Design of Various New Enzyme Inhibitors as Anti-Mycobacterial Agents Using *In-silico* High Throughput Screening

THESIS

Submitted in partial fulfillment of the

requirements for the degree of

DOCTOR OF PHILOSOPHY

By

PRITESH BHAT S.

2007PHXF442

Under the Supervision of

DR. P. YOGEESWARI

BIRLA INSTITUTE OF TECHNOLOGY & SCIENCE

PILANI (RAJASTHAN) INDIA

2011

BIRLA INSTITUTE OF TECHNOLOGY & SCIENCE

PILANI (RAJASTHAN)

This is to certify that the thesis entitled **"Design of Various New Enzyme Inhibitors as Anti-mycobacterial Agents Using In-silico High Throughput Screening"** which is submitted for award of Ph. D. degree of the Institute, embodies original work done by him under my supervision.

Signature in full of the Supervisor: P. Yogeeswari 29/10/11

Name in capital block letters: **P. YOGEESWARI**

Designation: **Associate Professor**

ACKNOWLEDGEMENTS

It is a great pleasure and immense satisfaction in expressing my deep gratitude towards my research supervisor, Dr. P. Yogeeswari Associate Professor and Head, Pharmacy Group, BITS-Pilani, Hyderabad Campus for her guidance, suggestions and support. She was always an inspiration to me for my work.

I deeply acknowledge and heartfelt thanks to Dr. D. Sriram, Associate Professor and Head, Pharmacy Group, BITS-Pilani, Hyderabad Campus for his valuable suggestions, guidance offered to me during the research.

I am grateful to Prof. Bijendra N. Jain, Vice-Chancellor, for allowing me to carry out my doctoral research work in the institute.

I am thankful to Prof. V. S. Rao, Director, BITS Pilani Hyderabad Campus and Prof G Raghurama, Director, BITS Pilani campus, for co-operation and encouragement.

I am thankful to Prof. Suman Kapur, Dean, Research and Consultancy Division, BITS Pilani Hyderabad Campus, for her co-operation and encouragement at every stage of this research work.

I am happy to express my sincere thanks to Prof. R. N. Saha, Deputy Director, Research and Consultancy, for his support during my research work and my stay at Pilani.

I would like to express my gratitude to Dr. R. Mahesh, Dean Faculty Affairs, for providing me with all the necessary laboratory facilities and for having helped me at various stages of my research work at Pilani.

I sincerely acknowledge the help rendered by Dr. Hemant Jadhav, Dr. Sajeev Chandran, Dr. Punna Rao, Dr. Shrikant Charde, Dr Archan Roy, Dr Vamsi Krishna, Dr Sajali Begam and Ms. Ramani.

I express my thanks to our laboratory attendants and demostrators Gokulji, Hariramji, Naveenji, Ramsutharji, Sunithaji, Shaliniji, Sarithaji, Rekhaji, Venkatji for all their help in one way or the other.

I am very much grateful to all my friends Monika, Jean, Rukkhayya, Mallika, Srividya, Petrisha, Rahul, Aditya, Senthil, Dinakaran, Sunil, Devadoss, Dilip, Thimmappa, Vaigunda Ragavendran, Debjani, Girish, Laila, Prakash, Pradeep, Kalidass, Sridhar, for the time they had spent for me and making my stay at BITS a memorable one.

I would also like to take names of my closest friends Arvind Semwal and Ram Kumar Mishra whose company made my moments delightful. Thank you my dearest friends for the continuous support and inspiration.

I would like to thank Amma, Anu, Prahanthanna, Honni, Pravenakka, Bavaji, Smrathi and cute kids Prajna, Prerana, Prathikasha, Pranav for all the support and having strong belief on me.

I deeply acknowledge the Department of Biotechnology (Centre of Excellence Project), New Delhi, India for their financial assistances.

At last, and above all, I would like to thank the God Almighty; for all that she has given to me.

Date: 29/10/11

Pritesh Bhat

List of Figures

List of Tables

List of abbreviations

A	Hydrogen bond acceptor
ADME	Adsorption, distribution, metabolism and excretion
ADP	Adenosine di phosphate
AFB	Acid fast bacilli
AG	Arabinogalactan
AIDS	Acquired immune deficiency syndrome
AMK	Amikacin
ATP	Adenosine tri phosphate
BCG	Bacille calmette-guerin
BCG	Bacille calmette guerin
BLAST	Basic local search alignment tool
BLOSUM	BLOcks of Amino Acid SUbstitution Matrix
BMGF	Bill and melinda gates foundation
BS	*Bacillus subtilis*
CDC	Centers for disease control and prevention
CDD	The collaborative drug discovery tuberculosis database
CG	Conjugate gradient
CHARMm	Chemistry at harvard molecular mechanics
CIP	Ciprofloxacin
CLR	Clarithromycin
CNS	Central nervous system
CFU	Colony Forming Units
CoMSIA	Comparative molecular similarity indices analysis
D	Hydrogen bond donor
D-AAT	D-amino acid transaminases
DevR	Dormancy regulon
DHFR	Dihydrofolate reductase
DNA	Deoxy ribonucleic acid
DOTS	Directly Observed Treatment, Short-course
EDCTP	European and developing countries clinical trials partnership
Efa	*Enterococcus faecalis*
FadD13	Fatty-acyl-coenzyme (co)a synthetase
FDA	Food and Drug Admnistration
GA	Genetic algorithm
GA-MLR	Genetic algorithm-multiple linear regression
GlmU	N-acetylglucosamine-1-phosphate uridyltransferase
GLP	Good laboratory practice

GluR	Glutamate Racemase
GMP	Good manufacturing practice
GOLD	Genetically Optimized Ligand Docking
g-PGA	gamma-poly-glutamic acid
GSK	Glaxosmithkline
H	Hydrophobic
HAART	Highly active antiretroviral therapy
HIV	Human immunodeficiency virus
HQSAR	Hologram quantitative structure–activity relation
HTS	High-throughput screening
ICL	Isocitrate lyase
INH	Isoniazid
IPTG	Isopropyl-1-thio-b-d-galactopyranoside
IRD	Institut de recherche pour le dévelopement
IRIS	Immune reconstitution inflammatory syndrome
KatG	Catalase-peroxidase-peroxynitritase
KM	Kanamycin
LBFGS	limited-memory Broyden-Fletcher-Goldfarb-Shanno algorithms
LM	Lipomannan
LZD	Linezolid
MAA	Marketing authorization application
ManLAM	Mannose-capped lipoarabinomannan
MBP	Myelin basic protein
MD	Molecular dynamic
MDR-TB	Multi-drug resistant tuberculosis
MIC	Minimum inhibitory concentration
MICL	2-methylisocitrate lyase
MLR	Multiple linear regression
MOE	Molecular operating environment
Mtb	*Mycobacterium tuberculosis*
MurB	Udp-n-acetylenolpyruvoylglucosamine reductase
MXF	Moxifloxacin
Myc Ac	Mycolicacids
N	Negative ionizable
NCE	New chemical entity
NDA	New drug application
NfnB	Fmn dependent nitroreductase
NIH	National institutes of health

NM4TB	New medicines 4 tuberculosis
NMR	Nuclear magnetic resonance
NNRTIs	Non-nucleoside reverse transcriptase inhibitors
NPT	Number-pressure-temperature
NVT	Number-volume-temperature
OPLS	Optimized Potentials for Liquid Simulations
P	Positive ionizable
PAS	*P*-aminosalicylic acid
PCA	Principal component analysis
PDB	Protein data bank
PG	Peptidoglycan
PGDBs	Pathway/genome databases
PGL	Phenolic glycolipid
PIMs	Phosphatidyl-myo-inositol mannosides
PIs	Protease inhibitors
PknB	Protein Kinase B
PLS-QSAR	Partial least squares quantitative structure–activity relation
PMSF	phenylmethanesulfonylfluoride
QSAR	Quantitative structure activity relationship
R	Aromatic ring
rmsd	Root mean square deviation
RNA	Ribonucleic acid
SCR	Structurally conserved regions
SD	Steepest descent
SL	Sulfolipid
SLDs	Second-line drugs
SP	Standard precision
STPKs	Ser/thr protein kinases
SVR	Structurally variable regions
T	Thioacetazone
TB	Tuberculosis
TBDB	Tuberculosis database
TBSGC	Tuberculosis Structural Genomics Consortium
TBTC	Tuberculosis trials consortium
TBTC	Tuberculosis trial consortium
TDM	Trehalose dimycolate
TDR	Research and training in tropical diseases
TGs	Triglycerides

TMPK	Thymidine monophosphate kinase
WHO	World health organization
WYY	H-tryptophan-tyrosine-tyrosine-oh
XDR-TB	Extremely drug resistant tuberculosis
XP	Extra precision

Abstract

Various enzyme targets from mycobacterium were taken and inhibitors designed by using different computational drug design approaches. The identified molecules were then either procured or synthesized and their activity was estimated by performing enzyme inhibition assays. They were also assessed for anti-mycobacterial assay. The enzyme targets studied include Glutamate Racemase (GluR), Protein Kinase B (PknB), and Isocitrate Lyase (ICL).

D-Glutamate is an essential component of peptidoglycan cell wall of Mtb which maintains the cell wall integrity of the cells against an elevated internal osmotic pressure. GluR is the only source for D-glutamate, which catalyzes conversion of L-glutamate to D-glutamate. Because of unavailability of structural information, the 3D model was built for the Mtb GluR. Newly built model was compared with already available model in Swiss-prot repository by running 1.2 ns molecular dynamics (MD) simulation. The structures evolved during the MD simulation presented a very high deformation especially in the catalytic loop region for the Swiss-prot model, where as our model was consistently stable throughout the MD simulation. The initial rotameric conformation of amino acid residues in Swiss-prot model changed in due course of simulation to adopt the conformation present in our model. A structure based design approach was followed using the Mtb GluR model developed by us to identifying the inhibitors.

PknB is essential for cellular signaling and growth of Mtb. It is expressed during the exponential phase of growth. Over or under expression results in impaired cell growth. Structure based and ligand based pharmacophore approach was used to identify various diverse molecules by virtual screening of Asinex database. In the first approach ligand based pharmacophore was

developed using known inhibitors. In the second approach energy based pharmacophore was developed based on the interaction energetics of co-crystalized inhibitor. The developed Pharmacophore models mimicked the important hinge region interaction in enzyme. The hits identified from the virtual screening of the database were docked to crystal structure and important interactions were assessed and compared with the pharmacophoric mapping pattern. The identified potential molecules were then subjected to enzyme inhibition study.

One of the hallmarks of TB is the persistent phase of infection. During this phase the bacteria are thought to be in a slow growing or non-growing state and are recalcitrant to treatment by conventional anti-TB drugs. The strategy for survival of TB during chronic stages of infection is thought to involve a metabolic shift in the bacteria's carbon source to C2 substrates generated by the β-oxidation of fatty acids. Isocitrate lyase (ICL) catalyzes the first step in the glyoxylate shunt, a carbon assimilatory pathway that allows the net synthesis of C4 dicarboxylic acids from C2 compounds such as acetate. Structure based drug design, fragment based drug design were used to identify the inhibitors of the ICL. Since a metal ion was involved at the active site for the betterment of docking simulation, quantum polarized docking study was employed. The identified molecules by, virtual screening of database, were checked for ICL inhibitory activity. The Mtb ICL was expressed from recombinant *E. coli* strain. The enzyme was purified and enzyme inhibition study was carried out. The identified molecules presented inhibitory activity in μM range.

S. No.	**Contents**	**Page No.**
	Certificate	i
	Acknowledgements	ii
	List of Figures	iv
	List of Tables	viii
	List of Abbreviations	ix
	Abstract	xiii
Chapter 1	**Introduction**	1
1.1	Primeval tuberculosis	2
1.1.1	Global epidemiology of tuberculosis	3
1.1.2	Mycobacterium tuberculosis (Mtb)	5
1.2.1	The mannosylated cell envelope components of Mtb	5
1.3	Treatment	8
Chapter 2	**Review of literature: Anti TB Drug discovery current status & future approaches**	15
2.1	Current Therapy for TB	14
2.2	Clinical Development	20
2.3	New Approaches in Tuberculosis Drug Discovery	35
2.3.1	Drug Targets identification and prioritization by genomic approach	36
2.3.2	Structural genomics approach to drug discovery	39
2.3.3	Computational approaches and cheminformatics tools for drug discovery	40
2.4	Discovery Phase	55
Chapter 3	**Objectives and plan of work**	59
Chapter 4	**Glutamate Racemase (GluR) as anti-TB target and design of its inhibitors**	62
4.1	Introduction	62
4.1.1	GluR Inhibitors	71
4.2	Materials and method	77
4.2.1	Retrieval of GluR protein sequence	77
4.2.2	Template identification	77
4.2.3	Sequence alignment	78
4.2.4	Model building	78
4.2.5	Active site identification	81
4.2.6	Docking	82
4.2.7	Molecular Dynamics	82
4.2.8	Database preparation	85
4.2.9	Virtual screening of the database for inhibitor for inhibitor identification	85

Nowhere in these ancient communities of the Eurasian land mass, where it is so common and feared, is there a record of its beginning. Throughout history, it had always been there, a familiar evil, yet forever changing, formless, unknowable. Where other epidemics might last weeks or months, where even the bubonic plague would be marked forever afterwards by the year it reigned, the epidemics of tuberculosis would last whole centuries and even multiples of centuries. Tuberculosis rose slowly, silently, seepinginto homes of millions, like an ageless miasma. And once arrived, it never went away again. Year after year, century after century, it tightened its relentless hold, worsening whenever war or famine reduced the peoples' resistance, infecting virtually everybody, inexplicably sparing some while destroying others, bringing the young down onto their sickbeds, where the flesh slowly fell from their bones and they were consumed in the years- long fever, their minds brilliantly alert until, in apocalyptic numbers, they died, like the fallen leaves of a dreadful and premature autumn.

The Forgotten Plague:
How the War against Tuberculosis was Won - and Lost
Frank Ryan, 1992

Tuberculosis (TB) has a long history. Itexisted even before the beginning of recorded history and has left its mark on human creativity, music, art, and literature; and has influenced the advance of biomedical sciences and healthcare. Its causative agent, *Mycobacterium tuberculosis*(Mtb), may have killed more persons than any other microbial pathogen[1].

Each year, it is estimated, tuberculosis kills two million people and approximately eight million people become sick with the disease. HIV (Human Immunodeficiency Virus) and tuberculosis (TB) are leading global causes of mortality and morbidity [2]. In 2000, 7–12% of the estimated 8.3 million new TB cases worldwide were attributed to HIV infection [2]. However, the incidence of TB in HIV patients remains high in areaswhere TB is prevalent [3]. The average prevalence of all forms of tuberculosis in India is estimated to be 5.05 per thousand, prevalence of smear-positive cases 2.27 per thousand and average annual incidence of smear-positive cases at 84 per 100,000 annually.The incidence of TB is highest among patients with advanced HIV disease [4].Not only does HIV increase the risk of reactivating a latent Mtb infection, it also increases the risk of rapid TB progression soon after infection or re-infection with MTB. Highly active antiretroviral therapy (HAART) dramatically decreases the incidence of opportunistic infections and death in patients with advanced HIV infection, including those with TB [2]. The immune recovery associated with HAART results in dramatic clinical benefits, but this restoration of immunity may result in immunopathological reactions and clinical deterioration when HAART is initiated in patients with TB [5]. Some patients experience temporary exacerbation or worsening of symptoms, signs, and/or radiographic manifestations of TB disease. This phenomenon is termed 'immune reconstitution inflammatory syndrome' (IRIS) [5].

1.1 Primeval tuberculosis

It is presumed that the genus Mycobacterium originated more than 150 million years ago [1]. An early progenitor of Mtbwas probably contemporaneous and co-evolved with early hominids in East Africa, three million years ago. The modern members ofMtbcomplex seem to have originated from a common progenitor about 15,000 - 35,000 years ago[6]. TB was documented in Egypt, India, and China as early as 5,000, 3,300, and 2,300 years ago, respectively [1].

The first evidence of the infection in humans was found in a cemetery near Heidelberg, in the Neolithic bone remains that show evidence of the type of angulation often seen with spinal tuberculosis. Some authors term tuberculosis the first disease known to mankind. Signs of the disease have also been found in Egyptian mummies dated between 3000 and 2400 BCE. Typical skeletal abnormalities, including Pott's deformities, were found in Egyptian and Andean mummies and were also depicted in early Egyptian and pre-colombian art [7].

The first references to tuberculosis in Asian civilization are found in the Vedas. The oldest of them (Rigveda, 1500 BCE) calls the disease yaksma. The Atharvaveda calls it another name: balasa. It is in the Atharvaveda that the first description of scrofula is given. The SushrutaSamhita, written around 600 BCE, recommends that the disease be treated with breast milk, various meats, alcohol and rest. The Yajurveda advises sufferers to move to higher altitudes. The Manu Smriti, written around 1500 BCE, states that sufferers of yaksma are impure and prohibits Brahmans from marrying any women that has a family history of the disease [7].

1.1.1 Global epidemiology of tuberculosis

The consequences of TB on society are immense. Worldwide, oneperson out of three is infected withMtb– two billion people in total. TB accounts for 2.5 % of the global burden of disease and is the commonest cause of death in young women, killing more women than all causes ofmaternal mortality combined. TB currently holds the seventh place in the globalranking of causes of death. Unless intensive efforts are made, it is likely to maintain that position throughout[8].

In 2007, World Health Organization (WHO) estimated 13.7 million people to have active TB disease, with 9.3 million new cases and 1.8 million deaths; the annual incidence rate varied from 363 per 100,000 in Africa to 32 per 100,000 in America. Tuberculosis is the world's greatest infectious killer of women of reproductive age and the leading cause of death among people with HIV/AIDS.TB hinders socioeconomic development: 75 % of people with TB were within theeconomically productive age group of 15-54 years. Ninety-five per cent of all casesand 99 % of deathsoccurred in developing countries, with the greatest burden in sub-Saharan Africa and South East Asia[9].

Effective drugs to treat and cure the disease have been available for more than 50 years, yet every 15 seconds, someone in the world dies from TB. Even more alarming fact is that one person is newly infected with Mtbevery minute. If left untreated, a person with active TB would infect at an average of 10 to 15 other people every year[9].

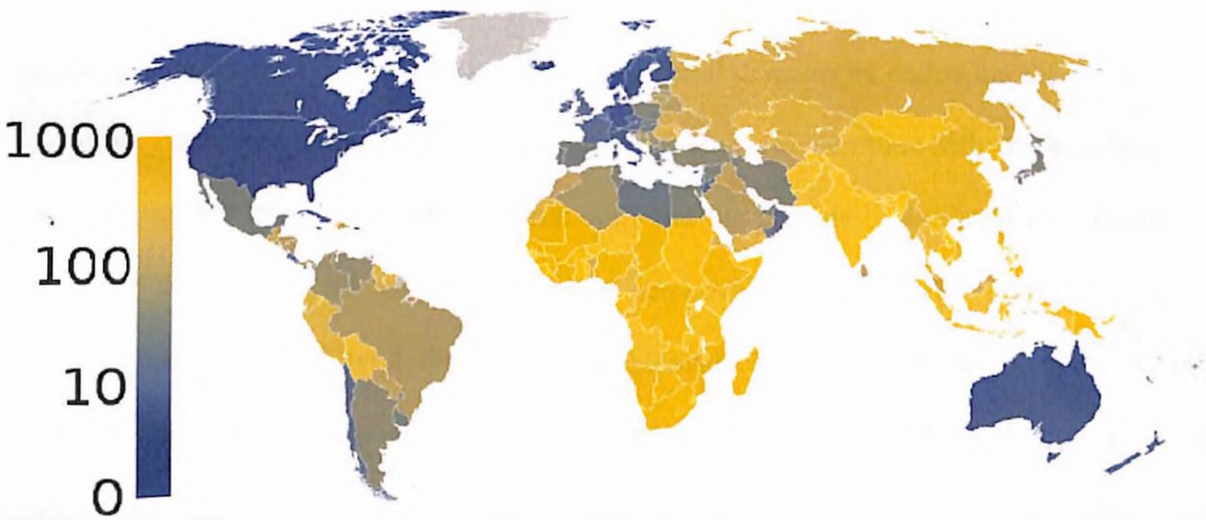

Figure 1: In 2007, the prevalence of TB per 100,000 people was highest in sub-Saharan Africa, and was also relatively high in Asia [10]

1.1.2*Mycobacterium tuberculosis (Mtb)*

Mtbthen known as the tubercle bacillus, was first described on 24 March 1882 by Robert Koch, who subsequently received the Nobel Prize in physiology or medicine for this discovery in 1905; the bacterium is also known as Koch's bacillus. Mtb is pathogenic bacterial species in the genus Mycobacterium and the causative agent of most cases of tuberculosis. Mtbhas an unusual, waxy coating on the cell surface (primarily mycolic acid), which makes the cells impervious to Gram staining so acid-fast detection techniques are used instead. The physiology of Mtbis highly aerobic and requires high levels of oxygen. Primarily a pathogen of the mammalian respiratory system, Mtb infects the lungs and is the causative agent of tuberculosis. The most frequently used diagnostic methods for TB are the tuberculin skin test, acid-fast stain, and chest radiographs.

1.2.1 The mannosylated cell envelope components of *M. tuberculosis*

The Mtb cell envelope is characterized by the presence of a variety of unique complex lipids, constituting 60% of the bacillus total weight. This lipid-rich low permeability matrix contributes to the difficulty in combatingmycobacterial diseases by endowing the organism with innate resistance to therapeutic agents and host defenses. The complex Mtb cell envelope can be divided into two major structures, the cell wall and the capsule-like outermost structures. The outermost components are solvent-extractable non-covalently bound free lipids, carbohydrates and proteins associated with the mycolyl-arabinogalactanepeptidoglycan complex (cell wall core). These surface components may be prone to release, shedding, and/ or cleavage upon contact with the host cell or within an appropriate intracellular environment of the cell. The surface of Mtb is particularly rich in mannose-containing biomolecules, including mannose-capped lipoarabinomannan (ManLAM), the related lipomannan (LM), phosphatidyl-myo-inositol mannosides (PIMs), arabinomannan, mannan and manno-glycoproteins (Figure 2). PIMs, LMandManLAMare incorporated into the plasmamembrane and also exposed on the Mtb cell surface. They act as ligands for host cell receptors and contribute to the pathogenesis of Mtb.

1.2.2 Microscopic morphology

The microscopic appearance does not allow the differentiation of the pathogenic agents of TB, mainlyMtb, from other mycobacteria although some characteristics may be indicative. In smears stained with carbolfuchsin or auramine and examined under light microscope, the tubercle bacilli typically appear as straight or slightly curved rods. According to growth conditions and age of the culture, bacilli may vary in size and shape from short coccobacilli to long rods. A typical curved shape has been described for *M. microti*[8]. The dimensions of the bacilli have been reported to be 1-10 μm in length (usually 3-5 μm), and 0.2-0.6 μm in width. Therefore, the length of the microorganism is comparable to the diameter of the nucleus of a lymphocyte. Unlike some fast growing mycobacteria and other actinomycetales, Mtbis rarely pleomorphic, it does not elongate into filaments, and does not branch in chains when observed in clinical specimens or culture. In the experimental macrophage infection, intracellular bacilli were described as being significantly elongated compared to broth-grown bacilli and, remarkably, to display bud-like structures.

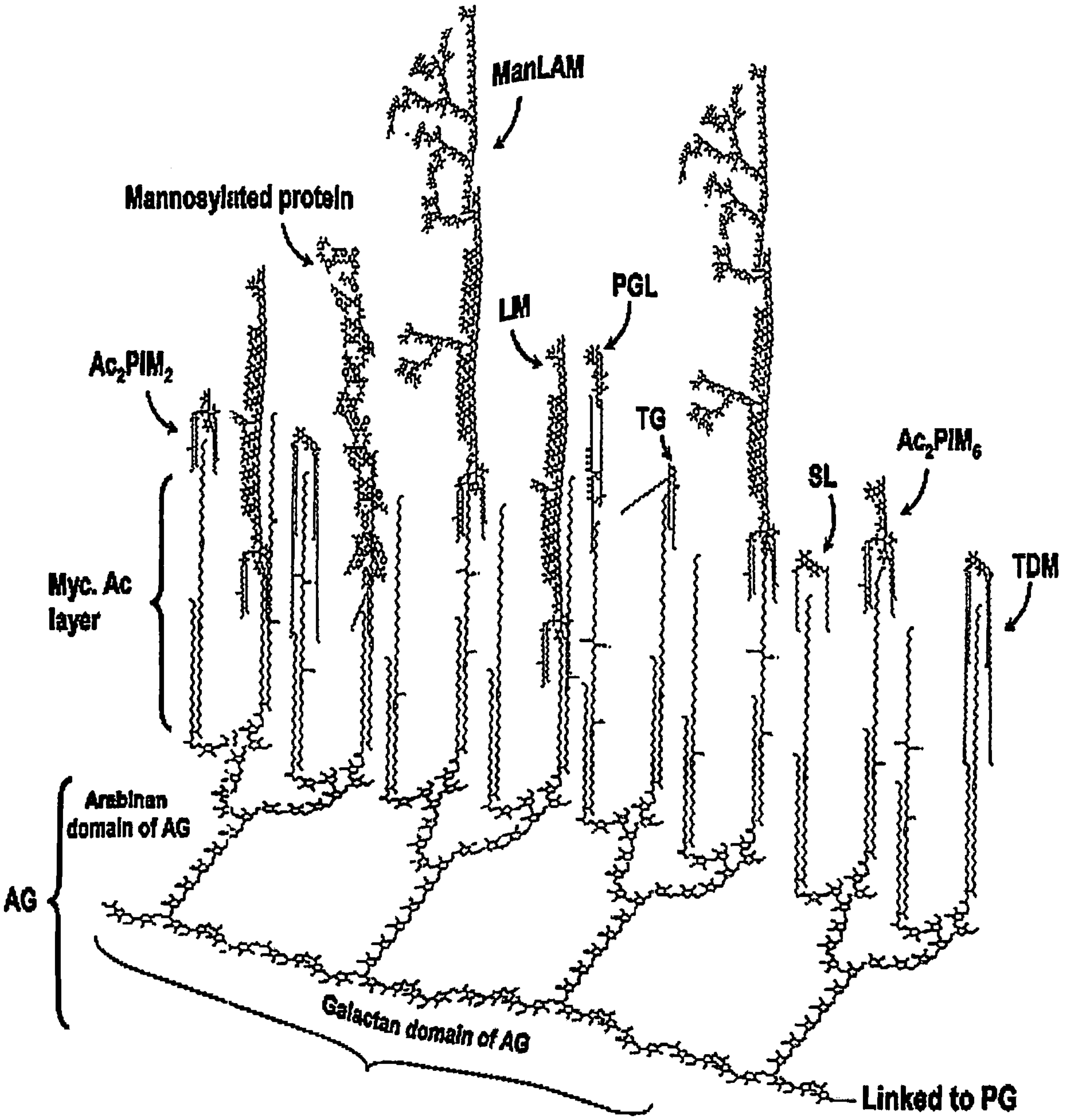

Figure 2.The cell envelope of Mtb with an emphasis on exposed mannosylated cell envelope components. This scheme depicts the cell envelope "skeleton or core" determinants (mycolyl-arabinogalactanepeptidoglycan complex) and emphasizes the distribution of intercalated major mannosylated cell envelope components that are exposed on the Mtb surface. AG is covalently linked to PG via the galactan chain and the arabinan chain is in turn linked to the mycolic acids (Myc Ac) which are shown perpendicular to the plasma membrane. The polar groups (i.e. carbohydrate domains) of several mannosylated cell envelope components are exposed on the cell surface and their lipid domains are intercalated with the Myc Ac acid layer. These envelope

components include ManLAM, LM, higher- and lower-order PIMs, and lipomannoproteins. Other known virulence factors described for M. tuberculosis that interact with the Myc Ac layer [i.e. TDM, SL; and TGs and PGL, the latter on some Mtb strains)] are also depicted. Not all Myc Ac are depicted interacting with cell surface components. Not shown are capsule-like components (i.e. arabinomannan, glucan, mannan, and xylan). In order to maintain simplicity, molecular quantities depicted (relative number of molecules) do not accurately reflect experimental data. AG (arabinogalactan); PG (peptidoglycan); Myc Ac (mycolicacids); ManLAM (mannose-capped lipoarabinomannan); LM (lipomannan); PIMs (phosphatidyl-myo-inositol mannosides); TDM (trehalosedimycolate); SL (sulfolipid); TGs (triglycerides); PGL (phenolic glycolipid). [11]

When numerous and actively multiplying, the bacilli are strongly acid fast and show an evident and distinctive tendency to form hydrophobic bundles. Free bacilli can also be seen, though, especially at the border of the swarms. In unlysed host tissue, the bacilli are more numerous within the phagocytic cells.

Once the disease has been controlled, dying bacilli become sparser, often faintly and unevenly colored, due to partial loss of the internal contents. Of course, irregular staining may also be the consequence of technical defectiveness of dyes or staining procedures.

1.3 Treatment

Tuberculosis treatment refers to the medical treatment of the infectious disease tuberculosis. Active tuberculosis will kill about two of every three people affected if left untreated. Treated tuberculosis has a mortality rate of less than 5%

The standard "short" course treatment for TB is isoniazid, rifampicin (also known as rifampin in the United States), pyrazinamide, and ethambutol for two months, then isoniazid and rifampicin alone for a further four months. The patient is considered cured at six months (although there is still a relapse rate of 2 to 3%). For latent tuberculosis, the standard treatment is six to nine months of isoniazid alone.

If the organism is known to be fully sensitive, then treatment is with isoniazid, rifampicin, and pyrazinamide for two months, followed by isoniazid and rifampicin for four months. Ethambutol need not be used.

First Line:

All first-line anti-tuberculous drug names have a standard three-letter and a single-letter abbreviation:

1. Ethambutol is EMB or E,
2. Isoniazid is INH or H,
3. Pyrazinamide is PZA or Z,
4. Rifampicin is RMP or R,
5. Streptomycin is STM or S.

Second Line:

There are six classes of second-line drugs (SLDs) used for the treatment of TB. A drug may be classed as second-line instead of first-line for one of three possible reasons: it may be less effective than the first-line drugs (e.g., p-aminosalicylic acid); or, it may have toxic side-effects (e.g., cycloserine); or it may be unavailable in many developing countries (e.g., fluoroquinolones):

1. Aminoglycosides: e.g., amikacin (AMK), kanamycin (KM);
2. Polypeptides: e.g., capreomycin, viomycin, enviomycin;
3. Fluoroquinolones: e.g., ciprofloxacin (CIP), levofloxacin, moxifloxacin (MXF);
4. Thioamides: e.g. ethionamide, prothionamide
5. Cycloserine (the only antibiotic in its class);
6. p-aminosalicylic acid (PAS or P).

Third Line:

Other drugs that may be useful, but are not on the WHO list of SLDs:

1. Rifabutin
2. Macrolides: e.g., clarithromycin (CLR);
3. Linezolid (LZD):
4. Thioacetazone (T);
5. Thioridazine;
6. Arginine;
7. Vitamin D;
8. R207910.

These drugs may be considered "third-line drugs" and are listed here either because they are not very effective (e.g., clarithromycin) or because their efficacy has not been proven (e.g., linezolid, R207910). Rifabutin is effective, but is not included on the WHO list because for most developing countries, it is impractically expensive.

Management and Treatment

The main objectives of anti-TB treatment are to

1. cure the patient of TB (by rapidly eliminating most of the tubercle bacilli),
2. prevent death from active TB or its late effects,
3. prevent relapse of TB (by eliminating the dormant tubercle bacilli),
4. prevent development of drug resistance (by using a combination of effective drugs),
5. decrease TB transmission.

Table 1 and Table 2 details different standard regimen followed with dosing frequency.

Table 1. Standard regimen for new TB patients

Intensive phase	Continuation Phase	Comments
2 months of HRZE[a]	4 months of HR	
2 months of HRZE	4 months of HRE	Applies only in countries with high levels of isoniazid resistance in new TB patients, and where isoniazid drug susceptibility testing in new patients is not done (or results are unavailable) before the continuation phase begins

[a] WHO no longer recommends omission of ethambutol during the intensive phase of treatment for patients with non-cavitary, smear-negative pulmonary TB or extrapulmonary disease who are known to be HIV-negative. Ethambutol is E, Isoniazid is H, Pyrazinamide is Z, Rifampicin is R.

Table 2. Dosing frequency for new TB patients

Dosing frequency		Comments
Intensive phase	Continuation phase	
Daily	Daily	optimal
daily	3 times per week	Acceptable alternative for any new TB patient receiving directly observed therapy
3 times per week	3 times per week	Acceptable alternative provided that the patient is receiving directly observed therapy and is not living with HIV or living in an HIV-prevalent setting

Note: daily (rather than three times weekly) intensive-phase dosing may help to prevent acquired drug resistance in TB patients starting treatment with isoniazid resistance.

Chapter II

Review of literature: Anti TB Drug discovery current status & future approaches

It has passed more than half a century after the introduction of effective chemotherapy for tuberculosis, but the disease still remains unconquered [12]. The multidrug regimens are available that can cure 95% of patients with active tuberculosis, newer and better drugs are needed because of poor patient compliance with the long 6 months of treatment duration, adverse interactions with antiretroviral drugs, and the emerging of resistance to drug. The longer treatment regimen is the greatest problem of all other, with reduction in the duration of the treatment; the success rate can be increased because more number of patients going for complete treatment, resulting in reduced relapse and development of resistance. WHO introduced their DOTS (Directly Observed Treatment, Short-course) strategy in 1993 [13], which involves direct observation by the trained personnel of patients taking their medications to ensure compliance. This has increased treatment success, meanwhile increasing the cost. Other than by shortening of the treatment time, new agents would be considered an advance if they are able to penetrate sites that are difficult to treat, such as pulmonary cavities, emphysema, or extra pulmonary locations, or had novel mechanisms of action that are active against infections that are either sensitive or resistant to current drugs [14]. Drugs with long half-lives are advantageous simplifying the treatment regimen. New agents which are able to target tubercle bacilli in its dormant state will be able to overcome the relapse of the disease and latency.

The reduced incidence of TB in the developed world resulted into fall in the commercial incentives for pharmaceutical companies to invest in anti-TB drug research and development. In

2000 the Rockefeller Foundation convened a meeting, in Cape Town, South Africa, to investigate ways to stimulate drug development. More than 120 organizations came forward to form a not for profit public private partnership the Global Alliance for TB Drug Development (TB Alliance) responsible for the development of improved and affordable therapies [15]. Three pharma majors AstraZeneca, GlaxoSmithKline, and Novartis developed discovery research units focused on tuberculosis. Other organizations like Otsuka Pharmaceuticals, Johnson and Johnson, Lupin, Sequella, the US National Institutes of Health (NIH), the Special Program for Research and Training in Tropical Diseases (TDR) sponsored by WHO, and the Tuberculosis Trials Consortium (TBTC) sponsored by the US Centers for Disease Control and Prevention aimed their work at finding and developing new therapies for TB. This renewed drug discovery interest and now there are potentially useful agents at every stage of the development pipeline with multiple organizations doing clinical trials. With all these efforts the development of a new drug active against Mtb has just started.

2.1 Current Therapy for TB

Current TB treatment capitalizes combination chemotherapy. Multiple drugs are used to increase efficacy that prevent the development of resistant organisms. Based on the mechanism of action, presently used drugs can be classed as inhibitors of, bacterial protein synthesis (aminoglycosides), electron transport across the bacterial membrane (a proposed mechanism of action for pyrazinamide), nucleic acid synthesis (rifampin, quinolones) and cell wall synthesis (isoniazid, ethambutol, ethionamide and cycloserine) (Figure 3). The requirement of long duration of treatment is attributed to physiologic heterogeneity of TB bacteria that is, subpopulations of organisms actively growing bacteria to metabolically quiescent ones. It duration of treatment is attributed to physiologic heterogeneity of TB bacteria that is, subpopulations of organisms actively growing bacteria to metabolically quiescent ones. It appears that subpopulations can display phenotypic drug-resistance and thereby survive long periods of drug treatment in an animal or human host. These bacteria have been called "persisters" [16, 17] i.e., those with latent tuberculosis infection who are clinically asymptomatic and noninfectious.

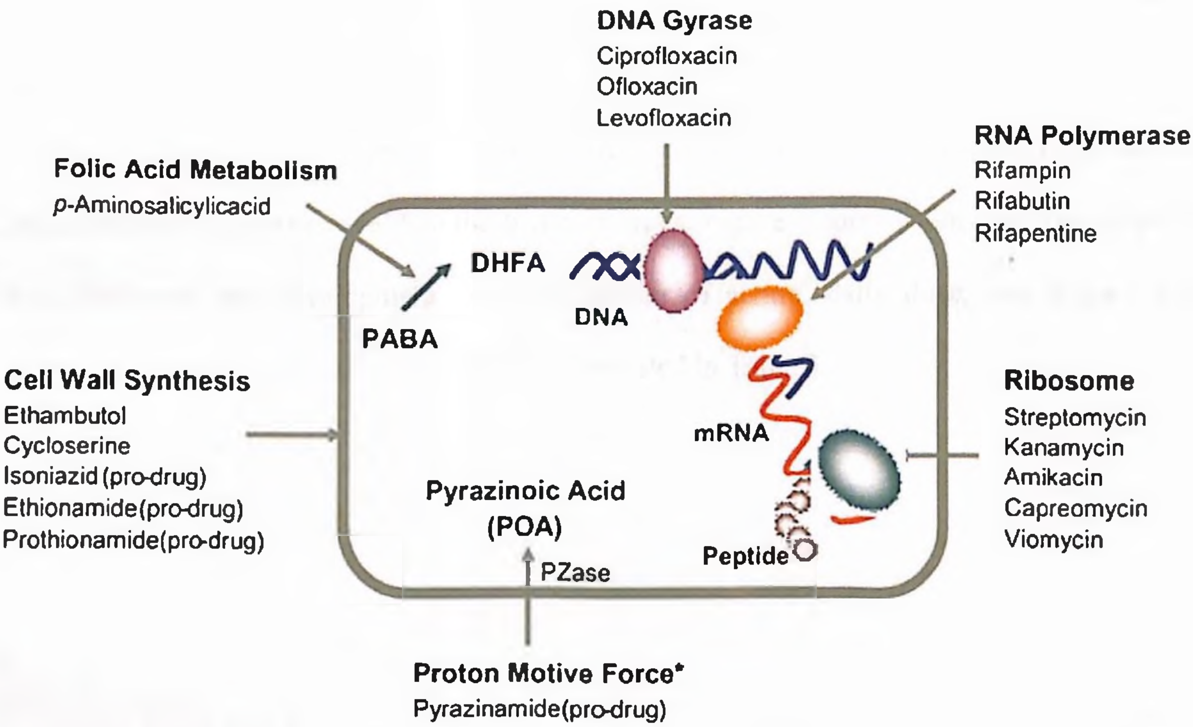

* Indicates a hypothetical mechanism.

Figure 3: Mechanism of action of currently prescribed anti-mycobacterial drugs [69].

Drugs acting with different mode of action are most likely needed to kill bacteria spanning spectra of different subpopulations. Isoniazid is the most effective of TB drugs at killing active replicating tubercle bacilli and rifampin an inhibitor of RNA synthesis, are active against both replicating and non-replicating or slowly replicating bacteria [18]. Pyrazinamide, effectiveness is seen only during first two months of therapy [19]. It is the combination of rifampin and pyrazinamide which reduced the duration of treatment from 18-24 months to 6-9 months [20]. The combination of three, or more typically, four drugs, i.e. isoniazid, rifampin, pyraziminamide and ethambutol when used, offer the best combination of efficacy and tolerability, and are therefore recommended for use as "first line" therapy. Less efficacious and tolerable drugs are used in cases of resistance to the first line drugs, and are referred to as "second line" products [21] (Table 3). They are streptomycin, capreomycin, kana-mycin, amikacin, ethionamide, para-aminosalicylic acid, cycloserine, ciprofloxacin, ofloxacin, levofloxacin, moxifloxacin, gatifloxacin and clofazimine. These products have low therapeutic index and are more expensive than the first line drugs. Figure 4 contains the time line of anti TB drug discovery and development. The mechanism of action, daily dose, and major adverse effects of first line and second line drugs are tabulated in Table 3.

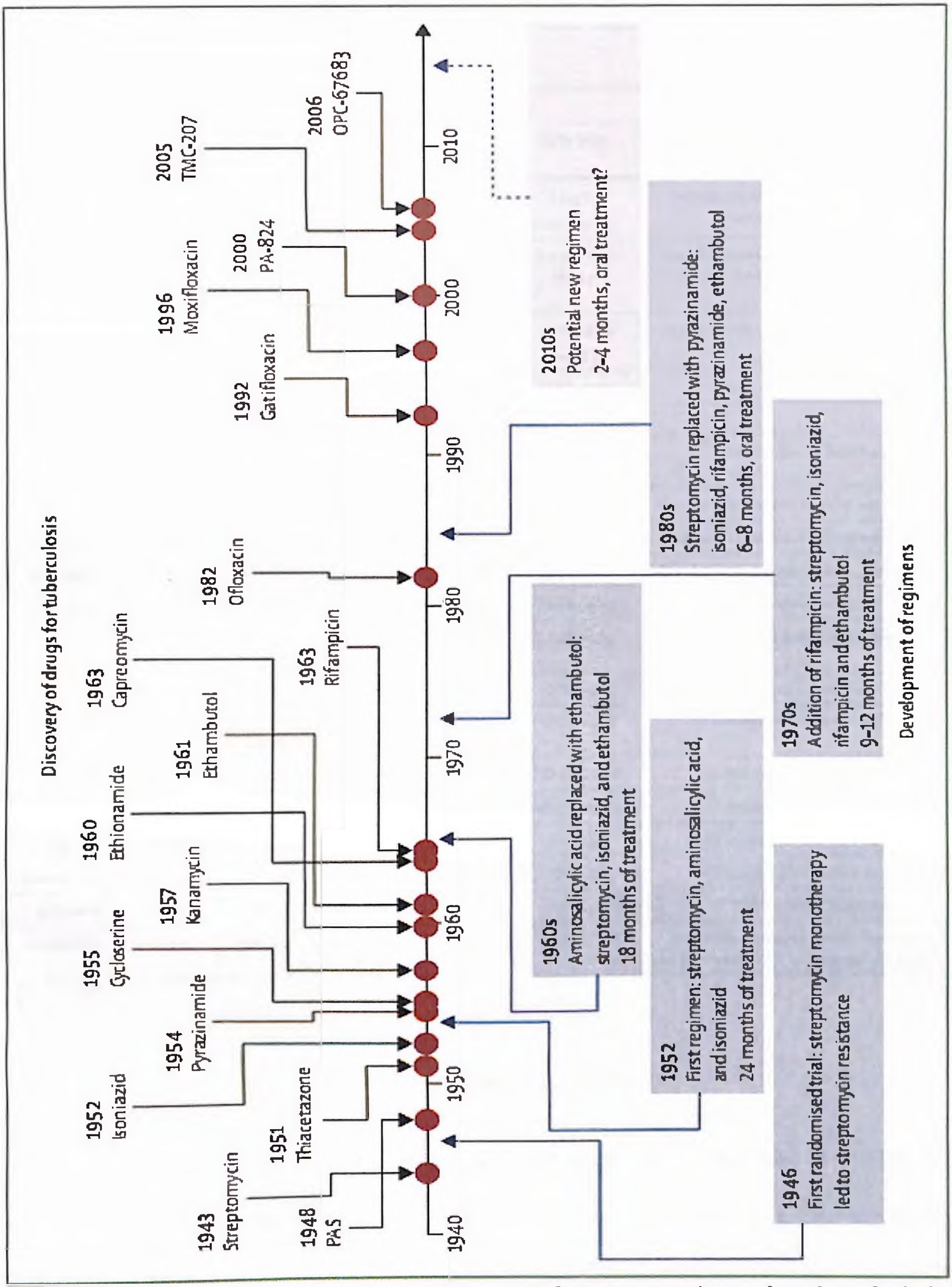

Figure 4: History of drug discovery and development of treatment regimens for tuberculosis [14].

Table 3: Year of Discovery, Main Characteristics and Most Frequently Reported Adverse Reactions of First and Second Line TB Drugs

First Line Drugs					
Drug	**Year discovered**	**MOA**	**Route**	**Daily Dose**	**Major Adverse Reactions**
Isoniazid	1952	Cell wall syntheis inhibitor	P Os	5 mg/kg (max 300 mg)	Hepatitis, peripheral neuropathy, lupus-like syndrome, drug interactions
Rifampin	1966	RNA synthesis Inhibitor	P Os	10 mg/kg (max 600 mg)	Drug interactions, orange color of body fluids, GI, hepatitis, fever, acute renal failure, hemolytic anemia
Pyrazinamide	1952	Disruption of electron transport across the membrane ♦	P Os	15-30 mg/kg (max 2 g)	Hyperuricemia, gouty arthritis, rarely nephritis
Ethambutol	1961	Cell wall synthesis inhibitor	P Os	15-25 mg/kg	Optic neuritis, exfoliative rash
Second Line Drugs					
Drug	**Year discovered**	**MOA**	**Route**	**Daily Dose**	**Major Adverse Reactions**
Streptomycin	1944	Protein synthesis inhibitor	IV/IM	15 mg/kg	Cochlear and vestibular toxicity, nephrotoxicity
Capreomycin	1956	Protein synthesis inhibitor	P Os	15-30 mg/kg	Cochlear and vestibular toxicity, nephrotoxicity
Kanamycin	1957	Protein synthesis inhibitor	IV/IM	15-30 mg/kg	Cochlear and vestibular toxicity, nephrotoxicity
Amikacin	1974	Protein synthesis inhibitor	IV/IM	15-30 mg/kg	Cochlear and vestibular toxicity, nephrotoxicity
Ethionamide	1956	Inhibition of mycolic acid synthesis (cell wall)	IV/IM	15-20 mg/kg	GI toxicity/hepatitis/dizziness
PAS	1946	Inhibition of folic acid	P Os/IV	15-20 mg/kg	GI toxicity, fever, rash
Cycloserine	1952	Inhibition of peptidoglycan synthesis	P Os	15-20 mg/kg	Dizziness, depression, CNS
Ciprofloxacin	1986	Inhibition of DNA gyrase	P Os/IV	750-1550 mg/d	GI toxicity, CNS, tendon rupture
Ofloxacin	1995*	Inhibition of DNA gyrase	P Os/IV	600-800 mg/day	GI toxicity, CNS, tendon rupture
Levofloxacin	1996*	Inhibition of DNA gyrase	P Os/IV	500 mg/d	GI toxicity, CNS, tendon rupture
Moxifloxacin	1999*	Inhibition of DNA gyrase	P Os/IV	400 mg/d	GI toxicity, CNS, tendon rupture
Gatifloxacin	1999*	Inhibition of DNA gyrase	P Os/IV	400 mg/d	GI toxicity, CNS, dysglycemia
Clofazimine	1954	Binding to mycobacterial DNA and mRNA ♦	P Os/IV	100-300 mg/d	GI toxicity, cutaneous, ocular discoloration/ pigmentation QT prolongation, dizziness

* Year of first US patent
♦ proposed

Limitations and Hurdles to Optimal Use of Current Therapy

As mentioned earlier the biggest hurdle is the length and complexity of the treatment protocols. DOTS is the program recommended by WHO, but its level of implementation varies as it is quite demanding for patients and for health care staff. Inefficient treatment has resulted severely to the individual and for public health. Over the decades, resistance has appeared to each one of the existing drugs; strains that are resistant to at least isoniazid and rifampin are referred to as "multi-drug resistant" (MDR-TB). Recently strains have appeared that are resistant to isoniazid, rifampin, fluoroquinolones, and at least one second line injectable drug (capreomycin, kanamycin, or amikacin) are defined as "Extremely Drug Resistant" (XDR-TB) [22]. During 2000—2004 survey carried out by the WHO globally, 20% were MDR and 2% were XDR. Other population-based estimates report a relative incidence of approximately 10% MDR-TB among all new TB cases [23]. In addition, population-based data on drug susceptibility of Mtb isolates obtained from the US (1993-2004), Latvia (2000-2002), and South Korea (2004), showed that 4%, 19%, and 15% of MDR TB cases, respectively, were XDR. The treatment regimens for MDR TB are less well defined; depend on second line drugs which are less effective and more toxic, and expensive overall. The mortality rate in a recent outbreak of XDR approached 100% a XDR TB has thus come to worldwide attention as a major therapeutic challenge and potential threat to public health.

The second hurdle in the treatment of TB is existence of co-infection with human immuno-deficiency virus (HIV). It is estimated that half the people living with HIV/AIDS develop active TB [2]. The risk of expression from latent TB to active disease is estimated to be on average fifty fold higher in HIV positive individuals [24-26]. Drug interaction between Anti TB and Anti HIV are also major concern rendering the treatment problematic. Interactions of rifampin, non-nucleoside reverse transcriptase inhibitors (NNRTIs) and protease inhibitors (PIs) with cytochrome P450 3A4, create a significant problem in treatment of patients co-infected with TB and HIV. Anti-retroviral and isoniazid can cause peripheral neuropathy, and toxicity is enhanced when used together in combination.

Improving TB treatment focuses on achieving several goals:

i. Shortening the duration of treatment for active TB to improve compliance, lessen the burden on public health infrastructure, and reduce the occurrence of MDR-TB.

ii. Developing safe, tolerable drugs with novel mechanisms of action that will therefore be effective against resistant disease (MDR-TB and XDR-TB).

iii. Developing TB drugs that lack liver cytochrome P450 enzyme induction and inhibition, to avoid drug-drug interactions.

iv. Developing safe and effective drugs to shorten the treatment of LTBI thus making it possible to address the problem of the biologic reservoir of Mtb.

2.2 Clinical Development

The portfolio of compounds currently in research and development is commonly referred to as a 'pipeline'. As a result of the combined efforts of the institutions described earlier and driven by the severity of the global public health needs, there is now a growing pipeline of compounds for the treatment of TB.

The probability of any given molecule moving successfully through the various phases of the drug development process is very limited; of the thousands of compounds screened only a few make it to the preclinical phase, and a fraction of those enter into human experimentation. Therefore the number of products entering in to the clinical development is considerably smaller than those in earlier stages of the pipeline. Currently there are seven new products in clinical trials for TB.

Phase I

Diamine SQ-109

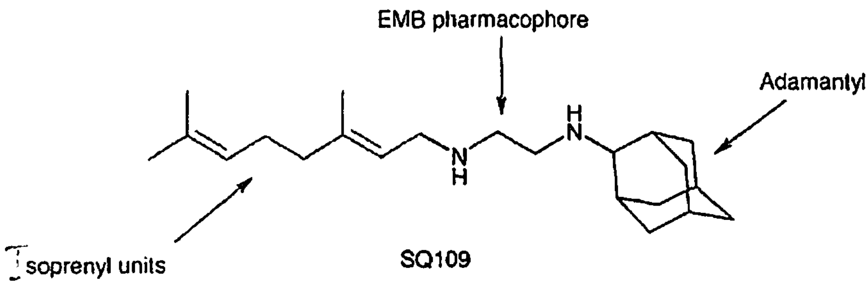

SQ109 is a diamine, being developed by Sequella, Inc. It was originally discovered during a collaborative effort with investigators at the U. S. National Institutes of Health (NIH) to identify promising analogs of ethambutol. Its structural dissimilarity to ethambuol and the potential differences in its intracellular target suggest that it may have a novel mechanism of action. The exact target has not been identified. It appears to be the synthesis of cell wall inhibition to be the mechanism but in a different manner than that of ethambutol. Both *in-vivo* and *in-vitro* studies have shown high potency as well as specificity to Mtb [27].

SQ109 has also been reported to be synergistic with rifampin and isoniazid both *in-vitro* and *in-vivo*. There were no antagonistic interactions observed when combined with other first-line drugs [28]. A particularly potent combination is SQ109/ rifampin with an inhibition of Mtb growth greater than 99% at very low concentrations, and that is also effective against rifampin resistant strains [28]. It has been reported that synergy arises from the activation of SQ109 by rifampin induced Mtb cytochrome P450 (CYP), producing active oxidized metabolites. Experiments with mice have also shown *in-vivo* synergy when SQ109 is used in combination with INH, RIF and PZA [29]. In September 2006 an IND for SQ109 was granted by the US FDA

[30]. SQ109 is hence a promising new drug that may shorten the duration of anti-TB regimens. By the completion of the first four doses (fasting) no serious adverse events had been reported. The first reports of Phase Ia clinical trials, completed in 2007, describe no serious side effects and fast and extensive distribution to tissues after oral administration with a long half-life, suggesting that once-a-week dosing may be achievable [31].

Pyrrole LL3858

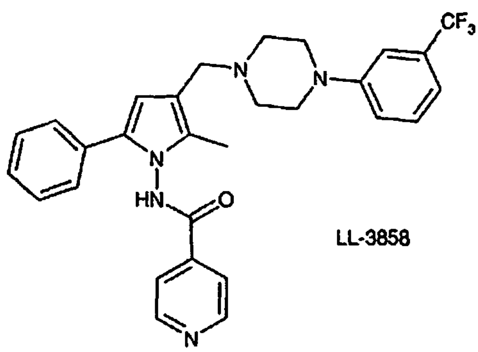

LL-3858

Named LL-3858 or sudoterb, after inventor Lupin Ltd., India, belongs to a class known as pyrroles derived from plant alkaloids. It has been suggested to act with novel mechanism, has showed potent anti Mtb activity *in-vitro* and *in-vivo*, against both drug-sensitive and drug-resistant strains of Mtb. Lupin Ltd. reported *in-vitro* bactericidal activity of sudoterb similar to isoniazid and is synergistic with rifampin, also the combination of with isoniazid, rifampin, and pyrazinamide has led to complete sterilization of sensitive and resistant Mtb strains in infected mice within two months, in a shorter timeframe than conventional therapy. These results suggest sudoterb could potentially reduce the time of TB treatment.

Nitroimidazole PA-824

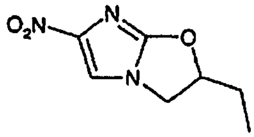

CGI 17341

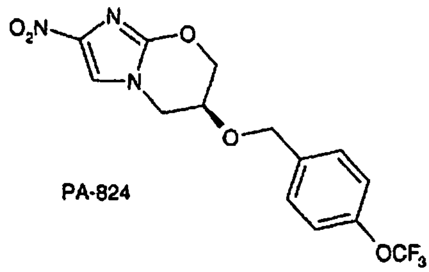

PA-824

PA-824 is a nitroimidazo-oxazine developed by the TB Alliance. With its novel mechanism of action it has shown the potential for both first-line treatment of active tuberculosis and for therapy of MDR/XDR. Initial nitroimidazoles were used in radio-sensitizing agents in cancer therapy, found to have anti-tuberculous activity. The Lead compound CGI-17341was found to be mutagenic [32]. In the 1990s, PathoGenesis further explored these and identified PA-824 potent compound against Mtb, later TB Alliance further developed it. The *in-vitro* studies indicted the molecule to be highly efficacious against both drug-sensitive and drug-resistant tuberculosis [15] and MIC similar to that of isoniazid [33, 34]. PA-824 has shown activity against strains with known resistance to standard TB treatment.

It is a prodrug, produces antibacterial activity by inhibiting the cell wall synthesis and the protein synthesis. Since it is also showing activity against the persistent Mtb there must be some other mechanism also involved. It induces an accumulation of hydroxymycolic acid and a concomitant reduction in ketomycolic acids, indicating inhibition of the enzyme responsible for the oxidation of hydroxymycolate to ketomycolate [35]. The pro-drug undergoes activation *via* an F420-dependent mechanism. *In-vitro* study has shown development of resistance by phenotype mutation in F420 enzyme [36]. PA-824 undergoes nitro-reduction producing highly reactive intermediates which interact with multiple intracellular targets. Thus the mechanism of action appears to be complex. The preclinical activity showed the substitution of PA-824 for INH resulted into rapid culture-negative conversion than standard therapy. The lung CFU (Colony Forming Units) counts after two months of treatment were significantly low and there was no relapse in mice after six months [37].

PA-824 entered Phase I clinical development in 2005. The Phase I study involving single and multi-dose study carried out on healthy subjects showed that PA-824 was well tolerated, with no dose-limiting adverse events or abnormal laboratory results. The time to maximum concentration (Tmax) was 4-5 hours, and the half-life ($t_{1/2}$) was approximately 18 hours. Presently the the renal effects of the PA-824, and Pharmacokinetic evaluation and drug-drug interaction with special focus on potential interaction with anti-retroviral drugs studies are underway.

PNU-100480

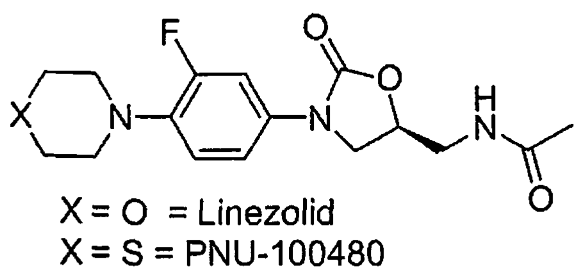

PNU-100480 is oxazolodinone developed by the Pfizer. The oxazolidinones comprise a new class of protein synthesis inhibitors that block translation through a novel mechanism by preventing the formation of the initiation complex. Linezolid is the only marketed oxazolidinone, approved for use for the treatment of complicated skin and skin structure infections and hospital-acquired pneumonia. The anti TB activity of PNU-100480 was first reported in 1996 [38]. Subsequent experiments with a murine model found that it was more active than linazolid. PNU-100480 significantly improves the initial bactericidal activity of several combinations of existing first-line drugs and moxifloxacin [39]. PNU-100480 has activity against persistent tubercle bacilli in mice such that the addition of PNU-100480 to the standard first-line tuberculosis regimen shortens the duration of treatment necessary for cure. These results suggest PNU-100480 may have the potential to improve the treatment of both drug-susceptible and drug-resistant tuberculosis. PNU-100480, is now in Phase I trials for TB [40].

AZD5847

AZD5847 is the oxazolodinone derivative developed by the Astrazenica. It works similar to other oxazolodinone that is by blocking translation through a novel mechanism by preventing the formation of the initiation complex.

Phase II

Nitroimidazole OPC-67683

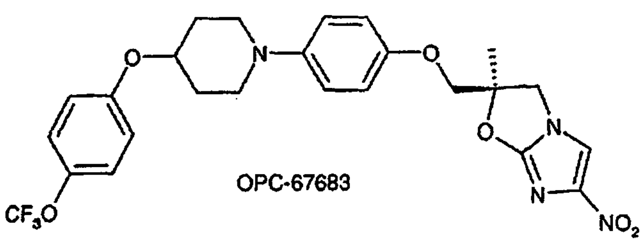

OPC-67683

OPC-67683 is a nitro-dihydroimidazo-oxazole derivative under development by Otsuka Pharmaceutical Co. Ltd. It has been already evaluated in a number of Phase I studies in healthy volunteers and in an early bactericidal activity study in TB patients. The compound has potent *in-vitro* anti-microbial activity against Mtb, and has no cross resistance with any of the currently used first-line tuberculosis drugs. Mechanism of action of OPC-67683 is similar to PA-824, so this compound could prove effective in the treatment of MDR/XDR TB. Pre-clinical studies in a chronic mouse model of tuberculosis showed superior efficacy of OPC-67683 to the currently used drugs. In other preclinical *in-vitro* and *in-vivo* studies, OPC-67683 showed synergistic effect with other first-line drugs with no appreciable interactions. A combination of OPC-67683 with rifampin and pyrazinamide for two months followed by a combination with rifampin for further two months virtually eliminated all lung bacterial load within three months, totally eliminating it after four months in mouse models, [41] The long half-life of OPC-67683, the lack of metabolisation by CYP enzymes and its efficacy in immunocompromised mice suggest that this drug may be useful for the treatment of co-infected TB/HIV patients. Otsuka has completed a small single dose level Phase II EBA study with OPC-67683 and has started a larger, multiple dose level EBA trial. This larger trial compares the safety, efficacy and pharmacokinetics in patients with uncomplicated, smear-positive pulmonary TB [42, 43].

Diarylquinoline TMC207

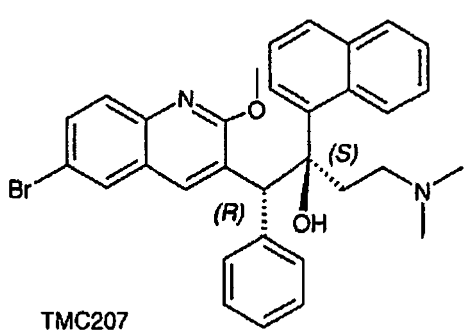

TMC207

TMC207 is a diarylquinoline discovered and under development by Tibotec Pharmaceuticals Ltd., a subsidiary of Johnson & Johnson. It has very unique and novel mechanism of action, inhibiting the mycobacterial ATP synthase proton pump one of the mycobacterial sources of energy [44] and thus explains the absence of development of cross-resistance in preclinical studies to the first-line drugs. In preclinical studies, TMC207 has shown potent anti-TB activity. In the mouse model, the combination of TMC207 with any two of the three first-line drugs i.e. isoniazid, rifampin and pyrazinamide was more effective than the standard regimen of isoniazid, rifampin and pyrazinamide and it resulted in negative spleen and lung cultures after 8 weeks of therapy [45]. The use of TMC207 alone is as effective as a combination of rifampin, INH and pyrazinamide and more effective than rifampin alone in mouse models [44]. TMC207 has a potent sterilising ability in guinea pigs, being 100 times more effective than the conventional combination of rifampin, INH and pyrazinamide [46].

TMC207 has completed several Phase I studies to evaluate safety, tolerability and pharmacokinetic parameters. These include a single ascending dose study, a multiple dose study, drug-drug interaction studies with rifampin, isoniazid and pyrazinamide, and an interaction study with ketoconazole. Results showed a positive food effect, a 2-fold increase in exposure, and metabolism by CYP450 3A4. Co-administration with rifampin, an inducer of CYP450 3A4 has lowered TMC207 plasma levels by 50%. Phase I trials in healthy human volunteers suggest that the drug is safe and, with a half-life greater than 24 hours, may allow for dosing at frequencies less than once per day.

Currently it is in Phase II development, an EBA trial [47]. The multidose study comparision between TMC207 vs. isoniazid/ rifampin, showed a decrease in colony forming units/ml/day over seven days, but observed reduction in clony forming units was less than that of observed with either isoniazid or rifampin over the same time period. The linear kinetics was observed in healthy volunteers as well as in patients. No serious adverse effects been reported till now patients trated with TMC207 in clinical trials. A Phase II dose-finding study in MDR patients, which includes safety and efficacy endpoints, is under consideration for TMC207 [47].

Rifapentine

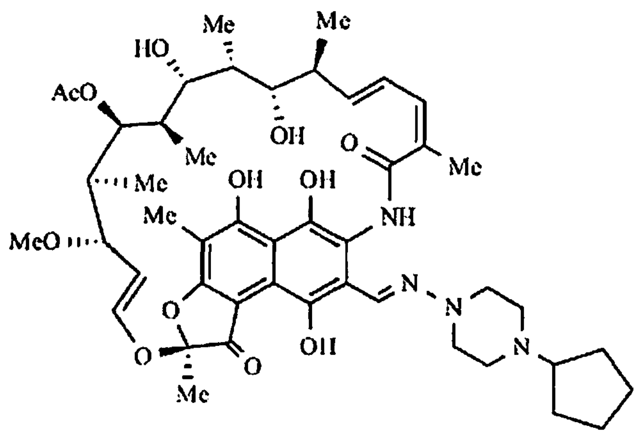

Rifapentine

Rifamycins are potent inhibitors of bacterial RNA polymerase [47]. Three semisynthetic rifamycins, rifampicin rifapentine and rifabutin have been introduced for the treatment of various microbial infections. Rifapentine, a more potent analogue with a longer half-life than rifampicin, is an attractive candidate for shortening treatment, and for intermittent treatment. [48, 49] However, as with rifampicin, rifapentine induces the expression of P450 enzymes [50]. Clinical studies are in progress to assess the effects of high doses of rifapentine once or twice per week given with moxifloxacin and daily rifapentine in the first-line regimen to shorten treatmen.

Phase III

Two products, Gatifloxacin and Moxifloxacin both being fluoroquinolones, are in the TB drug pipeline in Phase III development. The fluoroquinolones, originally introduced in the 1980s, have a broad spectrum of activity, and offer a favorable pharmacokinetic profile for the treatment of TB [51, 52]. These antibiotics have been used for several years for other indications and have become part of the second-line regimen for the treatment of MDR-TB [53]. Fluroquinalones have good oral bioavailability and are distributed widely in the body.

Fluoroquinolones act by inhibiting mycobacterial DNA gyrase. Given the common target for all fluoroquinolones, Very few data indicate the prevalence of resistance to fluoroquinolones is low in North America reported for ciprofloxacin [54], but considerably higher incidences in South East Asia. The fluoroquinolones are cleared by the kidney and/or by the liver [55, 56].

Data published by the Tuberculosis Research Centre in Chennai, India on a clinical trial with ofloxacin containing regimens showed negative sputum culture for 92-98% of participants in two months compared to an expected rate of approximately 80% with a standard four-drug treatment [57]. Clinical trial results also have shown that fluoroquinolones have the potential to shorten the duration of tuberculosis treatment.

Recent data shows gatifloxacin and moxifloxacin have more potent activity against Mtb than the older members of this class, including ofloxacin [58]. *In-vitro* evaluation with model of persistent Mtb infection also found that moxifloxacin had the greatest sterilizing activity of the fluoroquinolones tested. Gatifloxacin and moxifloxacin are now being developed specifically for the treatment of TB, and have reached Phase III. These programs could lead to the first new class of drugs approved for the treatment of tuberculosis in over 30 years.

Gatifloxacin

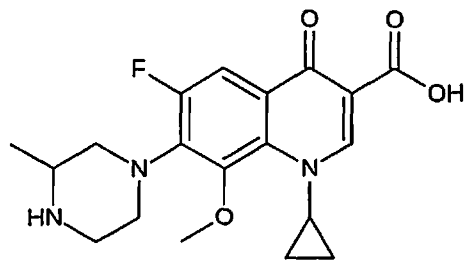

Gatifloxacin was approved in 1999 by the FDA for the treatment of pneumonia, bronchitis, uncomplicated gonorrhea, and various infections including those of the urinary tract, kidneys, and skin. Both *in-vivo* and *in-vitro* activity of gatifloxacin has shown bactericidal activity against Mtb [58-60]. In mice, gatifloxacin in combination with pyrazinamide and ethionamide, cleared the lungs of infected animals in two months [61].

The gatifloxacin clinical trial is conducted by the OFLOTUB consortium. OFLOTUB is a consortium of ten partners from Europe and Africa that was initiated in 2002 to undertake Phase II and Phase III trials to test the safety and efficacy of a gatifloxacin containing four month treatment regimen for the treatment of TB. It was established under the European Commission and is coordinated by the Institut de Recherche pour le Dévelopement (IRD) in Paris, France. It includes Phase II study conducted in Durban, South Africa, randomizing newly diagnosed patients to one of three fluoroquinolone containing regimens (ofloxacin, moxifloxacin, or gatifoxacin) in combination with isoniazid, rifampin, and pyrazinamide during the first two months of treatment called "Oflotub Phase II surrogate marker study". It was found that ethambutol substitution in standard therapy with either moxifloxacin or gatifloxacin killed Mtb significantly faster than the control or ofloxacin based regimens, supporting a potential for these fluoroquinolones to be able to reduce treatment duration by one, or possibly two months. The OFLOTUB consortium is continuing the evaluation of the gatifloxacin substituted regimen vs. standard six months treatment in Phase III design [62], which is a multicenter, open-label, randomized, controlled trial of four month gatifloxacin containing regimen vs. standard six month regimen for the treatment of adult, pulmonary TB [63]. This study is for testing the non-inferiority of a regimen of two months of gatifloxacin, isoniazid, rifampin and pyrazinamide followed by two months of gatifloxacin, isoniazid and rifampin vs. two months of ethambutol, isoniazid, rifampin and pyrazinamide followed by four months of rifampin and isoniazid, i.e. standard treatment guidelines. During the study percent of relapses at 24 months, time to relapse, patients cured in each arm by the end of treatment are evaluated. The post marketing surveillance activity indicated increased incidence of serious hypoglycemia and hyperglycemia in patients, especially the elderly and/or diabetic, receiving gatifloxacin. Due to which in February 2006, the FDA issued a specific warning [64], which has affected the phase III clinical trials of gatifloxacin. The study is continuing with stringent monitoring of glucose levels. To date, to the no dysglycemic events have been identified in the trial.

Moxifloxacin

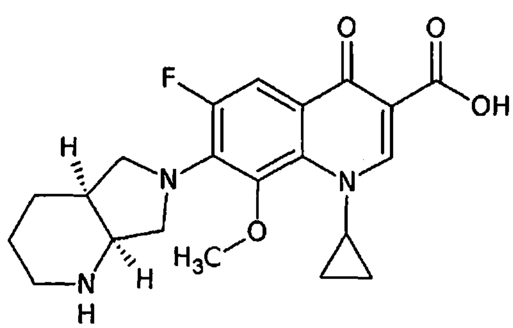

Moxifloxacin was first approved in 1999 by the FDA [65]. It is produced and marketed by Bayer Healthcare for the treatment of chronic bronchitis, acute bacterial sinusitis, community acquired pneumonia and uncomplicated skin and skin structure infections. Then in 2005, Bayer and the TB Alliance entered a partnership for global clinical development program to register moxifloxacin for a TB indication. Studies conducted at Johns Hopkins University in the mouse model, comparison of treatment with sparfloxacin, clinafloxacin, moxifloxacin or isoniazid; found that moxifloxacin had the greatest bactericidal activity [66, 67]. Another study involving the mouse model reflective of chemotherapy for human tuberculosis, the combination of moxifloxacin, rifampin, and pyrazinamide reduced the time needed to eradicate Mtb from the lungs of infected mice by two months when compared with the standard regimen of isoniazid, rifampin, and pyrazinamide. These findings suggest that this regimen has the potential to substantially shorten the duration of therapy needed to cure human tuberculosis [68]. The Phase II trial carried out by the US Centers for Disease Control and Prevention Tuberculosis Trial Consortium (CDC/ TBTC) is randomized HIV-positive and negative patients. Two standard regimens were given, either daily/ three times weekly and two analogous regimens in which moxifloxacin replaced ethambutol under double blind conditions. The study showed no significant difference between standard and moxifloxacin-based regimens in percent patients whose sputum converted to negative by eight weeks. The arm treated with moxifloxacin showed higher rates of sputum conversion after four and six weeks of therapy compared to the control arm, results consistent with the mouse model findings. The study demonstrated marked difference in the rates of two month culture conversion between African participants and North American participants (60% vs. 85% respectively. A similar Phase II study of a moxifloxacin substituted for ethambutol-based regimen is currently conducted by Johns Hopkins University in

Brazil. CDC/TBTC is currently conducting a multicenter, randomized, controlled, double-blind study to test the hypothesis, the replacement of INH with moxifloxacin in standard therapy during the intensive phase of treatment, would produce negative sputum culture in two months compared with the standard regimen.

Phase III trial is planned by the University College London in cooperation with the British Medical Research Council and with the support of the European and Developing Countries Clinical Trials Partnership (EDCTP) and the TB Alliance at a number of sites in Africa. This is double-blind, randomized, controlled, multi-center trial, called "Rapid Evaluation of Moxifloxacin in TB" (REMox TB) will test two different hypotheses: 1) two months of moxifloxacin, isoniazid, rifampin and pyrazinamide followed by two months of moxifloxacin, isoniazid and rifampin will be non-inferior to six months of standard therapy, and 2) two months of moxifloxacin, rifampin, pyrazinamide and ethambutol, followed by two months of moxifloxacin and rifampin will be non-inferior to six-months of standard therapy for newly-diagnosed, drug-sensitive, adult, pulmonary TB patients. By this study it could be made out whether moxifloxacin can be substituted to ethambutol and can the replacement reduce the treatment duration to two months.

Figure 5 and 6 presents the anti TB molecules in different clinical development phase stages and their mechanism of action.

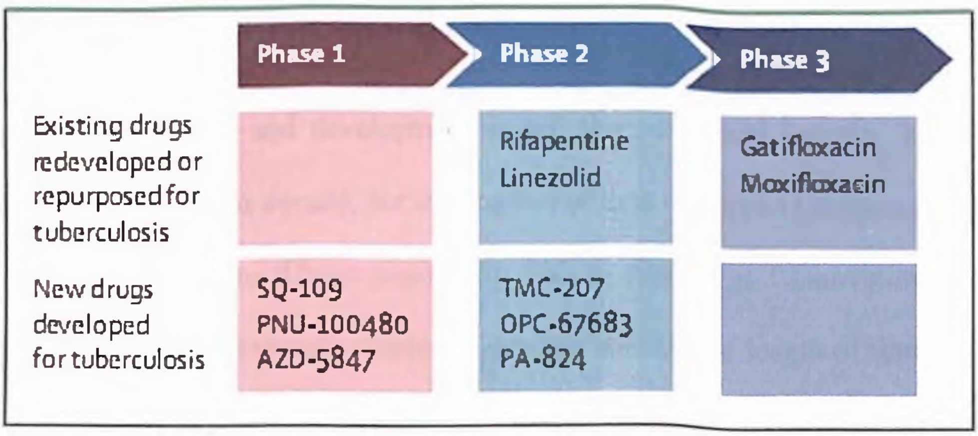

Figure 5: Compounds in clinical development for the treatment of active tuberculosis [14].

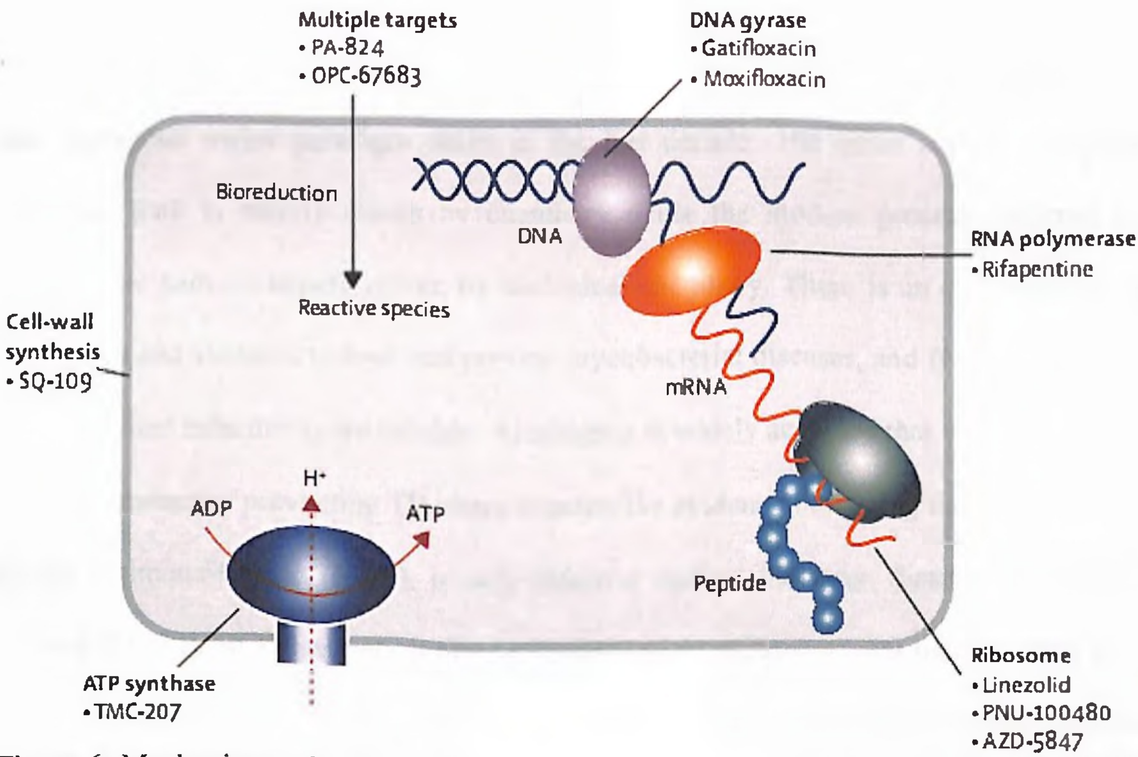

Figure 6: Mechanisms of action of new compounds in clinical development for tuberculosis [69].

2.3 New Approaches in Tuberculosis Drug Discovery

The cost of research and development in the pharmaceutical industry has been rising steeply and steadily in the last decade, but the amount of time required to bring a new product to market remains around ten to fifteen years [70]. This is labeled as "innovation gap," and it necessitates investment in inexpensive technologies that shorten the length of time spent in drug discovery. The success of a drug discovery program for combating infectious diseases rests on three major factors, viz. identification of key elements contributing to the pathogenicity of the microbe, an understanding of the interplay of responses between the host and the microbe and most importantly the properties of the candidate chemical compound. The drug discovery route has undergone major paradigm shifts in the last decade. The older version, the time tested empirical path is mainly driven by chemistry while the modern process, referred to as the mechanistic path, is largely driven by biological chemistry. There is an ever growing need for new drugs and vaccines to treat and prevent mycobacterial diseases, and for improved diagnostic tools to detect infection more reliably. Although it is widely accepted that vaccination is the most desirable means of preventing TB, there is extensive evidence indicating that the current vaccine, bacille Calmette-Guerin (BCG), is only effective against the rarer, disseminated forms of the disease [71, 72]. BCG has very limited efficacy against pulmonary TB that accounts for most of the disease burden [73] and has consistently failed to confer significant protection in developing countries despite inducing protective responses against leprosy in the same settings [74]. Ideally, antibacterial agents display bactericidal activity and target essential activities. One means of pinpointing such functions, which has never been applied to the tubercle bacillus, is to isolate and characterize mutants with conditionally lethal defects and then to screen for inhibitors capable of generating the same effect. Identification of new drugs can result from a rational, hypothesis driven approach inspired by genomics or from high-throughput screening of chemical or combinatorial libraries by a variety of automated methods.

2.3.1 Drug Targets identification and prioritization by genomic approach

The target identification stage is the first step in the drug discovery process and provides the foundation for years of dedicated research in the pharmaceutical industry. This stage of drug discovery is complicated by the fact that the identified drug target must satisfy a variety of criteria to permit progression to the next stage. Important factors include least homology between target and host to prevent host toxicity; activity of the target in the diseased state; and the essentiality of the target to the pathogen's growth and survival. Traditional prioritization approaches are purely by literature searches and mental integration of multiple criteria, which are becoming overwhelming for the researchers. A more effective alternative is computational integration over different criteria to create a ranking function. AssessDrugTarget is a new application that aims to rapidly prioritize potential drug targets in a genome [75]. The need to quickly identify new targets responsible for persistence and against growing organisms has been need of the time. By taking advantage of experiments published on the Mtb genome, comparative genomic data, and other structured data scoring schemes implemented for prioritizing new drug targets. The prioritized targets can be then validated by constructing a knockout or using chemical validation. To prioritize drug targets in TB by the three sets of criteria listed.

Metabolic drug target criterion. The top-prioritized target genes must be responsible for unique, growth essential roles in the TB metabolome. The ranking is further prioritized by lack of homology to the human host and members of the host gut flora, intended to minimize the chances of undesirable host-drug interactions.

Mtb specific drug target criterion. The prioritized targets must (i) represent growth-essential genes and (ii) share close homologs within the Actinobacteria class, but (iii) lack a close homolog in the host and host gut flora. The metabolic pathways of these targets need not be mapped, as required in the metabolic drug target criterion.

Persistence drug target criterion. The prioritized targets must play a role in the maintenance of the dormancy phase. For this the expression profiles of a few targets that have been implicated.

AssessDrugTarget provides a simple framework for integrating the vast amount of biological data that can be used in the drug target identification stage. The software can be extended to include scoring patterns for any kind of structured biological data. The weights given to each criterion can be set by an expert user or determined using a genetic algorithm if example targets are available. Out of two growth essentiality datasets, one was correctly identified 90% of studied active TB targets, whereas the other was 55% accurate in this respect. The chokepoint criterions of unique enzyme commission assignments are more useful for predicting Mtb targets. Predicting distinct structure based features, such as Pfam scores, are useful for prioritizing targets when sequence homology to a host protein is relatively high. Table 4 lists the properties observed for the studied targets and the contributions of individual features to the ranking of these targets.

homology to the human host and members of the host gut flora, intended to minimize the chances of undesirable host-drug interactions.

Mtb specific drug target criterion. The prioritized targets must (i) represent growth-essential genes and (ii) share close homologs within the Actinobacteria class, but (iii) lack a close homolog in the host and host gut flora. The metabolic pathways of these targets need not be mapped, as required in the metabolic drug target criterion.

Persistence drug target criterion. The prioritized targets must play a role in the maintenance of the dormancy phase. For this the expression profiles of a few targets that have been implicated.

AssessDrugTarget provides a simple framework for integrating the vast amount of biological data that can be used in the drug target identification stage. The software can be extended to include scoring patterns for any kind of structured biological data. The weights given to each criterion can be set by an expert user or determined using a genetic algorithm if example targets are available. Out of two growth essentiality datasets, one was correctly identified 90% of studied active TB targets, whereas the other was 55% accurate in this respect. The chokepoint criterions of unique enzyme commission assignments are more useful for predicting Mtb targets. Predicting distinct structure based features, such as Pfam scores, are useful for prioritizing targets when sequence homology to a host protein is relatively high. Table 4 lists the properties observed for the studied targets and the contributions of individual features to the ranking of these targets.

Table 4: Ranks of Studied Targets in Three Prioritized Lists

Target Status	Drug	Gene Name	Disrupted Mechanism	Metabolic Rank	Actinobacteria-Specific Rank	Optimized Persistence Rank
Current	Pyrazinamide[a]	—	M/P	—	—	—
	Rifampicin[a]	*rpoB*	R/P	1,759	2,762	1,604
	Ethambutol[a,b]	*embC*	C	554	219	3,626
		embA	C	2,115	628	3,893
		embB	C	678	321	3,908
	Streptomycin[a]	*rpsL*	T	1103	2,990	997
	INH[a,b]	*inhA*	C	231	2,679	2,915
	Quinolones[c]	*gyrA*	D	424	2,586	3,110
	Quinolones[c]	*gyrB*	D	65	1,569	1,706
	Ethionamide[b,c]	*inhA*	C	1.850	1,029	2,788
	D-cycloserine[c]	*alr*	C	6	282	1,519
		ddlA	C	350	550	1,558
Candidate	Epiroprim	*dfrA*	V	20	3,582	2,009
	Trimethoprim	*folP1*	V	1	596	809
	6-azido-6-deoxytrehalose	*fbpC*	C	2,995	1,412	521
		fbpB	C	1,850	1,029	2,788
		fbpD	C	116	220	3,134
		fbpA	C	1,516	549	2,131
	Azole drugs	*cyp51*	C	255	2,397	189
		cyp121	C	3,716	3,844	3,903
	BB-3497	*def*	T	360	521	2,469
	Diarylquinoline: R207910	*atpE*	E	1,910	2,655	3,867
Proposed		*icl*	P	593	481	77
		pcaA	C/P	2,622	1,827	1,116
		relA	P	2,851	3,077	2,868
		devR	P	955	880	108
		devS	P	46	724	173
	Alpha-difluoromethyl ornithine compounds based on similarity to *T. brucei* active site	*lysA*	A	3	927	1.835
		panD	V	3,164	3,081	1,733
		panC	V	283	2,006	2,507
		glnE	A	436	176	2,519
	Methionine sulphoximine (affects only membrane-bound target)	*glnA1*	A	742	1,376	1,602
		aroK	A	172	1,394	2,863
		glf	C	111	367	685
		ideR	V/P	510	391	11
		ompA	C/M	2.295	2,668	1,515
		mshC	D	599	2,088	2,031

Targets are ranked out of 4,000: Mtb genome; 4,000 genes; a First-line drug; b Current TB-specific drug; c Second-line drug; A, amino acid biosynthesis; C, cell wall biosynthesis; D, transcription; E, energy molecule biosynthesis; M, membrane integrity/energy production; P, persistence; R, RNA synthesis; T, translation; V, vitamin/co-factor biosynthesis/acquisition.

3.3.2 Structural genomics approach to drug discovery

Structural genomics is a route to understanding microbial organisms at a molecular level. Structural genomics refers to large scale efforts to determine as many of the unique structures of proteins in an organism as possible, primarily through X-ray crystallography. Structural genomics was born from advances in technology that made high throughput structure determination possible. With the advent of high intensity beam lines at synchrotrons and new phasing techniques, along with more powerful computational algorithms for data processing, refinement and model building [76-79] high resolution structures can be solved more systematically, faster, within few days of obtaining crystals. Coupling of new methods for expression, purification, and crystallization [80], efficiently result in a high throughput pipeline can solving the structures of many targets in a rapid and automated way.

The Tuberculosis Structural Genomics Consortium (TBSGC) was established in 2000, with centralized core facilities serving over 100 collaborating research labs around the world [81]. The TBSGC has applied the concept of a high throughput pipeline to determining the structures of functionally important proteins [82, 83] to improve our understanding of metabolic pathways, and ultimately to facilitate the drug discovery process. To date 118 of Mtb crystal structures of 257 determined and deposited in the Protein Data Bank (PDB) were contributed by TBSGC members. In some cases, structure determination has also revealed mistakes in annotation [84, 85].

Given that the mission of the TBSGC is based on defining the structures of new drug targets, targeting is not as straightforward a process as with other structural genomics programs. In the TBSGC, the method used is based on bioinformatics approach, by combining as much relevant data as possible to prioritize targets in terms of the likelihood that they will be good drug targets. This approach takes into account all available data on drug ability, enzyme pathway analysis, essentiality, and gene expression under different models of persistence to identify genes whose inhibition might lead to bacterial cell death. An interactive web service called Target Explorer has been implemented to allow investigators to experiment with dynamically adapting the weighting of different criteria, including multiple DNA micro-array datasets, for selecting preferred targets for structure determination. This is one of several informatics tools provided on the Consortium web site for information sharing, http://webtb.org.

2.3.3 Computational approaches and cheminformatics tools for drug discovery

Cheminformatics methods, occupy an important place in the pharmaceutical industry drug discovery workflow. These computational approaches manage, mine and/or simulate complex systems or processes, related to chemical, genomic, proteomic or clinical data. Ligand and protein based methods, for example, have been used for the virtual screening of compound libraries as a complement to high throughput screening *in-vitro* [86]. Integration of these methods guide the selection of compounds for *in-vitro* screens, and identifying new compounds as antitubercular hits or leads.

Databases for TB

Over 300 000 compounds are screened against Mtb in one laboratory alone. It is likely that several million compounds have been examined cumulatively to date by all groups. Recently a central location for these screening results has been developed. This has prevented repetition of screening by different groups, while also allowing large scale analysis of molecular properties of compounds with antitubercular whole cell activity [87]. Below is range of some of the major databases for TB from diverse areas such as genome databases to databases of active compounds,

BioHealthBase [88] is now incorporated into PATRIC (http://patricbrc.vbi.vt.edu/portal/portal/-patric/IncumbentBRCs?page=bhb) and includes rapid annotation using subsystem technology annotations for approximately 1850 of the 2000 complete bacterial genomes including Mtb. The website provides a genome browser, protein family sorter, metabolic pathways (using KEGG pathway maps), phylogenetic trees, pathway and BLAST searches, feature cart, PubMed integration and Google search.

The Collaborative Drug Discovery Tuberculosis Database (CDD TB, www.collaborativedrug .com) [89] software (Collaborative Drug Discovery Inc. Burlingame, CA) is focused on small molecule libraries of compounds tested against Mtb. CDD have collated over 15 public datasets on Mtb specific datasets representing well over 300000 compounds derived from patents, literature, and high-throughput screening data shared by academic and pharmaceutical laboratories. In addition, this web based database system can facilitate storing and sharing of private data. The CDD database has been used to find compounds with molecular similarity to known Mtb drugs and to build novel computational machine learning and pharmacophore models to rapidly identify potential inhibitors. To date, CDD, with funding from the Bill and Melinda Gates Foundation (BMGF), has developed a unique community with over 20 pilot groups in the TB field, including groups in the EU funded New Medicines 4 Tuberculosis (NM4TB) initiative [90] and groups funded by the BMGF Tuberculosis accelerator project.

GenoMycDB [91] is a database for the large scale comparative analyses of completely sequenced mycobacterial genomes (http://157.86.176.108/catanho/genomycdb/). It provides tools for functional classification and analysis of genome structure organization and evolution.

Tbrowse [92] is a resource for the integrative analysis of the TB genome, a genome browser across various online resources and datasets with over half a million data points (http://tbbrowse.osdd.-net) and is a part of the Open Source Drug Discovery Initiative (http://www.osdd.net/).

TDR targets database (http://tdrtargets.org) brings together genome sequencing and functional genomics projects, protein structural data, etc. [93]. Key features include computational assessment of target druggability and integration of large scale screening data with manually curated data, enabling the assembly of candidate targets to pursue.

Tuberculosis Drug Resistance Mutation Database [94] is a database listing mutations associated with TB drug resistance and the frequency of the most common mutations associated with resistance to specific drugs (http://www.tbdreamdb.com/).

TubercuList is widely recognized as the premier database for TB researchers. The TubercuList server [95] (http://genolist.pasteur.fr/TubercuList/help/about.html) represents a database focused on the analysis of the Mtb genomes and on collating and integrating various aspects of the genomic information. TubercuList provides a complete dataset of DNA and protein sequences derived from Mtb H37Rv, linked to annotations and functional assignments.

The Tuberculosis Database (TBDB [96] http://www.tbdb.org/) provides genomic data (for 28 annotated genomes) and resources including several thousand microarray datasets from *in-vitro* experiments and Mtb infected tissues. Researchers can freely deposit data before publication, browse gene detail pages, and perform genome visualization and comparative analysis using the genome map tool, the genomes synteny map or operon map browser.

WebTB.org is provided by the TB structural genomics consortium [97]. It contains tools to search and browse the TB genome, structure summary pages on all known TB proteins, the MTBreg database of proteins upregulated or downregulated in TB, top 100 persistence targets in TB and many more tools.

An integrated analysis of metabolic pathways, small molecule screening and structural databases would facilitate antiTB screening efficiency which is towards more of utilization system biology and computer aided drug discovery approach. System Bilogy is his is cross disciplinary field that endeavors to comprehend how the molecular components of life function together to create complex biological systems. It is usually represented by computational integration of very large quantities of genomic, proteomic and metabolomic information captured from underlying preexisting databases. A wide spectrum of approaches to systems modeling exists including: (i) statistical analysis of large datasets, (ii) models of system kinetics, (iii) flux balance techniques, (iv) evolutionary models of drug resistance, and (v) symbolic models of processes. Below are few system biology databases,

BioCyc, MetaCyc (SRI) [98, 99]: BioCyc (http://biocyc.org/MTBRV/)isa database collection together with a suite of tools supporting the generation of pathways and querying of them. The BioCyc database consists of organism specific Pathway/Genome Databases (PGDBs), including tier 2 (derived computationally using the PathoLogic program, and partially curated) PGDBs for two strains of Mtb, both virulent and drug susceptible, namely CDC1551 and H37Rv. The

PGDBs for Mtb are being adopted by the Tuberculosis Database (TBDB) consortium (www.tbdb.org). This is expected to lead to more frequent updates reflecting the latest knowledge. The BioCyc collection also includes MetaCyc, a database of non-redundant, experimentally elucidated metabolic pathways curated from the experimental literature. MetaCyc (http://metacyc.org/) contains more than 1200 pathways from more than 1600 different organisms. A PGDB describes the genome of an organism and the product of each gene; its metabolic network/pathways, reactions, enzymes, metabolites and transporter complement; and the genetic network of the organism, including its operons, transcription factors and the interactions between transcription factors and their small molecule ligands and DNA binding sites. The BioCyc Pathway Tools suite has three components. PathoLogic is used to create a new PGDB containing the predicted metabolic pathways of an organism, given an annotated genome (e.g. a GenBank entry and MetaCyc) as input. PathoLogic can predict metabolic pathways, genes coding for missing enzymes in metabolic pathways and operons. The Pathway/Genome Navigator supports query, visualization and analysis of PGDBs. The Pathway/Genome Editors also allow interactive editing of PGDBs. In addition, there is a computational interface to facilitate integration with external analysis tools such as the Pathway Tools Omics Viewer [101].

KEGG [102] is a major academic resource consisting of 16 databases covering genomic and chemical information and is a widely used reference resource (http://www.genome.jp/kegg/) valuable for linking compounds and metabolites to biological pathways.

LipidMaps [103] LIPID Metabolites And Pathways Strategy (LIPID MAPS) (http://www.lipid-maps.org/data/structure/LMSDSearch.php?Mode=SetupTextOntologySearch) was created in

2003 to identify and quantify all of the major and many minor lipid species in mammalian cells and the changes in these species in response to perturbation.

One example of utilization of TB systems biology research is gene expression data to identify stress response networks across the biological pathways before and after treatment with different drugs [103]. It was found that gene expression networks for isoniazid treatment indicated a generic stress response. This type of approach could create an expression signature related to the drug used from which the mechanism of action can be easily established. A chemical systems biology approach can compare binding sites for known drugs and identified off targets with similar binding sites, which can be used as starting drug discovery.

Computational cheminformatic tools

These methods have been generally used by specialists focused on a single target or series of compounds, and rarely in combination with other computational tools.

Quantitative structure–activity relation and molecular properties analysis

An analog is a molecule whose structure is related to that of another molecule but whose chemical and biological properties may be quite different. Analog based drug discovery is the process of predicting promising ligands with a set of analog, which have information active and inactive. It can be approached by the following ways, pharmacophore analysis and structure activity relationships e.g. Catalyst and 3D QSAR. Considerable success has been achieved in the development of new drugs based on the leads provided by established drugs. Ligand based approaches towards TB drug discovery have used similar strategies. Once a model is generated using the appropriate (usually commercial) software, testing is typically carried out by leaving out one or more groups of compounds at random. These models help to optimize activity for a specific target or starting hit or lead (Table 5). Several analyses have been used on large datasets of active and inactive compounds already reported with Mtb activity to calculate molecular descriptors or properties, and analyzed for differences between active and inactive compounds. Lipinski's 'Rule of Five'[104] as a method for selecting 'drug-like' compounds, hardly could be followed for identifying the Mtb inhibitors because of the complexity involved with organism specially the highly lipophilic cell wall. A known 112 anti TB compounds [105] when filtered with the Rule of Five, 40 (35.7%) failed, including the known clinical candidates OPC-67683 and TMC-207, because of their lipophilicity and molecular weight. Analysis of several datasets representing many active compounds suggested that the mean value for various simple molecular descriptors, such as polar surface area (PSA), is significantly different from that of FDA approved drugs. This analysis followed studies on molecular property values for antibiotics in general [106], including those that have evaluated logP and molecular mass [107], as well as earlier studies on anti TB compounds [108]. Generally, FDA approved TB drugs are more similar to inhaled drugs [molecular weight mean 370, PSA 89.2 $A^{\circ 2}$, logP of the compound (clogP) 1.7] [109].

Table 5: Descriptor based QSAR studies

Compound types	Number of molecules in training set	Number of descriptors used	Algorithm used and testing	Refs
Pyrazinoate esters	32	43	Genetic function approximation models. clogP was a key descriptor, and the model was tested with 11 external compounds	[110]
N-benzylsalicyl-thioamides	29	177	Two MLR models for TB with the STATOO program. clogP was a key descriptor, and there was no external	[111]

			testing	
Ring-substituted-2/4-quinolinecarbaldehyde derivatives	24		PCA[a] analysis, inclusion of logP did not improve model statistics. Actives appeared clustered in a small region of PCA plot	[112]
5-Aryl-2-thiol-3,4-oxadiazoles	41	Topological descriptors	Neural networks (q^2=0.8), not tested externally	[113]
Hydrazides	173	Abraham's descriptors, electronic, geometrical or steric descriptors	MLRb subsets were used for modeling. Hydrophobicity could not explain the biological response. For small subsets there were good correlations with test sets (R2 > 0.77)	[114]
Isoniazid derivatives	91	HQSAR[c] and Dragon descriptors	HQSAR and generated a test set (R2 =0.87) for 24 compounds. The results were better than for PLS-QSARd with 2D descriptors from Dragon (R2 =0.72)	[115]
Chalcones and flavonoids	9-33	48	Genetic function approximation, internally cross validated (q2=0.79–0.94)	[116]

[a]PCA, principal component analysis; [b]MLR, multiple linear regression; [c]HQSAR, hologram quantitative structure–activity relation; [d]PLS-QSAR, partial least squares quantitative structure–activity relation.

Comparative molecular field analysis and 3D-QSAR

An understanding of multiple molecular binding conformations binding to the same target provides useful information which can aid drug design. By super imposing these binding conformation molecular fields can be generate fields around the molecules and molecular descriptors, based on conformation or a representation of a molecular feature that can then be related to bioactivity, termed 3D-QSAR. 3D-QSARmodels (Table 6) have been generated from 21 to 100 molecules for structurally related compounds. In most cases studies contained <10 to <30 external testing compounds have generally good results. These models have rarely been used for other than data explanation but also with few virtual screening studies. There are very few examples of global models generated using these methods [117], although other pharmacophore methods are generally alignment independent and can be used for rapid database searching. Limitations of 3D-QSAR methods include the dependency on the molecule conformation, force fields and the active compounds selected to build the model.

Table 6: CoMFA and other 3D-QSAR models

Compound types	**Number of molecules in training set**	**Algorithm used**	**Statistics**	**Refs**
1,4-Dihydropyridines	35	CoMFA and CoMSIA[a]	Cross validated (R^2 of 0.56 and 0.62) and external validation (R^2 0.74 and 0.69)	[118]
Diaryloxymethano-phenanthrene derivatives	37	CoMFA and CoMSIA	CoMFA (q^2=0.625) and CoMSIA (q^2 =0.486) models and seven compound external test set with very good predictive value	[119]
Deoxythymidine monophosphate derivatives that inhibit thymidine monophosphate kinase	36	Molecular field analysis	Alignments performed with least squares (predictive R^2 =0.70), pharmacophore (0.56) or docked conformations (0.72). Receptor based alignment performed best	[120]
Nitrofuranyl derivatives	95	CoMFA and CoMSIA	ested with a set of 15 molecules. CoMFA (R^2 =0.78) outperformed CoMSIA. cLogP and polar surface area or steric bulk did not improve the models	[121]
4-Adamantan-1-yl-quinoline-2-carboxylic acid alkylidene hydrazides	30	CoMFA and CoMSIA	Models tested with 14 molecules CoMFA (R^2 0.49) and CoMSIA (R^2 0.49)	[122]
Ring-substituted quinolines	70	CoMFA and CoMSIA	Tested with 24 molecules. The CoMFA model (R^2 =0.42). 18 molecules were suggested for synthesis based on the CoMFA predictions.	[123]

Nitroimidazoles	21	Catalyst pharmacophore	Tested with 22 molecules. No test set correlation value reported, but correlation looked similar to the training set (R=0.96)	[124]
1,5-Diarylpyrrole derivatives		Catalyst pharmacophore	Had difficulty predicting N-methylpiperazine and thiomorpholine derivatives. No numerical prediction data were presented.	[125]

[a]CoMSIA, comparative molecular similarity indices analysis

Pharmacophore Based Drug Design

Perceiving a pharmacophore is the most important first step towards understanding the interaction between a receptor and a ligand. In the early 1900s, Paul Ehrilich offered the first definition for a pharmacophore, "molecular framework that carries (phoros) the essential features responsible for a drug's (pharmacon) biological activity" The current widely used definition was presented by Peter Gund in 1977, "a set of structural features in a molecule that is recognized at a receptor site and is responsible for that molecule's biological activity". A pharmacophore is a representation of generalized molecular features including 3 dimensional (3D) (hydrophobic groups, charged/ionizable groups, hydrogen bond donors/acceptors), 2D (substructures), and 1D (physical or biological properties) that may be essential for important binding interactions with a receptor in turn are considered to be responsible for a desired biological activity. In the absence of any knowledge of the 3D structure of a receptor, pharmacophores may provide such important information in the drug design process. The pharmacophores may be used in several ways, as a 3D query in searching 3D databases containing "drug like" small organic molecules to identify active and specific inhibitors or in evaluating a new compound for mapping on a known pharmacophore. This approach is powerful and found wide applications in drug design. The hypothesis generation methods (HipHop and HypoGen) of the Catalyst software, Phase from Schrodinger, have been successfully used in drug discovery research.

Docking, virtual screening and hybrid approaches

Docking is tool that can positively affect ligand or inhibitor design. Despite potential weaknesses from under sampling poses and the methods of calculating energetics through a scoring function, docking as a form of virtual screening has proved to be a useful tool outside the TB field [134]. Analysis of recent publications indicated that docking has been extensively used to identify small molecules with potency against a given Mtb target to find hits. Docking has also been used as integrated part of virtual screening processes, which can represent a complementary technology to biochemical high throughput screening. Many reports use docking methods preceded by some form of computational filtering of screening libraries using pharmacophores or QSAR models (Table 7).

Table 7: Hybrid methods combining docking and QSAR or pharmacophore methods

Method	**Results**	**Refs**
Homology models of DevR and pharmacophore used to screen 2.5million compounds, followed by docking with MOE and Gold	Resulted in 11 compounds screened and 4 hits including a phenylcoumarin derivative.	[126]
37 enoyl acyl carrier protein reductase carboxamide inhibitors were used to build CoMFA model (tested with 10 compounds R^2 =0.88) followed by the de-novo molecule design software LEAPFROG.	Suggested 13 molecules with improved binding energy values; however, these have not been synthesized or tested.	[127]
29 enoyl acyl carrier protein reductase arylamide inhibitors were used to build CoMFA and CoMSIA models (tested with eight molecules $R^2 > 0.87$). A pharmacophore was also used to screen the Maybridge database to retrieve 996 hits, which	The CoMFA and CoMSIA scores were used to suggest 20 molecules for future testing.	[128]

were then docked with FlexX.		
Docking and pharmacophore approach used to suggest type II dehydroquinase inhibitors, starting from 45 published inhibitors used to test docking approach and generate GAMLR QSAR model (35 train, ten test) using MOE QuaSAR Evolution (q^2 test and train > 0.95). The most active was used for FlexX pharmacophore generation. Also looked at interaction fingerprints.	Predicted 42 active compounds. No test data.	[129]
Combined experimental and computational approach with 12 new imidazoles and triazole derivatives using AUTODOCK to dock molecules in sterol 14a-demethylase followed by free energy of binding calculations	Good agreement between calculated DGbind and experimental data for MIC.	[130]
Thirty 5'-thiourea-substituted a thymidines analogues used to develop receptor independent 4D-QSAR models (q^2 =0.83) for thymidine monophosphate kinase inhibitors. The model was also put into the context of reported crystallographically characterized inhibitor-enzyme interactions	The model was tested with four compounds and three were predicted within the SD of the assay. Activity also increased with logP.	[131]
31 5'-O-[N–[(salicyl)sulfamoyl]adenosine inhibitors of MbtA (a salicyl AMP ligase) used with molecular dynamics simulations in a homology model to calculate linear interaction energy (R^2 =0.70).	A single validation molecule was predicted with the LIE models to have a Ki of 1.6 nmol/l and the actual value was 0.7 nmol/l.	[132]
Docking and molecular dynamics were used to study the binding of the isoniazid metabolite INH-NAD to the enoyl-acyl carrier protein reductase.	Suggested the role of a water molecule in binding. The modeling supported the role of KatG before InhA binding	[133]
FlexX and GOLDwere used to virtually screen the Chembridge and NCI databases (covering over half a million compounds) against the ATP phosphoribosyl transferase (HisG). Filtering for drug-likeness also used.	Fifty compounds were tested *in-vitro.* and seven were active at 10 μmol/l. Nitrobenzothiazoles were identified as active and co-crystallized, and 19 follow up compounds found in the ChemBridge database (two of which showed inhibition in the target and whole cell assays).	[134]
UNITY pharmacophore, FlexX docking and structure interaction fingerprint approaches were	Ten compounds were ultimately selected and five showed MIC < 12.5 μg/ml in	[135]

were then docked with FlexX.		
Docking and pharmacophore approach used to suggest type II dehydroquinase inhibitors, starting from 45 published inhibitors used to test docking approach and generate GAMLR QSAR model (35 train, ten test) using MOE QuaSAR Evolution (q^2 test and train > 0.95). The most active was used for FlexX pharmacophore generation. Also looked at interaction fingerprints.	Predicted 42 active compounds. No test data.	[129]
Combined experimental and computational approach with 12 new imidazoles and triazole derivatives using AUTODOCK to dock molecules in sterol 14a-demethylase followed by free energy of binding calculations	Good agreement between calculated DGbind and experimental data for MIC.	[130]
Thirty 5'-thiourea-substituted a thymidines analogues used to develop receptor independent 4D-QSAR models (q^2 =0.83) for thymidine monophosphate kinase inhibitors. The model was also put into the context of reported crystallographically characterized inhibitor-enzyme interactions	The model was tested with four compounds and three were predicted within the SD of the assay. Activity also increased with logP.	[131]
31 5'-O-[N–[(salicyl)sulfamoyl]adenosine inhibitors of MbtA (a salicyl AMP ligase) used with molecular dynamics simulations in a homology model to calculate linear interaction energy (R^2 =0.70).	A single validation molecule was predicted with the LIE models to have a Ki of 1.6 nmol/l and the actual value was 0.7 nmol/l.	[132]
Docking and molecular dynamics were used to study the binding of the isoniazid metabolite INH-NAD to the enoyl-acyl carrier protein reductase.	Suggested the role of a water molecule in binding. The modeling supported the role of KatG before InhA binding	[133]
FlexX and GOLDwere used to virtually screen the Chembridge and NCI databases (covering over half a million compounds) against the ATP phosphoribosyl transferase (HisG). Filtering for drug-likeness also used.	Fifty compounds were tested *in-vitro.* and seven were active at 10 µmol/l. Nitrobenzothiazoles were identified as active and co-crystallized, and 19 follow up compounds found in the ChemBridge database (two of which showed inhibition in the target and whole cell assays).	[134]
UNITY pharmacophore, FlexX docking and structure interaction fingerprint approaches were	Ten compounds were ultimately selected and five showed MIC < 12.5 µg/ml in	[135]

used to identify compounds in the Maybridge database (59,275 compounds) as potential thymidine monophosphate kinase inhibitors.	whole-cell assays with no cytotoxicity, although the binding of these compounds to enzyme remain to be demonstrated.	
CDOCKER used to dock tripeptides into the TB dihydrofolate reductase crystal structure. Molecular dynamics simulation was also performed.	WYY was predicted as potent and selective versus human DHFR. This prediction has yet to be verified.	[136]
FlexX used for docking a library of over 19 000 Vichem compounds and Tripos Lead quest compounds into NAD synthetase PknB.	Nine sub-micromolar inhibitors were found. Additional further docking for NAD kinase inhibitors found that 22 showed activity versus NAD synthetase and one against NAD kinase, out of 100 compounds tested	[137]
Catalyst Hypogen pharmacophore and GOLD docking were used to develop the composite model for screening potential thymidine monophosphate kinase inhibitors.	Screened an in-house database of 500 000 compounds, subsequently providing 186 virtual hits that do not appear to have been tested *in-vitro*.	[138]
ICM and DOCK were used to virtually screen the University of California, Irvine, ChemDB database and NCI databases to identify AccD5 inhibitors.	One ligand NCI-65828 was found to inhibit AccD5 (an essential acyl-CoA carboxylase carboxyl-transferase domain) competitively with an experimental K of 13.1 μM.	[139]
AutoDock used for docking inhibitors to MshB (a lcNAc-Ins deacetylase)	Docking used to explain mode of binding for inhibitors only	[140]
AutoDock and GOLD were used to find inhibitors for the adenylation domain of theNAD+ dependent ligase with bound AMP (LigA).	A novel class of inhibitors, glycosyl ureides, were identified to compete with the NAD+. 5 compounds with docking scores were tested *in-vitro* versus LigA, no assessment of correlation.	[141]

DevR, dormancy regulon; MOE, molecular operating environment; DHFR, dihydrofolate reductase; AccD5, acyl-CoA carboxylases domain 5; GA-MLR, genetic algorithm-multiple linear regression; KatG, catalase-peroxidase-peroxynitritase; WYY, H-tryptophan-tyrosine-tyrosine-OH.

These hybrid methods have validated the pharmacophore or QSAR model, with thymidine analogs as inhibitors of thymidine monophosphate kinase (TMPK) [142]. In another case of search for InhA inhibitors, a 3D-QSAR derived pharmacophore model was used to narrow down a set of 230000 compounds to 299 hits and ultimately to 30 compounds [143]. The predicted IC_{50} values were similar to the experimental values, although some of the molecules showed deviations. Another study of TMPK inhibitors used a 3D-pharmacophore model derived from four X-ray structures of the enzyme with bound substrate or three inhibitors to screen a 60000 compound vendor library [144]. Five of the eight virtual hits demonstrated whole-cell efficacy versus Mtb. A commercially available library of small molecules, chemically similar to the substrate, the product or the known inhibitor L-methionine-(S)-sulfoximine, was virtually screened with scoring via a rigid pharmacophore model. After visual inspection, four of the 29 virtual hits had IC_{50} values close to 1mmol/l, which are very weak hits, but they facilitated design of a 15 member analog library as a starting point for future efforts.

The docking studies used crystallographically characterized Mtb enzyme, in other instances homology model based on a closely related protein been used, when a crystal structure is unavailable e.g. work with UDP-N-acetylenolpyruvoylglucosamine reductase (MurB) [145] and fatty-acyl-coenzyme (Co)A synthetase (FadD13) [146], which are involved in the biosynthesis of peptidoglycan and fatty acids, respectively. These efforts are dependent on the quality of the homology model and the extent of similarity to the starting protein. Docking has also been used to investigate the metabolism of promising antitubercular small molecules. For example, Manina et al. studied the bioreduction of a nitro moiety in the BTZ043 family of inhibitors, which appears to target mycobacterial arabinogalactan and lipoarabinomannan polysaccharide biosynthesis [147]. Docking suggested potential BTZ043-*M.smegmatis* FMN dependent nitroreductase NfnB interactions and proposed modifications to the BTZ043 scaffold to avoid metabolism via NfnB and other nitroreductases. Docking, virtual screening and hybrid approaches have resulted in some promising results and yet, as discussed below, these methods and strategies require further significant refinements to be able to deliver on the promise of novel antitubercular therapeutics.

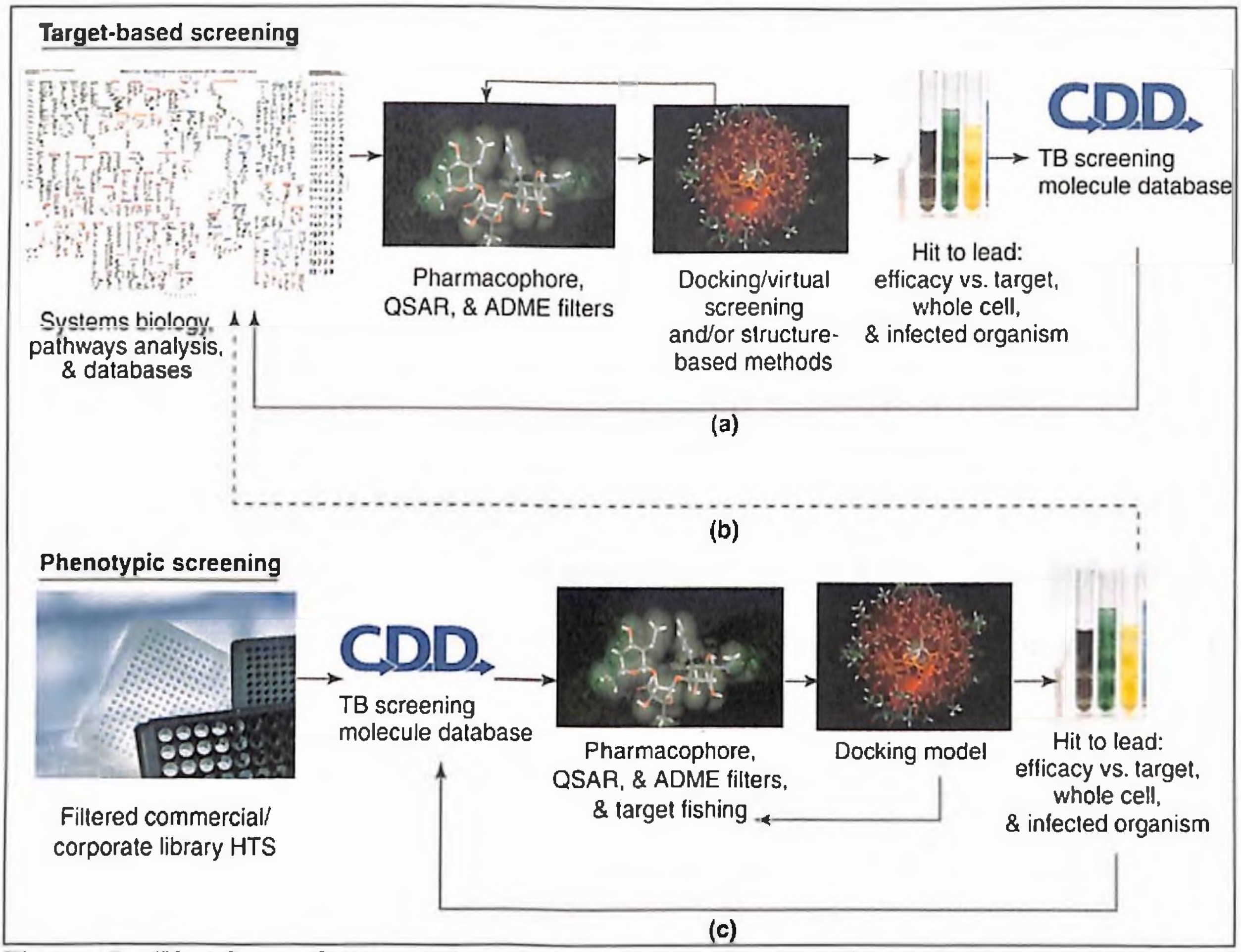

Figure 7. Workflows for target-based and phenotypic screening using several integrated computational components. Illustration of target based screening to find new compounds that inhibit an enzyme or protein–protein interaction using tightly integrated computational methods, followed by optimization and feedback of data to databases and pathways. Phenotypic screening data are used with integrated computational methods to suggest potential targets and optimize ADME properties in parallel, and then verify *in-vitro*. Target-based screening computational methods might include identification of target family interaction motifs; filtering and prioritization of compound source pools; design or selection for final screening collection; diversity, similarity and coverage calculation; and 2D or 3D descriptors (pharmacophore, shape or chemical substructure). Target-based screening could use structure-based methods, which could incorporate the following computational methods: 2D and 3D descriptor and pharmacophore based activity models; binding site assessment and mapping; ligand docking or virtual library screening; protein homology modeling; and fragment-based drug discovery. In both target-based screening and phenotypic screening, hit to lead screening data analysis and follow up might require computational tools for: 'hit picking' and filtering, clustering and

prioritizing; isostere selection; identifying structure–activity relationship trends; and calculating chemical substructures and properties, for example 2D or 3D descriptors. Phenotypic screening might require computational methods for hit explosion (such as the creation of a pharmacophore or by similarity searching in commercial data bases) and target fishing [13] to identify the target for a hit. Lead optimization requires the use of computational methods for identifying, tracking and optimizing structure–activity relations and ADME trends within data sets. (a) For chemical probe selection, a search is made new compounds that inhibit a target using tightly integrated computational methods, then the data are optimized and fed back to databases and pathways. (b) When a target is identified, the target based screening workflow can be pursued. (c) Phenotypic data are used with integrated computational methods to suggest potential target(s) and optimize ADME properties in parallel, then verify *in-vitro*. [148]

2.4 Discovery Phase

A New Chemical Class Addressing a Known Target: Pleuromutilins

These are novel class of compounds which inhibit bacterial protein synthesis. These have been reported to be active against a variety of pathogenic bacteria [149]. Pleuromutilins interact with the bacterial ribosome that is with 50S subunit [150]. Its exact mechanism in Mtb is not yet established. The resistance to pleuromutilins emerges slowly in a stepwise fashion [31]. The development to the resistance could be reduced by using them in combination therapy.

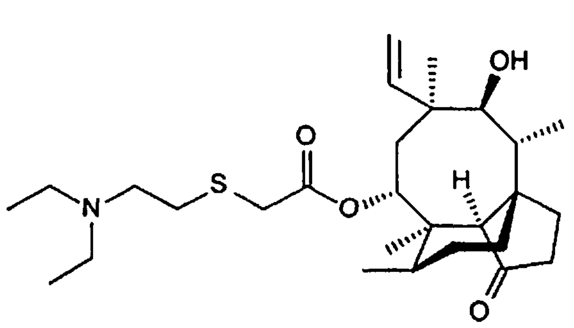

Tiamulin

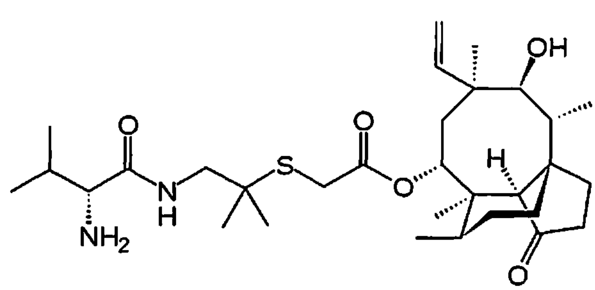

valnemulin

Tiamulin and valnemulin have been used for mycoplasma infections in farm animals [151] but for human usage, yet more developments has to take. They are found to be metabolized very fast in human by liver enzymes and eliminated from the body [152]. GlaxoSmithKline (GSK) has been working together with the TB Alliance to identify a semi-synthetic pleuromutilin optimized against both replicating and non-replicating Mtb for the treatment of respiratory tract infections, with respect to potency, pharmacokinetic, metabolic and safety characteristics. Cross resistance has, been reported between pleuromutilins and oxazolidinones with other microor-ganisms, [153] so this aspect will require careful evaluation in TB.

A New Chemical Class Addressing a Novel Targets

Desirable targets should be involved in vital aspects of bacterial growth, metabolism and viability, whose inactivation should lead to bacterial death or inability to persist. The availability of the Mtb genome sequence, mycobacterial genetic tools, such as transposon mutagenesis, gene knockout and gene transfer greatly facilitate target identification. Targets involved in the pathogenesis of the disease process should also be considered for drug development. For example, liquefaction from solid necrotic lesion to cavity formation is a key step in the spread of infection to other individuals. If the liquefaction and cavity formation could be interrupted, the bacilli in the lesion would not be coughed up and spread to others. Thus, inhibition of host liquefaction process represents a novel approach to the design of new drugs that stop the transmission of the disease.

It is increasingly acknowledged that new drugs should not only be active against drug resistant TB, but should also kill persisters and shorten the lengthy TB treatment, which underlies the problem of drug resistance due to poor compliance to the length of therapy. Enzymes in metabolic pathways that are not inhibited by current TB drugs could also be good targets. Mycobacterial two-component systems, sigma factors and virulence factors have also been proposed as targets for TB drug development. Novel drug targets for which new drugs can be developed are discussed in Table 8.

Table 8: Validated drug targets in Mycobacterium tuberculosis

Metabolic pathway	Gene product	Validation				
		Knockout *in vitro* growth	Human homologue	Knockout *in vivo* growth	Complexed with crystal structure	Small-molecule inhibitor
Cell wall biosynthesis						
Peptidoglycan biosynthesis	Alanine racemase	Not viable	None		D-cycloserine	D-cycloserine
	D-Ala-D-Ala ligase	Not viable	None			D-cycloserine
Arabinogalactan biosynthesis	EmbA–C	EmbA–B not viable	None		Cofactor (PLP)	Ethambutol
	AftA	Not viable	None			
	Phospho-ribosyltransferase	Not viable	None			
	Galactofuraosyl transferase	Not viable	None			
	dTDP-deoxy-hexulose reductase	Not viable	None			
	RmlA–D		None			
Mycolic acid biosynthesis	ENR (InhA)	Not viable	None			Isoniazid
	AcpM	Not viable	None			
	FabD	Not viable	None			
	FabH	Not viable	None		Lauroyl-CoA	
	MabA	Not viable	None			
	KasA	Not viable	None			Thiolactomycin
	KasB	Not viable	None			Thiolactomycin
	MmaA4		None	Attenuated		
	Pks13	Not viable	None			
	Acyl-AMP ligase	Not viable	None			
	FadD32	Not viable	None			
	AccD4	Not viable	None			
	AccA3	Not viable	None			
	AccD5	Not viable	None			
	AccE5	Not viable	None			
Amino acid biosynthesis	LysA		None	Attenuated	Lysine/coenzyme PLP	
	LeuD		None	Attenuated		
	TrpD		None	Attenuated		
	ProC		None	Attenuated		
	LeuA		None	Attenuated	Substrate/product/cofactor	Leucine
	Didydropicolinate reductase		None	Attenuated		
Shikimic acid pathway	AroA, B, C, E, G, K, Q	Not viable	None			
Arginine biosynthesis	ArgF	Not viable	None			Substrate
	ArgA		None	Attenuated		
Branched-chain amino acid biosynthesis	Acetolactate synthase		None			
	Branched-chain amino acid aminotransferase	Not viable	None			
Cofactor biosynthesis						
Folic acid biosynthesis	Dihydropteroate synthase	Not viable	None			Trimethoprim
	Dihydrofolate reductase	Not viable	Yes		NADP/methotrexate/trimethoprim	Trimethoprim
Pantothenic acid biosynthesis	PanB–PanE		None	PanCD attenuated		
CoA biosynthesis	CoA (PanK)	Not viable	None			
Riboflavin biosynthesis	LS, riboflavin synthase	Not viable	None		Purinetrione inhibitors	

Metabolic pathway	Gene product	Validation				
		Knockout *in vitro* growth	Human homologue	Knockout *in vivo* growth	Complexed with crystal structure	Small-molecule inhibitor
Reductive sulfur assimilation	APS reductase	Not viable	None			
Mycothiol biosynthesis	MshA–MshD	Not viable?	None		Octylglucoside for MshB/CoA and acetyl CoA for MshD	
Terpenoid biosynthesis	IspC–H	Not viable	None		Fosmidomycin for IspC	Fosmidomycin
DNA synthesis	Ribonucleotide reductase	Not viable	Yes			
	Thymidine monophosphate kinase	Not viable	Yes		3-azidodeoxythymidine monophosphate	3-azidodeoxythymidine monophosphate
	LigA	Not viable	None			Glycosyl ureides glycofuranosylated · diamines
	DNA gyrase	Not viable	Yes			Fluoroquinolones
Glyoxylate shunt	Icl 1/2		None	Attenuated	Nitropropionate	Nitropropionate
	Malate synthase		None	Attenuated?		
Regulatory proteins	GlnE	Not viable	None			
	MtrA	Not viable	None			
	IdeR	Not viable	None			
	DosR	Conditionally impaired	None			
Menaquinone biosynthesis	MenA-E and MenH	Not viable?	None			
Stringent response	RelMTB		None	Attenuated		
ATP synthesis	ATP synthase		Yes			R207910

Chapter III

Objectives and plan of work

Based on the literature review it can be understood that there is a very urgent need for the newer medication or newer treatment regimen for TB. Drugs for tuberculosis are inadequate to address the many inherent and emerging challenges of treatment. Despite the progress, the global drug pipeline for tuberculosis is still insufficient to address the unmet needs of treatment. The first significant hurdle to the successful treatment of TB with current drugs is the length and complexity of the treatment protocols, which negatively impact patient adherence and play a significant role in the emergence of drug resistant TB. The resurgence of drug resistant TB is a significant global healthcare challenge. Mtb evades the host immune system and drug regimens by entering prolonged periods of non-proliferation or dormancy. Based on all above said facts there is an urgent need for the new need for drugs to improve the treatment of TB.

Advances in genome biology and medicinal chemistry have influenced the new paradigm in drug discovery research. The mechanism driven modern process uses the knowledge of the target as the starting point for drug discovery. The basis of this approach is identifying and validating Mtb targets essential for survival in different environmental niches and physiological states. Glutamate Racemase (GluR), Protein Kinase B (PknB), and Isocitrate lyase (ICL) are known to be essential for Mtb for survival and cell homeostasis under different physiological states of micro-organism. Targeting and inhibiting these Mtb vital enzymes would be a very effective mean to kill the causative organism. Even though new promising targets have been identified based on molecular biology, to the extent of our knowledge, there exists very few or no lead for them so far. These newer targets are of immense importance in the development of anti-tubercular drugs as until now no systematic study has been made on these new targets. A rational study involving these targets could result in an introduction of a number of new classes of drugs in the market which can combat the problem of resistance and shorten the duration of treatment. So to identify the new inhibitors the structure based design and analogue based design approach was used followed by the virtual screening of the database to identify the potential hits.

Objective of the research work

Glutamate Racemase (GluR)

- Identification of the suitable structural template and building the structural model of Mtb GluR based on Homology modeling principle.
- Validation of structural stability of the newly built GluR model by running the molecular dynamic (MD) simulation.
- Virtual screening of the in-house and commercially available database to identify novel potential hits.

Protein kinase B (PknB)

- Identification of suitable structure from protein databank.
- Construction of the analogue based pharmacophore from already reported Mtb PknB inhibitors.

- Construction of the receptor based pharmacophore from the inhibitor bound structure of PknB.
- Virtual screening of the in-house and commercially available database.
- Assessment of the interaction pattern of the candidate molecules by docking in to active site of enzyme.

Isocitrate lyase (ICL)

- Virtual screening of the in-house available database.
- Assessment of the interaction pattern of the candidate molecules by docking in to active site of enzyme.
- Enzymatic and biochemical analysis of the newly identified hits in Mtb.

Chapter IV

Glutamate Racemase as anti-TB target & design of its Inhibitors

4.1 Introduction

Damage to the cell wall of bacteria leads to cell lyses and death due to the elevated internal osmotic pressure of the cell. The biogenesis of cell wall components is essential pathway for many pathogenic bacteria [154] and has long been well accepted as a target for antibiotic action [155-157] Penicillins, cephalosporins and glycopeptide are examples for the class of drugs which act by inhibiting key steps in biosynthesis of peptidoglycan layer of bacterial cell walls [158]. Till now successful work has been done on the inhibition of the last segment of the peptidoglycan layer biosynthesis which involves the extracellular cross linking and final maturation. The development of resistance has limited the therapeutic utility of both the existing and future compounds in these classes. The emergence of MDR-strains also has increased mortality rates with limiting options for therapeutic intervention for these existing classes of targets and put into need of alternate promising targets with novel mode of action. There are few clinically validated targets which have been subject to intense discovery efforts over the past decade, such as enzymes involved in synthesis and utilization of D-amino acids, which form components of the cell wall. The first step of peptidoglycan biosynthesis includes conversion of glucosamine-1-phosphate to UDP-N-acetylglucosamine (UDP-GlcNAc) and which then leads to form UDP-N-acetylmuramic acid-pentapeptide (UDP-MurNAc-pentapeptide). A key step of the peptidoglycan synthesis involves the incorporation of D-amino acids, D-glutamate by the ligase

MurD, and D-alanine in the form of dipeptide formed by enzyme D-ala-D-ala ligase, the substrate of MurF. Figure 8 shows the importance of the GluR in the biosynthesis of peptidoglycan cell wall. These unusual residues provide a defense against hydrolysis of the bacterial capsule, as host proteases are unable to recognize sequences containing D-amino acid residues [159].

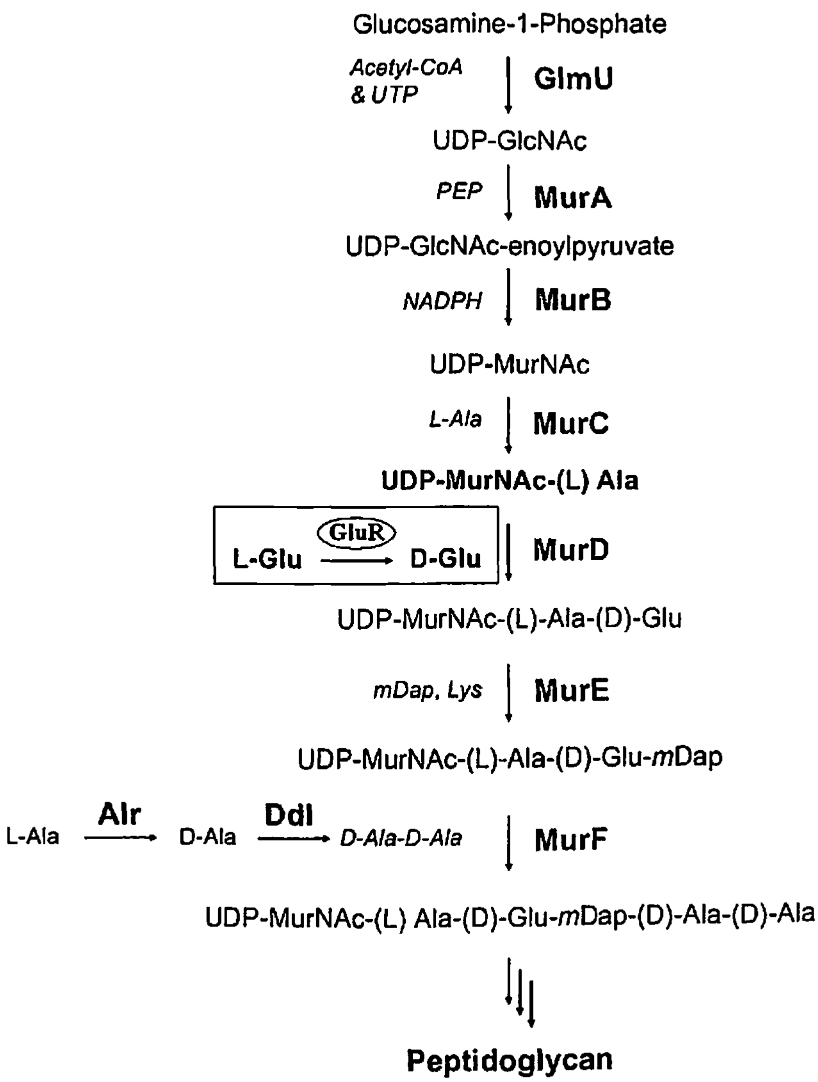

Figure 8: Schematic representation of peptidoglycan biosynthesis.

The role of GluR in peptidoglycan biosynthesis was not always so clear. Pioneering work in *Lactobacillus arabinosus* suggested the presence of GluR activity in cellular extracts [160, 161] and implicated its role in supporting growth when D-glutamate was substituted for L-glutamate in the growth medium. It was hypothesized that the primary route for D-glutamate production was through D-amino acid transaminases (D-AAT). Purification and biochemical characterization of GluR from *L. arabinosus* [162] and *Lactobacillus fermenti* [163] provided direct evidence for the existence of GluR enzyme activity in lactic acid bacteria. Further purification of enzyme, demonstrated that the enzyme required no cofactors for catalytic activity [164]. Additional biochemical studies with the enzyme derived from *Pediococcus pentosaceus* confirmed that the enzyme was a member of the cofactor independent family of racemases.

Elegant genetic studies using *E. coli* with the mutant strain WM355, GluR activity was unambiguously assigned to an open reading frame encoding a protein of 289 amino acids in the 90 min region of the chromosome, near the *murA* and *murB* genes, but quite distant from the remaining Phase I peptidoglycan biosynthetic genes [165] denoted *murI* using the nomenclature adopted for the peptidoglycan biosynthetic pathway. Disruption of *murI* resulted in to alteration in the peptidoglycan precursor pool distribution and ultimately leading to cell lysis [166]. Later detailed genetic dissection of the WM335 mutant strain [167] and plasmid based complementation of *murI* strains using either the *E. coli murI* gene [168] or the *murI* gene from *P. pentosaceus* [169] confirmed essentiality of GluR for bacterial survival.

Observation of effects on nucleoid separation and supercoiling of plasmids in strains over expressing the *E. coli* murI gene [168] led to an understanding that elevated levels of *E.coli MurI* inhibit the topoisomerases responsible for DNA replication, gyrase and topoisomerase IV.

Subsequent studies demonstrated that *E. coli MurI* is a potent inhibitor of gyrase-supercoiling activity [170] and similar findings have been observed with the GluR proteins from Mtb [167], *M. smegmatis* [172] and *B. subtilis* [173]. Mechanistic studies utilizing the recombinant enzymes from *M. smegmatis* and Mtb indicate that GluR inhibits DNA binding to gyrase and that GluR overexpression *in-vivo* provides protection against the action of the gyrase inhibitor ciprofloxacin.

In several *Bacillus* species, including *B. anthracis* and *B. subtilis*, encode two homologues of GluR. Subsequent biochemical studies have confirmed that both genes encode functional glutamate racemase enzymes with similar pH and substrate preferences; however, differences have been noted between the isozymes in their thermostability [178], solution oligomeric state [179, 180] and, for the *B. subtilis* enzymes, their overall catalytic efficiency.

D-Glutamate is one of the important biosynthetic building blocks present in peptidoglycan layer, produced from L-glutamate by the enzyme glutamate racemase (GluR) [181]. GluR has been found to be essential for the viability of *Streptococcus pneumonia* [182] *Escherichia coli* [172], *Staphylococcus haemolyticus* [183] and *B. subtilis* [184]. The pathogenic Mtb exclusively relies on the GluR enzyme for D-glutamate biosynthesis, which is vital for its cell envelop formation and in turn for bacterial survival. Absence of human counter part of the enzyme makes it a very safe and offers high potential for novel therapeutic intervention, perhaps with no toxicity issues to humans making it an attractive target [185, 186].

GluR belongs to amino acid racemases and epimerases, those operate in a cofactor independent manner like proline racemase, aspartate racemase and diaminopimelate epimerase [181]. Studies involving structure determination of GluR from different bacterial species like *A.*

pyrophilus [187], *B. subtilis* [188] and *S. pyogenes* [189], have revealed that there are two conserved cysteines which act as bases during the enzyme's catalytic cycle. The accepted catalytic mechanism for glutamate racemase involves deprotonation of the glutamate's R-proton, followed by substrate reprotonation on the stereochemical opposite face. Mutagenesis studies have shown that two cysteines are the catalytic acid/base residues [181, 190-192]. Mechanistic studies on the GluR enzyme have suggested that the catalysis uses a 'two-base' mechanism which involves deprotonation of the substrate at the position to form an anionic intermediate followed by reprotonation in the opposite stereochemical sense [181]. Studies by Knowles and co-workers on proline [193-195] and glutamate racemases [196-197] established that the enzymes employs a "two-base" racemization mechanism, in which two cysteine residues flank the glutamate's R-proton. Cys75 functions as the catalytic base in the case of D to L direction, abstracting the CR-proton to generate a carbanion intermediate, which is then protonated by Cys185 residue to yield the antipode and vice versa works for L to D direction (Figure 9). The physicochemical rationale underlying glutamate proton acidification and the catalytic acceleration of proton abstraction remain poorly understood. The carboxylate in fully protonated glutamate has pKa value of more than 21 making the proton abstraction challenging [191]. Anion stabilization may occur via delocalization of negative charge through many strong hydrogen bond donors. With pKa 8.4 in aqueous solution, at neutral pH, the sulfur

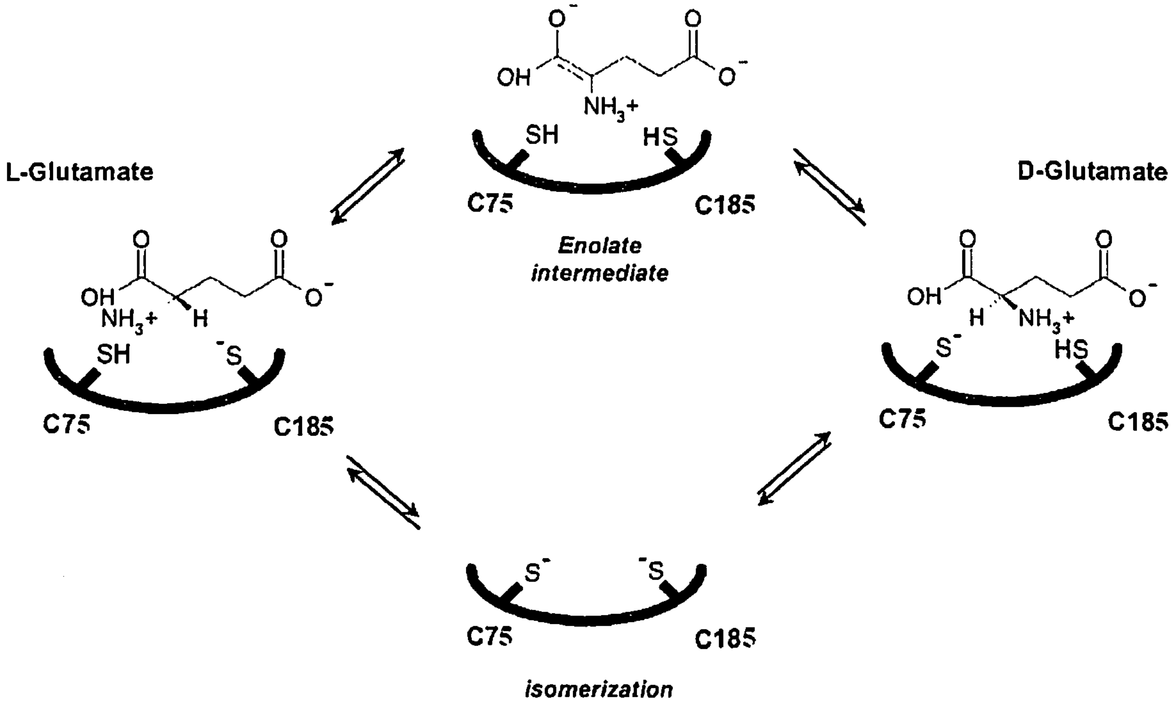

Figure 9: Proposed catalytic mechanism of glutamate racemase. Conserved active site cysteines shown schematically. Isomerization of the enzyme is represented proceeding through the fully deprotonated state; additional or other forms may be involved.

atom of the cysteine would be fully protonated, and will be unable to abstract the proton of the glutamate. But the electrostatic field inside the enzyme can highly perturb the original pKa in aqueous solution due to some specific interactions among residues making reaction possible [198]. A known example is the interconversion of L- and D-alanine by pyridoxal 5'-phosphate and alanine racemase. Tyr265' and Lys39 are two catalytic residues acting as an acid/base pair [199-202]. The pKa is 10.5, in aqueous solution of the phenolic hydroxyl of tyrosine and the conjugate acid of lysine. Therefore both residues would be protonated at neutral pH. The electric field in the active site of alanine racemase is stabilized by the His166 mediated interaction with Arg219, leading to the formation of a negative charge in the phenolic oxygen atom of Tyr265', thus pKa shifts to 7.315, by which Tyr265' can work as catalytic base for the conversion of L-alanine to D-alanine at near pH 8, where the enzyme is most likely active in nature [199].

Simlarly, Lys39 with pKa shifted, will be unprotonated amine, so acts as catalytic base for the conversion of D-alanine to L-alanine [199]. In case of GulR Asp10 and His187 stabilize the Cys75 thiolate and Cys185 thiols respectively. Analysis of structure of a complex of BS GluR with D-glutamate shows the conserved thiol groups, Cys74 and Cys185, are close to the side chains of Asp10 (3.9 Å) and His187 (4.2 Å). Many theoretical studies carried out have shown that these residues stabilize the cysteines or aid in abstraction of the proton from glutamaic acid [203-206]. This is also evident from mutational studies carried out by Glavas and Tanner, that the catalytic cysteines showed significant activity [177]. If intermediate formed was alkoxide ion which is expected in the case of metallo enzyme or enzymes with cofactor, after mutating the catalytic cysteine residues the enzyme should have turned out to be inactive.

Amongst the GluR form different species, differed the enzyme kinetics, structure, and inhibition characteristics, they also revealed significant differences in biophysical properties and steady-state kinetics [207]. *E. coli* GluR is monomeric in solution and has low intrinsic activity in either direction, and catalysis is up regulated by UDP-MurNAc-Ala, the product of the preceding enzyme in the peptidoglycan biosynthetic pathway, which is a feedback regulation mechanism for maintaining levels of D-glutamate to support cell growth, [208-210]. In contrast, *H. pylori* GluR forms a dimer, is unaffected by UDP-MurNAc-Ala, but presents a severe substrate inhibition by D-glutamate alone [200]. These findings indicate a totally different regulatory mechanism of enzyme activity for *H. pylori and E. coli.* MurI enzymes from the Gram-positive species *Staphylococcus aureus, Enterococcus faecalis* and *Enterococcus faecium* share similar biophysical, biochemical characteristics that they all form homodimers in solution, and are unaffected by UDP-MurNAc-Ala, and exhibit high intrinsic catalytic turnover. These enzymes displayed asymmetry in substrate preference with elevated L-glutamate Km values, but did not exhibit the severe substrate inhibition. As a result, the catalytic activity of these enzymes is not strictly governed; this may be because Gram-positive organisms require more D-glutamate because they have a thicker peptidoglycan layer. In addition, these organisms contain a D-amino acid transaminase [211, 183] and because GluR was shown to be essential in Gram-positive pathogens [212, 213] it is likely that the transaminase is used to salvage excess D-glutamate. The different kinetic profiles exhibited across the species suggested fundamental structural differences.

So far the crystal structure of Mtb GluR is not solved. The GluR monomers crystal structures from different species, shared a conserved topology and fold, that is comprised of two domains that exhibit a pseudo-symmetry axis. Catalysis takes place at the interface of the two domains, with each domain contributing the residues attributed to the enantiomeric deprotonations [187]. The domain that begins with the amino terminus (domain A) contains the conserved amino acids involved in deprotonation of D-glutamate (D7, S8, C70, T72), whereas the carboxy-terminal domain (domain B) contains the catalytic residues involved in L-glutamate deprotonation (E150, C181, T182, H183). It is apparent that the two domains move with respect to each other and this movement is largely restricted to a rotation around a single axis. This hinge movement occurs at the two crossovers between the domains and a coordinated hinge movement is required to form the active site and permit catalysis.

The observed hinge movement of GluR is not only critical for catalytic function, but also adopts activity to meet physiological demands. *E. coli* GluR co-crystallized as a monomer with both L-glutamate and its activator UDP-MurNAc-Ala, the activator binds in the hinge region on the side opposite to the catalytically active site through contacts between the uracil ring system and domain B and through specific salt bridge interactions with R104 in domain A and the alanyl moiety of the activator. These interactions are predicted to focus the hinge movement and to favor productive substrate binding, leading to higher catalytic efficiency in response to cell wall biosynthesis demand. *S. aureus, E. faecalis, E. faecium* and *B. subtilis* form homodimeric structures. The monomers oligomerize in a tail-to-tail orientation with active sites opposed and fully exposed to solvent. Oligomerization occurs through interactions across a C2 symmetry axis, mainly involving helices from the A and B domains of each monomer, to create an interface that is conserved in all of the Gram-positive GluR structurally characterized so far. In contrast to the Gram-positive GluR structures, the *H. pylori* GluR enzyme also forms a homodimer with the active sites in close proximity in a face-to-face orientation, shielded from the solvent. A similar interaction is observed in the asymmetric unit of the structure reported for *B. subtilis*; however, *B. subtilis* AB interface probably results from crystal packing interactions, [195]. The *H. pylori* GluR structure contained only D-glutamate in the active site, despite growing the crystals in the presence of saturating concentrations of racemic glutamate. This finding is consistent with the asymmetric, D-glutamate-inhibited kinetic profile of the enzyme and the structure most probably represents the substrate-inhibited, resting state of the enzyme. This arrangement suggests that the enzyme has evolved to stabilize the closed, glutamate-bound state to reduce overall catalytic turnover. Although dimerization occurs through inter-monomer interactions between both A and B domains, the B-domain interactions possess the majority of dimerization contacts. Logically, during hinge-movement transition between closed and open states, it is the A-domain interface that is predicted to separate to allow glutamate to enter and leave, whereas the B-domain interface is maintained. This hypothesis is supported by analysis of the nuclear magnetic resonance (NMR) titrations with glutamate, which indicate that domain A is more dynamic.

As mentioned earlier, the crustal structure of Mtb GluR is not yet reported. A three dimensional structural model is reported in Swiss-Prot Repository. It's an automatically generated model without human interruption or monitoring. The model was created on 27th September 2006 [214]. The model was constructed based on *Bacillus subtilis* GluR, (PDB entry 1ZUW, resolution 1.75 Å). The Mtb GluR model was derived by ModPipe, (http://salilab.org/-modpipe/) an automated modeling pipeline relying on the programs PSI-BLAST [215] and MODELLER.

4.1.1 GluR Inhibitors

Tunner and Miao, in 1994 first reported aziridino-glutamate, 4-(2-(2-carboxyethyl) aziridine-2-carboxylic acid) as inhibitors of GluR for *Lactobacillus* [216]. The rate of inactivation was decreased by the presence of substrate as expected for an active site directed inhibition process. Samples of aziridino-glutamate rapidly lost inhibitory activity when kept at neutral pH and room temperature due to the cyclization of aziridino-glutamate to lactone. The evidence for covalent attachment was obtained by electron spin mass spectrometry.

In 1997, Glavas S and Tanner ME reported D-N-hydroxyglutamate as first reversible competitive inhibitors of GluR [217]. The compound showed a K_I value of 56 μM to GluR of Lactobacilli. The compound acts as an alternate substrate and is converted into α-ketoglutarate and ammonia. An imine intermediate is likely to cause the inhibition.

In 2002, Alfonso de Dios et al., from Eli Lilly reported 4-substituted D-glutamic acid analogues to be the first potent, inhibitors of GluR with whole cell inhibitory activity against *S. pneumonia.* These compounds were substrate analogues and presumed to attack the active site of the GluR in a competitive way. Different substitution on the γ-carbon of glutamic acid was carried out. To avoid the CNS effects due to involvement of L-Glutamate in kainite and metabotropic glutamate receptor the D-Glutamate analogues only were synthesized. The elongated analogue was completely inactive indicating that the distance between carboxylic acids is very important for the activity. The simple alkyl substitution on γ-carbon substantially reduced the activity in enzyme and in cell assays they were totally inactive. Large aromatic groups were well-tolerated and retained or increased activity. A linear arrangement of aromatic rings was crucial for activity as 1-naphthyl substitution was 50-fold less potent than 2-naphthyl (IC_{50}=0.1 μg/mL, MIC=0.31 μM). (E)-Cinnamyl and arylpropargyl derivatives were also quite potent showing that elongation of the substitution in the right direction determined by C-4 stereochemistry was possible but clearly had a limit of 3 carbons. Other than carbon linkers were not tolerated indicating need of lipophilic character. For antibacterial activity, linear arylmethyl groups were preferred, and for other kind of linkers, a large decrease in whole cell growth inhibition. Different analogues of prepared by substitution on benzyl group of γ-benzyl-D-glutamate showed good activity. The conversion to γ-phenoxy-glutamate reduced the enzyme activity. *O*-benzyl substitution were detrimental compared to *p*/*m*-substitutions, which were either well tolerated or could potentially boost both activities. Moving a chlorine atom around the aromatic ring led to a large increase in activity (from *ortho* to *para*). Large lipophilic groups such as Br and Phenyl led to poorly active or inactive compounds at the *o*-position, but quite potent compounds at *m*/*p*-positions were obtained. With respect to possible electronic effects, several electron withdrawing and donating groups showed similar activity for the same substitutions and at both *m*/*p*-positions. All of these observations were consistent with the hypothesis of a large and linear lipophilic binding pocket in the catalytic domain of GluR. The aromatic nonpolar substituents m- or p-positions showed good activity consistent with the MIC values. Substitution of benzyl group to isostearic groups were well tolerated especially 2-benzothienyl substitution showed very good IC_{50} value as well as MIC value.

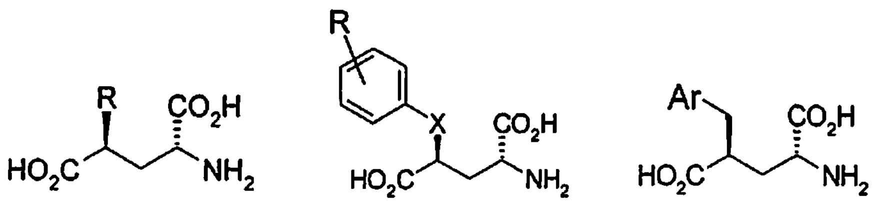

In 2008 reseach from Astra Zeneca R&D, reported many inhibitors of GluR of *Enterococcus faecalis, Enterococcus faecium, Staphylococcus aureus*[218]. From hit to lead identification efforts by high-throughput screening (HTS) of the Astra Zeneca compound collection, 9-benzyl purine scaffold was identified as a potential hit. Objectives during the lead identification phase were to increase MurI enzyme inhibitory potency, improve physical properties, especially solubility, and to expand the Gram-positive spectrum. To achieve this substituents on position 2, 6, and 9 of the purine scaffold, followed by purine core modification were carried out. Ortho substituents on the benzyl ring tended to increase potency (Type I).

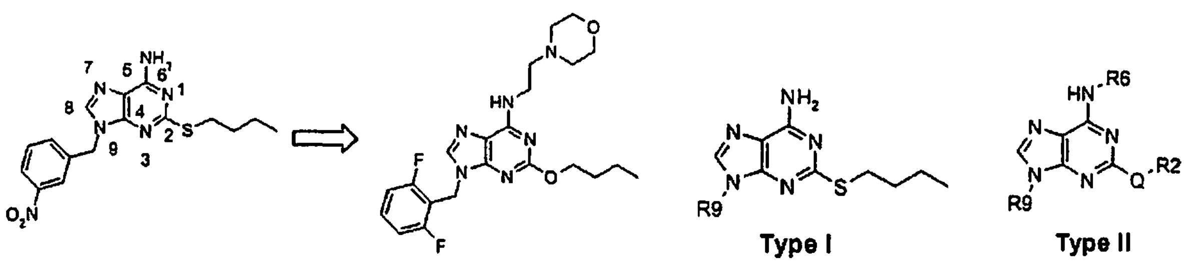

However, variations of the substituent on the benzyl ring afforded, in general, no significant potency improvements against *E. faecalis* and *E. faecium* GluR enzyme and no inhibition of the *St. aureus* enzyme activity was observed.

In another Hit-to-lead identification HTS program by Astra Zenica, pyrazolopyrimidine-dione was identified to be a hit selective towards *H. pylori* GluR [219]. To have an excellent enzyme inhibition resulting into potent antibacterial activity and for pharmacokinetics stability, pro-drug approach was implemented wherein a solubilizing sulfoxide moiety is oxidized *in-vivo* to a sulfone. The X-ray structure of the *H. pylori* GluR with and D-glutamate bound has been determined to 1.9 Å showing that the inhibitor occupying an allosteric binding site. The crystal

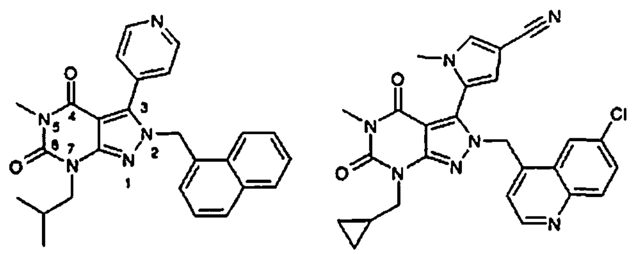

structure revealed that 7-position isobutyl group and the 2-position naphthalene of the inhibitor are deeply buried in hydrophobic regions of the inhibitor binding pocket. The pyrazolopyrimidinedione 5-position methyl group lies against a hydrophobic surface and otherwise faces solvent. From crystal structure it seemed best to target the region of the binding pocket surrounding the pyridine, analogously, the pyrrole of 2 for the incorporation of polar functionality. Replacing 1 with 2 in the inhibitor binding region showed the pyrrole methyl group surrounded by a nicely complementary hydrophobic environment whereas the region surrounding the cyano substituent is lined with the hydrogen bonding atoms of a series of more polar side-chain functionalities (Ser152, Gln248, Arg247, and Trp 252) and reaches outward to solvent(Pdb id 2jfz). New molecules were made where the cyano group is replaced with the sulfur substitutions: sulfones, sulfoxides, and sulfonamides. These functionalities were sterically accommodated by the crystallographic model and offered the potential to form hydrogen bonds with enzyme side chains or bridging water molecules. Substitution with 5-membered aromatic rings at the 3-position over 6-membered ring improved inhibitory potencies. Small methyl placement on 5-membered aromatic ring in a 1–2 relationship to the bond connecting to the scaffold improved antimicrobial activity. Potency is further improved when polar groups are situated in a 1–3 relationship with the linkage to the scaffold. Substituents on sulfonamide slightly decreased the inhibitory potency but improved MICs through the increase in lipophilicity.

Another hit identified by Astra Zenica 9-benzyl purines, was subjected to scaffold hopping to the 8-benzyl pteridinediones which led to compounds with μM enzyme potency and antibacterial activity [220] including Gram positive organism *S. aureus*. Fragmenting the 5-membered ring gave a monocyclic template; the highly functionalized pyrimidine as shown in figure below, which was used for substructure search, identified 2-benzylthio 8-benzyl pteridinedione as hit. This molecule upon screening showed activity against the *S. aureus* enzyme as well as *E. faecalis and E. faecium* a broad spectrum GluR inhibitor. Introduction of small cyclic groups at the 2-position retained activity against *E. faecalis* but led to loss of potency against *S. aureus*.

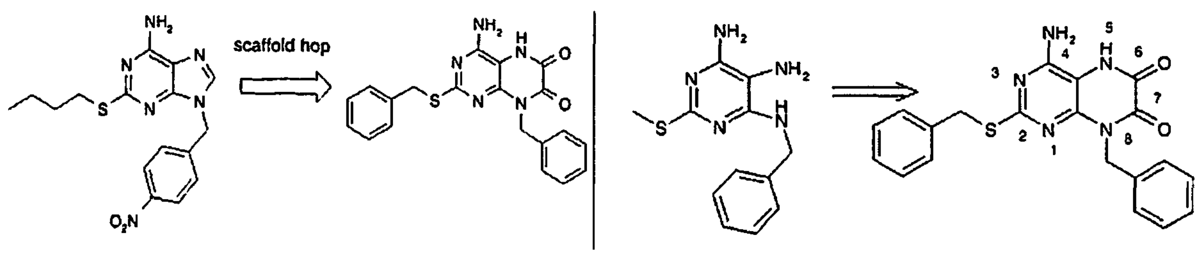

Benzodiazepine amine is another hit identified by Astra Zenica by HTS of their prioritory compound collection [221]. The benzodiazepin amine was higly selective and potent towards *H. pylori* with IC_{50} of 1.7 μM and MIC of 0.5 lg/mL. An X-ray structure of H. pylori GluR in a ternary complex with Hit2 and D-glutamate was obtained (Pdb id 2w4i) demonstrating a distinctive non competitive binding interaction at the enzyme dimer interface at allosteric site.

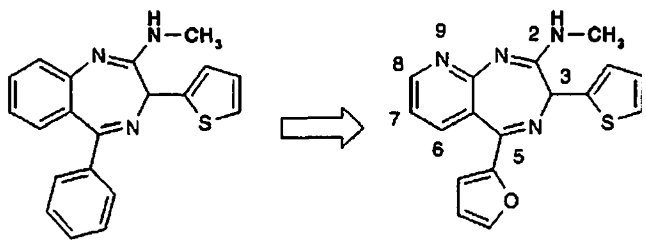

Hit   Lead

Variations of the 2-position amine (R2) did not produce any compounds that markedly improved solubility or decreased plasma protein binding. For inhibitory potency, only small alkylamines were tolerated, with methylamino remaining the best.

Leone PA et al., reported first natural product, exiguaquinol as inhibitor of *H. pylori* GluR [222]. Exiguaquinol, is a pentacyclic hydroquinone that inhibited *H. pylori* GluR with an IC_{50} of 4.4 μM. It was isolated from methanol extract of the Australian sponge *Neopetrosia exigua.*

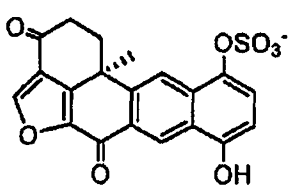

Recently Whalen KL et al., disconected active site directed competitive inhibitors of GluR from *Bacillus* [223]. They in their effort to identify totally new class of GluR inhibitors by explioting the plasticity of the enzyme active site efficiently by using the transition state of the enzyme collected based on molecular dynamic and quantum mechanic studies. They conducted a virtual screening by docking a million molecules to the active site bound with substarte. The highest scored molecules were then screened for the activity. They reported 8 new molecules with very highest potency in the form of enzyme dessociation constant, which are not amno acid analogues.

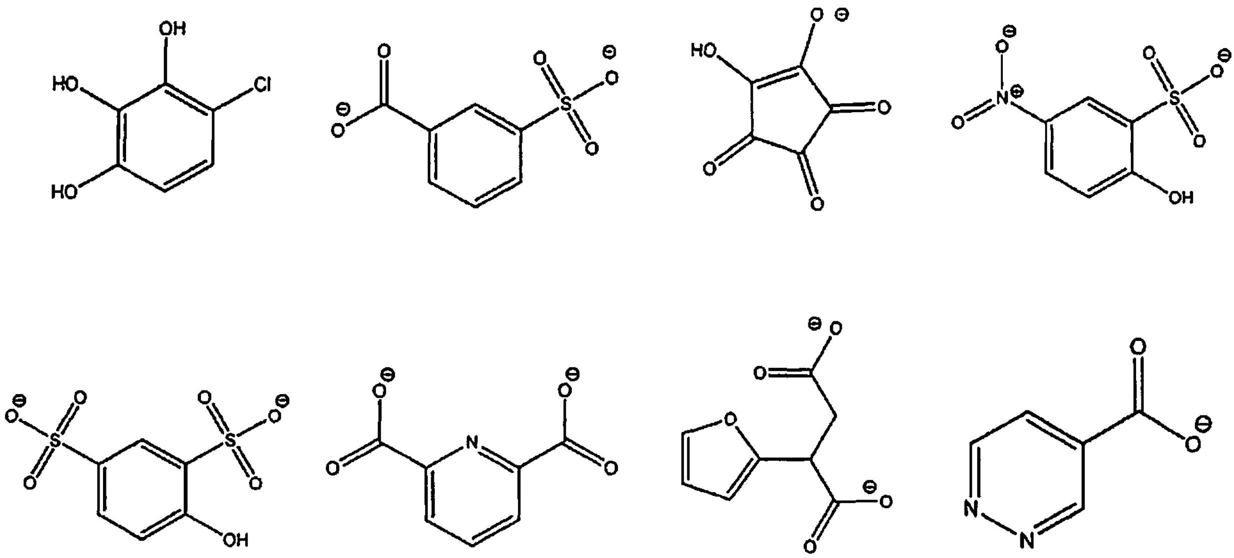

4.2 Materials and methods

4.1.1 Retrieval of GluR protein sequence The amino acid sequences of the target protein, Mtb GluR was collected from the Swiss-prot protein sequence database (Swiss-prot Accession No. P63635). The Mtb GluR sequence consisted of 271 residues. It was ascertained that the three dimensional structure of GluR from Mtb is not available in PDB database, hence an attempt has been made to determine the structure.

4.2.2 Template identification The NCBI BLAST (Basic Local Search Alignment Tool) was used to identify the template or modeling the three dimensional structure of GluR from Mtb. The template for the model building was considered based on high percentage homology to Mtb GluR, the high crystallographic resolution of the template structure and low BLSAT alignment error values (E value).

4.2.3 Sequence alignment Sequence alignment was derived with the ClustalW 1.8 package using the BLOSUM matrices [224] for scoring the alignments. Getting a very good quality alignment of the target sequence with the template sequence is an important step in protein homology modeling to yield a high quality model. Openings and extension GAP penalty were changed systematically, and the obtained alignment was checked for deletions and insertions in structurally conserved regions and finally fine-tuned manually.

4.2.4 Model building The resulting alignment was used as an input for the prediction of three dimensional structure of Mtb GluR using automated homology modeling program MODELLER v9.2 [225]. The alignment obtained from ClustalW program was converted to "pir" format and submitted to MODELLER program with the file name "aligment.ali" which has an alignment between the Mtb GluR and template sequences (Figure 10). 3D model was then obtained using the script "model-default.py" based on the generated alignment (Figure 11). Either the single template or the multiple template alignments were used to obtain the primary 3D models of Mtb GluR. This program assigns atomic co-ordinates to regions structurally aligned with the template, builds intervening loops, optimizes the rotamers of amino acid side chains, and performs an initial energy optimization of the structure. MODELLER generates protein 3D structures by satisfying spatial restraints imposed by the sequence alignment with the template structure. These spatial restraints consist of homology derived restraints on the distances and dihedral angles in the target sequence based on its alignment with template structures, stereo chemical restraints such as bond length and bond angle terms obtained from CHARMm force field, and statistical preferences for dihedral angles and non-bonded inter atomic distances obtained from a representative set of protein structures. These restraints are expressed in terms of probability density functions (PDF). A 3D protein model is obtained by optimizing the probability density function with the variable target function procedure in cartesian space that employs methods of conjugate gradients and molecular dynamics with simulated annealing. To guarantee sufficient conformational sampling of each active site residue, several homology models are generated in this step. The MODELLER generated 100 models of Mtb GluR for each template protein used, from which the best model was selected based on the Dope score [221, 226]. A comparative study was made on the Mtb GuR models developed from the different templates to select best model of Mtb GluR based on Ramachandrans plots and G score. The Mtb GluR model developed from *Enterococcus faecalis* (Efa) (PDB id 2VVT) was the best model compared to the model developed from other templates or from combination of multiple templates.

The best Mtb GluR model was subjected to protein preparation wizard [227] in Schrodinger where hydrogen atoms were added to the model. By explicitly specifying the pH as 7.0, the protonation states for all the amino acid side chains were set in accordance with their typical pKa values. The initial model was energy minimized, employing the Impact [228] module of Schrodinger, in a stepwise fashion following a standard procedure consisting of 1000 steps of steepest descent and 2000 steps of conjugate gradient minimization with a root mean square gradient of the potential energy of 0.001 Kcal/mol Å in each step for which OPLS parameters, a distance dependent dielectric constant and a non-bond cutoff distance of 10.0 Å were employed. In the first step, all newly added hydrogen atoms were minimized followed by energy minimization of the loop side chains, loop main chains, all core side chains, and finally the core main chains.

```
Efa GluR MGSSHHHHHHSSGLVPRGSHMSNQEAIGLIDSGVGGLTVLKEALKQLPNE 50
Mtb GluR ---------MNSPLAP----------VGVFDSGVGGLTVARAIIDQLPDE 31
                   .* *.*          :*::********* :  :.***:*

Efa GluR RLIYLGDTARCPYGPRPAEQVVQFTWEMADFLLKKRIKMLVIACNTATAV 100
Mtb GluR DIVYVGDTGNGPYGPLTIPEIRAHALAIGDDLVGRGVKALVIACNSASSA 81
          ::*:***.. ****  .  ::  .:  :.* *: : :* ******:*::.

Efa GluR ALEEIKAALPIPVVGVILPGARAAVKVTKNNKIGVIGTLGTIKSASYEIA 150
Mtb GluR CLRDARERYQVPVVEVILPAVRRAVAATRNGRIGVIGTRATITSHAYQDA 131
         .*.: :    :*** ****..* ** .*:*.:****** .**.* :*: *

Efa GluR IKSKAPAIEVTSLACPKFVPIVESNQYRSSVAKKIVAETLQALQLKGLDT 200
Mtb GluR FAAAR-DTEITAVACPRFVDFVERGVTSGRQVLGLAQGYLEPLQRAEVDT 180
         : :     *:*::***:** :** .   .  .  :.   *:.**   :**

Efa GluR LILGCTHYPLLRPVIQNVMGSHVTLIDSGAETVGEVSMLLDYFDIAHTPE 250
Mtb GluR LVLGCTHYPLLSGLIQLAMGENVTLVSSAEETAKEVVRVLTEIDLLRPHD 230
         *:*********  :** .**.:***:.*. **. **  :*  :*: :. :

Efa GluR APTQPHEFYTTGSAKMFEEIASSWLGIENLKAQQIHLGGN- 290
Mtb GluR APPATRIFEATGDPEAFTKLAARFLGPVLGGVQPVHPSRIH 271
         **. .: * :**..: * ::*: :**     .* :* .
```

Figure 10: Sequence alignment of Efa GluR and Mtb GluR usedin the "alignment.ali", submitted to MODELLER program for the construction of Mtb GluR model. Sequence alignment carried out using ClustalW server. The conserved regions (identical residues) are indicated by '*', residues with highly similar physicochemical properties are represented by ":", residues with considerable similar physicochemical properties are represented by ".".

```
# Homology modeling by the automodel class
from modeller import *              # Load standard Modeller classes
from modeller.automodel import *    # Load the automodel class

log.verbose()    # request verbose output
env = environ()  # create a new MODELLER environment to build this model in

# directories for input atom files
env.io.atom_files_directory = './atom_files'
a = automodel(env,
              alnfile  = 'alignment.ali',     # alignment filename
              knowns   = '2VVT',              # codes of the templates
              sequence = 'GluR_2vvt_mod',     # code of the target
```

```
                assess_methods=(assess.DOPE))
a.starting_model= 1              # index of the first model
a.ending_model  = 100            # index of the last model
                                 # (determines how many models to calculate)
a.make()                         # do the actual homology modeling
```

Figure 11: Script "model-default.py" used in MODELLER for generation of 3D models of Mtb GluR from Efa GluR.

The quality of the final refined model was assessed by subjecting it to a series of tests for its internal consistency and reliability. The Procheck [229] analyses bonds length, bond angle, and torsion. The Profile-3D [230] program was used to check the structure and sequence compatibility, to evaluate the fitness of the model structure to their sequence at current 3D environment, while the Procheck suite of programs was used for assessing the ''stereo chemical quality'' of the modeled protein structure. Root mean square deviation for protein backbone was also calculated for the structure before and after minimization to show there was no gross change.

4.2.5 Active site identification For the identification of binding site two strategies were used. The GluR of different bacterial species whose crystal structure already has been solved out with the ligand and having amino acid sequence identity more than 34% to Mtb GluR were collected and using ClustalW, they were subjected to multiple sequence alignment together with the GluR of Mtb. For the study GluR from six different bacterial species *Bacillus anthracis* (PDB id 2GZM), *Bacillus subtilis* (PDB id 1ZUW), *Enterococcus faecium* (PDB id 2JFV), *Enterococcus faecalis* (PDB id 2VVT), *Staphylococcus aureus* (PDB id 2JFQ), and *Helicobacter pylori* (PDB id 2JFX) were used. The amino acid residues of Mtb GluR corresponding to the amino acid residues involved with the ligand interactions (residues within range of 10 Å from the) at the active site of relative species were identified. Then using the active site pocket detecting program from Schrödinger SiteMap, in the modeled structure of Mtb GluR, those amino acid residues were checked for practical possibility of interaction with the ligand or to surround the active site pocket [231].

4.2.6 Docking A protein ligand complex would offer a more detailed and accurate information of the interactions and structural complementarities between the ligands and the active site. To identify possible active site for docking and to understand the ligand binding pattern, the PDB was searched for solved crystal structures of GluR in complex with ligands. The crystal structure of Efa GluR (PDB id 2VVT), which used as template for homology modeling, was structurally aligned with Mtb GluR. Active sites of both structures were analyzed, and differences in the residue positions were identified. Initially the Mtb GluR model was superimposed with 2VVT. The atomic co-ordinates of the ligands from 2VVT were then transferred to the Mtb GluR, which was taken as initial point for the docking simulation. Using the protein preparation wizard in Schrödinger Maestro software, the bond order was assigned for all atoms of the modeled Mtb GluR receptor. The H-bond was optimized by the exhaustive sampling method. The protein was minimized using the OPLS force field to the extent of 0.3 Å root mean square deviations (rmsd) by keeping the protein back bone constrained. Docking simulations were run using Glide [232] module in Schrodinger. This binary complex was used as input for the receptor grid generation where the centroid of the work place ligand was used as origin for the grid with all other default setting. The docking was run with Standard Precision (SP) and post docking minimization was carried for each pose.

4.2.7 Molecular Dynamics The molecular dynamic (MD) simulation was carried out using Desmond software [233, 234]. The initial docked and refined structures from previous steps were taken as starting points for MD simulation. By explicitly specifying the pH as 7.0, the protonation states for all the amino acid side chains were set in accordance with their typical pKa values. Using the System Builder in Desmond, an orthorhombic box of TIP3P water molecules added [235] such that there was at least 10.0 Å of water between the surface of the protein and the edge of the simulation box. This was to overcome the errors that could have generated during long range columbic interactions which was set 9Å. The solvated system was minimized by force field to relax water molecules added. The system builder removes any water molecules added to the bulk of the protein. The total charge of the solvated protein system calculated from force field parameters. To maintain charge neutrality of the system, appropriate numbers of ions were added using system builder option. The ion placement was excluded for the placement within a range of 7.0 Å from the docked glutamate. To relax the water molecules minimization was carried out by fixing the protein using combination of steepest descent LBFGS method provided in Desmond package till a convergence threshold of 0.01 Kcal/mol/Å was reached. Restraint energy of 50 Kcal/mol was given on water molecules during minimization. The minimized structure was subjected to MD simulation. The MD simulation was run on workstation having Xeon Quad core Processor (5405 2.0 Ghz x 2, 8 processors) with 8 GB Fully buffered Ram and FX 1700 NVIDIA Quadro graphics card. The simulation was carried out for 1.2 ns using NPT ensemble at temperature of 300K and pressure 1.01325 bar. The time duration for the simulation was decided based on the earlier experience on working with same protein in our laboratory. Berendsen Thermostat/ Barostat method was used during simulation. [236] A relaxation time of 200 ps with isotropic cooling style was used. The particle mesh Ewald method [237] for the long-range electrostatics, a 9 Å cutoff for columbic interactions were set up for the series of simulations. All covalent bonds involving hydrogen were constrained using the SHAKE algorithm [238]. A time step of 2 fs was used to integrate the equations of motion. Before starting the production-run phase, a six step relaxation protocols which involves the force field minimization and MD simulation with different temperature and pressure for smaller time interval present in Desmond was used to minimize the whole system. 1000 structures were sampled during the simulation into the trajectory to monitor the simulation. The same protocol was run for both the models of Mtb GluR. To compare two different structures, first the protein structures generated during MD simulation were reoriented in order to minimize the rmsd of the backbone atoms of the enzyme and ligand system with respect to the corresponding atoms of the first structure. Then rmsd of backbone atoms of the protein and ligand of the reoriented second structure with respect to the corresponding atoms of the first structure were calculated.

The stages in the relaxation protocol:

1. Minimize with the solute restrained.

2. Minimize without restraints.

3. Simulate in the NVT ensemble using a Berendsen thermostat with: (i) a simulation time of 12ps, (ii) a temperature of 10K, (iii) a fast temperature relaxation constant, (iv) velocity resampling every 1ps, (v) non-hydrogen solute atoms restrained.

4. Simulate in the NPT ensemble using a Berendsen thermostat and a Berendsen barostat with: (i) a simulation time of 12ps, (ii) a temperature of 10K and a pressure of 1 atm, (iii) a fast temperature relaxation constant, (iv) a slow pressure relaxation constant, (v) velocity resampling every 1ps, (vi) non-hydrogen solute atoms restrained.

5. Simulate in the NPT ensemble using a Berendsen thermostat and a Berendsen barostat with: (i) a simulation time of 24ps, (ii) a temperature of 300K and a pressure of 1 atm, (iii) a fast temperature relaxation constant, (iv) a slow pressure relaxation constant, (v) velocity resampling every 1ps, (vi) non-hydrogen solute atoms restrained.

6. Simulate in the NPT ensemble using a Berendsen thermostat and a Berendsen barostat with: (i) a simulation time of 24ps, (ii) a temperature of 300K and a pressure of 1 atm, (iii) a fast temperature relaxation constant, (iv) a normal pressure relaxation constant

4.2.8 Database preparation In-house database molecules were used for the identification of the potential inhibitors of Mtb GluR. The molecular structures were built using Schrodinger Maestro. The 2D structures were saved in SDF format and then they were subjected to Schrodinger LigPrep (LigPrep, version 2.3, Schrodinger, LLC, New York, NY) program, where the 2D molecules were converted to 3D form, hydrogens added to the molecules, different tautomeric forms generated, proper ionization state generated at pH 7±2 and finally molecules were minimized to local minima. The prepared molecules were then used for further study.

4.2.9 Virtual screening of the database for inhibitor identification The prepared in-house database was used for the virtual screening, to identify the potential inhibitors of the Mtb GluR. The virtual screening was carried out by docking the molecules into active site. The programs like Glide and GOLD were used for docking the database molecules. The Mtb GluR model was subjected to the protein preparation wizard, all the water molecules were removed and the hydrogens were added, H-bonds optimized by the exhaustive sampling method. The protein was subjected initially to 10,000 steps of Steepest Descent (SD) minimization, followed by 15,000 steps of Conjugate Gradient (CG). The minimized protein was used for running the docking simulations. In the case of Glide the center of ligand D-Glutamate present at the active site was taken as the center of grid. As the active site was large, different sized grids constructed ranging between 7.5 to 15 Å. The Glide docking simulation was carried out with SP and XP (extra precision) mode. Another docking program GOLD v3.2 was used. In the case of the GOLD the ligand D-glutamate was removed from the active site before starting the docking. The co-ordinate of the center of the grid generated using Glide was taken as the center of the active site pocket. From this co-ordinate different size of grid were constructed by considering the different radius starting from 7.5 to 15 Å. All of the amino acids within that particular radius were considered to constitute the active site. Docking was carried out using GOLD, which uses the genetic algorithm (GA). For each of the 50 independent GA runs, a maximum number of 100,000 GA operations were performed, whereby all variables for the GA were set to their default values. Default cutoff values of 2.9 Å (dH-X) for hydrogen bonds and 6.0 Å for Van-der-waals were employed. When the top three solutions attained (room mean square deviation) values within 1.5 Å, GA docking was terminated. The common top ranked molecules from each docking method and the highest scoring molecules from each docking method common amongst the different grid size used (but may not be common for all the different docking method) were short listed and studied for their interaction with receptor.

4.3 Results and discussion

4.3.1 Template identification Glutamate Racemase [MurI, EC 5.1.1.3] is a cofactor independent enzyme that catalyzes the inter conversion of the enantiomers of glutamic acid. Mtb GluR sequence contains 271 amino acids with molecular weight of 29 KDa has been cloned, purified [171]. Several proteins homologous to Mtb GluR with known 3D protein structures within PDB were found using Protein BLAST search having good identity percentage and E-values (expectation values). The E-value represents the number of different alignments with scores equivalent to or better than scores that are expected to occur in a random database search. Lower E-values indicate higher scores. The Protein BLAST with PDB presented 19 homologous proteins crystal structures of GluR with score more than 95 to Mtb GluR. These protein crystals presented 32 to 40% identity to Mtb GluR amino acids and Positive residues (identical + similar; similar are amino acid residues which have similar physicochemical properties) ranging from 48 to 60%. Table 9 shows details of PDB entry, number of amino acid residues, percentage identities, percentage of positive residues, resolution of crystal structure, and name of species from which enzyme was crystalized. Out of these, three homologues proteins crystals, showed

Table 9: Homologous proteins crystal structures of GluR with score more than 95 to Mtb GluR belonging to different species.

S. No.	PDB id	Number of Amino acids	% identity/ Positive	Resolution [Å]	Species
1	3hfr	256	42/57	2.3	*Listeria monocytogenes*
2	2gzm	263	38/60	1.99	*Bacillus anthracis*
3	1zuw	259	42/59	1.75	*Bacillus subtilis*
4	2jfw	254	40/58	2	*Enterococcus faecium*
5	2vvt	260	40/58	1.65	*Enterococcus faecalis*
6	2jfo	260	40/58	2.5	*Enterococcus faecalis*
7	2jfp	260	40/58	1.98	*Enterococcus faecalis*
8	2dwu	251	40/59	1.6	*Bacillus anthracis*
9	2oho	250	36/55	2.25	*Streptococcus pyogenes*
10	2ohg	250	36/55	2.5	*Streptococcus pyogenes*
11	2ohv	250	36/55	2.5	*Streptococcus pyogenes*
12	2jfq	252	39/55	2.15	*Staphylococcus aureus*
13	1b73	203	41/59	2.3	*Aquifex pyrophilus*
14	1b74	203	41/59	2.3	*Aquifex pyrophilus*
15	2jfx	195	35/56	2.3	*Helicobacter pylori*
16	2jfz	195	35/56	1.86	*Helicobacter pylori*
17	2jfy	195	35/56	1.9	*Helicobacter pylori*
18	2w4i	195	35/56	1.87	*Helicobacter pylori*
19	2jfn	235	34/48	1.9	*Escherichia coli*

very good identity and had high crystal resolution compared to others. Table 10 presents the comparison of percentage identity and resolution of these homologues proteins to Mtb GluR. Models were built taking these three proteins as templates. The primary analysis of these models is presented in Table 10. It could be seen that the Mtb GluR model developed based on Efa GluR was very good compared to other templates. Model developed based on the Efa GluR presented highest (96%) of the residues in the core region (most favored region) of the Ramachandran plot compared to other models. The G-factor tells about the overall quality of the protein structure. The values between 0 to -0.5 is considered as good for a structure. The model generated from

Table 10: Comparison of percentage identity and resolution of these homologues proteins to Mtb GluR

Name of Protein	Micro-organism	Resolution [Å]	% Identity	Residues in core region of RC plot	G-factor of model	Amino acids
1zuw	*Bacillus subtilis*	1.75	42	92.8	-0.01	259
2vvt	*Enterococcus faecalis*	1.65	40	96.0	-0.05	260
2dwu	*Bacillus anthracis*	1.6	40	90.6	-0.01	251

Efa presented better G-factor value (-0.05) compared to the other models. The Efa crystal had a good resolution and comparable total length of amino acids to the Mtb GluR. Based on these primary results the model developed based on Efa GluR was considered for further study. The GluR of Efa has 40% identities and 58% positives (amino acid residues with similar physicochemical properties) to Mtb GluR. Structurally conserved regions (SCRs) for the model and the template were determined by superimposition of the two proteins amino acid sequence and pair wise alignment. Coordinates from the reference protein (2VVT) to the SCRs, SVRs, N-termini and C-termini were assigned to the target sequence based on the satisfaction of spatial restraints. All side chains of the model protein were set by rotamers.

The model available in Swiss-Prot Repository was built based on GluR of *Bacillus subtilis* (PDB entry 1zuw). Even though the resolution and amino acid length of the GluR from

Bacillus subtilis was comparable to Efa GluR, the crystallographic resolution was better for Efa GluR. The time, during which the Swiss-Prot Repository model was constructed, the Efa GluR crystal structure was not available. The Swiss-Prot Repository model was generated by using an automated procedure using the MODELLER without involvement of human interference. More over the website where the model was presented does not claim assurance for the correctness of the generated model by automated method. The website suggests a thorough inspection of the models before its use. For the ease of discussion model developed from Efa GluR, was named model1. The model available in Swiss-Model Repository was named model2.

The model1 was refined by force field minimization method and the final structure of the GluR enzyme obtained is shown in Figure 12. It is evident from the Figure 12 that this enzyme contains nine α helices and nine β strands. The model1 consists of two compact domains of α/β structure. The N-domain includes residues 1–97 and 207-264, and the C-domain includes residues 98–206. The two domains are related by pseudo 2-fold symmetry, and the active site of the enzyme is located at the interface of the two domains. The N-domain is composed of a five β-strands flanked by four helices, with two helices on each side. The C-domain consists of four β-sheet flanked by four helices, with two on each side. The C-domain 45 residues do not have equivalent pairs, so β9 and α10 are unique to the N-domain.

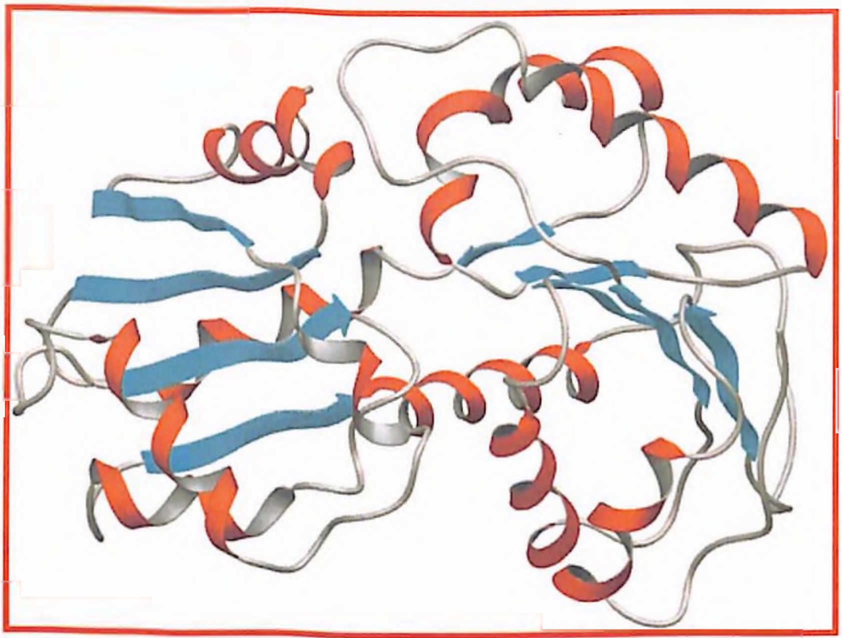

Figure 12: Refined model of Mtb GluR developed from Efa GluR. The model contains nine α helices and nine β sheets. Position of the active site between two domains is indicated by spear.

The quality of the structures of model1, model2 and Efa GluR was evaluated with Procheck. Both the structures were very similar. There were not many differences between the results of the validation parameters used for these structures. The stereo-chemical parameters calculated by Procheck can be found in Table 10. There are 37 per 100 residues, bad contacts between nonbonded atoms in the Efa GluR, but in the initial structure of model1 it was reduced to 6 per 100 residues. The energy minimization in the gas phase could be the reason for reduced bad contacts which removed disfavored interactions. The Ramachandran plot for initial structure of model1 showed 96.0% of the residues present in the most favored regions, 3.5% in allowed regions, accounting for a total of 99.5%. The corresponding plot of the Efa GluR revealed presence of 91.3% in most favored region and 8.7% of the residues in the allowed regions, respectively, with a total of 100%. Using Procheck of other stereochemical parameters as dihedral angles, covalent geometry, main-chain hydrogen bonding energy, and planarity were also examined. The G-factor was -0.05 for the initial structure of model1, compared to Efa GluR which is found to be 0.14, the larger G-factor than model1, indicated better quality for our models of the Mtb GluR. 0 to -0.5 is the most reasonable values for the G-factor in Procheck. Best models display values close to zero. Thus, the parameters obtained from the structural validation showed similar or better quality values for the initial structures of model1 compared to those of Efa GluR. Stereochemical parameters measured for model2 revealed 8 disfavorable non bonded contacts per 100 residues. The Ramachandran plot displayed 94.5% of the residues presence in the most favored regions, 4.6% in allowed regions, total of 99.1%. The G-factor was -0.08 for model2, indicating model1 is slightly better compared to model2. Procheck structural validation was also done for the models of model1 derived from MD simulation. The derived structure was minimized before the validation to remove bad contacts resulted from MD simulation. The bad contacts between non-bonded atoms were reduced from 6 to 3 per 100 residues, compared to the initial structure. The G-factor was decreased to -0.37 from -0.05 for model1. The changes were due to the increased number of bad dihedral angles of the structures, during MD simulation but at the same time it removed disfavorable non-bonded contacts. The Ramachandran plot of φ-ψ combination displayed by the MD structure of Model1 was consistent with change of the G-factor discussed above, with a decreased percentage of the residues in the core regions (83.6%) and higher percentage (15.9%) of residues in additionally allowed regions, totaling to 99.5%. which was equal to the initial structure. The temperature and velocity energy provided during MD simulation can enable protein to pass through the high energy barrier and bring unfavorable dihedral angles. This is the reason for the lower number of favorable dihedral angles in the structure resulting from MD simulation

Table 11: Results of protein structure check by PROCHECK

	Model1	Efa GluR	Model2
Residues in most favored regions	96.0%	91.3%	94.5
Residues in additional allowed regions	3.5%	8.7%	4.6
Residues in generously allowed regions	0.0%	0.0%	0.0%
Residues in disallowed regions	0.5%	0.0%	0.9%
Number of non-glycine and non-proline residues	226	231	226
Number of end-residues (excl. Gly and Pro)	2	1	2
Number of glycine residues	25	19	25
Number of proline residues	18	15	18
Total number of residues	271	266	271
G-factor	-0.05	0.14	-0.08
Bad non-bonded contact	6	37	8

PROSTAT assesses the stereochemical quality of the model. This program verifies the accuracy of parameters such as bond length, bond angle, torsion angle, and correctness of amino acid chirality. The cut-off used was 10 standard deviations from the reference value. No spurious angle or bond length was detected in model1 even after MD simulation. These geometric criteria of model1 compares well with the X-ray structure of the Efa GluR structure which is used as template. Another important indicator of the stereo chemical quality of the model is the distribution of the main chain torsion angles φ-ψ examined in a Ramachandran plot. The φ-ψ plots for model1 are shown in Figure 13, while the more detailed results are listed in Table 11. The plot showed the vast majority of the amino acids were consistent with right-handed α-helices and the remaining residues that fall into the random or beta configuration geometries of

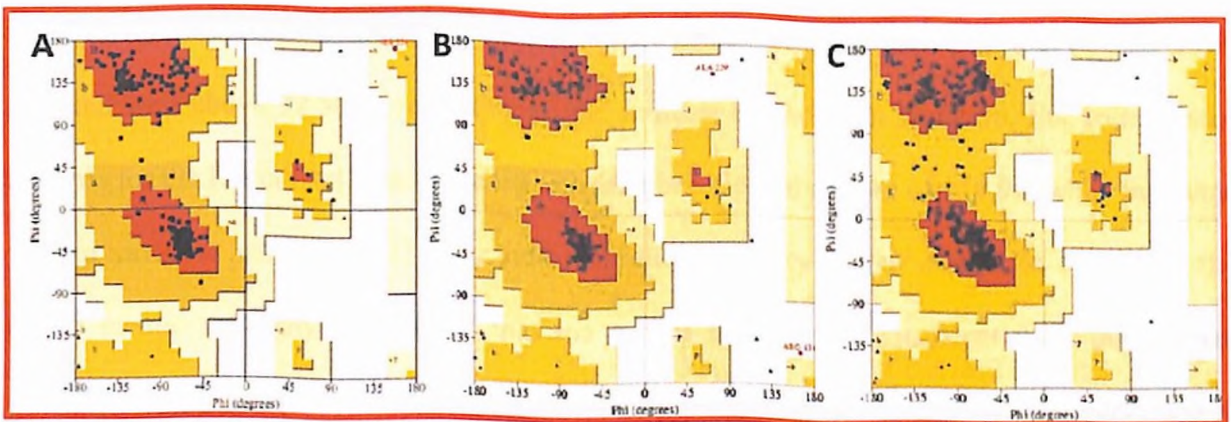

Figure 13. **A.** Ramachandran plot of the homology modeled structure of Mtb GluR (model1) based on the structure of Efa GluR. **B**. Ramachandran plot of the model2, the model available in Swiss-Prot Repository, of Mtb GluR. **C.** Ramachandran plot of the X-ray structure of Efa GluR (PDB entry 2VVT). The different colored areas indicate "disallowed" (white), "generously allowed" (light yellow), "additional allowed" (yellow), and "most favored" (red) regions.

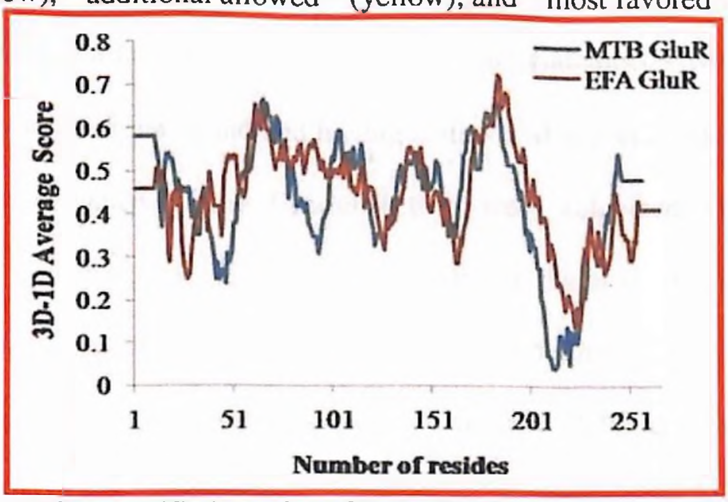

Figure 14. The 3D profiles verified results of Mtb GluR model1 in comparison to Efa GluR (template protein), where residues with positive compatibility score are reasonably folded.

the protein. A check of amino acid side chain integrity in initial structure of model1 did not show any amino acid side chain clashes with one another or with the backbone. No residues were outside the allowed regions. The initial structure of model1 was subsequently checked by Profile-3D graph. The compatibility score above zero in the Profile-3D graph corresponded to acceptable side chain environments. All residues appeared to be reasonable from Figure 14. The comparison of Profile-3D parameter for initial model1 with the Efa GluR crystal structure is shown in Figure 14. A smoothing window size of 10 residues was used. The analysis yielded an overall score of 116.80 similar to the typical score of 124.37 for a native protein of equivalent size and well above 52.56, a score that would indicate an incorrect structure. For comparison, analysis for the Efa crystal structure used as a template yielded a score of 114.96, while the range for the structure was 51.73–133.54, indicating the reliability of the model. In summary, the above mentioned analyses indicate that the model structure is consistent with our current understanding of the protein structure. The rmsd values for the minimized initial model1 and to the Efa GluR crystal structure was calculated by superimposing on each other. There was significant difference found of 10.2 Å.

4.3.2 Active site identification The GluR of different bacterial species whose crystal structure already has been solved with the ligand and having amino acid sequence identity more than 34% to Mtb GluR were collected. Using ClustalW they were subjected to multiple sequence alignment together with the GluR of Mtb (Figure 15). For the study GluR from six different bacterial species *Bacillus anthracis* (PDB id 2GZM), *Bacillus subtilis* (PDB id 1ZUW), *Enterococcus faecium* (PDB id 2JFV), *Enterococcus faecalis* (PDB id 2VVT), *Staphylococcus aureus* (PDB id 2JFQ), and *Helicobacter pylori* (PDB id 2JFX) were used. The amino acid residues around 10 Å of bound substrate were located and corresponding residues aligned to the Mtb GluR amino acid sequence were identified. These were amino acids identified to be involved in the active site of Mtb GluR. They were Asp12-Gly17, Asp38, Gly40-Tyr44, Ala74-Ala78, Gly118-Thr119, Ala121-Thr122, Val149, Gly184-Tyr188. After the final model was built, the probable binding sites in Mtb GluR were searched using the SiteMap for possible sites. These sites were compared with conserved amino acid residues identified from multiple

```
2GZM|      ----------------------KLNRAIGVIDSGVGGLTVAKELIRQLPKERIIYLGDTA 38
1ZUW|      ----------------------MLEQPIGVIDSGVGGLTVAKEIMRQLPKENIIYVGDTK 38
2JFV|      MGSSHHHHHHSSGTIEGRMIRLTDNRPIGFIDSGVGGLTVVKEALKQLPNENILFVGDTA 60
2VVT|      MGSSHHHHHHSSGLVP-RGSHMSNQEAIGLIDSGVGGLTVLKEALKQLPNERLIYLGDTA 59
2JFQ|      MGSSHHHHHHSSGLVP---RGSHMNKPIGVIDSGVGGLTVAKEIMRQLPNETIYYLGDIG 57
MtbGluR|   --------------------MNSPLAPVGVFDSGVGGLTVARAIIDQLPDEDIVYVGDTG 40
2JFX|      -------------------------MKIGVFDSGVGGFSVLKSLLKARLFDEIIYYGDSA 35
                                      :*.:******::* :  :     : : : **

2GZM|      RCPYGPRSREEVRQFTWEMTEHLLD-LNIKMLVIACNTATAVVLEEMQKQLPIPVVGVIH 97
1ZUW|      RCPYGPRPEEEVLQYTWELTNYLLENHHIKMLVIACNTATAIALDDIQRSVGIPVVGVIQ 98
2JFV|      RCPYGPRPAEQVIQYTWEMTDYLVE-QGIKMLVIACNTATAVALEEIKAALSIPVIGVIL 119
2VVT|      RCPYGPRPAEQVVQFTWEMADFLLK-KRIKMLVIACNTATAVALEEIKAALPIPVVGVIL 118
2JFQ|      RCPYGPRPGEQVKQYTVEIARKLME-FDIKMLVIACNTATAVALEYLQKTLSISVIGVIE 116
MtbGluR|   NGPYGPLTIPEIRAHALAIGDDLVG-RGVKALVIACNSASSACLRDARERYQVPVVEVIL 99
2JFX|      RVPYGTKDPTTIKQFGLEALDFFKP-HEIELLIVACNTASALALEEMQKYSKIPIVGVIE 94
           . ***.     :  .       :     :: *::***:*::  *   :    :.:: **

2GZM|      PGSRTALKVTN--TYHVGIIGTIGTVKSGAYEEALKSINNRVMVESLACPPFVELVESGN 155
1ZUW|      PGARAAIKVTD--NQHIGVIGTENTIKSNAYEEALLALNPDLKVENLACPLLVPFVESGK 156
2JFV|      PGTRAAVKKTQ--NKQVGIIGTIGTVKSQAYEKALKEKVPELTVTSLACPKFVSVVESNE 177
2VVT|      PGARAAVKVTK--NNKIGVIGTLGTIKSASYEIAIKSKAPAIEVTSLACPKFVPIVESNQ 176
2JFQ|      PGARTAIMTTR--NQNVLVLGTEGTIKSEAYRTHIKRINPHVEVHGVACPGFVPLVEQMR 174
MtbGluR|   PAVRRAVAATR--NGRIGVIGTRATITSHAYQDAFAAAR-DTEITAVACPRFVDFVERGV 156
2JFX|      PSILAIKRQVEDKNAPILVLGTKATIQSNAYDNALKQQG-YLNISHLATSLFVPLIEESI 153
           *.       .   .  : ::**  *: * :*   :        :  :* . :* .:*

2GZM|      FES-EMAYEVVRETLQPLKNTDIDTLILGCTHYPILGPVIKQVMGDKVQLISS--GDETA 212
1ZUW|      FLD-QTADEIVKTSLYPLKDTSIDSLILGCTHYPILKEAIQRYMGEHVNIISS--GDETA 213
2JFV|      YHS-SVAKKIVAETLAPLTTKKIDTLILGCTHYPLLRPIIQNVMGENVQLIDS--GAETV 234
2VVT|      YRS-SVAKKIVAETLQALQLKGLDTLILGCTHYPLLRPVIQNVMGSHVTLIDS--GAETV 233
2JFQ|      YSDPTITSIVIHQTLKRWRNSESDTVILGCTHYPLLYKPIYDYFGGKKTVISS--GLETA 232
MtbGluR|   TSG-RQVLGLAQGYLEPLQRAEVDTLVLGCTHYPLLSGLIQLAMGENVTLVSS--AEETA 213
2JFX|      LEG-ELLETCMHYYFTPLEILP-EVIILGCTHFPLIAQKIEGYFMGHFALPTPPLLIHSG 211
              .          :        : ::*****:*::   *   :  :  :  .    .:

2GZM|      REVSTILYHSKMLNEGEE-QSDHLFLTTGKIGLFKEIASKWFGQPIENVKHIHLEK---- 267
1ZUW|      REVSTILSYKGLLNQSPI-APDHQFLTTGARDQFAKIADDWFGHEVGHVECISLQEPIKR 272
2JFV|      GEVSMLLDYFNLSNSPQNGRTLCQFYTTGSAKLFEEIAEDWLGIGHLNVEHIELGGK--- 291
2VVT|      GEVSMLLDYFDIAHTPEAPTQPHEFYTTGSAKMFEEIASSWLGIENLKAQQIHLGGN--- 290
2JFQ|      REVSALLTFSN-EHASYTEHPDHRFFATGDTTHITNIIKEWLNLSVN-VERISVND---- 286
MtbGluR|   KEVVRVLTEIDLLRPHDAPPATRIFEATGDPEAFTKLAARFLGPVLGGVQPVHPSRIH-- 271
2JFX|      DAIVEYLQQKYALKNNACTFPKVEFHASGDVIWLERQAKEWLKL---------------- 255
             :   *      .          * ::*    : .    ::
```

Figure 15: Multiple sequence alignment together with Mtb GluR. The residues inside box are amino acid residues around 10 Å of bound substrate. They were Asp12-Gly17, Asp38, Gly40-Tyr44, Ala74-Ala78, Gly118-Thr119, Ala121-Thr122, Val149, Gly184-tyr188. For the study GluR from six different bacterial species *B. anthracis* (PDB id 2GZM), *B. subtilis* (PDB id 1ZUW), *E. faecium* (PDB id 2JFV), *E. faecalis* (PDB id 2VVT), *S. aureus* (PDB id 2JFQ), and *H. pylori* (PDB id 2JFX) were used.

alignment process. The site1 was common and matched with site identified by multiple sequence alignment process. There were two important amino acid residues in Mtb GluR Cys75 and Cys185 (Cys94 and Cys205 in Efa GluR) which are mainly involved in the racemization of D and L glutamate by deprotonation and reprotonation. These residues were seen at site1 further confirmed the ligand binding site. The 85% of amino acid residues in site1 was found to be conserved. It is observed that the amino acid residues at site1 Asp12, Ser13, Gly14, Val15, Gly16, Gly17, Gly37, Asp38, Pro43, Tyr44, Gly45, Ala74, Cys75, Asn76, Ala78, Gly118, Thr119, Val149, Gly184, Cys185, His187 and Tyr188 were conserved with the active site of template protein Efa GluR (Figure 16). Other than these residues at the active site of Efa GluR has Thr96 which has been replaced with similar but smaller polar amino acid Ser77, Cys61 has been replaced with much smaller hydrophobic amino acids Gly42, amino acid Arg60 has been replaced with much less polar smaller amino acid Asn41, and Gly140 has been replaced with more non polar Ala121 respectively in Mtb GluR. Thus the replacement of the residues in Mtb GluR has made its active site more hydrophobic and larger cavity compared to the template. Thus, site1 was chosen as the most favorable binding site to dock the substrate and the inhibitors and the remaining sites identified by SiteMap was therefore not discussed further. Since both the proteins have very high homology at active site, ligands and inhibitors are suggested to bind in a similar manner for both the Mtb and Efa GluR.

4.3.3 Molecular Docking A protein ligand complex would offer a more detailed and accurate information of the interactions and structural complementarities between the ligands and the active site. To identify possible active site for docking and to understand the ligand binding pattern of the ligands, the PDB was searched for solved crystal structures of GluR in complex with ligands. The crystal structure of Efa GluR, which used as template for homology modeling, was structurally aligned with model1. Active sites of both structures were carefully analyzed, and differences in the residue positions were identified. The active site of Efa GluR was highly conserved to the extent of 85%. There are only a few different amino acid residues within the active site of both GluR such as, Gly42, Asn41, Ser77 and Gly121. All the amino acid replacements were with residues of similar physicochemical properties. Hence a similar binding pattern of ligand binding to the protein was expected with Mtb GluR to that of Efa GluR. Initially the Mtb GluR model was superimposed with 2VVT. The atomic co-ordinates of the ligands from 2VVT were then transferred to the Mtb GluR, which was taken as initial point for the docking simulation. Docking simulation was run using Standard Precision (SP) in Glide module present in Schrodinger. Before running the docking simulation for our model the docking parameters were set by redocking the glutamate to 2VVT, which resulted into a docking pose with rmsd 0.415 Å to the crystal pose. The same parameters were then used for docking glutamate to Mtb GluR. All the top ten docking poses for the glutamate with Mtb GluR had rmsd less than 2 Å to the initial crystal co-ordinates obtained from 2VVT indicating consistent docking poses. The best pose had least rmsd of 1.38 Å. Side chains of Asp12, Ser13 and Thr186 are involved in the stabilization of α-amino group by H-bond formation, side chains of Cys75, Ser77 and Thr186, amino group of peptide backbones of Ser77, Asn76 and Thr186 were stabilizing the α-carbonyl group by formation of H-bond. Hydrophobic pocket formed by the side chains of amino acid residues Val15, Pro43, Thr119, Val149, Glu153, Cys185, His187 were stabilizing the side chain atoms of glutamate to give the required orientation for racemization reaction (Figure 16). Other than these Gly14, Val15, Gly16, Asp38, Gly40, Gly42, Tyr44, Ala121, Thr122, were present within 10 Å of glutamate. The electrostatic surface view shows a prominent extension of the hydrophobic pocket towards the exterior of the receptor.

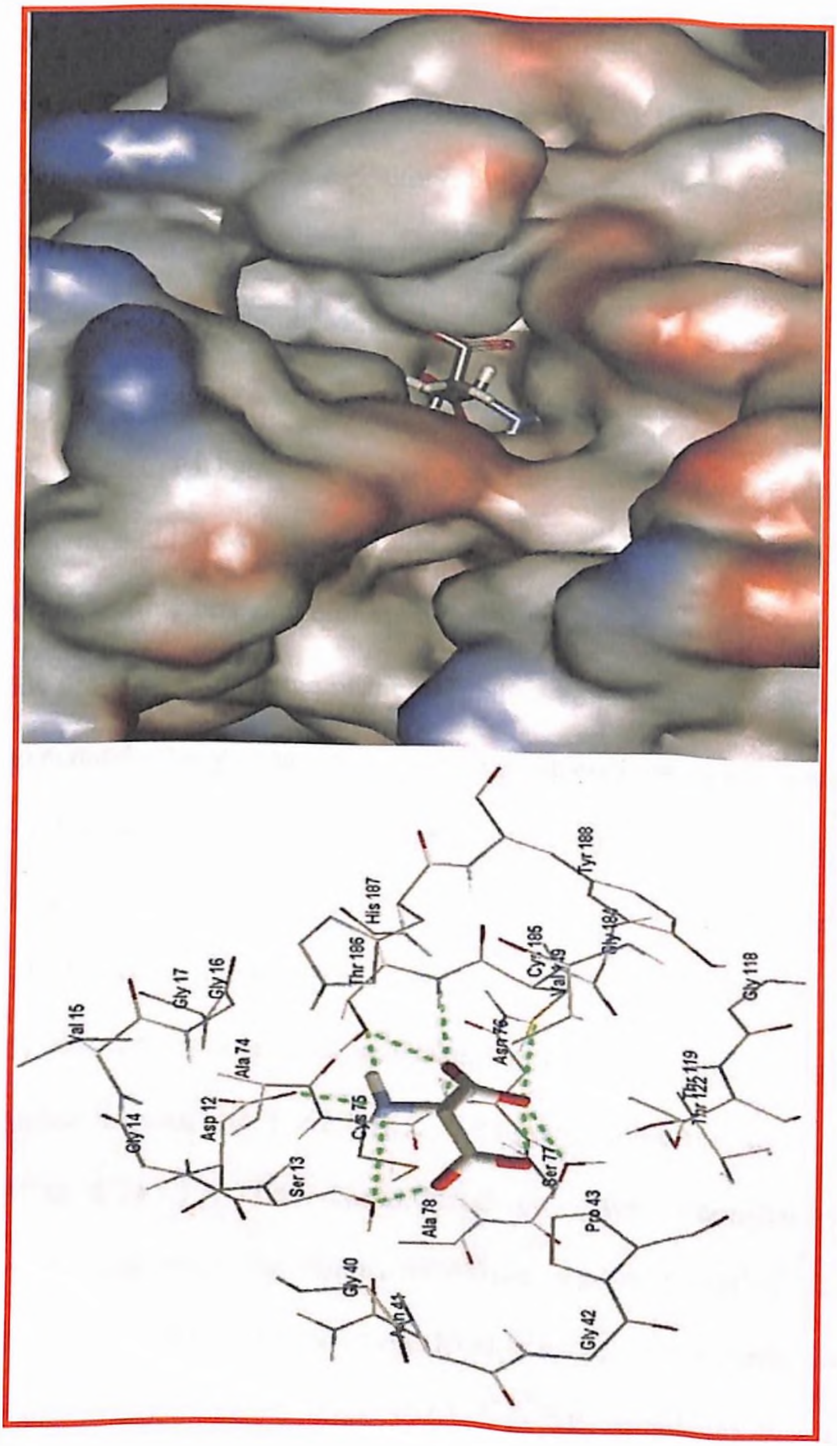

Figure 16: Schematic representation of interactions of the glutamate and Mtb GluR complex in the active site (left), H-bonds are shown as green colored dashed lines. Surface view of Mtb GluR with glutamate docked inside the active site pocket (right).

4.3.4 MD simulation There were two models for Mtb GluR, one called model1 the model developed by us using Efa GluR crystal structure (PDB entry 2VVT), and the model2 the model available at Swiss prot repository, built based on the crystal structure of *B. subtilis* GluR (PDB entry 1ZUW). The only difference between the two models was observed large across amino acid residue back bone. Molecular dynamics was run to compare the stability of both models and to check which is a better model compared to each other. For this both model1 and model2 was subjected to MD simulation. The simulations were run using explicit water model. The Desmond system builder was used to add TIP3P water molecules. Water molecules were added in an orthorhombic box shape of such that there was at least 10.0 Å of water between the surface of the protein and the edge of the simulation box. This was to overcome the errors that could have generated during long range columbic interactions which was set 9Å. For model1, a total of 13,036 water molecules were added, after removing the overlapping water molecules on protein, in an orthorhombic box of 80.77 X 72.07 X 80.99. The overall charge on the system was -8 which was neutralized by addition of Na+ ions. The sodium ions were added at random positions by system builder but care was taken not to include counter ion within 7Å distance from ligand molecule glutamate. For model2, 10,836 water molecules were added in an orthorhombic box of 71.16 X 74.23 X 71.59. The solvated system was minimized by force field to relax the added water molecules. The minimized system was subjected to 1.2 ns MD simulation. The time duration for the simulation was decided based on the earlier experience on working with the same protein in our laboratory. [A 5 ns MD simulation was run on the same protein using explicit water model (continuum water model) did not show much deviation after a time span of 0.6 ns.] To compare two different structures first, the protein structures generated during MD simulation were reoriented in order to minimize the rmsd of the backbone atoms of the enzyme and ligand system with respect to the corresponding atoms of the first structure. Then rmsd of backbone atoms of the protein and ligand of the reoriented second structure with respect to the corresponding atoms of the first structure were calculated. For both the models, based on the measurement of the root-mean-square deviation (rmsd) of the positions of the backbone atoms from those in the initial structure along the simulation time, the MD simulation showed drastic changes for about initial 50 ps, then after about 200 ps the system showed a steady dynamics. The rmsd of the backbone of protein and ligands for model1 and model2 are shown in Figure 18A. After 200 ps, the total rmsd of backbone of model1 stabilized at around 1.66 to 2.10 Å. From 200 ps to till end of 1200 ps of simulation, that is for 1000 ps duration the total rmsd of model1 was stabilized within a range of 0.44 Å, suggesting that 1.2 ns of simulation was more than sufficient for stabilizing a fully relaxed model and the core structure of the protein was stable during the MD simulation. The rmsd of the ligand drastically changed for initial 50 ps. From 50 to 1200 ps the rmsd of ligand in model1 remained stable within range of 0.37 and 0.69 Å Efa to the initial structure. The rmsd of the ligand with respect to, the initial structure of model1 and the last structure generated during the simulation is small and remained constant within range of 0.32 Å throughout the trajectory. This indicates that there is a very small difference between the two reference structures. During the first 50 ps there was larger change which was to reach a more stable conformation. The average rmsd of the ligand calculated was 0.45 ± 0.09 Å with respect to the initial and the last frame generated during the MD simulation trajectory, which is very close and is relatively small compared to the calculations made for ligand in model2. For model2 after 200 ps, the total rmsd of backbone stabilized at around 2.05 to 2.75 Å. The model2 back bone rmsd changed over a range of 0.70 Å for 1000 ps duration during the simulation. The rmsd of the ligand drastically changed for initial 50 ps, then there was a drift in rmsd for around 135 ps duration from 230ps to 365ps (0.6–1.32 Å) then again it remained within range of 0.18 to 0.7 Å, except for 10 ps duration near 880-890 ps where again there was a large drift in rmsd. The rmsd of the ligand with respect to the initial structure of model2 and the last structure generated during the simulation changed over a range of 1.14 Å throughout the trajectory. The average rmsd of the ligand calculated was 0.47 ± 0.26 Å with respect to the initial and the last frame generated during the MD simulation trajectory, which has relatively far large standard deviation compared to the calculations made for ligand in model1. This indicated the better stability of the model1 over model2 as far as case of ligand binding is concerned. The overall rmsd across the backbone of the model1 remained constant compared to model2. The model2 exhibited higher range of change in backbone. The overall rmsd change observed during the MD simulation for the backbone was also higher for model2 compared to model1. The ligand exhibited lot of fluctuations in model2 during the simulation evident from the large deviation observed in rmsd. The Figure 17A shows the rmsd across the back bones and ligand for model1 and model2 evolved during MD simulation.

Tenner and Glavas established the mechanism for cofactor independent GluR enzyme by carrying out several site directed mutation study. Their work evidenced the importance of two cysteine residues at active site, which bring out the racemization of glutamate. They explained two base mechanism where the first cysteine deprotonates the α-carbon of glutamic acid and the second cysteine present at the opposite side reprotonates the glutamic acid resulting in an inverted stereochemistry for the final product. Thus the distance between the C75 and C185 is a critical parameter, which was considered to check the quality of the GluR models during MD simulation. The Figure 17B shows the evolution of the distance between two cysteine sulphur moieties during the 1.2 ns MD simulation for model1 and model2. For model1 the distance between the two sulphur moieties of cysteine, from trajectory of 200 to 1000 frames recorded during simulation was within the range of 6.80 to 8.84 Å. On an average for model1 the distance observed was 7.7 ± 0.44 Å from initial point to last structure generated during dynamics run. The model2 exhibited the distance between the sulphur of the two catalytic cysteine moieties was within range of 7.33 to 9.95 Å, from frame 200 to 1000, and the average distance from initial frame to last frame was 8.48 ± 0.39 Å. For Efa GluR crystal and the *B. subtilis* (BS) GluR crystal, the distance observed was 7.40 and 7.36 Å respectively. The distance observed for the model2 was higher compared to the model1. The average distance measured was 0.3 Å more than what was observed for the crystal structure of Efa GluR, which was used as template. This difference was within the range of standard deviation observed for model1. The difference was more than 1 Å for model2 and the crystal structure of GluR of BS. The observed large range is unusual compared to both the crystal structures of Efa and BS GluR.

Glavas and coworkers, from mutation study identified that the nearby residues are also involved in catalysis; that is by stabilizing the generated thiolate intermediates. These residues are Asp10 and His188, which are highly conserved residues. These are situated within 3.8 to 4.7 Å to the catalytic cysteine sulphur in Efa and BS GluR. The first step of the racemization corresponds to the abstraction of a proton from the thiol group of the Cys75 from D-glutamate to form thiolate intermediate. The thiolate intermediate formed is stabilized by side chain carboxyl group of Asp10. In case of model1 the average distance measured from initial frame of the trajectory to the final frame was 4.4 ± 0.39 Å. The model2 showed average distance of 4.4 ± 0.79 Å. These average distances were higher compared to the distances observed in both Efa and BS GluR crystal structures, which were 3.82 and 3.80 Å respectively. The next step in the catalysis is the reprotonation of ligand, which is brought about by proton donation by C185. The intermediate formed in this step is stabilized by His187. For model1 the distance between cysteine sulphur and the histidine amine group ranged 3.62 to 5.63 Å with an average distance 4.5 ± 0.28 Å. For model2 the distance ranged between 3.46 to 5.78 Å with average value 4.9 ± 0.37 Å. The crystal structure of Efa GluR exhibited the distance of 4.30 Å and the BS showed a distance of 4.20 Å. The difference in the values observed for model1 and the crystal structures was within the range of the standard deviation observed, but the model2 showed slightly higher average value than that observed for the modlel during the MD simulation. The model2, for initial 200 ps, the distance was at lower side but in later phase of simulation, when the protein got relaxed the distance increased and stabilized around 4.94 Å. The Figure 17C and Figure 17D show the evolution of distances between Cys185 and His187 and Cys75 and Asp10 during the MD simulation.

The distance between the sulphur atom of C75 and the α-carbon of glutamate is very important factor during the proton abstraction. The distance varied from 3.38 to 5.94 Å for model1 during the MD simulation. The average distance throughout the simulation was 4.0 ± 0.38 Å. For the first 60 ps in the evolution of the MD simulation the distance increased, but later it got stabilized. In the crystal structures of Efa and BS GluR the sulphur of C75 and α-carbon atom are located at a distance of 3.44 Å and 3.51 Å respectively. The distance varied from 3.53 to 6.10 Å for model2 during the simulation and the average distance was 4.45 ± 0.35 Å. The distance observed in the case of both the models were higher than the distance present in both the crystal structure, but the model2 showed about 1 Å higher distance than the BS GluR, which was used as template for its model construction. The distance between the sulphur atom of C185 and the α-carbon of glutamate varied from 3.49 to 4.85 Å for model1 during the simulation. The average distance throughout the simulation was 4.01 ± 0.20 Å. The distance varied from 3.71 to 5.33 Å for model2 during the simulation and the average distance was 4.53 ± 0.23 Å. In the crystal structures of Efa and BS GluR the sulphur of C185 and α-carbon atom are located at a distance of 4.38 Å and 4.27 Å respectively. The distance observed was less for model1, compared to both the Efa and BS GluR crystals, but model2 showed a higher distance between sulphur of C185 and α-carbon of glutamate. It was also evident that the distance between sulphur moieties of two catalytic cysteine residues was higher than the observed distance in both of GluR crystals used as templates for building respective models. Figure 18E and Figure 18F shows the evolution of distance between the sulphur atom of C75 and C185 to α-carbon atom of Glutamate.

The Asn76, Ser77 and Thr186 in the active site of GluR stabilize the ligand, glutamate by forming multiple H-bonds. The backbone NH forms H-bond with α-carboy group. The average distance throughout the simulation, between the backbone NH of Asn76 with α-carboy group was 3.0 Å, comparable to the distances observed in the Efa and BS GluR crystals, which was 3.0 Å and 3.02 Å respectively. The model2 exhibited 2.90 Å, which was not different from that observed for the Efa and BS GluR crystals. The Ser77 backbone NH and the side chain OH forms H-Bond with the glutamate. In model1 the average distance throughout the MD simulation between sidechain OH of Ser77 to α-carboy group of glutamate was 1.76 Å and the average distance between the backbone NH of Ser77 to α-carboy group of glutamate was 1.73 Å. In model2 average distance throughout the simulation between sidechain OH of Ser77 to α-carboy group of glutamate was 1.85 Å and the average distance between the backbone NH of Ser77 to α-carboy group of glutamate was 1.81 Å. In Efa and BS GluR crystals The Ser77 is replaced with Thr77. The distance between sidechain OH of Thr77 to α-carboy group of glutamate was

1.78 Å and 1.66 Å Efa and BS GluR crystals respectively. The distance observed in case of backbone NH of Thr77 to α-carboy group of glutamate was 1.66 Å and 1.67 Å for Efa and BS GluR crystals respectively. The Thr186 backbone NH and the side chain OH forms H-Bond with the glutamate. In model1 the average distance throughout the MD simulation between sidechain OH of Thr186 to amine group of glutamate was 1.80 Å and the average distance between the backbone NH of Thr186 to α-carboy group of glutamate was 1.74 Å. In model2 average distance throughout the simulation between sidechain OH of Thr186 to amine group of glutamate was 1.74 Å and the average distance between the backbone NH of Thr186 to α-carboy group of glutamate was 1.84 Å. In Efa and BS GluR crystals the distance between side chain OH of Thr186 to amine group of glutamate was 1.82 Å and 1.92 Å respectively. The distance observed in case of backbone NH of Thr186 to α-carboy group of glutamate was 1.80 Å and 1.93 Å for Efa and BS GluR crystals respectively. The comparison all these H-bond distances of model1 and model2, with the crystal structures did not show much difference. They were all in same range without exhibiting differences in the models.

The residues Ser10, Tyr44 and Gly45 form the H-Bond with the γ-carboxyl group of glutamate. These amino acid are located on the loop regions of GluR. They by forming H-bond not only stabilize the glutmate but also provide the correct orientation so that the racemization takes place by two base mechanisms as explained by Tunner and Glavans. The side chain OH of Ser10 forms H-Bond with γ-carboxyl group of glutamate. Distance measured during the MD simulation of model1 from 200 ps to 1200 ps showed a range of 1.58 to 3.29 Å, with an average value of 2.51 ± 0.25 Å. The crystal structures exhibited a distance of 2.53 Å and 2.54 Å for Efa and BS GluR crystals respectively, which was within the range standard deviation of the average distance calculated from the structures generated during MD simulation. The distance recorded during the MD simulation indicated that the H-bond stabilization was present in all structures evolved during simulation of model1. In the case of model2 the H-bond stabilization was absent, which is evident from distances calculated from the structural samples from MD simulation. The distance between the OH of Ser10and the γ-carboxyl group of glutamate in the simulation ranged from 5.69 to 9.39 Å with an average value of 6.80 ± 0.59 Å. In this distance range no H-bond formation is possible. The amino acid residue Tyr44 by forms H-bond through backbone NH group with γ-carboxyl group of glutamate. Distance measured during the simulation of model1 from 200 ps to 1200 ps ranged between 1.50 to 2.73 Å, with an average value of 1.87 ± 0.16 Å. The crystal structures exhibited a distance of 1.71 Å and 1.82 Å for Efa and BS GluR crystals respectively, the distance calculated for model1 was within the range standard deviation of the average distance calculated from the structures generated during MD simulation. The distance recorded during the MD simulation indicated presence of strong H-bond stabilization in all structures generated during simulation of model1. In the case of the model2 the H-bond stabilization was weak or absent, evident from the distances calculated from the structures sampled during simulation. The distance between the backbone NH of Tyr44 and the γ-carboxyl group of glutamate in the simulation ranged from 1.62 to 6.95 Å with an average value of 3.93 ± 0.73 Å. The distance between the backbone NH of Tyr44 and the γ-carboxyl group of glutamate was small initially, but gradually increased during simulation. The H-bond became weak along the MD simulation for model2. Similar type of tendency was observed with the Gly45 during MD simulation for model2. The backbone NH group forms H-bond with γ-carboxyl group of glutamate. The distance between the backbone NH of Gly45 and the γ-carboxyl group of glutamate in the simulation ranged from 1.54 to 8.56 Å with an average value of 3.33 ± 1.40 Å. The distance between the backbone NH of Tyr44 and the γ-carboxyl group of glutamate was small initially, but gradually increased during simulation. The H-bond was absent in the frames collected after 250 till the last frame. Distance measured for model1 between the backbone NH of Gly45 and the γ-carboxyl group of glutamate, during the simulation of model1 from 200 ps to 1200 ps ranged between 1.49 to 2.25 Å, with an average value of 1.92 ± 0.11 Å. The crystal structures exhibited a distance of 1.87 Å and 2.11 Å for Efa and BS GluR crystals respectively. The average distance calculated during simulation for model1 was shorter than distance present in both GluR crystals. The distance recorded during the MD simulation indicated presence of very strong H-bond stabilization in all structures generated during MD simulation of model1. Figure 18 shows the evolution of distance between Ser10, Tyr44 and Gly45 to γ-carboxylate moiety of glutamate.

The Figure 19C presents the comparison of the different distance parameter used to bring comparison of model1 and model2 with the crystal structures of Efa and BS GluR, which was used as template to build the respective homology models. From the graph it can be seen that in most of the instances the red pillar is prominently emerging outside, corresponding to the model2, specially the three residues which are involved in stabilization of γ-carboxylic group of glutamate, the Ser10, Tyr44 and Gly45. The average distance between the two catalytic cysteine sulphurs was also very high for model2 compared to other structures. From this graph it is very much evident that the model1 presented a better structure for the Mtb GluR compared to the model2. Even though there were no drastic changes observed in the back bone rmsd for model2, it showed large rmsd deviation for the ligand during MD simulation. The fluctuation in the ligand indicated internal destabilization of the protein ligand complex, where as in model1, throughout the simulation the system was very stable Figure 19A and 19B presents the superimposed few representative structures (frame0, frame400, frame600, frame800, frame1000) of the model1and model2 generated during the 1.2 ns MD simulation. From the figure it is clear that for model2 there was large fluctuation in the glutamate binding pattern, the glutamate presented a flip during the simulation. This is mainly because of the absence on the H-bonds with Ser10, Tyr44 and Gly45. In model2, during the MD simulation the loop changed the conformation, the loop moved away from the original position. From the Figure 19B it can be seen that the loop took an extended conformation, due to which the loop moved far away from the ligand. In this extended conformation formation of the H-bonds was not possible. All the three H-bond was present in the initial structure of model2, but after about 200 ps the residues involved in the loop started adopting the extended conformation. In the absence of the H-bond the ligand was free to rotate. The comparison of the crystalized structure with and without the ligand of BS and for *A. pyrophilus* GluR structures did not show much difference and the rmsd difference was within 0.5 Å for the structures. This indicates there are no much structural changes occurring due to ligand binding in the GluR. Under such circumstances the loop moment occurring in the model2 is not acceptable. The loop moment did not occur in model1, indicated good stability of the model1 over model2.

The rotameric conformation generated for the model2 was different from Model1. Figure 20 shows the superimposed structure of active site from initial structure of model1 and model2. In the picture it is very much evident that the amino acid residues Ser72, Asn76, Thr114 and Val144 have taken different conformation. These are amino acids which stabiles the ligand glutamate by forming H-bonding and Van-der-waals interaction. These interactions are responsible for the proper positioning and the orientation of the D-Glu within the active site. Since the conformers of these amino acid residues were different the ligand glutamate has docked with different orientation in model2. There was large rmsd difference of 1.07 Å was observed between the docked poses of glutamate in model1 and model2. The α-carbon of glutamate was tilted in position compared to the orientation observed in model1. In model1 the α-carbon of glutamate is almost exactly on the line joining the two sulphurs Cys74 and Cys185. But in the case of model2 the α-carbon of glutamate does not fall on the line joining the two sulphurs Cys74 and Cys185, but is little bit upside, also its position is moved so that the amine moiety is falling close to the Cys185, and forms H-bond with sulphur.

The model2 has different rotamers for the amino acids, mainly for Ser72, Asn76, Thr114 and Val144. The Figure 20 is the superimposed active site of few structures samples from MD simulation of model2 with initial structure of model1. The superimposition of the active site from the first frame of model2 with initial structure of model1 revealed occupancy of different conformation for the amino acid residues Ser72, Asn76, Thr114 and Val144. The conformation for both catalytic cysteines was same in both models of Mtb GluR, also for the Ser10. But during the simulation rum the conformation started changing in model2. The model2, during simulation changed its conformation to the one which model1 is already having, which is evident from the snaps recorded during the simulation run (Figure 20). This was also evident from the potential energy of model2 recorded during the simulation time. The initial conformation of the model was corresponding to higher energy levels. During MD simulation the conformation of the amino acid residues changed and the potential energy of the protein got reduced. This is the reason for the internal instability of the model2, due to which the ligand showed fluctuations during the simulation. The change of rotamers towards the model1 indicated that the model1 is more stable, and MODELLER had predicted the correct rotamers for the amino acid residues from the probability density functions. There was no much changes observed in the amino acid residues conformation for model1 during the MD simulation. The change in the conformation bought about in model2 during the MD simulation distracted the overall arrangement of the structure, especially on the loop region, which moved away from the original position during the simulation by taking extended conformation. This movement in the loop caused the breakage of the H-bond, which resulted in to the flipping of the ligand within the active site of model2.

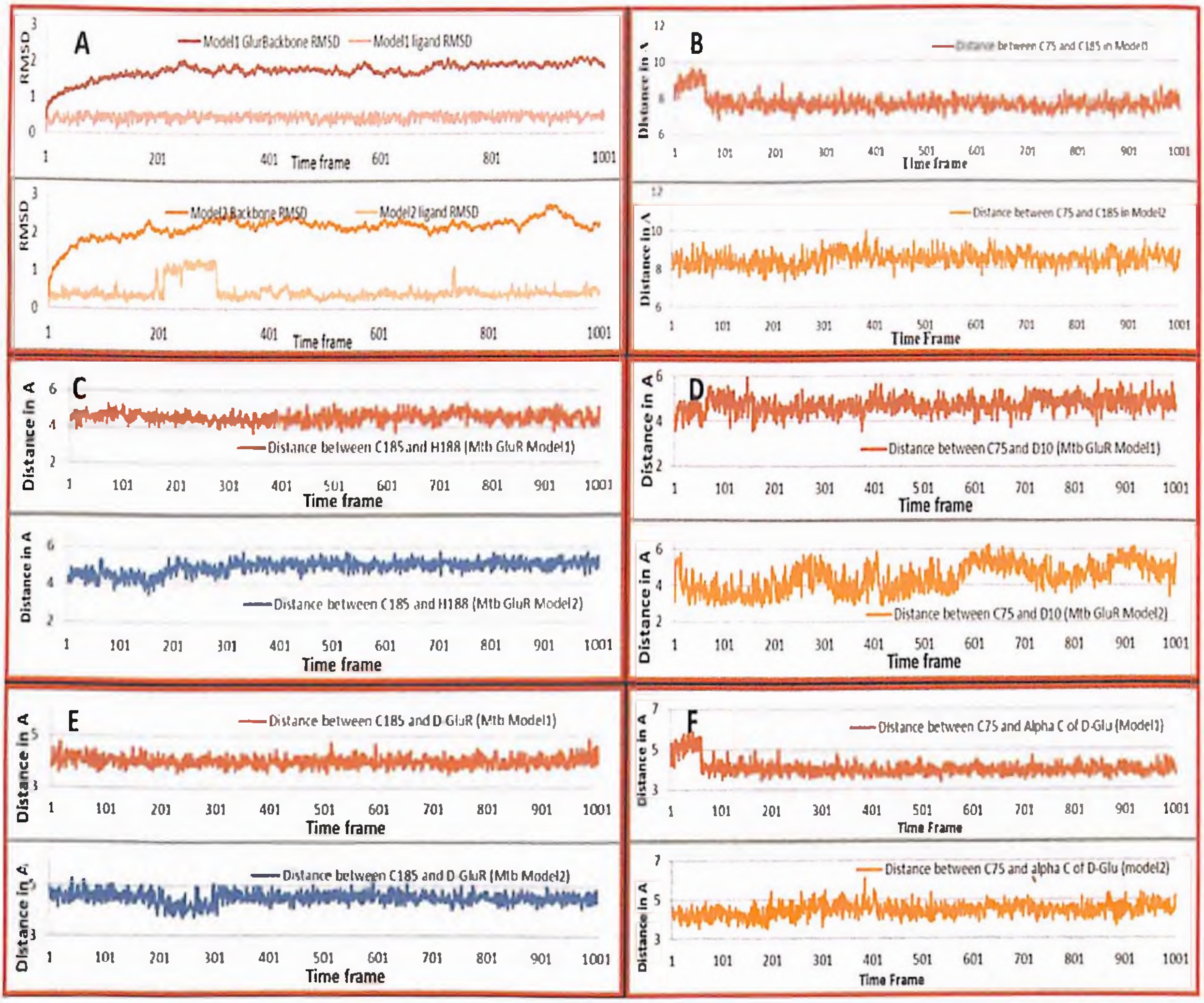

Figure 17. **A.** The rmsd across the back bones and ligand evolved during MD simulation for model1, modeled based on the structure of Efa GluR and model2 model available in Swiss-Prot Repository. **B.** Distance evolved between Cys75 and Cys185 during MD simulation of model1and model2. **C.** Distance evolved between Cys185 and His187 during MD simulation of model1and model2. **D.** Distance evolved between Cys75 and Asp10 during MD simulation of model1and model2. **E.** Distance evolved between Cys185 and α-carbon of glutamate during MD simulation of model1and model2. **F.** Distance evolved between Cys75 and α-carbon of glutamate during MD simulation of model1and model2.

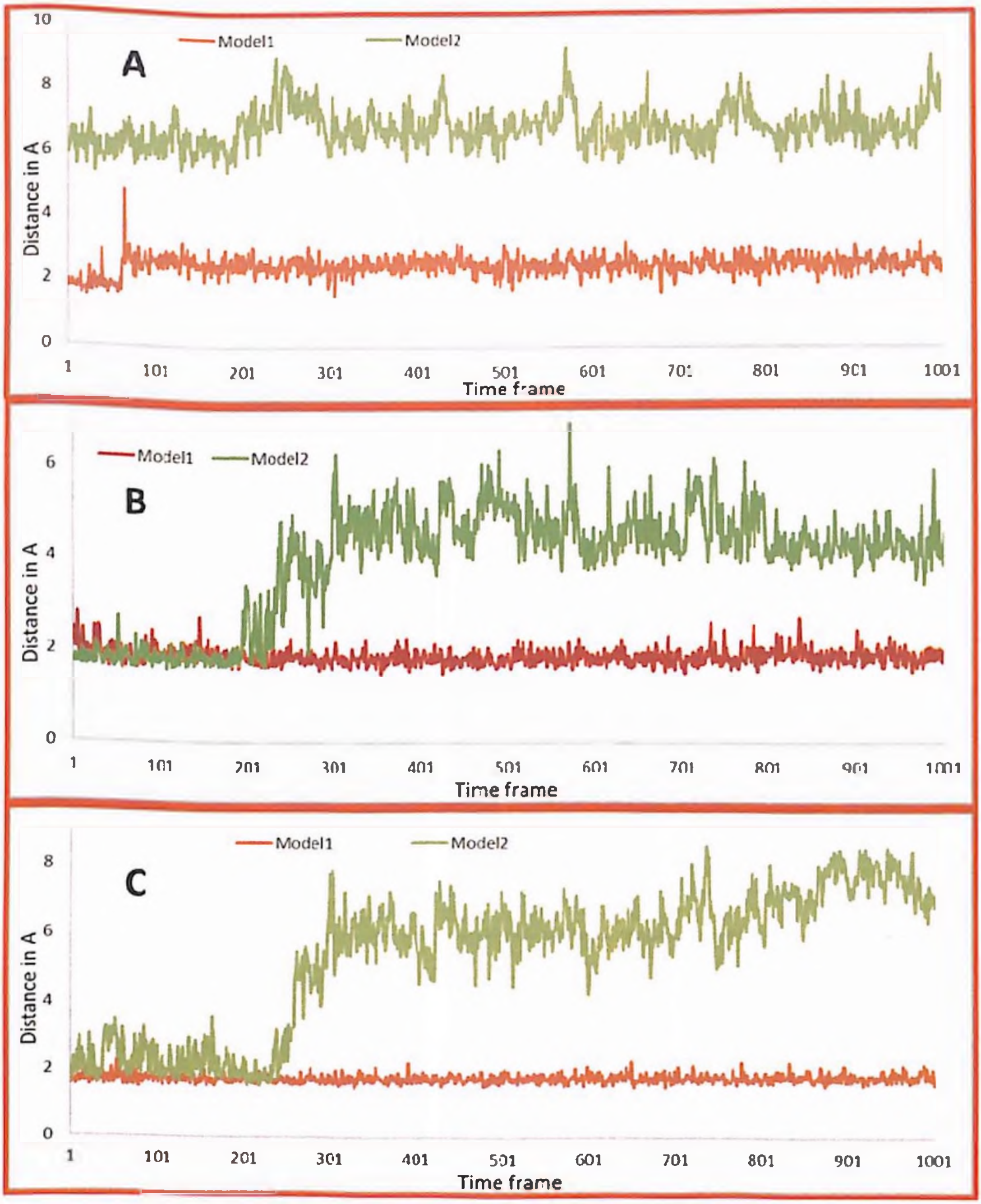

Figure 18. **A.** Distance evolved between OH of Ser10 and γ-carboxyl moiety of glutamate during MD simulation of model1and model2. **B.** Distance evolved between backbone NH of Tyr44 and γ-carboxyl moiety of glutamate during MD simulation of model1and model2. **C.** Distance evolved between backbone NH of Gly45 and γ-carboxyl moiety of glutamate during MD simulation of model1and model2.

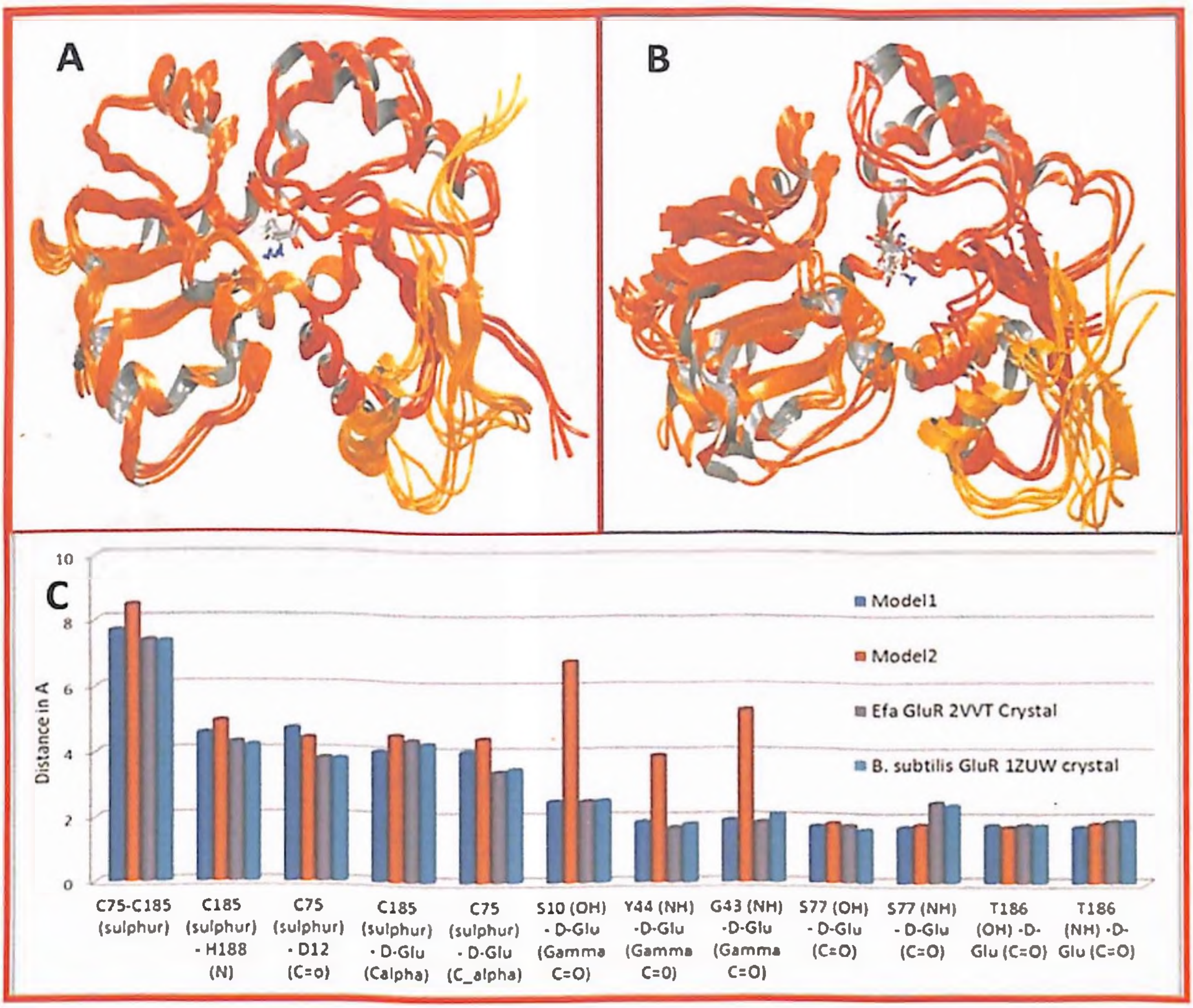

Figure 19. **A.** Superimposed few representative structures (Frame0, Frame400, Frame600, Frame800 and Frame1000) of the model1 generated during the 1.2 ns MD simulation. **B.** Superimposed few representative structures (Fame0, Frame400, Frame600, Frame800 and Frame1000) of the model2 generated during the 1.2 ns MD simulation. **C.** Comparison of the different distance parameter used to bring comparison of model1 and model2.

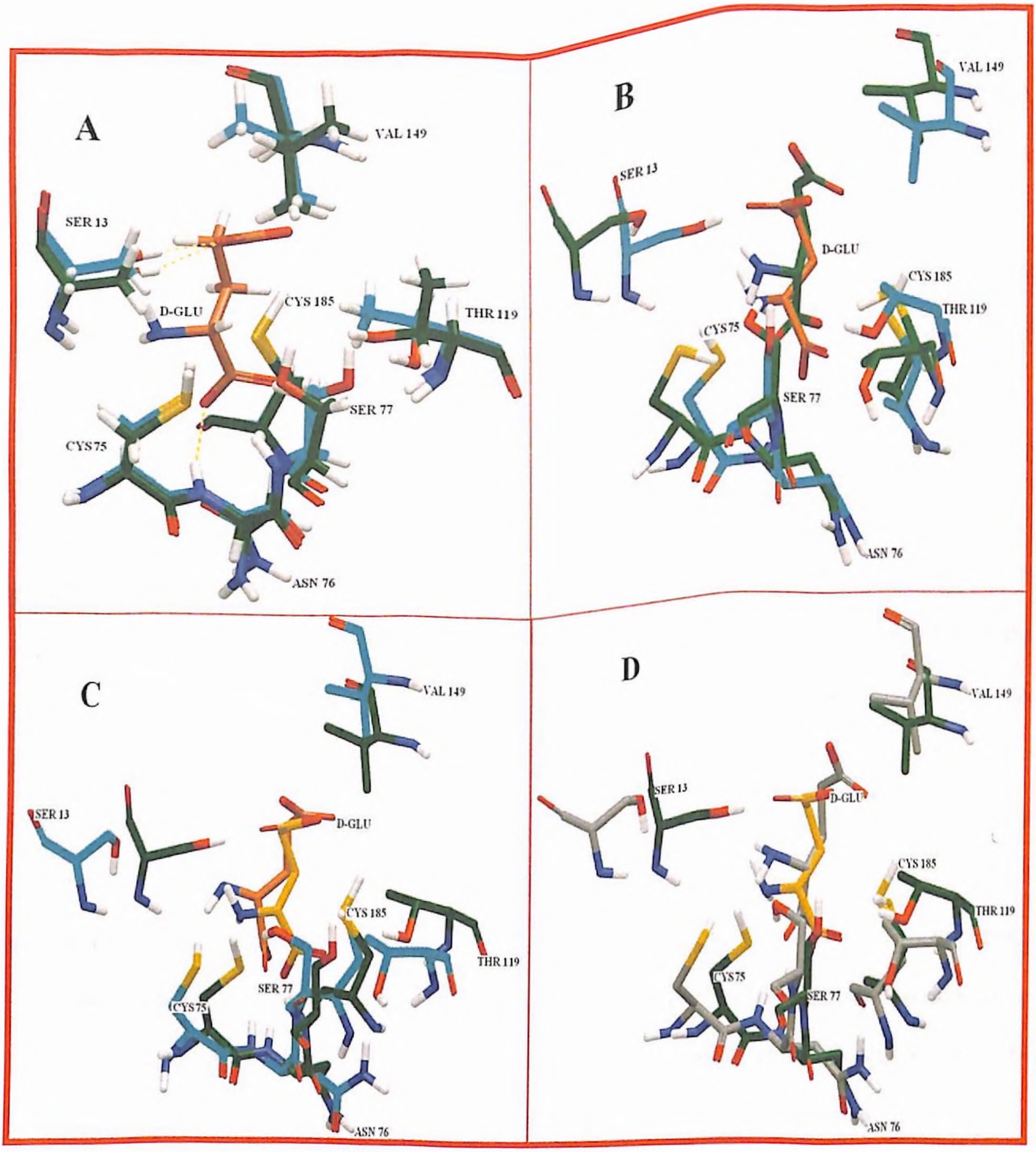

Figure 20. The superimposed structure of active site from initial structure of model1 and model2, the amino acid residues Ser72, Asn76, Thr114 & Val144 have taken different conformation. Comparison of changes evolved in the conformation during the MD simulation from Frame0 (A), Frame400 (B), Frame600 (C) and Frame1000 (D). (model1 is presented with green color, model2 is presented with blue in frames A, B & C, gray in frame D)

GluR has been identified as a promising drug target in protozoan parasites and the structural information of Mtb GluR is of great importance to design specific inhibitors of mycobacteria. The lack of the availability of the crystal structure necessitated the need to go for the homology based model building of the Mtb GluR, and the structural information could be used for the design of the inhibitors. The 3D structural model of Mtb GluR was constructed, based on known crystal structures of Efa GluR. It was found that there was one more model of Mtb GluR available in Swiss-prot repository. Since the developmental methodology was not known for the Swiss-prot repository model, to check the genuineness of the model, a thorough validation of the model structure was needed. The primary evaluation of the model did not present much difference between the two models. So for validation of the both models, 1.2 ns MD simulation was run for both the model. Different distance parameters were studied from the trajectory recorded, for the comparison of the two models. The comparison showed model developed by us of Mtb GluR is better to the model reported in Swiss-prot repository. The structures evolved during the MD simulation showed drastic changes especially in the loop region. This resulted into loss of important H-bond between the ligand glutamate and residues involved in the loop regions in model collected from Swiss-prot repository. The backbone interactions of Tyr44 and Gly45; side chain interaction from Ser10 was very important in stabilizing the glutamate to hold the glutamate in proper orientation at active site of GluR. In Swiss-prot repository model all the three H-bond got broken during the MD simulation, which resulted in to flipping of the glutamate, whereas the model generated by us was steady throughout the simulation with not much change in the structures of protein or ligand glutamate. These results ensured that our structural model generated by using Efa GluR as template is better compared to the Swiss-prot model. Structural models built in this study can be used in inhibitor design for discovery of new lead compounds which can inhibit Mtb GluR.

4.4 Virtual screening of the database for inhibitor for inhibitor identification The virtual screening of the database was carried by docking the in-house database molecules to the active site of the modeled Mtb GluR. The combination of the Glide SP, XP and GOLD docking program was used for the purpose. Figure 21 which details the virtual screening protocol followed for of the potential inhibitors is shown below.

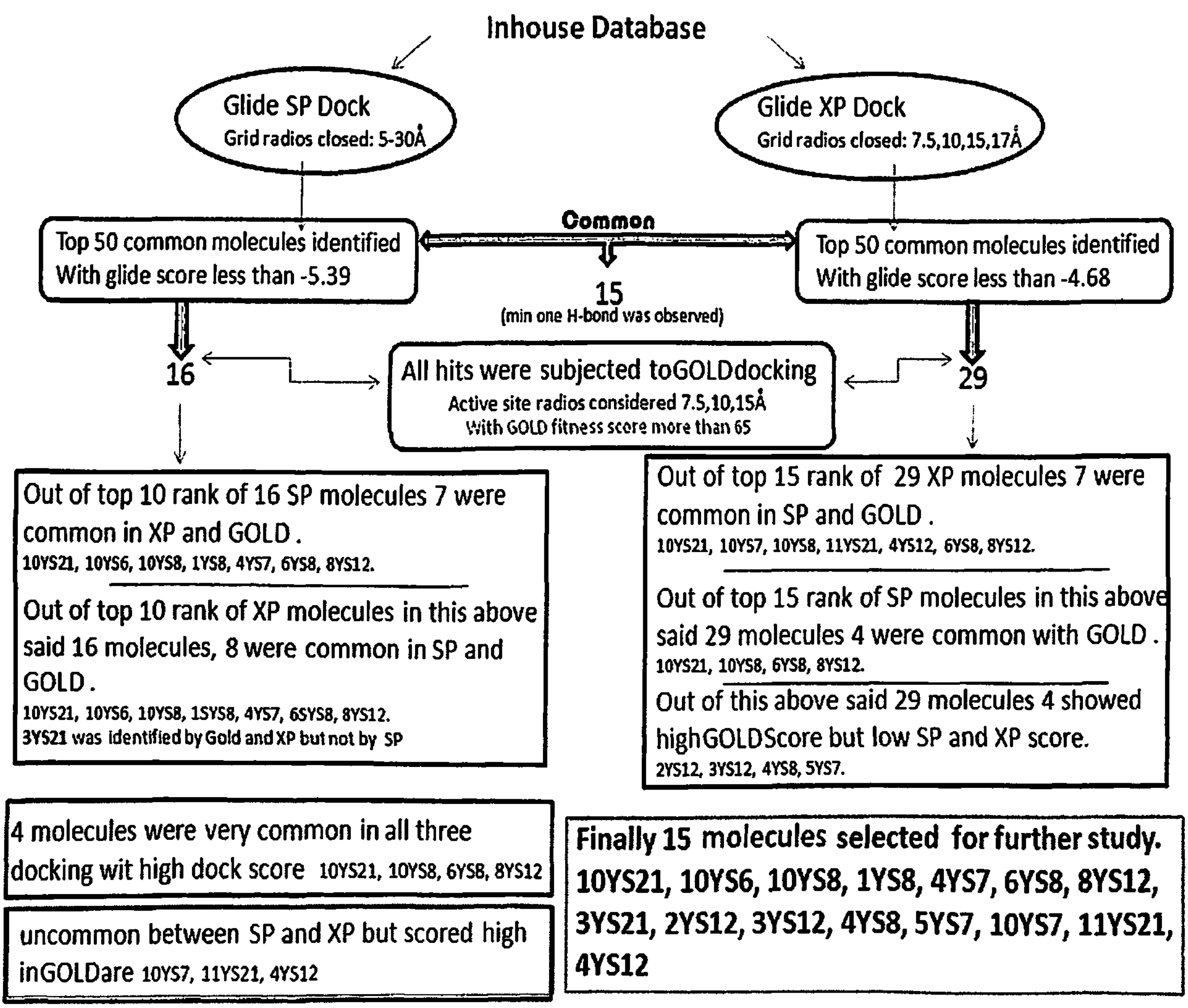

Figure 21: Virtual screening protocol used in identifying the potential inhibitors of Mtb GluR

The prepared in-house database was fist subjected to the Glide SP and XP docking. Since till now no inhibitors were reported, there was lack of knowledge regarding the suitable size of the inhibitor needed to inhibit the Mtb GluR. So to identify potential inhibitors Glide grids with different size 7.5, 10, 12.5 and 15 Å were constructed and used in SP and XP docking simulation. The successfully docked molecules were ranked according to the Glide score. The common top 50 highest scored molecules from different grid were identified from SP and XP docking. While shortlisting the molecules the molecular interaction with the receptor was thoroughly observed and molecules with at least one H-bond was considered. The lowest scoring molecule of the top 50 molecules from SP docking had a Glide energy score of -5.40, whereas the lowest scoring molecule of the top 50 molecules from XP docking had a score of -4.68. These 50 shortlisted molecules were then again docked in to Mtb GluR model using GOLD. For GOLD docking also different active site radius was considered i.e., 7.5, 10, 15 Å. The resulting molecules were ranked according to the fitness scores.

Out of fifty top scored molecules from SP and XP docking, 15 molecules were found common. 16 molecules were common hits from SP and GOLD docking, out of these 7 molecules were common in XP and GOLD docking. Those were **10YS21**, **10YS6**, **10YS8**, **1YS8**, **4YS7**, **6YS8**, **8YS12**. Out of top ten rank of XP molecules in this above said sixteen molecules (common to SP and Glod), 8 molecules were common in SP and GOLD docking. Those were **10YS21**, **10YS6**, **10YS8**, **1YS8**, **4YS7**, **6YS8**, **8YS12** and **3YS21**. Except **3YS21**, all other molecules were common top ranked in all the three docking methods. **3YS21** was one of the top score molecule common to XP and GOLD docking. 29 molecules were common hits from XP and GOLD docking. Out of these, 7 molecules were common in top fifteen ranked molecules from SP and GOLD which were mentioned above (**10YS21**, **10YS7**, **10YS8**, **11YS21**, **4YS12**,

6YS8, 8YS12). Out of these seven common hits from all three docking program, 4 molecules had high dock score in all the three docking program, they were **10YS21, 10YS8, 6YS8, 8YS12.** Another set of four molecules from 29 XP and GOLD common hits, **2YS12, 3YS12, 4YS8, 5YS7** had high GOLD docking fitness scores but had comparably low SP and XP Glide energy scores. There were three other molecules which were not in the common top ranked molecules from SP and XP, but scored very high in GOLD docking simulation. They are **10YS7, 11YS21** and **4YS12.**

By considering all these facts finally 15 molecules were shortlisted. They are **10YS21, 10YS6, 10YS8, 1YS8, 4YS7, 6YS8, 8YS12, 3YS21, 2YS12, 3YS12, 4YS8, 5YS7, 10YS7, 11YS21, 4YS12.** These molecules were either coming top hits in all the three docking programs, or were highest scoring molecule from any one of the docking program. Table 12 is the structure of these 15 molecules shortlisted from the virtual screening protocol. Table 13 contains the GOLD fitness scores, Glide SP docking scores and XP docking scores of the 15 shortlisted molecules.

Table 12: Structure of 15 molecules shortlisted from the virtual screening protocol.

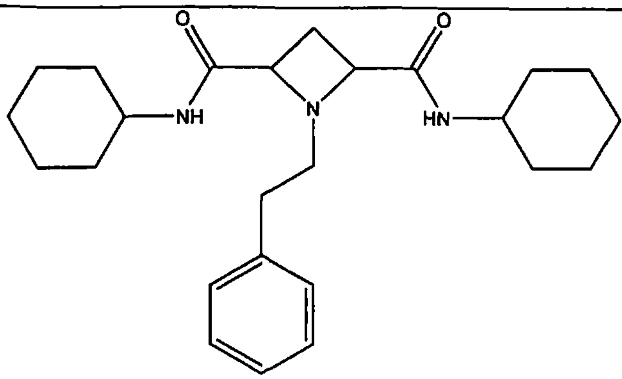 10YS6, Mol. Wt. 411.58	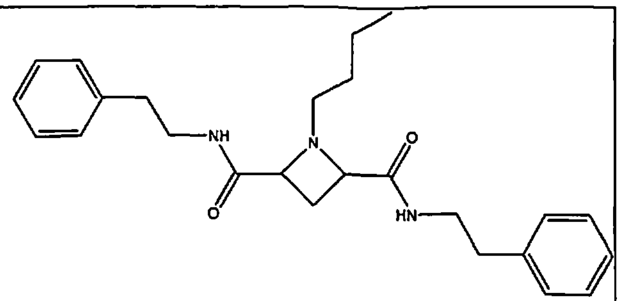 4YS8, Mol. Wt. 407.55

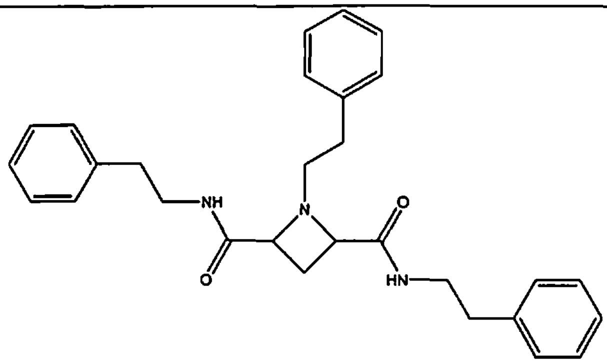

10YS8,Mol. Wt. 455.59

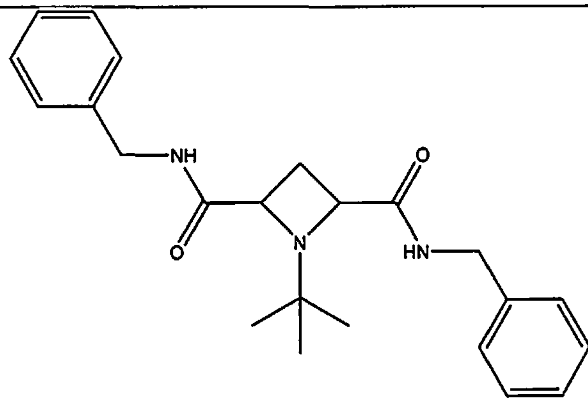

5YS7, Mol. Wt. 379.50

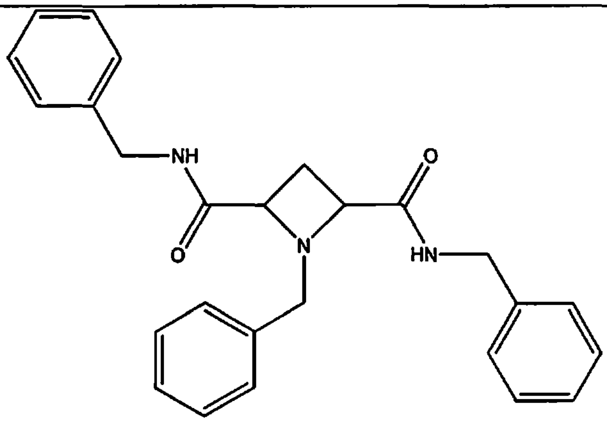

10YS7, Mol. Wt. 413.51

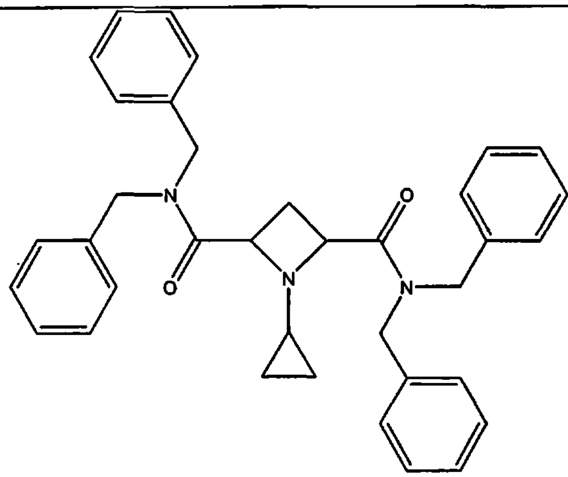

3YS12, Mol. Wt. 543.70

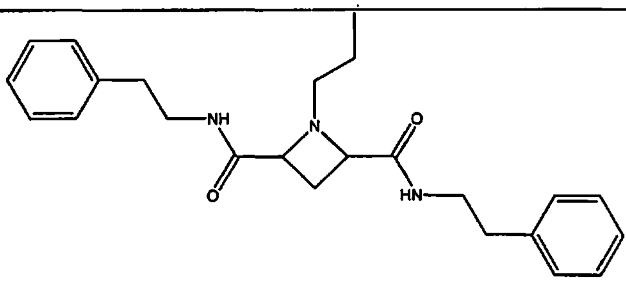

1YS7, Mol. Wt. 393.58

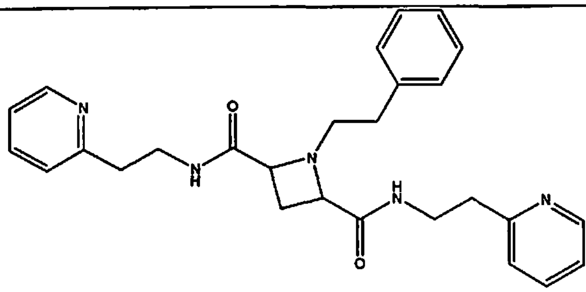

11YS21, Mol. Wt. 457.57

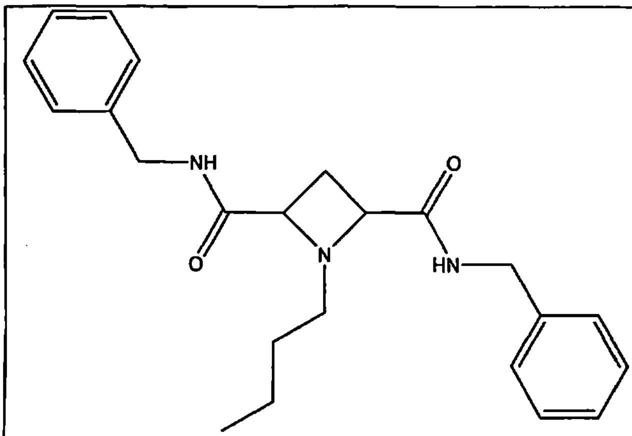

4YS7, Mol. Wt. 379.50

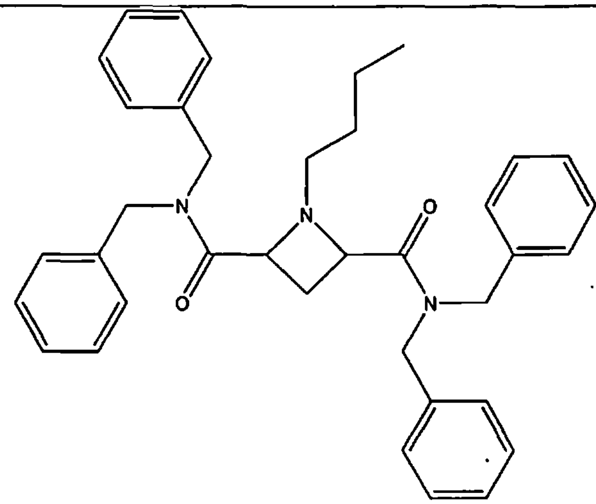

4YS12, Mol. Wt. 559.74

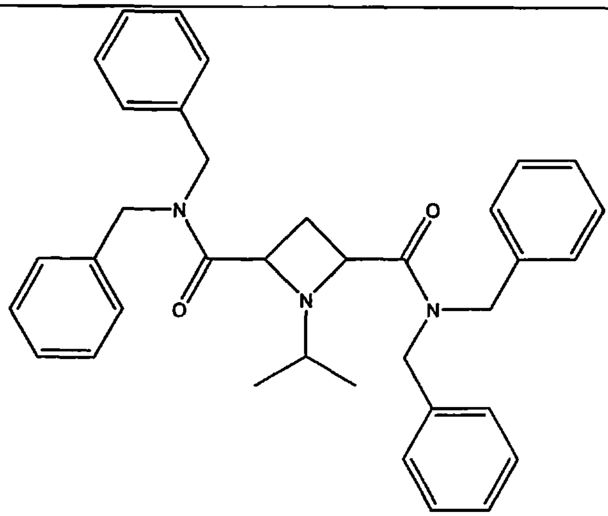

2YS12, Mol. Wt. 541.97

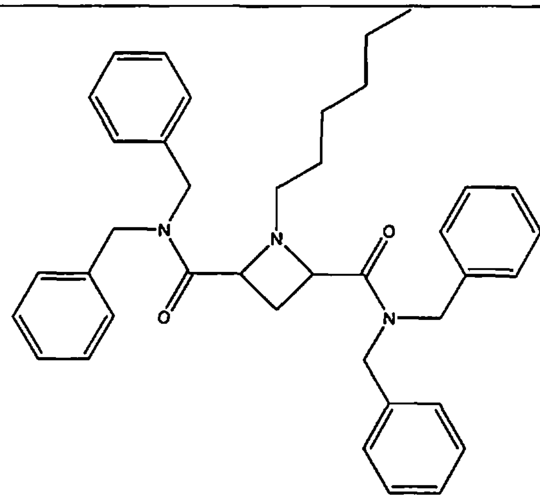

8YS12, Mol. Wt. 587.79

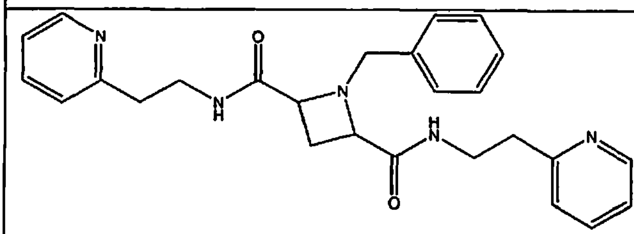

10YS21, Mol. Wt. 443.54

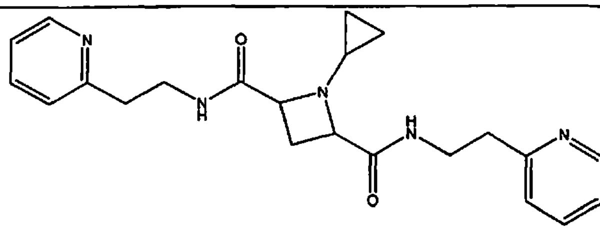

3YS21, Mol. Wt. 379.50

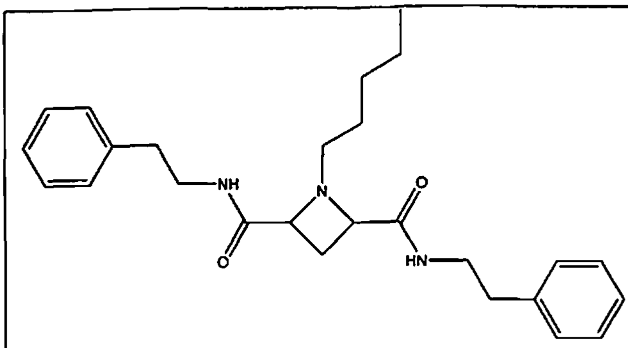6YS8, Mol. Wt. 421.57	

The **11YS21** docking with Mtb GluR showed very good interaction pattern. It was one of the molecules which were not a common hit between SP and XP glide docking but was scored very high in GOLD docking. Its GOLD fitness score was 74.23 and the XP docking score was -6.83. The docking calculations showed very good polar and hydrophobic interaction for the ligand, indicating a high affinity to the enzyme (Figure 22). Polar interactions such as H-bond and electrostatic interactions were predominant at the anterior part of the active site, whereas hydrophobic/van-der-waals interactions were overwhelming at the posterior part. Following interaction pattern was seen between Mtb GluR and the ligand **11YS21**. There were strong electrostatic interactions in the form of three H-bond was observed between ligand atom and enzyme. Nitrogen atom of one of the pyridine moiety formed strong H-bond with back bone NH of Val15 (V15:NH...N9 (pyridine); 2.8 Å), the N atom from pyridine ethyl amine moiety formed H-bond with side chain carboxyl group of Glu153 (N153:C=O...N5(from **11YS21**); 3.1 Å), the one of the carboxyl group attached with azetidine moiety formed H-bond with amino group of Gly40 (G40:NH...C4=O (from **11YS21**); 2.9 Å). The strong hydrophobic interactions were seen from ethyl benzene moiety of **11YS21** and the hydrophobic region formed by amino residues Pro43, Cys75, Val149. The pyridine ethyl amine group occupying posterior part of receptor pocket showed hydrophobic interaction in the form of Van-der-waals interaction with side chain of amino acid residues Pro43, Tyr44, Pro146, and Val149. Pyridine ethyl amine group occupying posterior part of receptor pocket showed hydrophobic interaction with side chain of amino acid residues Val15, Ala240 and Phe247. The counter map generated using the SiteMap program shows very good tolerance to **11YS21**. The yellow colored mesh represented for hydrophobic environment, the blue for electron donor and the red for electron acceptors regions in SiteMap. It can be seen that the hydrophobic parts of the receptor are very well mapped especially the ethyl benzene group of **11YS21** perfectly matching. It can be seen that the white dots are well covered with **11YS21** by ethyl benzene moiety and ethyl pyridine moieties. The site map is also properly depicting the electrostatic interactions resulted in to H-bond formation, the -NH of amino ethyl pyridine moiety is properly facing the blue donor environment (Figure 22).

The **4YS8** was one of the molecules, which scored very less in SP and XP docking but was scored very high in GOLD docking. Its GOLD fitness score was 72.56. Similar to the **11YS21** the **4YS8** presented a combination of electrostatic and hydrophobic interactions, but the hydrophobic interactions in the form of Van-der-waals interactions were predominating. That may be a reason it got identified in GOLD docking with high scoring compared to SP and XP docking. There were strong electrostatic interactions in the form of three H-bonds. Nitrogen atom of one of the amino ethyl benzene formed strong H-bond with back bone carbonyl group (C=O) of Ser13 (S13:C=O...N41 (from **4YS11**); 3.2 Å), the one of the carboxyl group attached with azetidine moiety manifested bifurcated H-bond, one with back bone amino group of Val15, (V15:NH... C39=O (from **4YS8**); 3.0 Å), another one with back bone amino group of Gly14, (G14:NH... C39=O (from **4YS8**); 3.1 Å). The strong hydrophobic interactions were seen from butyl chain attached to azetidine moiety of **4YS8** and the hydrophobic region formed by side chains of amino residues Ser13, Pro43, Cys75, and Val149. The amino ethyl benzene group occupying posterior part of receptor pocket manifested hydrophobic interaction with side chain of amino acid residues Pro43, Tyr44, Pro146, and Val149. Amino ethyl benzene moiety from anterior part of receptor pocket manifested hydrophobic interaction with side chain of amino acid residues Val15, Ala240, Ala246 and Phe247. The counter map generated using the SiteMap program shows very good hydrophobic integrations for **4YS8**. It can be seen that almost all parts of the hydrophobic regions of the receptor are very well mapped to the ligand especially at the ethyl benzene moiety and butane chain attached to the azetidine. The site map is also properly depicting the electrostatic interactions resulted in to formation of bifurcated H-bond with amino ethyl benzene moiety. The C=O is properly occupying the red acceptor rich part of the receptor (Figure 23).

The **6YS8** was one of the molecules, which scored very high SP and XP docking but was scored moderately by GOLD docking. Its XP and SP docking scores were -6.47 and -6.96 respectively, GOLD fitness score was 61.78. The interaction pattern was almost similar to the other two molecules explained above. **6YS8** had two H-bonds representing the electrostatic interactions. Nitrogen atom of anterior side of the amino ethyl benzene formed strong H-bond with side chain carbonyl group (C=O) of Glu153 (E153:C=O...N44 (from **6YS8**); 2.34 Å), the carboxyl group attached at anterior side of azetidine moiety manifested a H-bond, one with backbone amide hydrogen of Gly40, (G40:NH...C42=O (from **6YS8**); 3.3 Å). The strong hydrophobic interactions were seen from butyl chain attached to azetidine moiety of **6YS8** and the hydrophobic pocket formed by side chains of amino residues Ser13, Pro43, Cys75, and Val149, Cys185. The amino ethyl benzene group occupying posterior part of receptor pocket manifested hydrophobic interaction with side chain of amino acid residues Pro43, Tyr44, and Val149. Amino ethyl benzene moiety from anterior part of receptor pocket manifested hydrophobic interaction with side chain of amino acid residues Val15, Ala240, Ala246 and Phe247. It can be seen from SiteMap counter map that the yellow hydrophobic parts of the receptor are very well mapped specially the ethyl benzene group and pentyl side chains of **6YS8**. It can be seen that the white dots are well covered with ligand by ethyl benzene moiety and ethyl pyridine moieties. The site map is also properly depicting the electrostatic interactions resulting in H-bond formation, the -NH of amino ethyl benzene moiety is exactly coinciding donor environment required to satisfy the side chain carbonyl group of Glu153 (Figure 24).

The **3YS21** was only hit molecule identified from GOLD and XP docking but not by SP. Its GOLD fitness score was 64.97 and XP score was -5.98. **3YS21** manifested a different binding pattern compared to other molecules discussed above. The cyclopropane attached to the azetidine moiety was found occupying the solvent exposed part of the active site pocket and one amino ethyl pyridine moiety found extended towards the catalytic cysteine, the other one occupied the anterior part of the active site. It presented four H-bonds presenting very strong electrostatic interactions. The nitrogen atom of anterior side of the amino ethyl pyridine formed strong H-bond with side chain hydroxyl (OH) of Thr39 (T39:OH...N40 (from **3YS21**); 2.08 Å), the carboxyl group attached at anterior side of azetidine moiety manifested a H-bond with backbone NH of Val15 (V15:NH...C33=O (from **3YS21**); 2.57 Å), the nitrogen atom of the amino ethyl pyridine extended towards the catalytic pocket formed strong H-bond with side chain carboxyl group (C=O) of Glu153 (E153:C=O...N5 (from **3YS21**); 2.03 Å), the other carboxyl group attached to azetidine moiety manifested a H-bond with NH of Gly40 (G40:NH...C4=O (from **3YS21**); 3.0 Å). The hydrophobic interactions were seen from pyridine moiety occupying the anterior part of the receptor and the hydrophobic pocket formed by side chains of amino residues Val15, Ala246, Phe247 and Leu250. The pyridine moiety occupying catalytic site of receptor pocket manifested hydrophobic interaction with side chain of amino acid residues Pro43, Tyr44, Cys75, Thr119, Val149 and Cys185. It can be seen that the counter maps generated from SiteMap representing yellow hydrophobic parts of the receptor are very well mapped specially the ethyl pyridine group at catalytic site and pyridine moiety at anterior part of receptor. It can be seen that the donor regions and acceptor regions are exactly mapping to **3YS21** properly depicting the electrostatic interactions resulting in formation of H-bonds. (Figure 25).

Table 13: The GOLD fitness scores, Glide SP docking scores and XP docking scores of the shortlisted molecules.

Molecule Name	**GOLD fitness score**	**Glide SP score**	**Glide XP score**
10YS21	64.71	-6.42	-5.75
10YS6	60.58	-6.16	-5.55
10YS7	64.50	-	-5.97
10YS8	65.59	-6.37	-5.55
11YS21	74.23	-	-6.83
1YS8	57.08	-6.11	-5.65
2YS12	61.67	-5.62	-4.90
3YS12	67.73	-	-5.25
3YS21	64.97	-	-5.98
4YS12	62.16	-	-5.49
4YS7	60.68	-5.75	-5.42
4YS8	72.56	-	-4.88
5YS7	58.72	-	-4.83
6YS8	61.78	-6.96	-6.47
8YS12	61.94	-6.04	-5.60

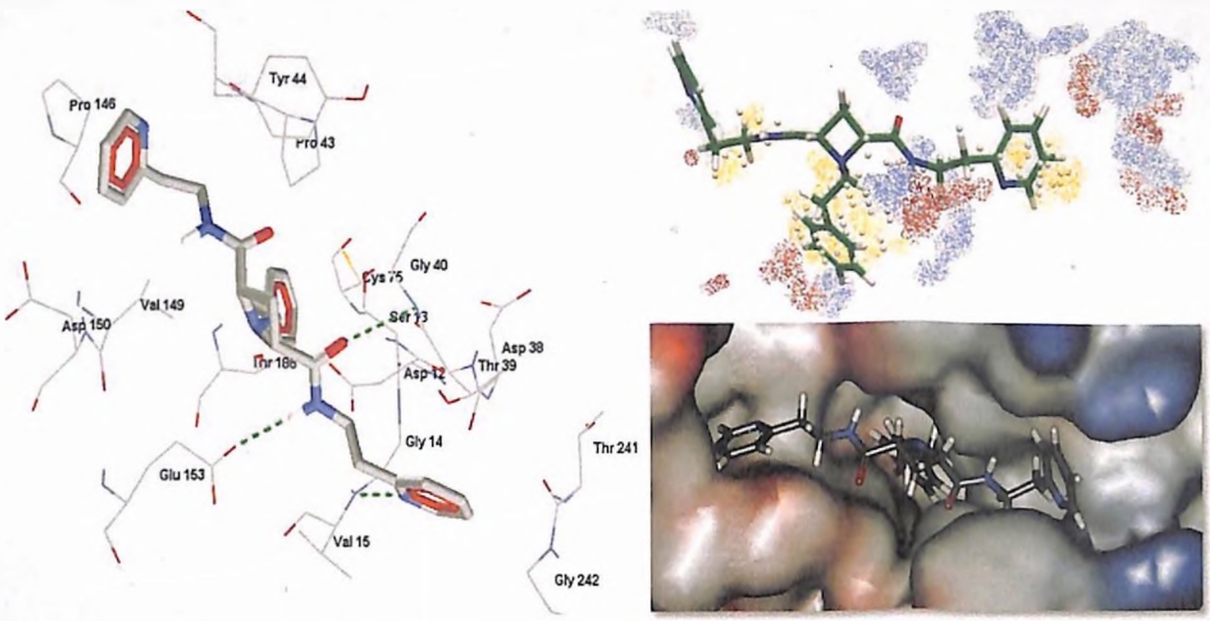

Figure 22: Schematic representation of the contact residues of **11YS21** with Mtb GluR generated by Glide docking (left). H-bonds are represented in green color. The **11YS21** mapped to the counter map generated from SiteMap, (right up side) the yellow color corresponds to the hydrophobic area, the red represents the electron acceptor area, the blue color represents the electron donor parts of the receptor surface. Electrostatic surface view of active site pocket of Mtb GluR bound to **11YS21** (Right side down).

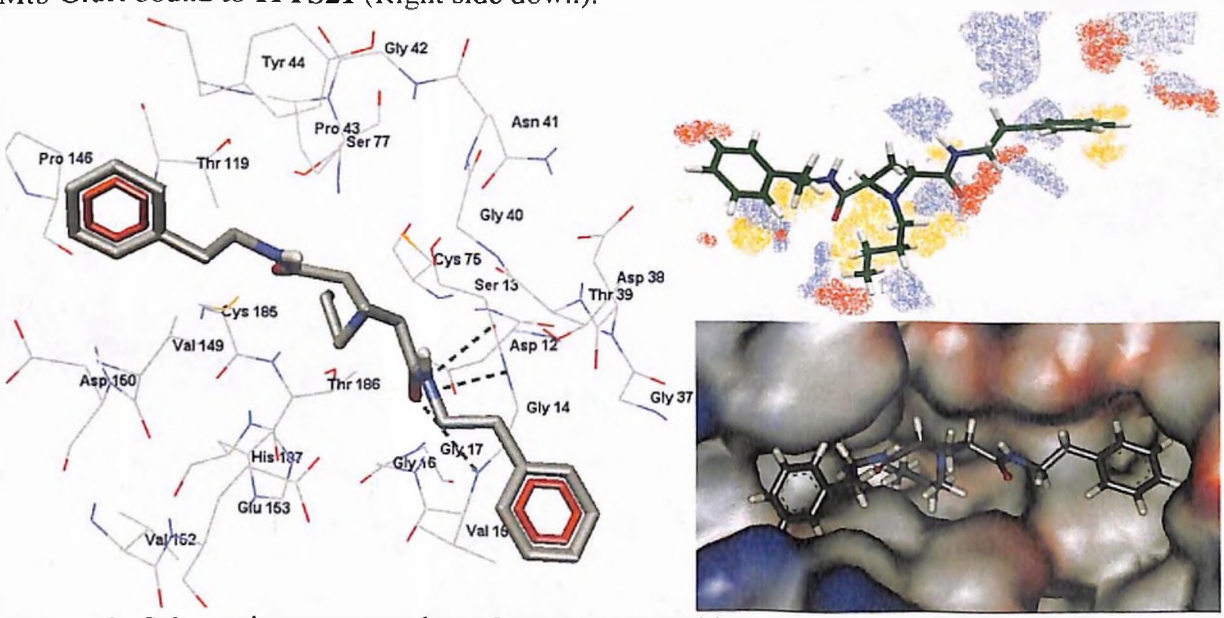

Figure 23: Schematic representation of the contact residues of **4YS8** with Mtb GluR generated by Glide docking (left). H-bonds are represented in green color. The **4YS8** mapped to the counter map generated from SiteMap, (right up side) the yellow color corresponds to the hydrophobic area, the red represents the electron acceptor area, the blue color represents the electron donor parts of the receptor surface. Electrostatic surface view of active site pocket of Mtb GluR bound to **4YS8** (Right side down).

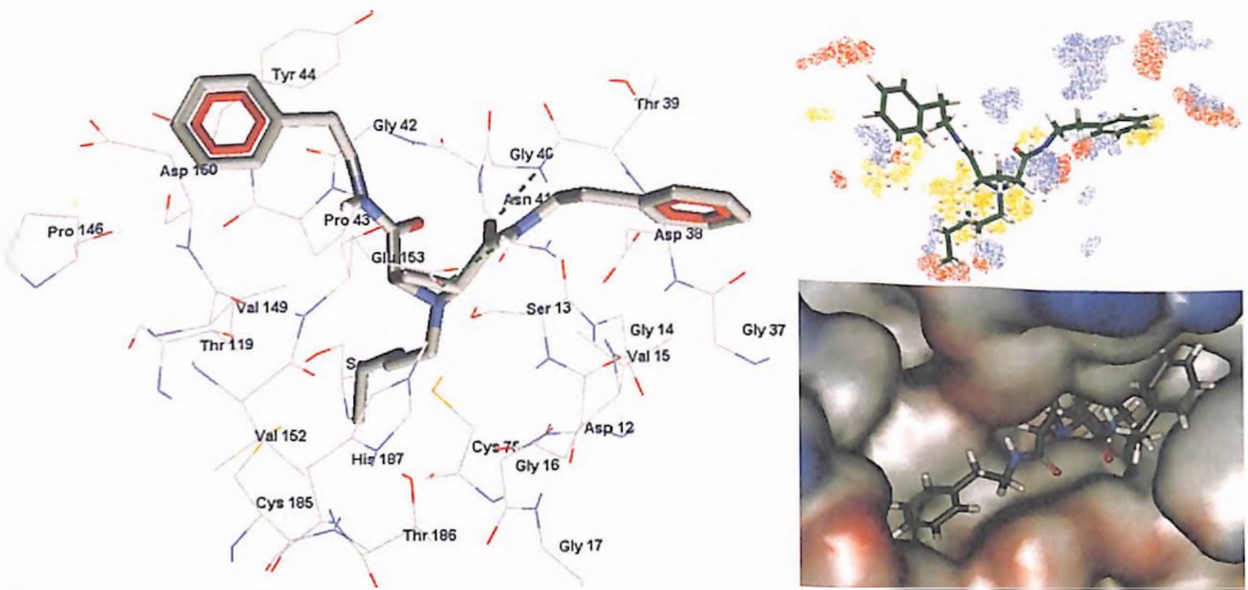

Figure 24: Schematic representation of the contact residues of **6YS8** with Mtb GluR generated by Glide docking (left). H-bonds are represented in green color. The **6YS8** mapped to the counter map generated from SiteMap, (right up side) the yellow color corresponds to the hydrophobic area, the red represents the electron acceptor area, the blue color represents the electron donor parts of the receptor surface. Electrostatic surface view of active site pocket of Mtb GluR bound to **6YS8** (Right side down).

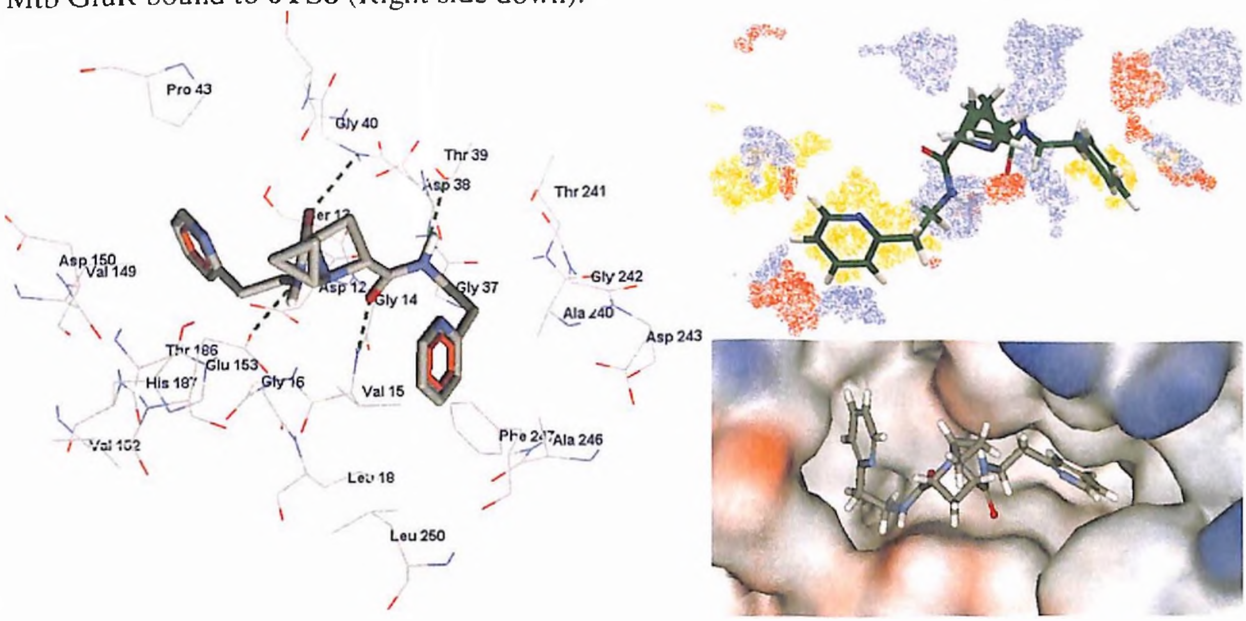

Figure 25: Schematic representation of the contact residues of **3YS21** with Mtb GluR generated by Glide docking (left). H-bonds are represented in green color. The **3YS21** mapped to the counter map generated from SiteMap, (right up side) the yellow color corresponds to the hydrophobic area, the red represents the electron acceptor area, the blue color represents the electron donor parts of the receptor surface. Electrostatic surface view of active site pocket of Mtb GluR bound to **3YS21** (Right side down).

Chapter V

Protein Kinase B as anti-TB target & design of its Inhibitors

5.1 Introduction

The study of signaling elements, Ser/Thr protein kinases (STPKs), is of outstanding interest, given their likely important roles in mycobacterial physiology and virulence. Signal transduction in prokaryotes is primarily conducted by two-component regulatory systems, basically consisting of a sensor histidine kinase and a response regulator [239]. The Mtb genome encodes 11 complete two-component systems [240, 241] several of which contribute to the virulence of Mtb, [242-246] but only one system (*MtrA*, *MtrB*) was found to be essential for cell growth [247]. This relatively low number of two-component systems is offset by alternative signal transduction mechanisms involving Ser/Thr phosphorylation that are generally less common in bacteria than in eukaryotes. Mtb has genes for one phospho-Ser/Thr phosphatase (*pstP*) and as many as 11 Ser/Thr protein kinases (STPKs) (PknA to PknL) [240]. In mycobacteria with larger genomes such as *M. marinum* or *M. smegmatis* STPK outnumber two-component systems, suggesting that the bulk of signal transduction is *via* Ser/Thr (de)phosphorylation.

Most of STPKs do not appear to control essential physiological processes. *M. leprae,* a closely related species that has undergone extensive gene decay [248], has retained only four STPKs, and orthologs of just three of them (PknA, PknB, and PknG) were found to be required for optimal growth of Mtb using saturation transposon mutagenesis [249]. Furthermore, inactivation of the PknG gene in Mtb was reported to decrease viability both *in-vitro* and upon infection of BALB/c mice [250], although independent work showed that the *in-vitro* growth of *M. bovis* BCG lacking PknG was identical to that of the wild type [251]. In a similar way, wild-type-like growth was observed for Mtb strains lacking either the PknD or the PknH gene [252, 253] and down regulation of PknF protein synthesis in Mtb using an antisense strategy also confirmed a viable phenotype, with faster-growing and shorter cells than the wild-type strain [254].

PknB was proposed to be a potential regulator of cell growth and division because of its localization close to the chromosomal origin of replication and since the operon also includes genes known to be important for these processes (*pbpA* and *rodA*, *pbpA* belongs to the family of penicillin binding proteins, membrane proteins that play key roles in cell wall synthesis, and *RodA* is known to control bacterial cell shape and elongation) [255]. Recent results demonstrated that PknB is predominantly expressed during exponential growth, and that its depletion or overexpression alters cell morphology [256], lending support to its involvement in cell shape and cell division control. The essentiality of the PknB for the Mtb survival was further confirmed later by allelic gene knockout experiments [257] and the nonselective ATP competitive inhibitors, K-252-a and K-252-b showed the IC_{50} values around 100 μM for PknB, with MIC for Mtb at a range of 5-20 μM. To further confirm PknB as the molecular target, the *M. segmentis* was transfected with Mtb PknB, and was over expressed during exponential phase of growth, showed lower MIC value compared to the MIC value observed with wild type, due to nonselective ATP competitive inhibitor. However, the physiological substrates of PknB are currently unknown.

The STPKs from a variety of different bacteria catalyze autophosphorylation [258-262] The isolated catalytic domains of Mtb PknA, B, D, E, F, G, H and I [263-266] were found to be catalytically active, suggested that the sensor domains may not be needed. In comparison to eukaryotic STPKs, the Mtb kinase domains are phosphorylated on more sites. Three to six autophosphorylation sites were discovered on PknB, that is on the activation loop, of two threonines and up to two serines [267, 268] Phosphorylation of the activation loop segment, located between the conserved DFG motif and the following APE sequence, activates many eukaryotic STPKs [269], suggesting that bacterial and eukaryotic STPKs are regulated by a similar chemical mechanism [267]. Alzari and coworkers showed that PknB dephosphorylated by the *PstP* phosphatase to inactivate PknB, and the phosphorylation of Thr171 and Thr173 in the activation loop enhanced kinase activity by approximately 20-fold [268].

A model was expanded by testing the *in-vitro* phosphorylation specificity of PknB, PknD, PknE and PknF for the FHA-domain-containing proteins Rv0020c, Rv1747 [270] and GarA [271]. These studies showed that kinase domains phosphorylate a specific subset of FHA proteins *in-vitro*. GarA and Rv1747-FHA-A mediated phosphorylation by all four kinase domains, whereas the other FHA domains were more restrictive to particular protein kinases. Using a proteomic approach, Alzari and coworkers showed that GarA (Rv1827), the most abundant soluble phosphoprotein produced by Mtb PknB, [271, 272] that has been linked both to glycogen degradation during exponential growth of *M. smegmatis* [273] and to regulation of the tricarboxylic acid cycle in *Corynebacterium glutamicum* [274].The phosphorylation site was mapped to Thr 22 in a conserved region of the protein N-terminal to the FHA domain. The only pThr residues in the PknB construct was in the activation loop, and Ala substitutions at these sites reduced GarA binding, kinase activity and GarA phosphorylation. The authors proposed that the FHA domains bind directly to the phosphorylated activation loop of the cognate STPKs. Because activation-loop phosphates are generally buried in a conserved receptor site in activated eukaryotic STPKs [269], this model suggests a distinct mechanism of substrate recognition in which the activation-loop phosphates are accessible to engage the FHA domain. To test this model, several groups are working to co-crystallize Mtb STPK segments with FHA-domain constructs. The roles of FHA-domains have yet to be defined. The FHA domains may mediate binding of a subset of cellular substrates (such as Rv1747). Alternatively, the FHA domains may function as kinase inhibitors by blocking the binding of other substrates to the activation-loop in activated STPKs. The functions of FHA-domain protein phosphorylation also have not been determined. Phosphorylation may mediate the effector functions of FHA-domain proteins through allosteric changes or by creating additional FHA-domain binding sites. On the other hand, phosphorylation may promote auto-inhibition of the FHA-domain by favoring intra-molecular binding to the pThr binding site. These alternative functions are not mutually exclusive, and different mechanisms may operate in different systems in diverse bacteria.

Husson and coworkers recently reported the first Mtb STPK substrates lacking a FHA domain [256]. A peptide-specificity screen indicated that PknA and PknB showed a preference for phosphorylation of Ser/Thr followed by Gln [256]. Using p(Ser/Thr)Gln antibodies and mass spectrometry, phosphoproteins enriched in Mtb extracts over expressing PknA and PknB in early stationary phase were detected. Two *in-vivo* substrates were identified are Rv1422 (a hypothetical protein) and Rv2145c (*Wag31*, a homolog of *B. subtilis DivIVA,* involved in cell shape regulation) [256]. *In-vitro*, the kinase domains of either PknA or PknB phosphorylated purified Rv1422c [256]. While PknB did not phosphorylate *Wag31* and PknA phosphorylated it weakly, *Wag31* phosphorylation was enhanced when PknA and PknB acted in concert [256]. The phosphorylation site of *Wag31* was mapped to Thr73, the morphologies of Mtb strains overexpressing wild-type, Thr73Ala, or Thr73Glu *Wag31* variants were analyzed [256]. While overexpression of wild-type and the Thr73Glu phosphorylation mimic produced the same bulbous-cell phenotype as PknB overexpression, expression of the Thr73Ala *Wag31* mutant resulted in normal cell shape [256]. This combination of *in-vivo* and *in-vitro* phosphorylation data with corroborating genetic data indicated that PknA and PknB regulate cell division or morphology by phosphorylating Rv1422 and *Wag31*.

The extracellular domain of PknB has been described as a penicillin binding and Ser/Thr kinase-associated (PASTA) domain that is also found in the bifunctional, high molecular mass penicillin binding proteins involved in peptidoglycan synthesis. It has recently been suggested that, this domain may bind both penicillins and peptidoglycan-related analogues [250]. A possible clue to their function came from the structure of the penicillin-binding protein from *Streptococcus pneumoniae*, which contains two PASTA domains and was found to bind the β-lactam antibiotic cefuroxime [275]. This observation led [276] to propose PASTA domains might specifically recognize stem-peptides from unlinked peptidoglycan, suggesting a role of STPKs in the control of peptidoglycan remodeling during cell growth [277] and the reactivation of dormant bacteria [278]. However, these hypotheses remain speculative because the peptidoglycan binding specificity of PASTA domains has yet to be proven.

In a study Chopra P. et al., showed Rv0018c gene of Mtb, designated as mycobacterial Ser/Thr phosphatase (*Pstp*), dephosphorylates phosphorylated PknA and PknB [279]. *Pstp* dephosphorylated the phosphorylated Ser/Thr residues of myelin basic protein (MBP), histone, and casein but failed to dephosphorylate phosphor-tyrosine residue of these substrates, suggesting that this phosphatase is specific for Ser/Thr residues. Further parallel research conducted by Boitel B. et al., demonstrate that *Pstp* dephosphorylates specifically phospho-Ser/Thr residues and that its activity is strictly dependent on the presence of Mn^{++}, which subsequently exhibits decreased kinase activity [268]. Mass spectrometry analysis identified two phosphothreonine residues in the activation loop of PknB. Mutagenesis of these threonines in alanine demonstrate their role in regulating PknB kinase activity. Thus combination of the *Pstp* and PknB plays regulatory roles in mycobacteria.

SigH is a key regulator of an extensive transcriptional network that responds to oxidative, nitrosative, and heat stresses in Mtb, and this sigma factor is required for virulence in animal models of infection [280-383] SigH is negatively regulated by RshA, its cognate anti-sigma factor, which functions as a stress sensor and redox switch. While RshA provides a direct mechanism for sensing stress and activating transcription, bacteria use several types of signal transduction systems to sense the external environment [284-286]. Husson and coworkers demonstrated SigH and RshA are phosphorylated *in-vitro* and *in-vivo* by PknB [287]. Further showed that, phosphorylation of SigH does not affect the SigH-RshA interaction and phosphorylation of RshA results in decreased binding of SigH by RshA. Consistently, negative regulation of SigH activity by RshA *in-vivo* is partially relieved in strains in which pknB is over-expressed, resulting in increased resistance to oxidative stress. These findings demonstrate an interaction between the signaling pathways mediated by PknB and the stress response regulation controlled by SigH. Coordination of the PknB and SigH regulatory pathways through phosphorylation of RshA may lead to adaptive responses that are important in the pathogenesis of Mtb infection.

The enzyme N-acetylglucosamine-1-phosphate uridyltransferase (GlmU) of Mtb is a novel substrate of PknB and is phosphorylated on threonine residues [288]. GlmU carries out two important biochemical activities, a C-terminal domain catalyzes the transfer of acetyl group from acetyl coenzyme A to glucosamine-1-phosphate to produce N-acetylglucosamine-1-phosphate, which is converted into UDP-N-acetylglucosamine by the transfer of uridine 5'-monophosphate (from uridine 5′-triphosphate), a reaction catalyzed by the N-terminal domain. The phosphorylation mediated by PknB regulates the acetyltransferase activity of GlmU. The mutational studies revealed one of the five threonines present in region 414–439 to be phosphorylated by PknB.

Recent work on GarA, a small protein mainly occupied by the FHA domain, has provided an indirect link to regulation of the mycobacterial metabolism by STPKs PknB and PknG [289, 290]. The phosphoindependent interaction of GarA with metabolic enzymes was shown to be blocked by an intramolecular inhibition mechanism triggered by PknG/PknB-mediated GarA phosphorylation.

Jan Maarten van Dijl and coworkers report that the serine/threonine kinase PknB from the important pathogen *Staphylococcus aureus* is released into the external milieu, which opens up the possibility that PknB does not only phosphorylate bacterial proteins but also proteins of the human host [291]. To identify possible human targets of purified PknB, they studied *in-vitro* phosphorylation of peptide microarrays and detected 68 possible human targets for phosphorylation. These results show that PknB is a proline-directed kinase with MAP kinase-like enzymatic activity. As the potential cellular targets for PknB are involved in apoptosis, immune responses, transport, and metabolism, PknB secretion may help the bacterium to evade intracellular killing and facilitate its growth.

Other putative PknB substrates that could be involved in downstream signaling events have also been proposed, such as penicillin-binding protein *PbpA* [292] or Rv1422 [256]. *C. glutamicum* and Mtb are both Actinomycetes with 4,000 genes, but *C. glutamicum* contains only four STPK genes, in contrast to 11 in Mtb. The four orthologous kinases are PknA, PknB, PknG and PknL. These shared STPKs may phosphorylate the majority of the substrate proteins in both species, or at the other extreme, each STPK may phosphorylate approximately the same number of unique proteins. (This latter assumption clearly breaks down for *Myxococcus* or *Streptomyces* species, which contain 100s or 36 STPKs, respectively.) These considerations support idea that Mtb may contain on the order of 500–1000 pSer/pThr proteins. This number is much larger than handful of Mtb phosphoproteins detected by *in-vitro* phosphorylation of lysates [271] or Western blotting of Mtb lysates with pSer/pThr-reactive antibodies [256]. Because nine of the Mtb STPKs and the Ser/Thr phosphatase PstP are predicted membrane proteins, structural analyses of these systems have relied on protein dissection strategies to produce soluble domains. These studies leave open question of how the sensor domains regulate the respective kinase domains.

Studies of Mtb PknB yielded the first structure of a kinase domain from a bacterial STPK [285, 311]. Despite <30% sequence identity to the most related human STPK, the PknB kinase domain conformed closely to the classical architecture associated with this protein family (Figure 26a). As in other members of the STPK family, the nucleotide was sandwiched between the N- and C-terminal lobes, engaging characteristic sequence motifs including the P-loop, catalytic a

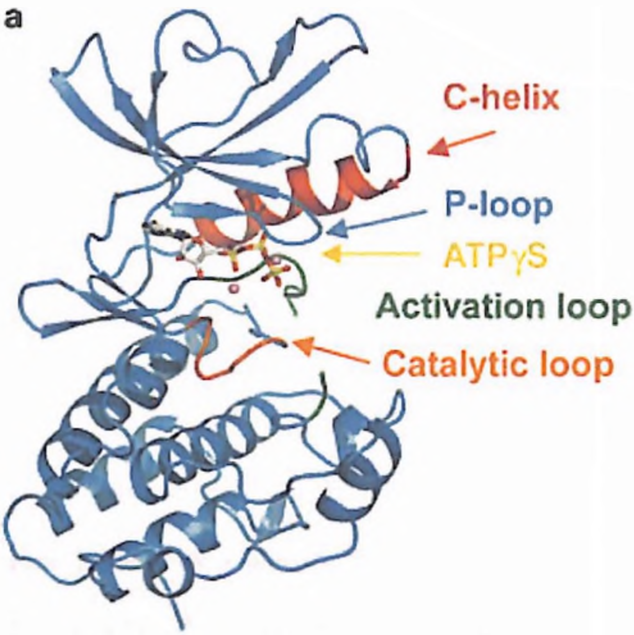

b

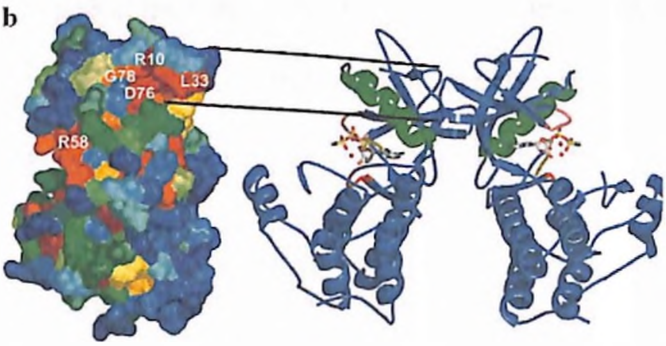

Figure 26: PknB adopts a classic STPK structure that dimerizes through a conserved interface.

a. Ribbon drawing showing the conserved fold and functional motifs of the PknB- ATPγS complex. Characteristic features of the STPK fold include the P-loop (which engages the phosphate groups of the nucleotide), the C helix (which orients key residues in the active site and forms an allosteric docking site for protein substrates), and the catalytic loop (which contains residues essential for catalysis). Most of the activation loop is disordered in the PknB crystal structures. The high structural similarity to the eukaryotic STPK fold suggests catalysis and regulation occur by similar mechanisms in eukaryotic and prokaryotic STPKs.

b. PknB dimerizes (right) through a conserved surface (red, left surface drawing) at the C-terminal end of the C helix on the opposite side of the N-terminal domain relative to the active site. Allosteric interactions at a position analogous to this dimerization interface control the position of the C helix in several eukaryotic protein kinases, such as c-Src. These structural similarities in light of the great functional divergence of PknB and c-Src suggest that the PknB dimer interface defines a universal allosteric site in STPKs.

loop, DFG motif and a regulatory helix called the C helix. Despite phosphorylation of the activation loop at 2–4 sites, this segment was disordered in the crystals of both PknB-nucleotide complexes. As a result, the C-helix, which forms part of the binding site for the phosphorylated activation loop in activated STPKs, was tipped away from the active site in a characteristic inactive conformation [294]. In this position, the conserved Glu59 in the C-helix did not form an ion pair with Lys40 in the active site, also distinguishing the conformation of the PknB kinase domain from activated STPK structures. PknB orthologs are widely distributed in prokaryotes.

Consequently, unlike more unique bacterial STPKs or orthologous eukaryotic STPKs (which show little sequence divergence), putative functional sites in the PknB kinase domain could be detected by mapping sequence conservation in orthologs onto the structure (Figure 26) [267]. Conserved surfaces of the PknB kinase domain include the ATP binding cleft, residues adjacent to the ATP γ-phosphate and a groove on the C-terminal lobe adjacent to the catalytic site.

Unexpectedly, PknB orthologs also showed conservation of a site on the opposite side of the N-terminal lobe relative to the active site (Figure 26) [267]. This conserved surface forms a dimerization interface in both crystal forms of the nucleotide complexes of the PknB STPK domain [267, 293]. The dimer interface includes conserved Leu33, as well as the docking site for Leu33 at the C-terminus of the C helix in the adjacent monomer. The existence of this conserved dimer interface strongly suggested that it is functionally important. The Leu33 binding pocket is analogous to an autoinhibitory site in c-Src [295, 296] suggesting that dimerization of PknB regulates the kinase domain and that the dimer interface contains a universal allosteric site that controls the position of the C helix.

Research group of Alzari, crystalized the Mtb PknB with an inhibitor mitoxantrone, an anticancer compound [297]. Kinase assays revealed that mitoxantrone (1,4-dihydroxy-5,8-bis[2-(hydroxyethylamino)-ethylamino]-9,10-anthracenedione) was able to inhibit PknB with an IC_{50} in the micro molar range ($IC_{50} = 0.8 \pm 0.05$ µM, MIC = 400 µM). The overall structure of the enzyme is similar to those previously described for PknB in complex with ATP analogs with the kinase domain in an overall closed conformation and a disordered activation loop. The most noticeable structural change involves the glycine-rich loop, which in the absence of ATP moves further towards the C-terminal lobe. Clear electron density is observed for mitoxantrone in the nucleotide binding cleft of PknB (ATP binding site). The planar dihydroxyanthraquinone moiety of the inhibitor occupies hydrophobic cage that binds the adenosine moiety of ATP. An important number of residues of both the N- and C-terminal lobes make van der Waals contacts with the inhibitor, including Leu17, Gly18, Val25, Ala38, Met 92, Glu93, Tyr94 and Val95 in the N-terminal lobe, Met145 and Met155 in the C-terminal lobe. The main-chain amide group of Val95, which in the PknB-AMPPCP complex is hydrogen bonded to the N1atom of adenosine, now forms a hydrogen bonding interaction with one hydroxyl group of the inhibitor, which may account for the observed lateral positioning of the inhibitor within the wide hydrophobic binding pocket (Figure 27). The partial occupancy of the cleft leaves space to accommodate bulkier substituents at the three-ring moiety, which might be exploited to improve the inhibitory properties of the compound.

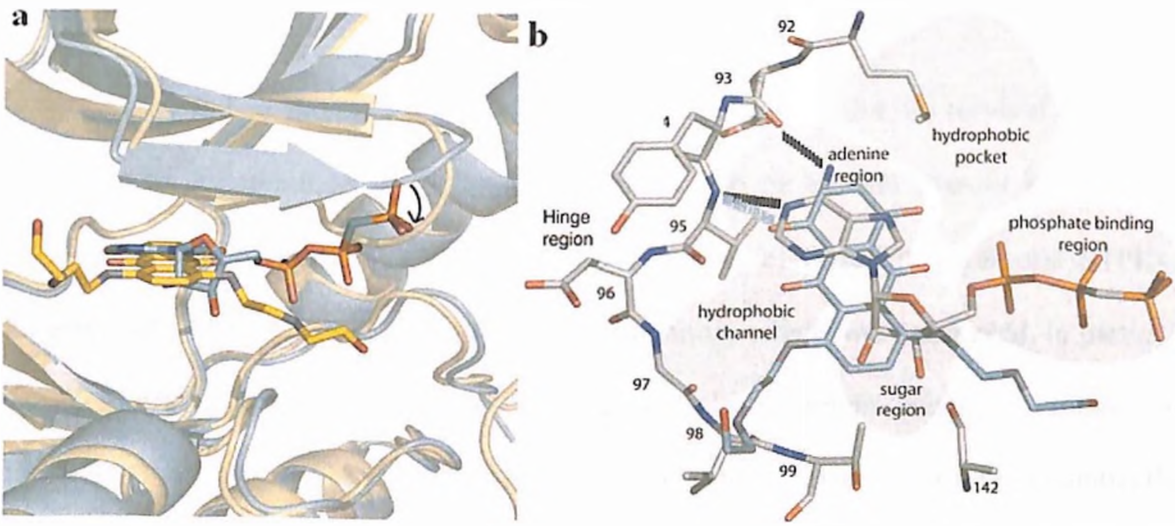

Figure 27. Structure of the PknB-mitoxantrone complex. (**a**) Superposition of the PknB-mitoxantrone complex (in yellow) and the PknB-AMPPCP complex (1O6Y, in cyan). Note the movement of the Gly-rich loop (black arrow). (**b**) Schematic view (represented as in Ref. [26]) of the PknB ATP-binding site showing hydrogen bonding interactions with both the inhibitor (in blue) and AMP-PCP (PDB code 1O6Y).

Av-Gay and coworkers first reported the potential to use protein kinase inhibitors to be antibacterial [298]. The protein kinase inhibitor 1-(5-isoquinolinesulfonyl)-2-methylpiperazine (H7) was found to inhibit the growth of two different mycobacterial strains, the slow-growing *Mycobacterium bovis* Bacille Calmette Guerin (BCG) and the fast-growing saprophyte *Mycobacterium smegmatis* mc2 155, in a dose-dependent manner. While screening for the effect of kinase inhibitors on mycobacterial growth, millimolar concentrations of H7 induced a 40% decrease in the growth of *M. bovis* BCG when measured as a function of oxidative phosphorylation. This H7-induced decrease in growth was shown to involve a 2-log fold decrease in the viable counts of *M. smegmatis* within a 48-h period and a 50% reduction in the number of BCG viable counts within a 10-day period. Micro molar concentrations of H7 compound induced a significant decrease in the activity of the Mtb protein serine/threonine kinase (PSTK) PknB.

Alzari and coworkers to establish the essentiality of PknB for the survival of Mtb; carried out the gene disruption by allelic replacement and also by Ser/Thr protein kinase inhibitors. Nonspecific commercially available known inactivators of different eukaryotic STPKs were screened for the inhibitory activity. Significant inhibitory effects were observed, in particular for K-252-a and K-252-b, two natural products that contain the indole carbazole chromophore and staurosporine, thought to target the ATP-binding site. The IC_{50} values for these compounds were determined by quantification and graphical analysis of radiolabeled spots from serial twofold dilution and found to be 0.096 μM for K-252-a, 0.106 μM for K-252-b, and 0.6 ± 0.05 μM for staurosporine. K-252-a inhibited the growth of both Mtb H37Rv and *M. smegmatis mc2* 155 at a concentration of 20 μM and that of *M. aurum* A+ at 5 μM. As a control, staurosporine also showed inhibitory effects on H37Rv between 25-50 μM. In contrast, K-252-b failed to inhibit the growth of all mycobacterial species at the highest concentration tested (40 μM), due to the low permeability of the envelope to this compound.

In 2008 Rita Szekely et al., reported six novel Mtb PknB inhibitors with the IC_{50} values bellow 3 μM [299]. They used 970 NCL library compounds in an *in-vitro* set-up assaying PknB activity. Based on these results, using their in-house developed modeling software, utilizing 606 data points they constructed a QSAR, utilizing 26 descriptors from a pool of 3355 descriptors. The value of 0.6546 of the cross-correlated correlation coefficient (Q2) indicates that the model is reliable and suitable for virtual screening. Figure 28 consists of Mtb PknB inhibitors shown below.

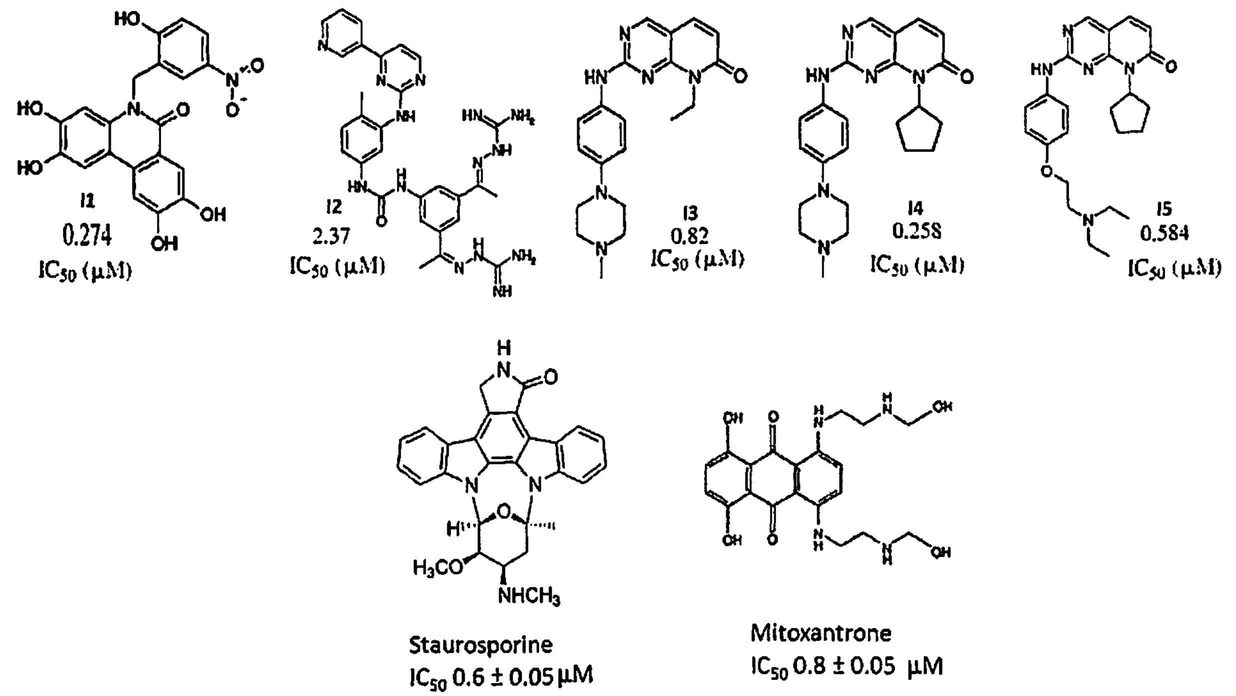

Figure 28: Chemical structure of the Mtb PknB inhibitors.

5.2 Materials and method

5.2.1 Ligand based pharmacophore The previously reported inhibitor structures were drawn using 'Build' option and then added to the project table. These were then imported from project table into the "Develop Pharmacophore Hypotheses" panel and geometrically refined using LigPrep module (LigPrep, version 2.3, Schrodinger, LLC, New York, NY). Conformers were generated for each molecule by using torsional search method with distance dependent dielectric solution treatment and OPLS_2005 force field. For all molecules a maximum of 500 conformations were developed. For each molecule, conformers with the maximum energy difference of 10 kcal/mol and within 1 Å rmsd relative to global energy minimum conformer were obtained.

Inhibitors with IC_{50} value 0.80 μM or less than that were considered as active in "Pharmaset", and IC_{50} values above 2.0 μM were considered as inactive. The molecules present in the Pharmacset are utilized for the generation of the Hypothesis. These active molecules were later used to score hypothesis. The pharmacophore features namely hydrogen bond acceptor (A), hydrogen bond donor (D), hydrophobic group (H), negatively charged group (N), positively charged group (P) and aromatic ring (R) were defined by a set of chemical structure patterns by Phase. Phase assigns the features by using SMARTS queries as one of the three possible geometries defining physical characteristics of the site into point, vector, or group. In the find common pharmacophore step, pharmacophores from all conformations of the ligand in the active site are examined, and those pharmacophores that contain identical sets of features with very similar spatial arrangements are grouped together. If a given group was found to contain at least one pharmacophore from each ligand, then this group gives rise to a common pharmacophore. Any single pharmacophore in the group ultimately becomes a common pharmacophore hypothesis which gives an explanation how ligands bind to the receptor. Common pharmacophores were then identified from set of variants (i.e., a set of feature types that define a possible pharmacophore) using tree-based partition algorithm with the maximum tree depth of three. The final size of pharmacophore box, which governs the tolerance on matching, was 2 Å. Any pharmacophore in the group could ultimately become a hypothesis. These hypotheses were examined using a scoring function to yield the best alignment of the active ligands. In the score hypotheses step, common pharmacophores were examined, and a scoring procedure was applied to identify the pharmacophore from each surviving n-dimensional box that yields the best alignment of the active set ligands. That pharmacophore provides a hypothesis to explain how the active molecules bind to the receptor. The scoring procedure provides a ranking of the different hypotheses, allowing making rational choices about which hypotheses were most appropriate for further investigation. Scoring with respect to actives was conducted using default parameters for site, vector, and volume terms. Ligand activity, expressed as $-\log_{10}(IC_{50})$, was incorporated into the score with a weight of 1.0, and relative conformational energy (kJ/mol) was included with a weight of 0.01. Hypotheses that emerged from this process were subsequently scored with respect to inactives, using a weight of 1.0.The inactive molecules were scored to observe the alignment of these molecules with respect to the pharmacophore hypothesis to enable making a decision on the selection of the hypothesis. Larger is the difference between the scores of active and inactives, better is the hypothesis at distinguishing the actives from inactives. The generated hypothesis was validated by mapping to already known hypothesis. A second method of validation carried out was by comparing the molecular interaction pattern of known inhibitors with the receptor to features present in the hypothesis at the ATP binding site. A third method of validation carried was carried out by measuring the rmsd of the docking poses of the known inhibitor at the active site with the pharmacophoric conformation.

5.2.2 Hypothesis generation for energy-optimized structure based pharmacophore (e-Pharmacophore) Collection of crystal structures The protein structural database, Protein Data

Bank (PDB) was searched for the solved Mtb PknB X-ray crystals. There were five crystals structures reported of catalytic domain that is of ATP binding site. One of which was reported bound with inhibitor mitoxantrone (Mtz) with considerable good resolution of 2.2 Å resolution (2fum), other three were reported with bound substrate ATP analogues, ACP and ADP respectively at active site, and fifth one was reported with amino acid mutation at the activation loop.

Protein preparation Coordinates for PknB inhibitor bound crystal structure 2fum was taken from the PDB and prepared using the Protein Preparation Wizard, which is part of the Maestro software package (Maestro, v8.5, Schrodinger, LLC, New York, NY). Bond orders and formal charges were added for hetero groups, and hydrogens were added to all atoms in the system. To optimize the hydrogen bond network, Histidine tautomers and ionization states were predicted, 180° rotations of the terminal χ angle of Asn, Gln, and His residues were assigned, and hydroxyl and thiol hydrogens were sampled. Water molecules were removed. A brief relaxation was performed using an all-atom constrained minimization carried out with the Impact Refinement module (Impref) (Impact v5.0, Schrodinger, LLC, New York, NY) using the OPLS-2005 force field to alleviate steric clashes that may exist in the original PDB structures. The minimization was terminated when the energy converged or the rmsd reached a maximum cutoff of 0.30 Å.

Ligand Docking/Refinement Glide energy grid was generated for the prepared complexes. The binding site was defined by a rectangular box surrounding the X-ray ligand. The prepared and energy minimized Mtb PknB crystal with bound inhibitor (2fum) was taken for the grid generation. Glide grid was constructed considering the center of the work space ligand as the center of the Grid. The grid size was constructed with default options, but it was kept in mind that the generated grid should be such that it covers the whole of the active site.

E-Pharmacophore generation All the previously reported inhibitors were considered for the XP docking. While running docking simulation Glide XP descriptor information was chosen (Glide v5.0, Schrodinger, LLC, New York, NY). Default settings were used for the refinement and scoring. Based on docking interaction energy, E-Pharmacophore was generated.

Pharmacophore sites were automatically generated with Phase (Phase, v3.0, Schrodinger, LLC, New York, NY) using the default set of six chemical features: hydrogen bond acceptor (A), hydrogen bond donor (D), hydrophobe (H), negative ionizable (N), positive ionizable (P), and aromatic ring (R). Phase treats most cationic groups exclusively as positive ionizable, primary and secondary amines from guanidinium and amidine groups were represented with a complementary set of hydrogen bond donors. Hydrogen bond acceptor sites were represented as vectors along the hydrogen bond axis in accordance with the hybridization of the acceptor atom. Hydrogen bond donors were represented as projected points, located at the corresponding hydrogen bond acceptor positions in the binding site. Projected-points allow the possibility for structurally dissimilar active compounds to form hydrogen bonds to the same location, regardless of their point of origin and directionality.

Each pharmacophore feature site is first assigned an energetic value equal to the sum of the Glide XP contributions of the atoms comprising the site. This allows sites to be quantified and ranked on the basis of these energetic terms. Glide XP descriptors include terms for hydrophobic enclosure, hydrophobically packed hydrogen bonds, hydrophobically packed correlated hydrogen bonds, electrostatic rewards, $\pi...\pi$ stacking, π...cation, and other interactions

[281]. ChemScore [300] hydrogen bonding and lipophilic atom pair interaction terms are included when the Glide XP terms for hydrogen binding and hydrophobic enclosure are zero. Sites with less than half of the heavy atoms contributing to the pharmacophore feature are excluded from the final hypothesis. Thus based on the docking interactions final energy optimized hypothesis (e-pharmacophore) was generated.

5.2.3 Database preparation In-house database molecules and freely available molecular database Asinex was used in the study. The database molecules were removed for the redundancy, the wrong structures were removed and the solvent molecules if present were stripped out. Database molecules were prepared using LigPrep (LigPrep v2.2, Schrodinger LLC, New York, NY) with Epik (Epik v1.6, Schrodinger, LLC, New York, NY) to expand protonation and tautomeric states at 7.0 ± 2.0 pH units. Conformational sampling was performed on all database molecules using the ConfGen search algorithm [301]. ConfGen samples conformations based on a heuristic search algorithm and energetic evaluations to efficiently explore diversity around rotatable bonds, flexible ring systems, and nitrogen inversions. ConfGen was employed with the OPLS_2005 force field and a duplicate pose elimination criterion of 1.0 Å rmsd to remove redundant conformers. A distance-dependent dielectric solvation treatment was used to screen electrostatic interactions. The maximum relative energy difference of 10.0 kcal/mol was chosen to exclude high-energy structures. Using Phase, the database was indexed with the automatic creation of pharmacophore sites for each conformer to allow rapid database alignments and screening.

Virtual screening of database The ligand based Pharmacophore and E-pharmacophore were taken and the prepared database was mapped to hypothesis. The highest active molecule had showed fitness of 3.0 to the pharmacophore. So the molecules with fitness vales less than 70% of this value were discarded. A distance matching tolerance of 2 Å was given during the pharmacophore mapping to database molecules. A maximum of 5000 hits mapped to the each pharmacophore were saved (initial hits).

The hits obtained by virtual screening of the database were docked to ATP binding site. The pharmacophoric alignment pattern of the hits obtained was compared with binding pattern to ATP binding site. The binding poses were manually inspected for binding poses at ATP binding site of PknB. The molecular docking poses were compared with pharmacophore alignment and the molecules which align in same way were considered. The molecules with minimum two H-bond interactions, one of which should be with hinge region amino acid (Val95) were only considered. Hits from virtual screening of database were docked into the PknB ATP binding site using Glide 5.0 (Glide v5.0 Schrodinger, LLC, New York, NY) utilizing the standard precision (SP) scoring function to estimate protein-ligand binding affinities. A maximum of 3000 molecular poses were saved form SP docking run. The docking poses were visually inspected and the molecules possessing good interaction pattern common to the pharmacophore were shortlisted. The molecules with best interaction and the good score only are considered. The only compounds with docking score more than Mtz Glide score were considered. The shortlisted molecules were subjected to the chemical clustering. The molecules with similar structure were clustered together. With aim of collecting diverse molecular structures, the structures from each cluster are examined for interaction pattern with Mtb PknB. The shortlisted Hits were further subjected to the Glide docking with extra precision (XP). The docking was carried out using the inhibitor bound crystal structure of Mtb PknB (PDB entry 2fum). The center of the Glide grid was defined by the position of the co-crystallized inhibitor. Default settings were used for both the grid generation and docking. The flexible docking was carried out with SP or XP scoring. Epik state penalties were considered during the docking run. Top five poses for each molecule were saved from docking runs. Before running the docking for the hits resulted from the virtual screening of the data base the docking parameters were set by running the crystal bound known inhibitor Mtz. Then same parameters were utilized for docking the database hits.

5.3 Results and discussion

5.3.1 Pharmacophore generation

Ligand based Pharmacophore The pharmacophore was built using seven reported inhibitors of Mtb PknB. The molecules below 0.8 μM were considered as active molecules and molecules with IC_{50} activity higher than 2.0 μM were considered as inactive in the Pharmaset. There were 4 active molecules in the Pharmaset, which was utilized to develop the pharmacophore. Mtz with the activity, 0.80 μM, was available with crystal co-ordinates, was present in the set of actives. Phase generated many hypotheses. There were 2 inactive molecules utilized for the scoring and identifying the better hypothesis. The Find common hypotheses step was run with option to generate minimum four pharmacophore sites, generated total of 28 pharmacophores with three different combinations of features. 7 pharmacophores were generated with AAAR combination, 15 pharmacophores were generated with ADRR combination and the third combination was AADR, with which 6 pharmacophores were generated. These pharmacophores were scored according to the fitness to the inhibitors. Upon clustering the scored hypothesis resulted to 14 groups. Out of these pharmacophores hypotheses 12 was chosen best based on the scoring. It had highest survival score compared to all other pharmacophores (3.084) as well as highest survival inactive score (1.095). The hypothesis 12 also featured with highest volume score (0.424), vector score (0.916) and site score (0.74) compared to other pharmacophores, because of which it was selected as the best hypothesis. It had four features in it, one hydrogen donor (D5), one hydrogen acceptor (A4), and two ring aromatic groups (R8 and R10). Below is the picture of the Hypotheses 12 with the distances between the features mentioned in Å units (Figure 29).

Validation of Pharmacophore Before using the pharmacophore for virtual screening it has to be validated. The hypotheses mapped to the Pharmaset molecules. The extent of mapping of a molecule to the hypotheses was expressed in terms of fitness. The hypotheses mapped well to the high active molecules with high fitness value. **I5** was a high active molecule present in Pharmaset with inhibitory activity (IC_{50}) of 0.58 μM, showed highest mapping (100%) with fitness value of 3.0 (Figure 30). **I4** and **I1** were other molecules present in Pharmaset showed mapping of 2.66 and 2.44 respectively to hypotheses (Figure 30). **I2** was the molecule with lowest activity, hypothesis showed a lowest fitness value of 0.77 (Figure 30).

The pharmacophore represents the binding pattern of the ligand to the receptor. The comparison of the receptor complementarity with the generated pharmacophore is a very effective way of validation the pharmacophore. The ligand based pharmacophore generated was compared with the active site of the Mtb PknB crystal structure bound with the Mtz (PDB entry 2fum). The four features present in the pharmacophore were compared to the ATP binding site of enzyme. The crystal bound form of the Mtz as well as the highest active compound **I4** docking presented an H-bond donor interaction with the hinge region amino acid Val95. This H-bond corresponds to the D5 donor feature present in the Pharmacophore. There are two ring aromatic features, which represented the hydrophobic cavity formed by the side chains of the amino acids Val25, Leu17, Val72, Met92, Tyr94, Val95, Met145, and Met155. There are two lysine residues situated in the active site, Lys40 and Lys140. The side chain amine group of the lysine was found to 3.75 to 4.0 Å distance from the acceptor feature present in the pharmacophore (measured based on the atom mapping to the A4 feature from **I4**). Since the lysine side chain is very flexible in nature it may change its conformation to and may take favorable conformation so that it can form an H-bond. Figure 31 is the picture of the pharmacophoric features mapped to the ATP binding site of Mtz bound crystal structure of Mtb PknB. For the comparison the highest active molecule I4 mapped to the pharmacophore also presented. It can be seen that the pharmacophoric features present a very good complementarity to the receptor features.

The comparison of the pharmacophore mapping pose to the crystal binding pose or docking pose has been very efficiently used and for the validating the pharmacophore by David E. Shaw and coworkers in their research article published on the Phase pharmacophore generation [302]. The same was used for the validation of the ligand based PknB inhibitor pharmacophore. The inhibitor bound crystal was taken and the active molecules from the Pharmaset were docked to the ATP binding site. To obtain high precision docking, the simulation was carried out with XP mode of Glide. The first pose with the highest docking score was considered for the comparison. The Mtz binding pose was compared directly with the crystal pose. The comparison of pharmacophore aligned pose to the docking pose presented an amazing result where all the four molecules presented rms deviation less than 2 Å. The **I5** presented a highest rms deviation, which was 1.79 Å. The highest active molecule **I4** presented a least rms deviation of 0.81 Å, and the **I1** had an rms deviation of 1.47 Å. The Mtz mapped with the pharmacophore posed was superimposed with the crystalline pose collected from crystalized PDB structure 2fum. It showed a very less rms deviation of 0.97 Å, inferring the generated ligand based pharmacophore is exactly presenting the receptor binding conformation for the

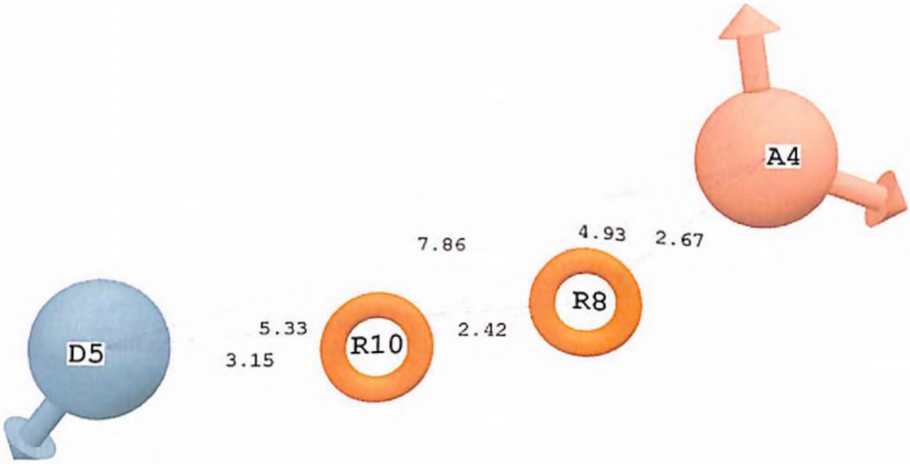

Figure 29: Ligand based pharmacophore of PknB inhibitor, has four features in it. A donor (D5) depicted in blue color, a acceptor (A4) depicted in pink color, and two ring aromatic features (R8 and R10) depicted in brown rings. The numbers mentioned are distance between the features expressed in Å units.

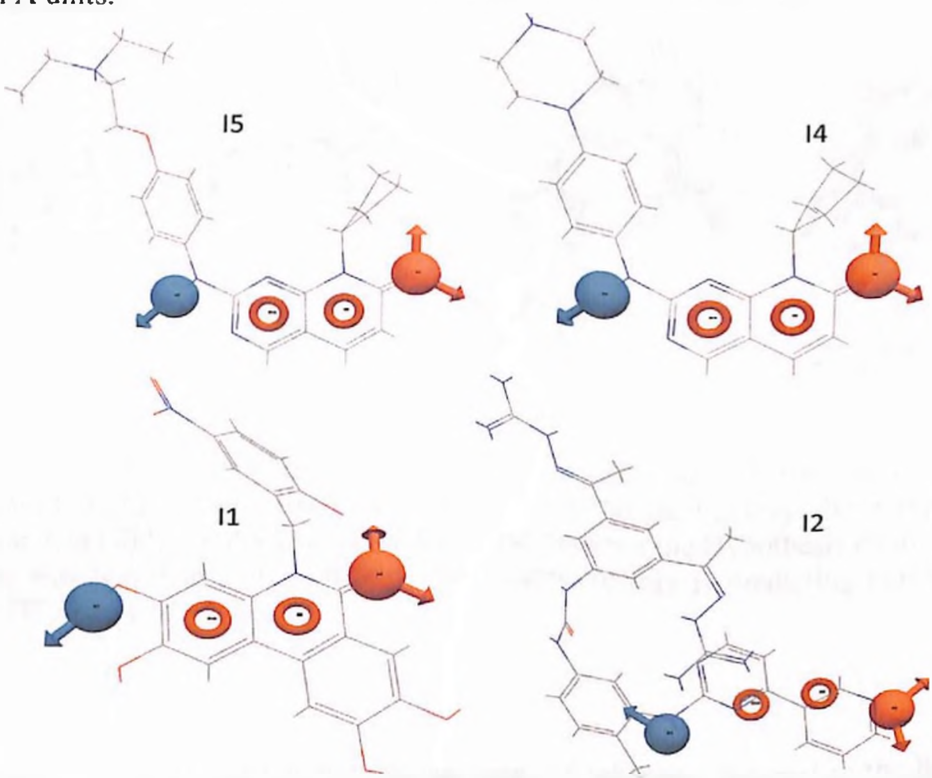

Figure 30: Pharmaset molecules mapped with PknB Ligand based pharmacophore, **I5**, **I4** and **I1** belonged to active molecules from Pharmaset and showed fitness of 3.0, 2.66 and 2.44 respectively. The **I2** belonged to inactive molecule, had fitness 0.7.

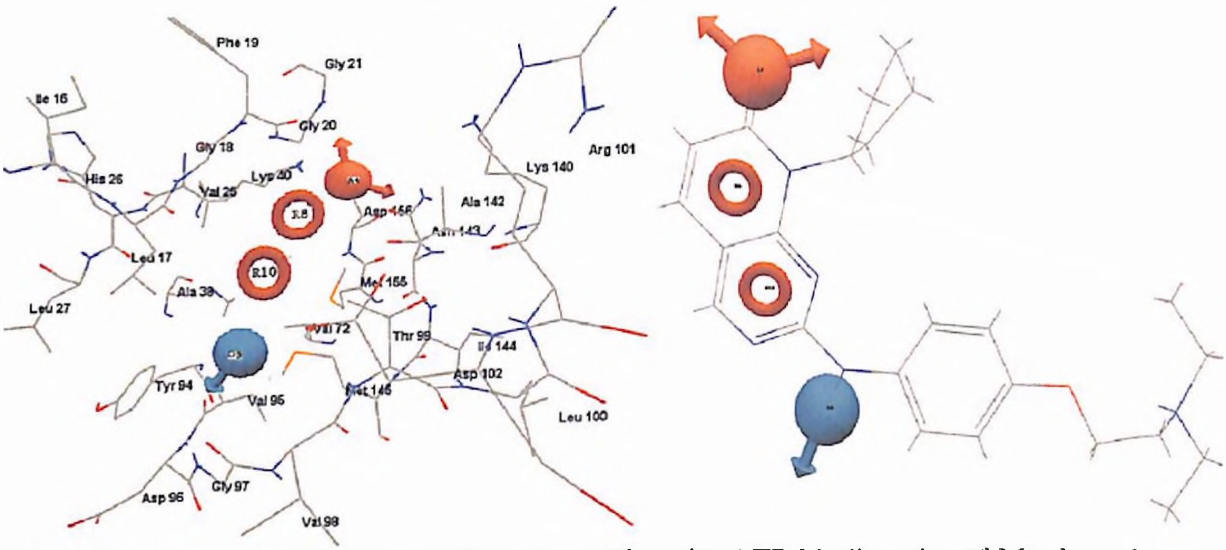

Figure 31: The pharmacophoric features mapped to the ATP binding site of Mtz bound crystal structure of Mtb PknB (PDB entry 2fum). For the comparison the highest active molecule **I4** mapped to the pharmacophore also presented.

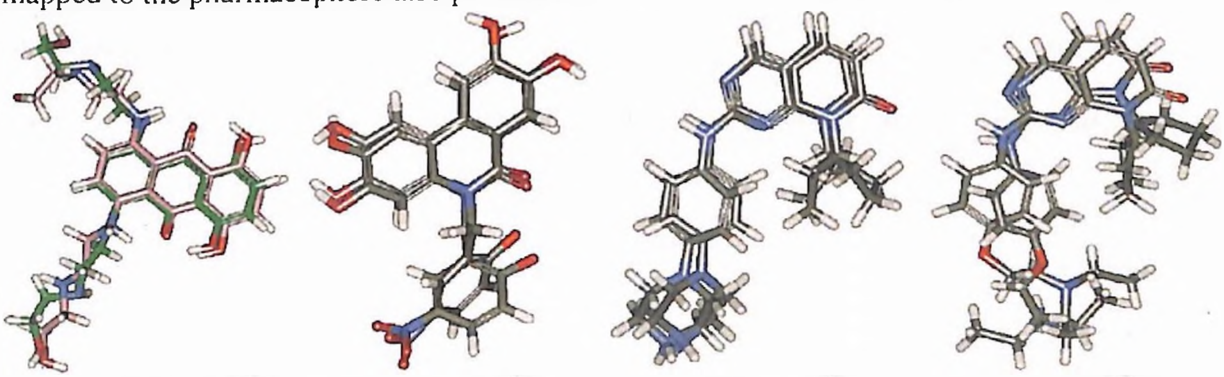

Mtz rmsd 0.975 Å | I1 rmsd 1.472 Å | I4 rmsd 0.814 Å | I5 rmsd 1.797 Å

Figure 32: The Mtz, pharmacophore mapped pose superimposed with the crystal bound pose collected from PDB 2fum. The active Pharmaset molecules aligned to Hypothesis super imposed with highest scored Glide XP docking pose. The rmsd between the Hypothesis conformation and docking pose was less than 2 Å, indicating the pharmacophore is predicting correct mode of binding at ATP binding site.

inhibitors. Figure 32 presents the superimposed poses of inhibitors mapped to the ligand based pharmacophore and to the docking pose of the ligand.

Since there were only few inhibitors reported till now for Mtb PknB a thorough validation of the pharmacophore was needed. The parameters used in all three methods of validation presented good results with generated ligand based pharmacophore indicating generation of fairly good pharmacophore.

Energy optimized structure based pharmacophore The E-pharmacophore was developed using the six default Phase features, hydrogen bond acceptor (A), hydrogen bond donor (D), hydrophobe (H), negative ionizable (N), positive ionizable (P), and aromatic ring (R). The sites with score less than -1.0 were only selected to make pharmacophore. The E-Pharmacophore developed had four features, one hydrogen donor (D4), one hydrogen acceptor (A2), and two ring aromatic groups (R9 & R11) (Figure 33). The energy descriptors presented a high importance to the hinge region interaction, which was represented as two distinct sites in the E-pharmacophore. The acceptor site (A2) had site score of -2.16, mapped to electrostatic interaction corresponding to the H-bond between the back bone amine group, similarly the donor site (D4) had a site score of -2.20 mapped to H-bond involving back bone carboxyl group of Val95. The other two sites present were two ring aromatic features. The R9 had a site score of -1.1, presented the hydrophobic pocket formed by the side chains of amino acids Val25, Ala38, Met92, Val72 and Met155. The R11 had a site score of -1.0, presented the hydrophobic pocket formed by the side chains of residues Leu17, Tyr94 and Met145.

The XP-descriptor information is the various scoring terms from the XP scoring function. Based on this energy scoring, utilizing the Phase default site features the E-pharmacophore is generated. Any feature (site) with score value less than -1.0 is considered an important site of interaction. The XP descriptor information showed very high weightage to the LipophilicEvdW feature (Lipophilic term derived from hydrophobic grid potential and fraction of the total protein-ligand Van-der-wall energy) indicting presence of strong hydrophobic interaction with in the active site pocket. The value was above -5.5, constituting about 50% of the total glide score.

The XP-descriptor information showed strong reward for hydrophobically packed H-bond (PhobEnHB) of -3.0, indicating the presence of strong bipolar interaction at the active site. Other than these the major contributor in the interaction was electrostatic interaction, mainly the in H-bond interaction present at the hinge region amino acid Val95 (Figure 35). The score of above -2.20 was shown for the electrostatic rewards.

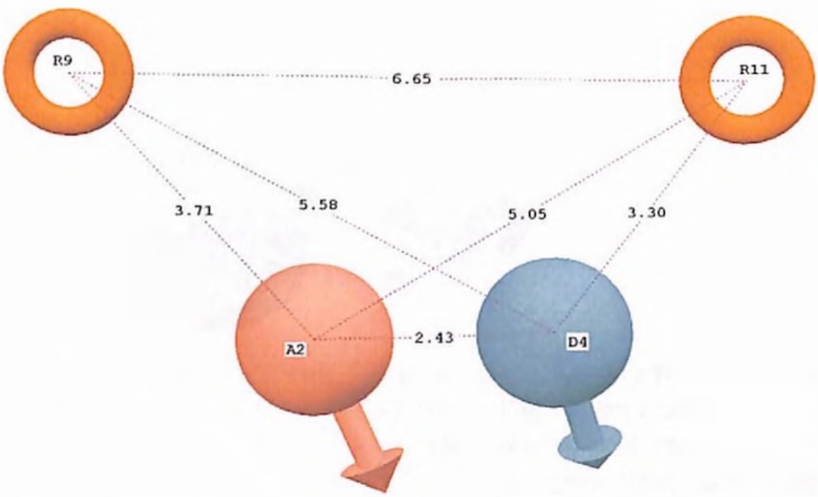

Figure 33: Energy based pharmacophore of PknB inhibitor, has four features in it. A donor (D4) depicted in blue color, an acceptor (A2) depicted in pink color, and two ring aromatic features (R9 and R11) depicted in brown rings. The numbers mentioned are distance between the features expressed in Å units.

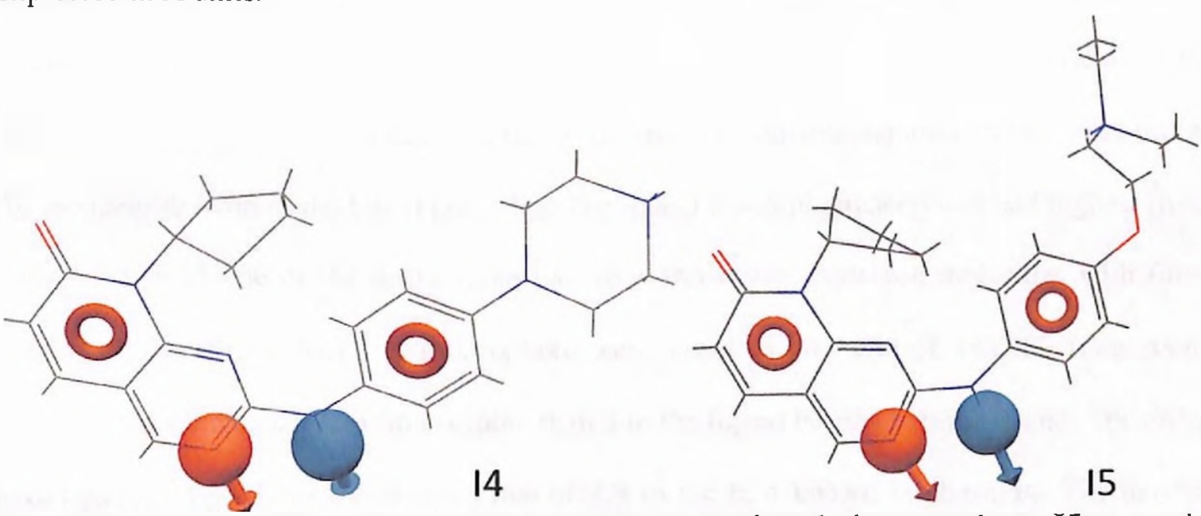

Figure 34: Highest active molecule **I4** mapped to energy based pharmacophore. **I5** mapped to energy based pharmacophore.

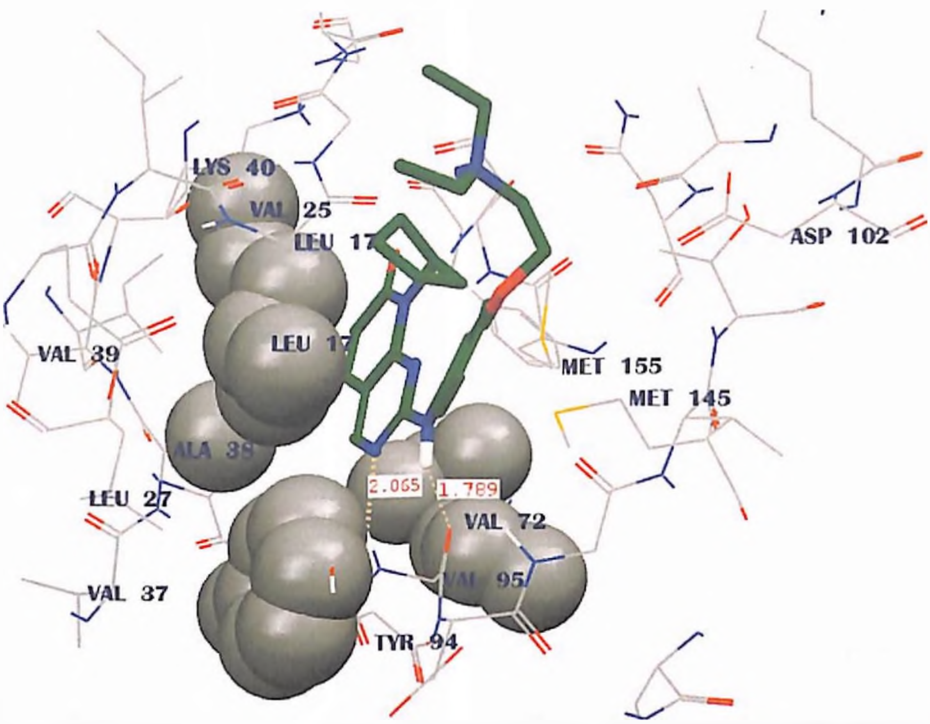

Figure 35: One of the high active molecule **I5** showing the XP-descriptor information presenting the strong reward for hydrophobically packed H-bond. The amino acids represented in spears are contributing to the hydrophobic interaction. The yellow colored interaction depicts the electrostatic interaction in the form of H-bond with hinge region amino acid Val95.

5.4 Virtual screening The in-house Database and commercially available database, Asinex was used for the virtual screening to identify the potential inhibitor of Mtb PknB. Before use the database was prepared so that it will be suitable to use. Both the pharmacophores could not pick up any hits from in-house database, so the commercially available database Asinex was utilized for the identification of the hits (Figure 36). The ligand based pharmacophore had highest fitness value of 3 to **I5** one of the active molecule from Pharmaset. Database molecules with fitness more than 2 to ligand based pharmacophore were saved as hits. Out of 393,000 from Asinex database 2017 molecules had fitness more than 2 to the ligand based pharmacophore. The energy based pharmacophore had a fitness value of 2.8 to the best known inhibitor **I4**. The database molecules with fitness more than 70% of this value (1.87) were saved. Energy based pharmacophore of PknB inhibitor identified 2709 molecules from Asinex database.

These hits collected from pharmacophore mapping were then subjected to Glide docking at ATP binding site with standard precision (SP). Two docking programs were tried for carrying out the docking simulation GOLD and Glide. Even after trying various options like changing the active site radius, changing the center of the active site, putting constrains during docking like H-bond and/or hydrophobic constrains, GOLD failed to redock the Mtz to ATP site, but Glide efficiently docked the Mtz in to the ATP binding site. So for future studies involving docking for shortlisting of the hits, only Glide docking was utilized.

The Glide docking parameter was set initially by docking the crystal ligand into the active site. The Glide grid was used for carrying out the calculation during the docking simulations. The grid was generated by considering the crystal ligand as the center of the grid. The docking was carried out with default options; with no constrain application during the docking. The top pose resulted from the Glide SP redocking had a Glide score of -6.54, and had an rms deviation of 1.2 Å. The rms deviation of the redocked ligand less than 2 Å to the crystal pose indicates good docking. The same parameters were utilized for carrying out the docking of the shortlisted hits from both pharmacophores. The Glide redocking score obtained for Mtz -6.5 was used as lower ceiling score for the hits identified by pharmacophore mapping during SP docking. This resulted into the short listing of 924 molecules, which were grouped into clusters based on their chemical diversity, resulted into 19 different clusters for the molecules shortlisted from ligand based pharmacophore. From energy based pharmacophore, 1235 molecules were shortlisted, belonging to 32 clusters. The top pose with highest glide SP score was saved for each molecule. The saved molecular poses were checked for the presence of at least two H-bonds. Both the pharmacophores had the sites corresponding to the hinge region interaction, and also the XP descriptors generated during E-pharmacophore generation presented high weightage to hinge region interactions during energy evaluation. So during shortlisting of the molecules from docking poses, only those poses were considered with the presence of the hinge region H-bond as one of the H-bond. Then pose was examined for presence of any other additional H-bond so as to contain each molecule minimum of two H-bonds with the enzyme. In the next step manual inspection of the docking poses were carried out where the docking poses compared with the pharmacophore mapping pose. The molecules presenting similar orientation were only considered. As the main motto was to identify the inhibitors of Mtb PknB belonging to the diverse class of chemicals, so only best and promising molecules belonging to each cluster was shortlisted. This resulted into shortlisting of total 77 molecules, 22 molecules from ligand based pharmacophore and 55 molecules from energy based pharmacophore.

These 77 molecules were subjected to another set of docking simulation. These were docked with extra precision (XP) mode of Glide. The docking pose collected from SP docking was used as the starting pose for XP docking. This was to check that the SP dock had predicted the minimum energy stable binding pose. The XP docking covers a large conformational space compared to the normal SP docking. So even if the ligand is at local minima, during XP docking the molecule is pushed to the global minima with best binding pose. If the molecule is already at global minima then the XP docking pose will not have a change in pose or intern will not have large rms deviation to the initial pose generated by SP docking. The rms deviation within 2 Å is accepted as same pose. The docked poses were also checked for the binding pattern and hydrogen bonding patterns, and compared with the pharmacophore binding pattern. This resulted into shortlisting of 13 molecules from ligand based pharmacophore and 45 molecules from energy based pharmacophore. Thus totally 58 molecules were shortlisted. Below Figure 36 shows the structure of 58 molecules shortlisted with the potential to inhibit Mtb PknB enzyme.

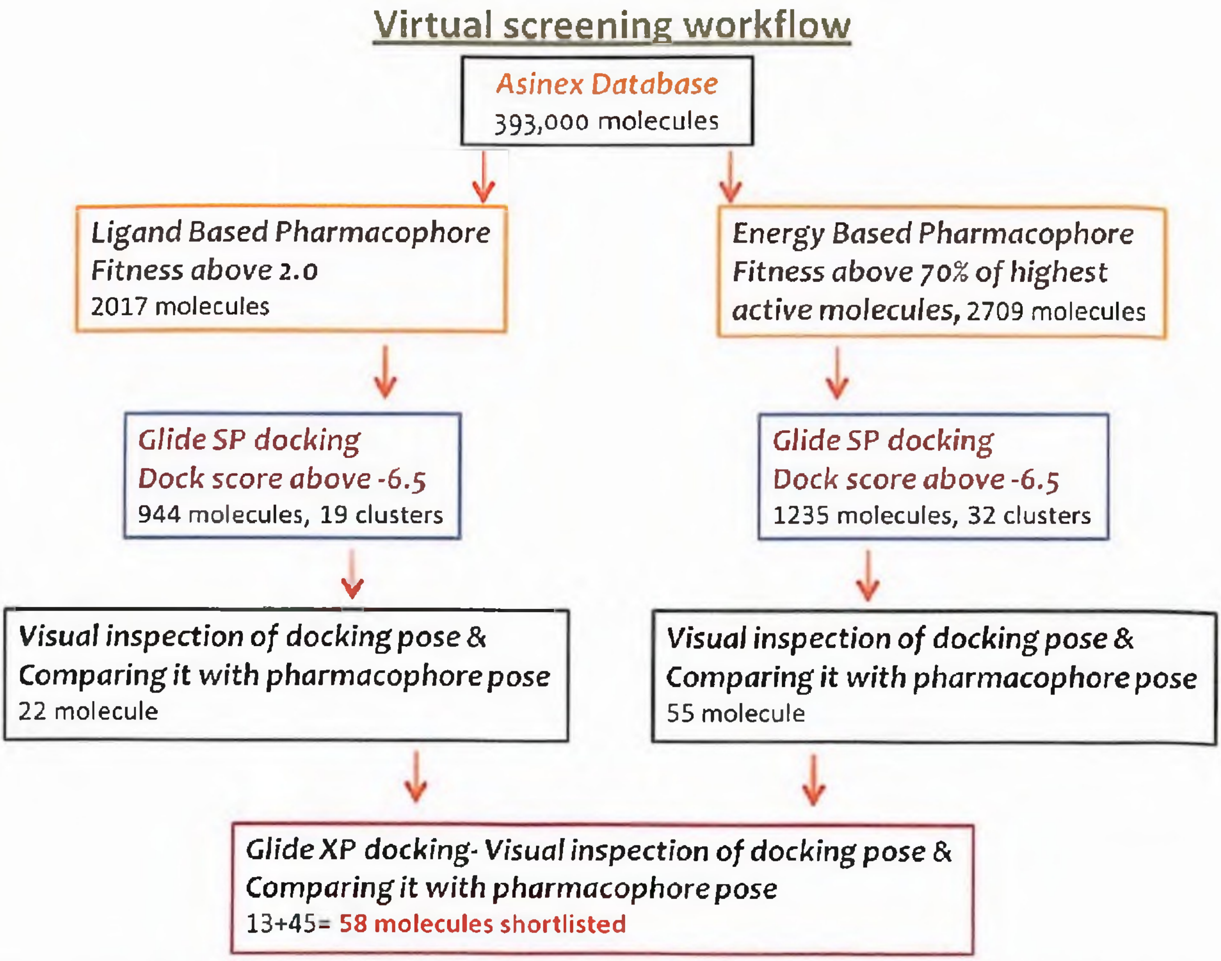

Figure 36: Schematic representation of different steps followed during the virtual screening of asinex database to identify the potential hits which can inhibit the Mtb PknB.

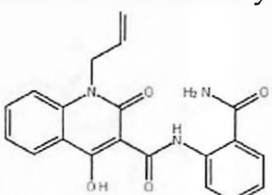

title: YS201
Fitness: 2.323
GLIDE Score: -7.45

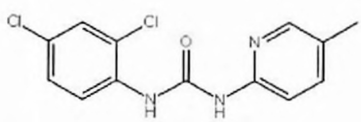

title: YS202
Fitness: 2.318
GLIDE Score: -7.82

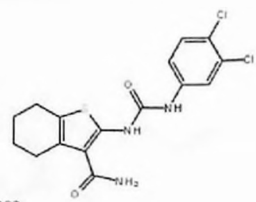

title: YS203
Fitness: 2.245
GLIDE Score: -7.74

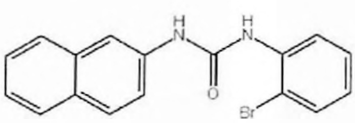

title: YS204
Fitness: 2.24
GLIDE Score: -7.99

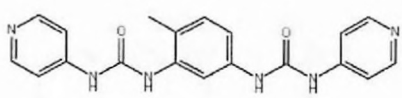

title: YS205
Fitness: 2.164
GLIDE Score: -8.14

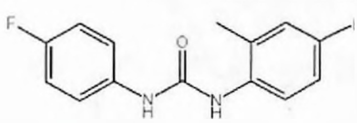

title: YS206
Fitness: 2.078
GLIDE Score: -7.06

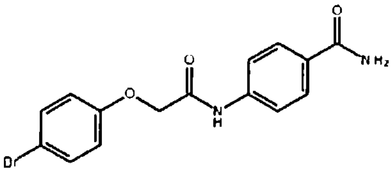

title: YS207
Fitness: 2.012
GLIDE Score: -6.85

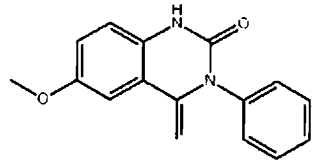

title: YS208
Fitness: 2.311
GLIDE Score: -9.07

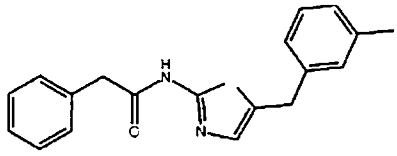

title: YS209
Fitness: 2.25
GLIDE Score: -8.73820705032

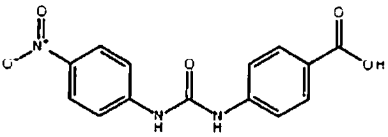

title: YS210
Fitness: 2.196
GLIDE Score: -7.77

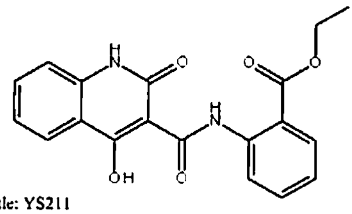

title: YS211
Fitness: 2.145
GLIDE Score: -6.95

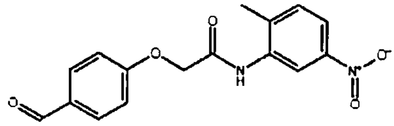

title: YS212
Fitness: 2.139
GLIDE Score: -7.52

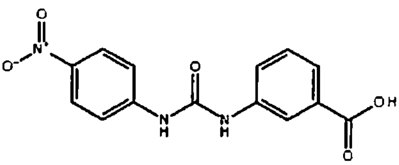

title: YS213
Fitness: 2.129
GLIDE Score: -8.44

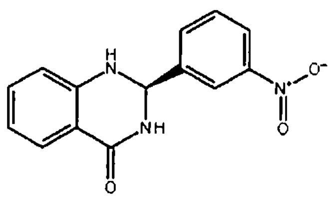

title: YS214
Fitness: 2.019
GLIDE Score: -8.63

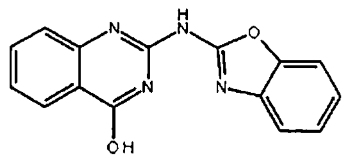

title: YS215
Fitness: 2.453
GLIDE Score: -8.56

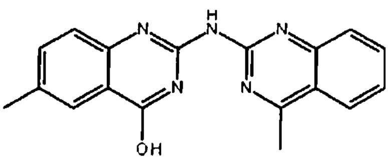

title: YS216
Fitness: 2.44
GLIDE Score: -7.73

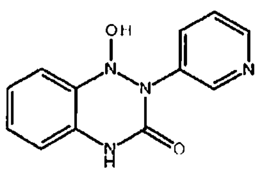

title: YS217
Fitness: 2.283
GLIDE Score: -9.1

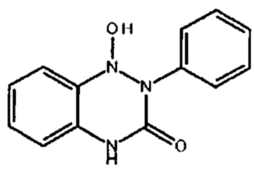

title: YS218
Fitness: 2.276
GLIDE Score: -9.24

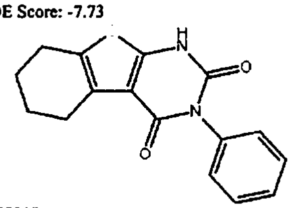

title: YS219
Fitness: 2.239
GLIDE Score: -8.39

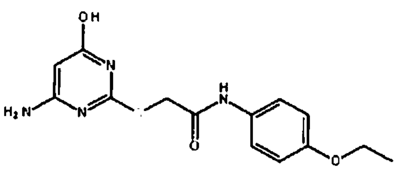

title: YS220
Fitness: 2.029
GLIDE Score: -7.08

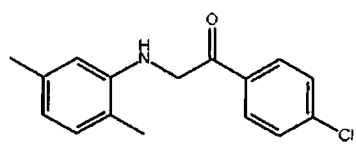

title: YS221
Fitness: 2.018
GLIDE Score: -8.08

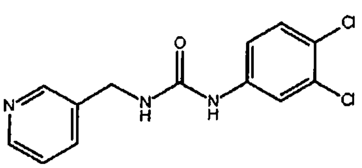

title: YS222
Fitness: 2.014
GLIDE Score: -7.17

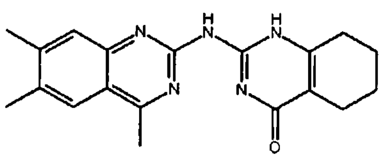

title: YS223
Fitness: 2.453
GLIDE Score: -7.22

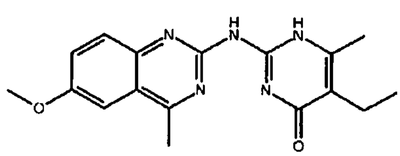

title: YS224
Fitness: 2.414
GLIDE Score: -8.52

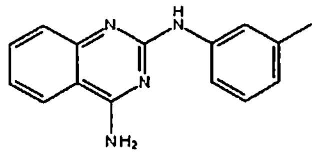

title: YS225
Fitness: 2.388
GLIDE Score: -7.18

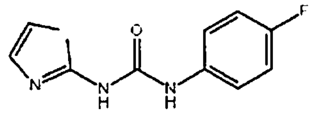

title: YS226
Fitness: 2.264
GLIDE Score: -7.69

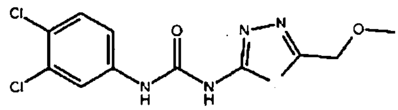

title: YS227
Fitness: 2.264
GLIDE Score: -7.5

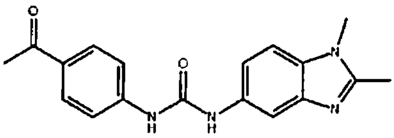

title: YS228
Fitness: 2.252
GLIDE Score: -8.62

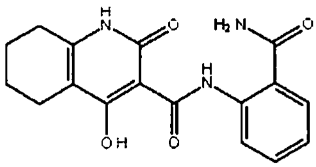

title: YS229
Fitness: 2.238
GLIDE Score: -8.18

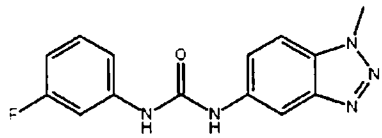

title: YS230
Fitness: 2.212
GLIDE Score: -7.93

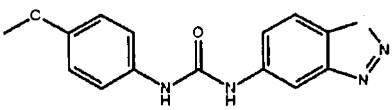

title: YS231
Fitness: 2.203
GLIDE Score: -7.81

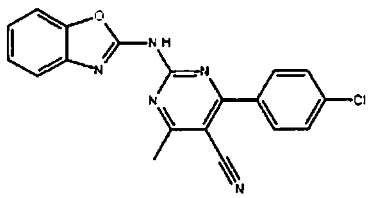

title: YS232
Fitness: 2.191
GLIDE Score: -8.28

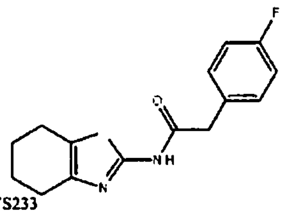

title: YS233
Fitness: 2.113
GLIDE Score: -7.89

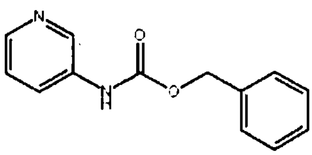

title: YS234
Fitness: 2.047
GLIDE Score: -6.95

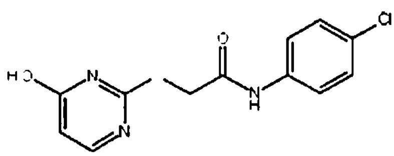

title: YS235
Fitness: 2.009
GLIDE Score: -7.2

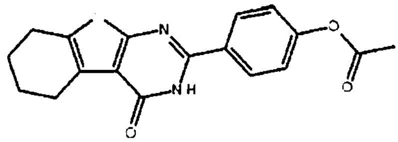

title: YS236
Fitness: 2.005
GLIDE Score: -9.1

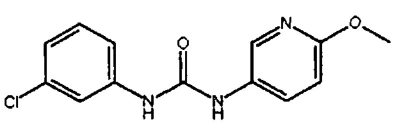

title: YS237
Fitness: 2.228
GLIDE Score: -7,77

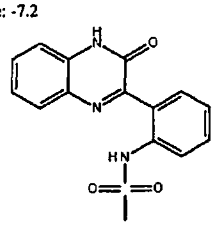

title: YS238
Fitness: 2.162
GLIDE Score: -8.56

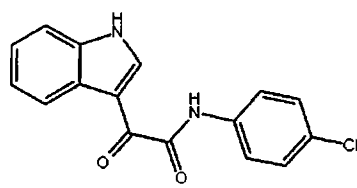

title: YS239
Fitness: 2.144
GLIDE Score: -8.46

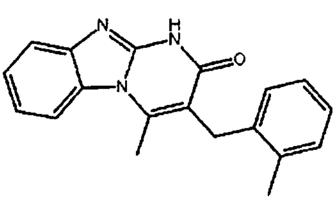

title: YS240
Fitness: 2.028
GLIDE Score: -8.14

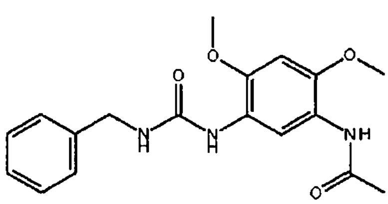

title: YS241
Fitness: 2.011
GLIDE Score: -7.96

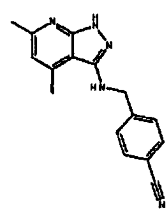

title: YS242
Fitness: 2.008
GLIDE Score: -8.85

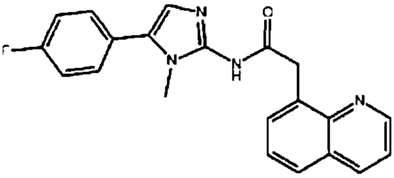

title: YS243
Fitness: 2.103
GLIDE Score: -8.28

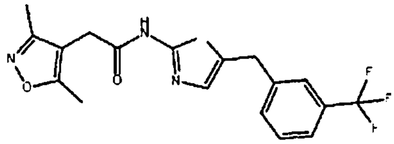

title: YS244
Fitness: 2.067
GLIDE Score: -7.24

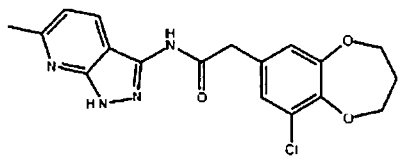

title: YS245
Fitness: 2.026
GLIDE Score: -8.25

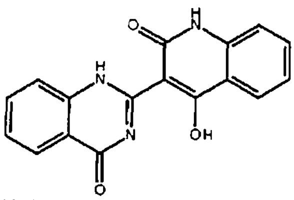

title: YS246
Fitness: 1.957
GLIDE Score: -6.82

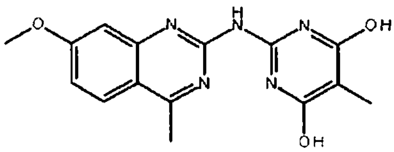

title: YS247
Fitness: 2.335
GLIDE Score: -8.79

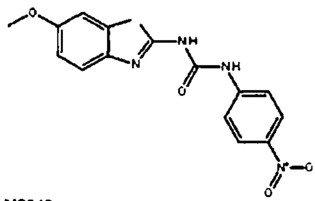

title: YS248
Fitness: 2.079
GLIDE Score: -7.45

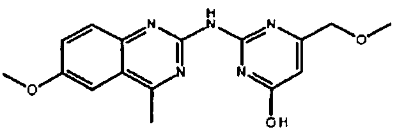

title: YS249
Fitness: 2.172
GLIDE Score: -9.74

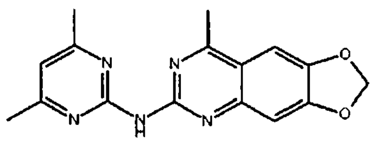

title: YS250
Fitness: 2.089
GLIDE Score: -6.94

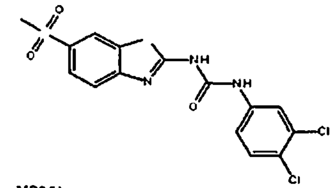

title: YS251
Fitness: 2.091
GLIDE Score: -7.04

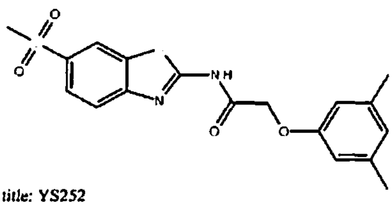

title: YS252
Fitness: 2.086
GLIDE Score: -6.62

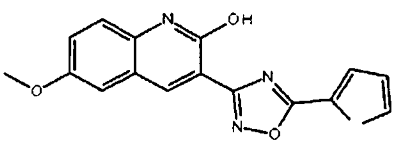

title: YS253
Fitness: 2.041
GLIDE Score: -6.83

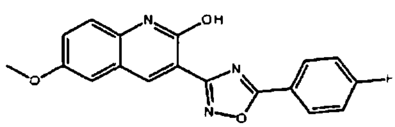

title: YS254
Fitness: 2.039
GLIDE Score: -6.98

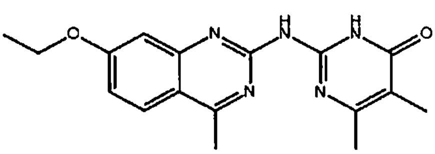

title: YS255
Fitness: 2.289
GLIDE Score: -8.34

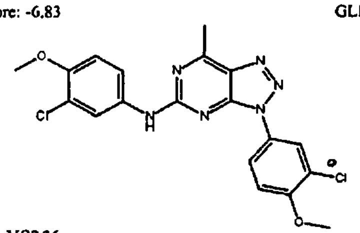

title: YS256
Fitness: 2.07
GLIDE Score: -6.93

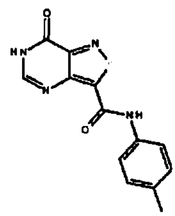

title: YS257
Fitness: 2.074
GLIDE Score: -7.89

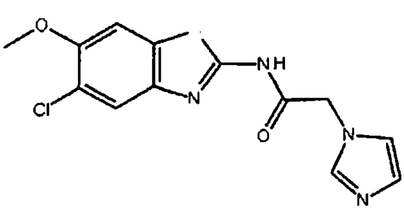

title: YS258
Fitness: 1.998
GLIDE Score: -6.66

The active site of Mtb PknB was formed by the presence of combination of the polar and non-polar surface areas, which constituted the Van-der-wall interaction, charge induced and electrostatic interactions with the ligands. The amino acid residues Val95, Tyr94 forms the base of the active site pocket. The number of residues of both the N- and C-terminal lobes makes Van- der-waals Surface, include Leu17, Gly18, Val25, Ala38, Met 92, Glu93, Tyr94 and Val95 in the N-terminal lobe, Met145 and Met155 in the C-terminal lobe. These constitute a strong hydrophobic pocket of Mtb PknB. The residues Asp96, Gly97, Thr99 and Asp102 present the water exposed area of active site pocket, provided the polar surface area. The inner side of the pocket is constituted by amino acid residues Lys40, Lys140, Asn143 and Asp153 which provide the electrostatic surface areas.

Table 13 presents the interaction pattern of each molecule with the amino acid residues of Mtb PknB. In the table the side chain and back bone interactions are listed with the nature of interaction present between molecule and the amino acid residue (polar, charge, acceptor, donor, hydrophobic, ring aromatic). The Figure 37 reprasents the graphcal reprsentation of the contact interaction pattern of the shortlisted potential Mtb PknB inhibitor with the enzyme. Based on the the interaction patern seen between the amino acid and the ligands the amino acids can be grouped into three catogories. The residues providing the polar interactions, the residues with non-polar interactions and the amino acid residues provinding both polar and non polar interactions.

The amino acids seen prvioding the strong polar interactions are Asp156, Asp102, Thr99, Gly97 and Asp96. In all aspartic acid residues interactions the side chain was involved. Asp156 produced charge interaction with all the ligand exceptfew ligands (**YS202**, **YS207**, **YS214**,

YS232, **YS233** and **YS258**). Through backbone amine moiety iteraction it povided the donor interactins for ligands **YS210**, **YS212**, **YS220**, **YS226**, **YS228**, **YS230**, **YS231**, **YS249**, **YS251** and **YS252**, and through side chains it has provided aceptor interaction for ligands **YS205**, **YS213**, **YS220** and **YS235**. Asp102 was located at the water exposed surface of enzyme pocket, provided the charge interaction throgh its sidechain. Thr99 was located near to Asp102, confining the water exposed area, povided the polar interactions throgh the hydroxyl sidechain. The Gly97and the Asp96 prvided the polar interaction throgh the back bone interactions, from table it can be seen that The Asp96 also formed charge interaction with few ligands for example **YS250**, **YS251**, **YS252**, **YS253**, **YS254**).

Other than this amino acids Lys40 and Glu93 provided the moderated number of polar interaction with ligands. The lysine is located inner side of the active site pocket. The interaction were through highly flexible side chain, provided a strong charge interaction. Glu93 interaction was through back bone interactions; with **YS256**, **YS255**, **YS249**, **YS247**, **YS232**, **YS233** and **YS215** it formed C=O...CH charge interactions. With **YS201**, **YS203** and **YS232** Glu93 through acceptor interaction formed the H-bond. Other than these amino acids Glu18, Phe19, Gly20 provided contact with the ligand throgh back bone interactions. Lys140 povided charge interaction with **YS205**; Arg101 with **YS223** and **YS257** through sidechain interactions.

The Val25, Val38, Val72, Met92, Met145 and Met155 povided the strong hydrophobic interactions in the form of Van-der-walls interactios with all the hits. These amino acids were located at the core of active site pocket. The hydrophobic pocket formed was picked by both the pharmacophores the e-pharmacophore as well as the ligand based pharmacophore. Ala38 also additionally formed the backbone interaction contact with ligands **YS212**, **YS233**, **YS240**, **YS255** and **YS256**. The three methionines Met92, Met145 and Met155 produced strong hydrobhobic interaction through sidechain interactions. Met92 formed the H-bond with the ligand **YS239** and **YS239** through acceptor natured suphur atom present at the sidechain.

Certain residues in the Mtb PknB presented a combitnation of the polar and non-plar interaction. The part of amino acid provided the Van-der-walls interaction and a part of the same residue provided the electrostatic interactions. The amino acid residues Leu17, Tyr94 and Val95 formed very strong dual interactions with all the molecules. The Leu17 produced more of nonpolar inctions with ligands through the side chain interaction. The backbone cotact provided some polar interactions. Three of the molecules **YS229, YS246** and **YS247** formed H-bond with the backbone amine moiety. The Tyr94 and the Val95 were located at the hinge regon Mtb PknB enzyme. From Figure 37 it is evident that the all the molecules shortlited are presenting strong interaction pattern with Val95. The sidechain presented strong hydrophobic Van-der-walls interaction between the ligands and ezyme. The back bone interaction resuted into strong electrostatic interaction leading to the formation of H-bonds. The backbone carbonyl moiety of the Val95 presented a strong acceptor interactions to ligands and the backbone amine moiety acted as a donor. Thus the amino acid Val95 provided two different types of interaction to hold the molecule in active site. Smilarly the amino acid residue Tyr94 provided both polar and non polar interaction with all the molecules. The sidechain phenyl ring fromed a part of the hydrophobic pocket. The backbone contact formed the polar interactions. The open form of the enzyme is inactive, upon binding of substrate there occurs a conformational change resulting into the closed conformation, which is the active form of the enzyme. This movement between two domains is brought about at hinge region. The active site is located at the hinge region and the two domains cover the active site from both the sides. The molecules with high afinity to the hinge region amino acid will have higher potential to stay at the active site. Other than Tyr94 and Val95, Ala142 and Phe152 provided combined polar and non-polar interactions to some ligands. The backbone contact with the ligands provided the polar inteaction with thee two amino acids. The Phe152 ring aromatic interactins with ligands **YS210**, **YS220**, **YS227** and **YS248**. Table 14 details the different types of interactions of each molecules with active site amino acid residues of Mtb PknB. Figure 38 to 48 shows the contact residues and electrostatic surface view of Mtb PknB with some shortlisted potential inhibitors.

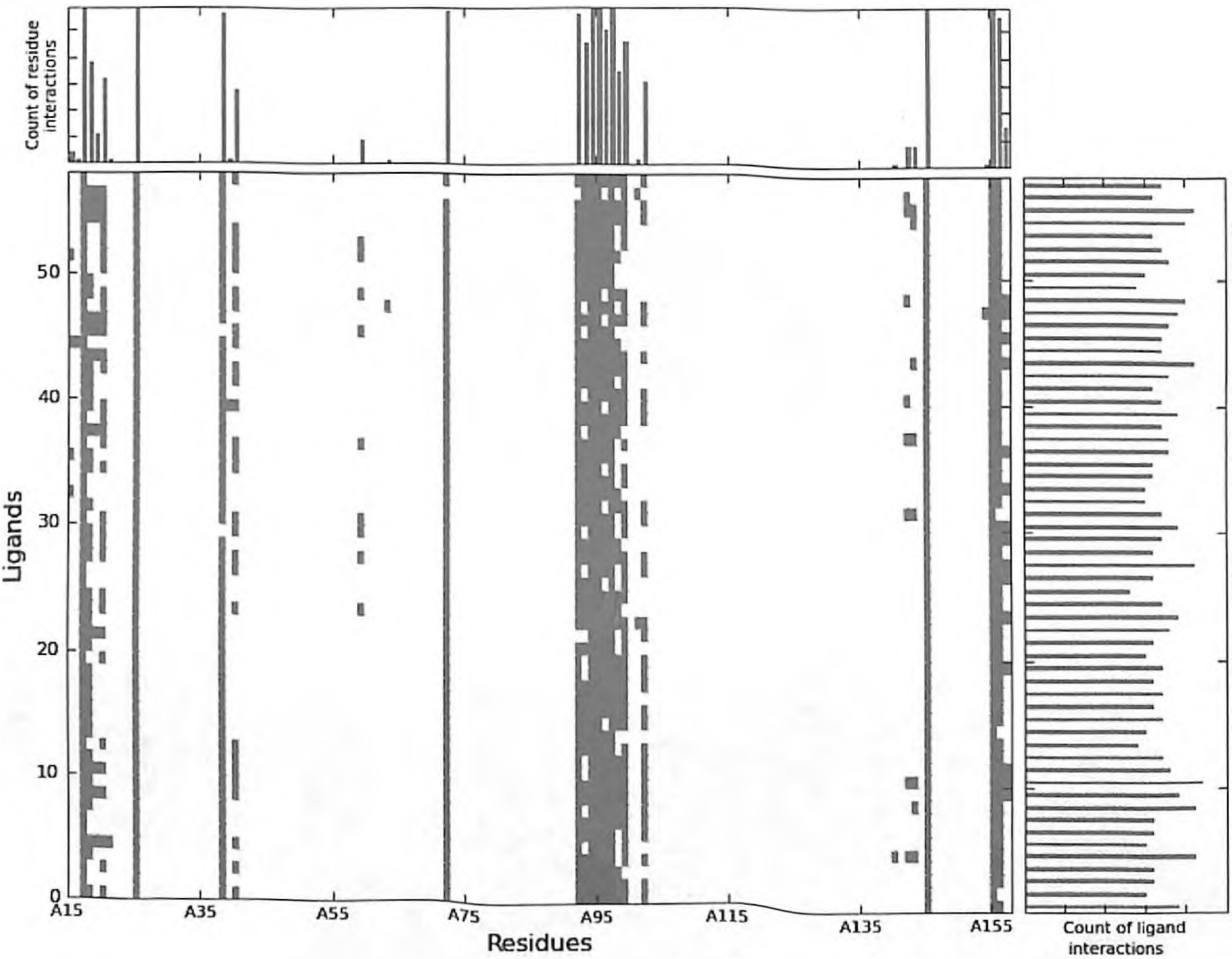

Figure 37: Graphical representation of interaction contacts of the shortlisted potential Mtb PknB inhibitors with enzyme.

Table 14: The interaction pattern of each molecule with the amino acid residues of Mtb PknB. The side chain and back bone interactions are listed with the nature of interaction present between molecule and the amino acid residue.

Molecule	E15	I16	L17	G18	F19	G20	G21	V25	A38	V39	K40	E59	V72	M92	E93	Y94	V95	D96	G97	V98	T99	R101	D102	K140	A142	N143	M145	M155	D156	F157
YS201			SBH	B		B		SH	SH		SPC		SH	SH	BPACS	BSHR	BSHAD	BSPC	B	B	BSP		SPC				SH	SH	BSPC	
YS202			SBH					SH	SH				SH	SH	B	BSHR	BSHAD	B	B	BSH	BSP		SPC				SH	SH		
YS203			SBH			B		SH	SH		SPC		SH	SH	BPACS	BSHR	BSHAD	BSPC	B	SH							SH	SH		
YS204			SBH	B				SH	SH				SH	SH	B	BSHR	BSHAD	B	B		SP		SPC				SH	SHB	BSPC	
YS205			SBH	B	B	B	B	SH	SH		SPC		SH	SH		BSHR	BSHAD	B	B		SP			SC	BSH	SP	SH	SH	BSPCA	
YS206			SBH					SH	SH				SH	SH	B	BSHR	BSHAD	B	B		SP		SPC				SH	SH	BSPC	
YS207			SH					SH	SH				SH	SH	B	BSHR	BSHA	B	B	BSH	BSP		SPCA				SH	SH	B	
YS208			SBH	B				SH	SH				SH	SH		BSHR	BSHAD	B	B	BSH	BSP		SPC				SH	SH	BSPC	
YS209			SBH	B	B	B		SH	SH		SPC		SH	SH	B	BSHR	BSHAD	B	B	B	BSP		SPC			SP	SH	SH	BSPC	
YS210			SBH	B				SH	SH		SPC		SH	SH	B	BSHR	BSHAD	B	B	BSH	BSP		SPCA				SH	SHB	BSPCD	BSR
YS211			SBH	B	B	B		SH	SH		SPC		SH	SH		BSHR	BSHAD	B	B	BSH	SP		SPC		B	BSP	SH	SHB	BSPC	B
YS212			SBH	B				SH	SHB		SPC		SH	SH		BSHR	BSHA	B	B	B	SP		SPC				SH	SHB	BSPCD	B
YS213			SBH			B		SH	SH		SPC		SH	SH	B	BSHR	BSHAD	B	B		SP		SPC				SH	SH	BSPCA	
YS214			SBH	B				SH	SH				SH	SH	B	BSHR	BSHAD	BSPC	BD								SH	SH	BSPC	
YS215			SBH	B				SH	SH				SH	SH	BPCS	BSHR	BSHAD		BA	BSH	SP		SPC				SH	SH		
YS216			SBH	B				SH	SH				SH	SH	B	BSHR	BSHAD	B	B	BSH	SP		SPC				SH	SH	BSPC	
YS217			SBH	B				SH	SH				SH	SH	B	BSHR	BSHAD	B	B	B	SP						SH	SH	BSPC	
YS218			SBH	B				SH	SH				SH	SH	B	BSHR	BSHAD	B	B	B	SP		SPC				SH	SH	BSPC	
YS219			SBH	B				SH	SH				SH	SH		BSHR	BSHAD	B	B	BSH	BSP		SPC				SH	SH	BSPC	
YS220			SBH			B		SH	SH				SH	SH		BSHR	BSHD	B	B	BSH	BSP		SPC				SH	SHB	BSPCDA	BSR
YS221			SBH	B				SH	SH				SH	SH	B	BSHR	BSHAD	BSPC	B		SP						SH	SH	BSPC	
YS222			SBH	B	B	B		SH	SH				SH			BSHR	BSHAD	B	B		SP		SPC				SH	SH	BSPC	
YS223			SBH	B				SH	SH				SH	SH	B	BSHR	BSHAD	B	B	BSH	SP	SPC	SPC				SH	SH	BSPC	
YS224			SBH	B		B		SH	SH		SPC	SPC	SH	SH	BPCS	BSHR	BSHAD	BSPC	B	BSH							SH	SH	BSPC	B
YS225			SBH	B		B		SH	SH				SH	SH	BPCSA	BSHR	BSHAD	B	B	B	SP						SH	SH	BSPC	
YS226			SBH					SH	SH				SH	SH	B	BSHR	BSHAD		B		SP						SH	SH	BSPCD	
YS227			SBH					SH	SH		SPC		SH	SH		BSHR	BSHAD	B	B		SP		SPC				SH	SHB	BSPC	BSR
YS228			SBH	B		B		SH	SH		SPC	SPC	SH	SH	B	BSHR	BSHAD	B	B	SH	SP		SPC				SH	SH	BSPCD	B
YS229			SBHA	B		B		SH	SH				SH	SHBA	B	BSHR	BSHA	B	B	B							SH	SH	BSPC	
YS230			SBH	B		B		SH			SPC	SPC	SH	SH		BSHR	BSHAD	B	B		SP						SH	SH	BSPCD	B
YS231			SBH			B		SH	SH		SPC	SPC	SH	SH	B	BSHR	BSHAD	B	B		SP		SPC				SH	SH	BSPCD	B
YS232			SBH	B				SH	SH				SH	SH	BPCS	BSHR	BSHAD		B	BSH	SP		SPC		BSH	B	SH	SH		
YS233	SPC		SBH					SH	SHB				SH	SHB	BPCS	BSHR	BSHAD	B	B	B							SH	SH	B	
YS234			SBH					SH	SH				SH	SH	B	BSHR	BSHAD	B	B		SP						SH	SH	BSPC	B
YS235			SBH	B		B		SH	SH		SPC		SH	SH	B	BSHR	BSHD		B		SP						SH	SH	BSPCA	
YS236	SPC		SBH	B				SH	SH		SPC		SH	SH	B	BSHR	BSHAD	B	B								SH	SHB	BSPC	
YS237			SBH			B		SH	SH		SPC	SPC	SH	SH	B	BSHR	BSHAD	B	B		SP						SH	SH	BSPC	B
YS238			SBH	B	B	B		SH	SH				SH	SH		BSHR	BSHAD	B	B	B					B	SP	SH	SH	BSPC	
YS239			SBH			B		SH	SH				SH	SHA	B	BSHR	BSHAD	B	B	B	SP		SPC				SH	SH	BSPC	
YS240			SBH	B		B		SH	SHB	B	SPC		SH	SH	B	BSHR	BSHAD		B	B	SP		SPC				SH	SHB	BSPC	
YS241			SBH	B				SH	SH				SH	SH		BSHR	BSHAD	BSPC	B	BSH	BSP		SPC		BSH		SH	SH	BSPC	
YS242			SBH	B				SH	SH		SPC		SH	SH	B	BSHR	BSHAD	B	B		SP						SH	SH	BSPC	
YS243			SBH	B		B		SH	SH		SPC		SH	SH	B	BSHR	BSHAD	BSPC	BD	B	SP						SH	SH	BSPC	
YS244			SBH	B	B	B		SH	SH				SH	SH	B	BSHR	BSHAD	BSPC	B	B	SP		SPC			SP	SH	SHB	BSPC	B
YS245	SPC	BSH	SBH					SH	SH		SPC		SH	SH	B	BSHR	BSHAD	B	B	B							SH	SH	BSPC	
YS246			SBHA	B	B	B		SH	SH		SPC	SPC	SH	SH		SHR	BSHA	B	B								SH	SH	BSPC	B
YS247			SBHA	B	B	B		SH	SH				SH	SH	BPCS	BSHR	BSHAD		BA	B	SP		SPC				SH	SH	BSPC	
YS248			SBH			B		SH	SH		SPC		SHB	SH		BSHR	BSHAD	B	B		SP		SPC				SH	SHB	BSPC	BSR
YS249			SBH	B		B		SH	SH		SPC	SPC	SH	SH	BPCS	BSHR	BSHAD		BA	B	SP				B		SH	SH	BSPCD	B
YS250			SBH	B				SH	SH				SH	SH	B	BSHR	BSHA	BSPC	BD								SH	SHB	BSPC	
YS251			SBH			B		SH	SH		SPC		SH	SH	B	BSHR	BSHAD	BSPC	B								SH	SHB	BSPCD	
YS252	SPC		SBH			B		SH	SH		SPC	SPC	SH	SH	B	BSHR	BSHAD	BSPC	BD	B							SH	SHB	BSPCD	
YS253			SH			B		SH	SH		SPC	SPC	SH	SH	B	BSHR	BSHAD	BSPC	B		SP						SH	SH	BSPC	
YS254			SH			B		SH	SH		SPC		SH	SH	B	BSHR	BSHAD	BSPC	B		SP						SH	SH	BSPC	
YS255			SBH	B	B	B		SH	SHB				SH	SH	BPCS	BSHR	BSHAD	B	B	BSH	SP		SPC			SP	SH	SH	BSPC	
YS256			SBH	B	B	B		SH	SHB				SH	SH	BPCS	BSHR	BSHAD	B	B	BSH	SPB		SPC		BSH	SP	SH	SH	BSPC	
YS257			SH	B	B	B		SH	SH						B	BSHR	BSHAD		B		SP	SPC			BSH		SH	SH	BSPC	
YS258			SBH					SH	SH		SPC		SH	SH	B	BSHR	BSHD	B	B	B	SPB		SPC				SH	SHB	B	

The pink color column are the amino acid with both polar and non-polar interaction, green color column are the amino acid with polar interactions, violet color column are the amino acid with non-polar interactions. S=Saidechain, B=Backbone, P=Polar, C=Charge, A=Acceptor, D=Donor, H=Hydrophobic, A=RingAromatic.

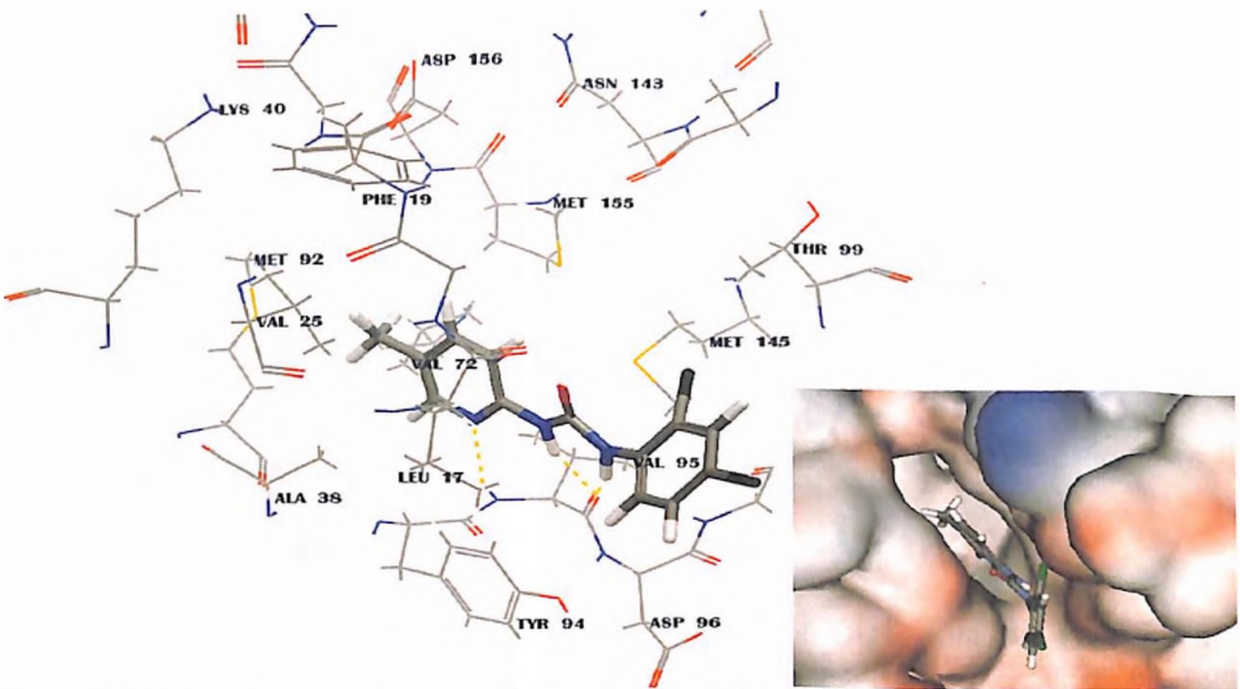

Figure 38: Schematic representation of the contact residues of **YS202** with Mtb PknB (left). Three H-bonds can be seen between Val95 and **YS202** in the form of yellow color dotted lines. Electrostatic surface view of active site pocket of Mtb PknB bound to **YS202** (down).

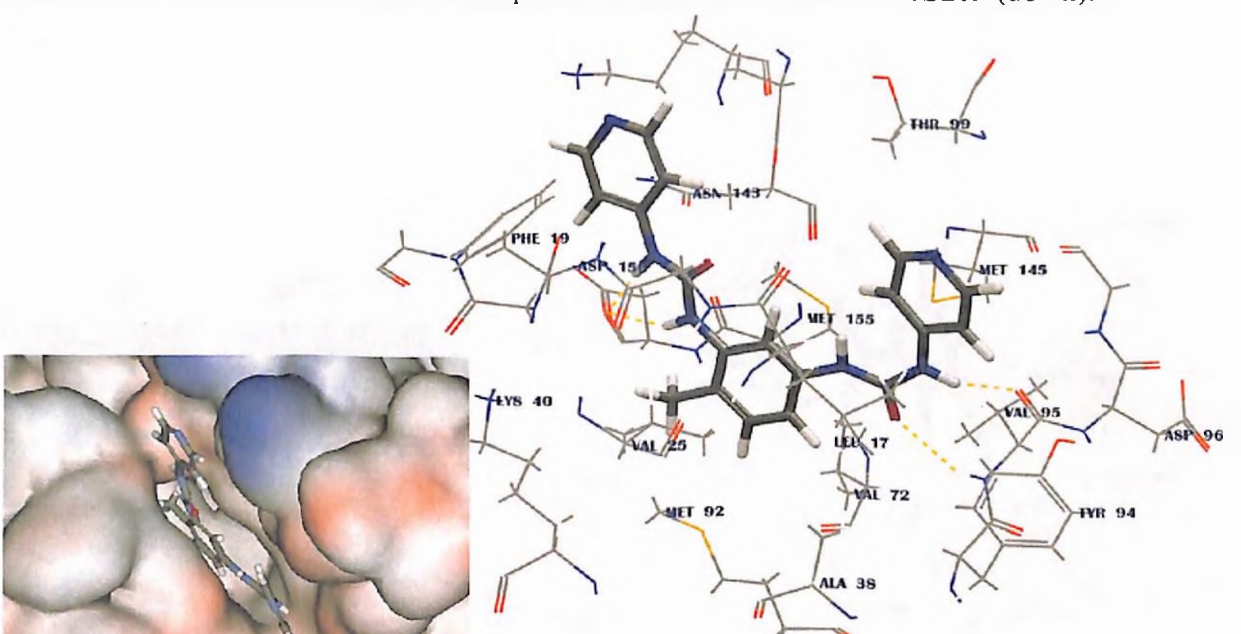

Figure 39: Schematic representation of the contact residues of **YS205** with Mtb PknB (left). H-bonds can be seen between Val95 and **YS205** in the form of yellow color dotted lines. Electrostatic surface view of active site pocket of Mtb PknB bound to **YS205** (down).

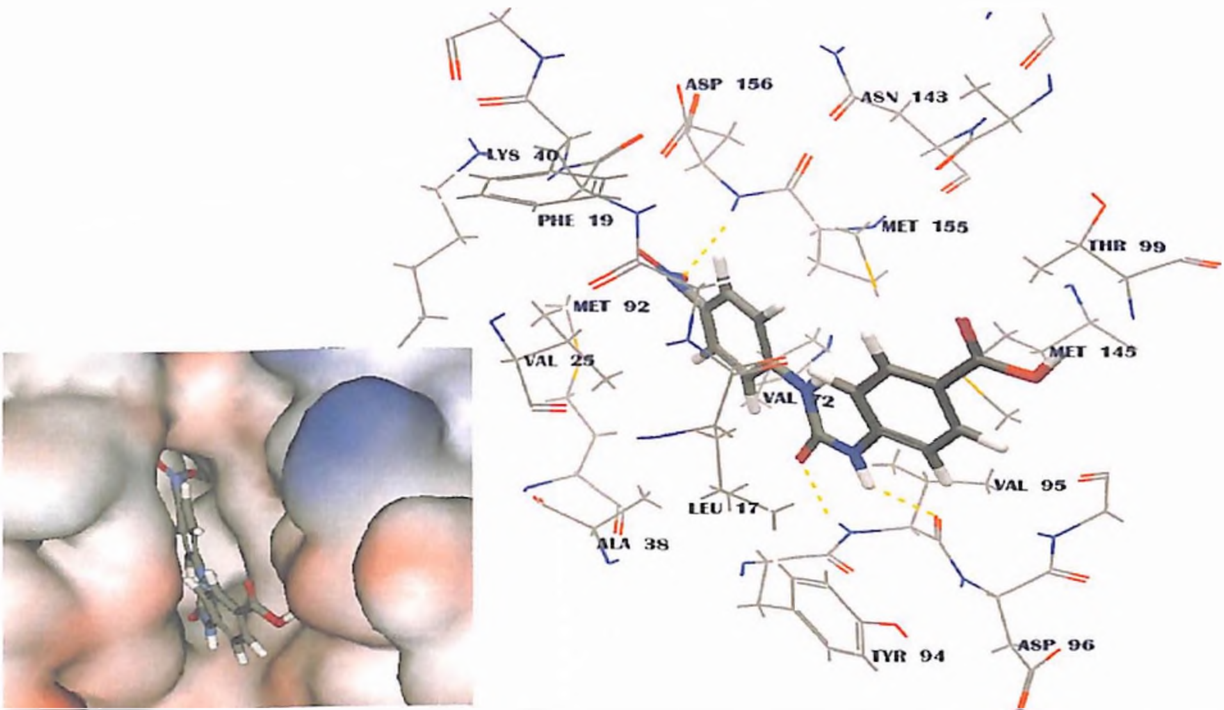

Figure 40: Schematic representation of the contact residues of **YS213** with Mtb PknB (right). Three H-bonds can be seen between **YS205** and residues Val95 and Asp156 in the form of yellow dotted lines. Electrostatic surface view of active site of Mtb PknB bound to **YS205** (down).

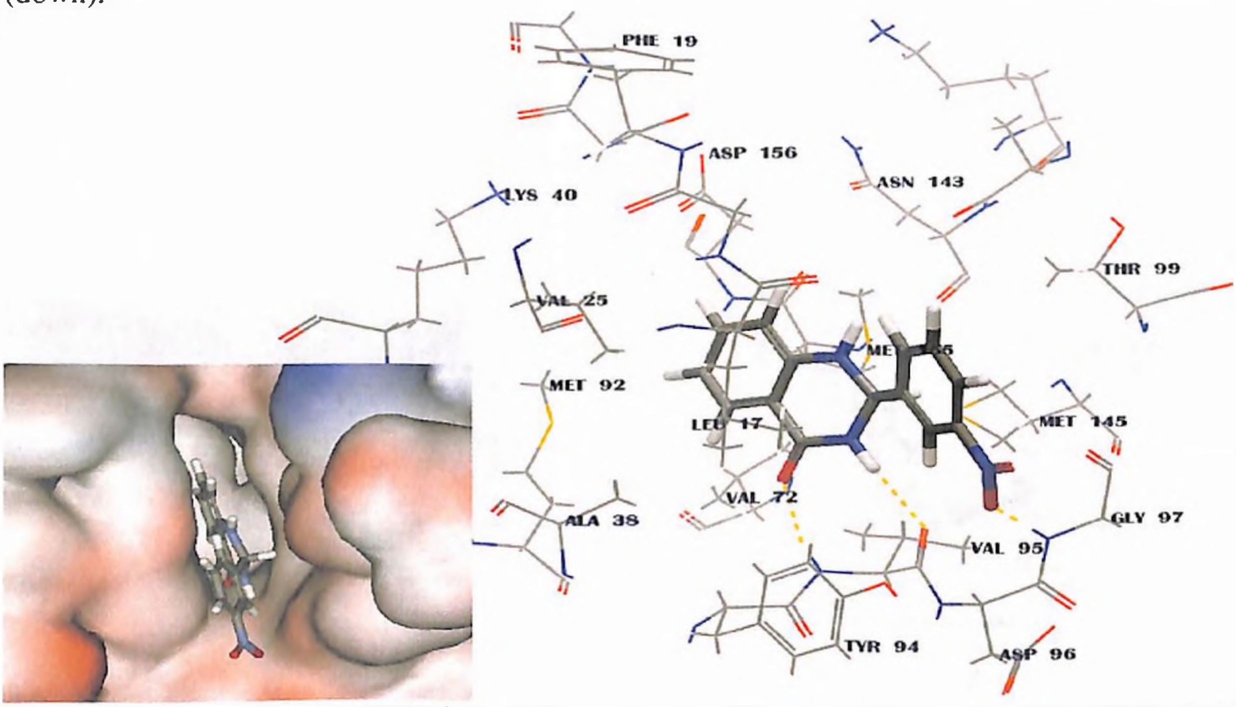

Figure 41: Schematic representation of the contact residues of **YS214** with Mtb PknB (left). Three H-bonds can be seen between Val95, Tyr94 and **YS214** in the form of yellow color dotted lines. Electrostatic surface view of active site pocket of Mtb PknB bound to **YS214** (down).

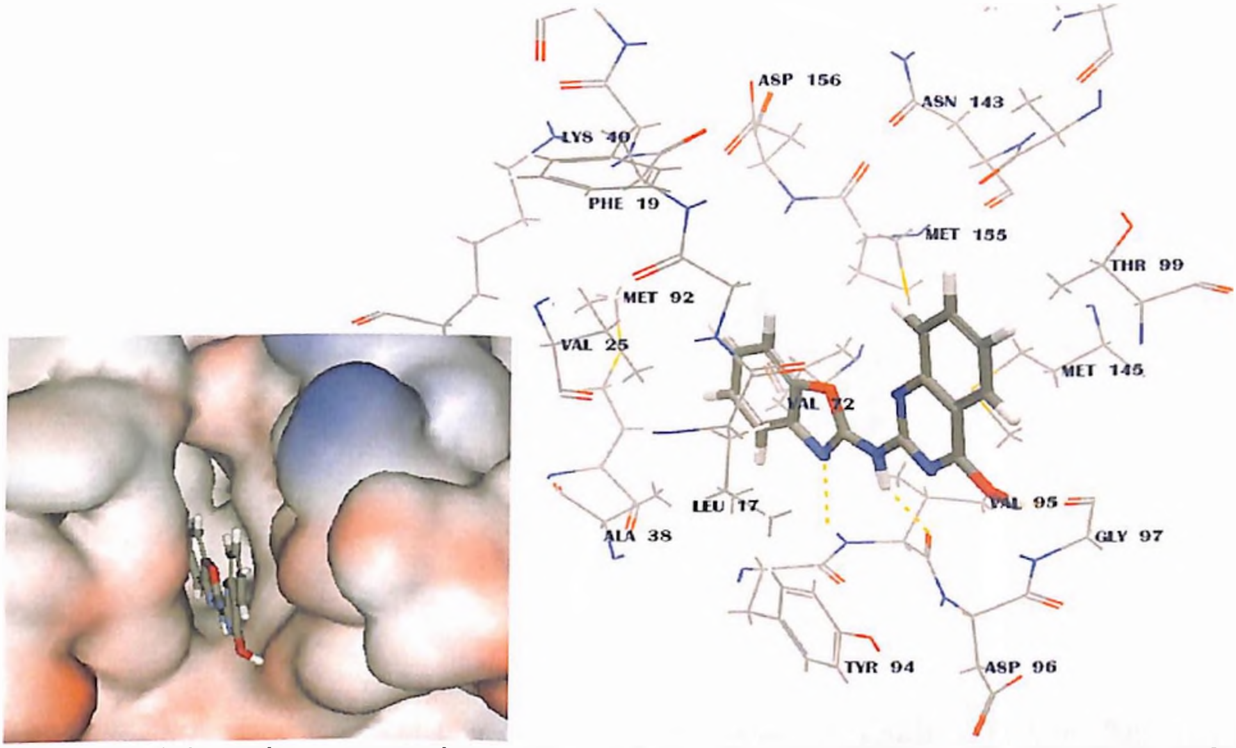

Figure 42: Schematic representation of the contact residues of **YS215** with Mtb PknB (left). Three H-bonds can be seen between Val95, Gly97 and **YS215** in the form of yellow color dotted lines. Electrostatic surface view of active site pocket of Mtb PknB bound to **YS215** (down).

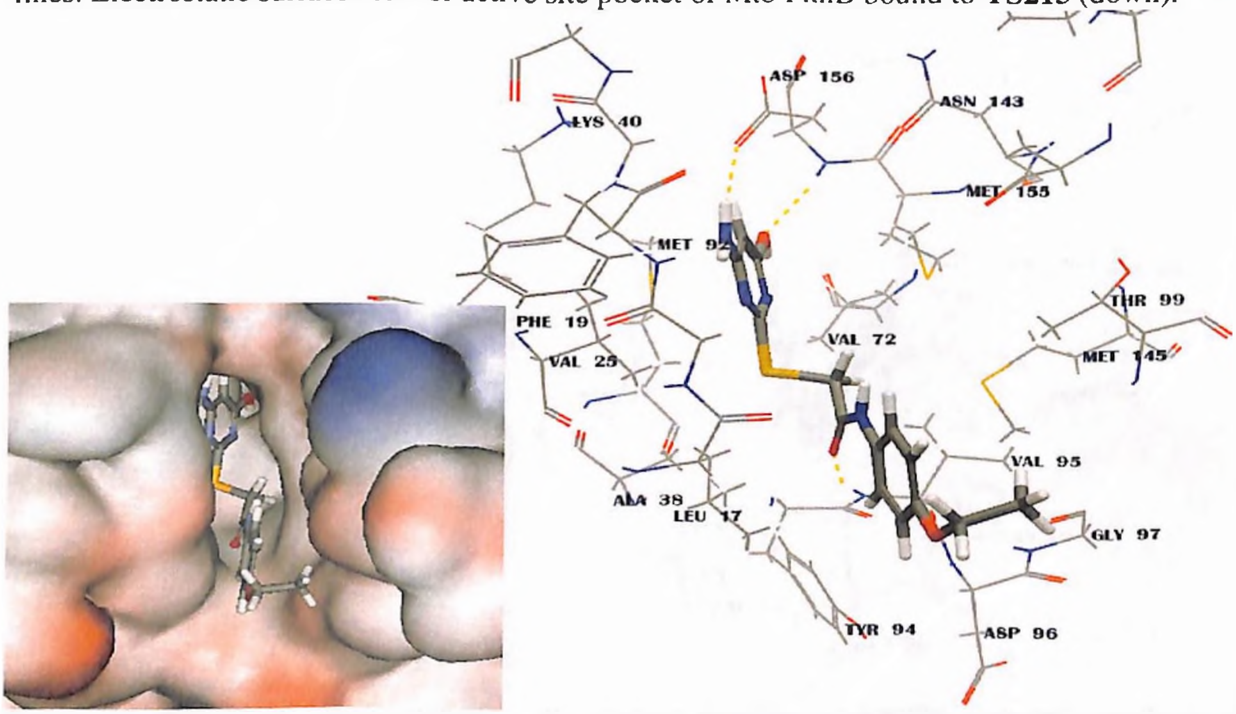

Figure 43: Schematic representation of the contact residues of **YS220** with Mtb PknB (left). Three H-bonds can be seen between Val95, Asp156 and **YS220** in the form of yellow dotted lines. Electrostatic surface view of active site pocket of Mtb PknB bound to **YS220** (down).

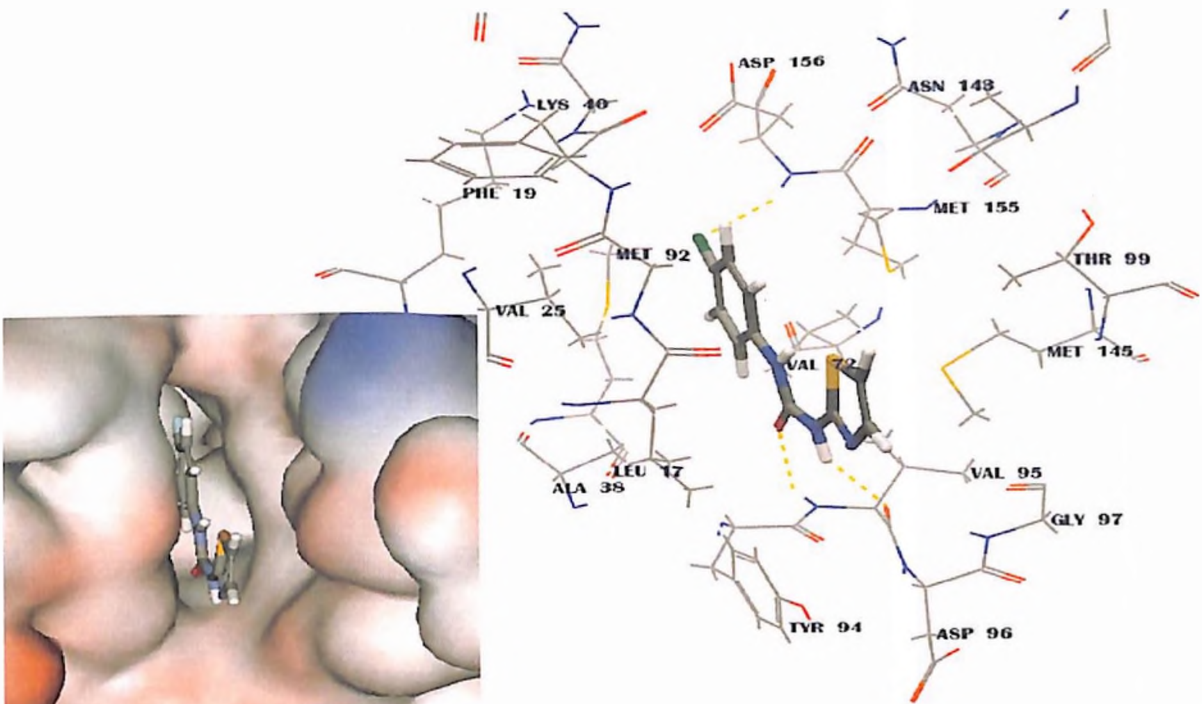

Figure 44: Schematic representation of the contact residues of **YS226** with Mtb PknB (left). Three H-bonds can be seen between Val95, Asp156 and **YS226** in the form of yellow dotted lines. Electrostatic surface view of active site pocket of Mtb PknB bound to **YS226** (down).

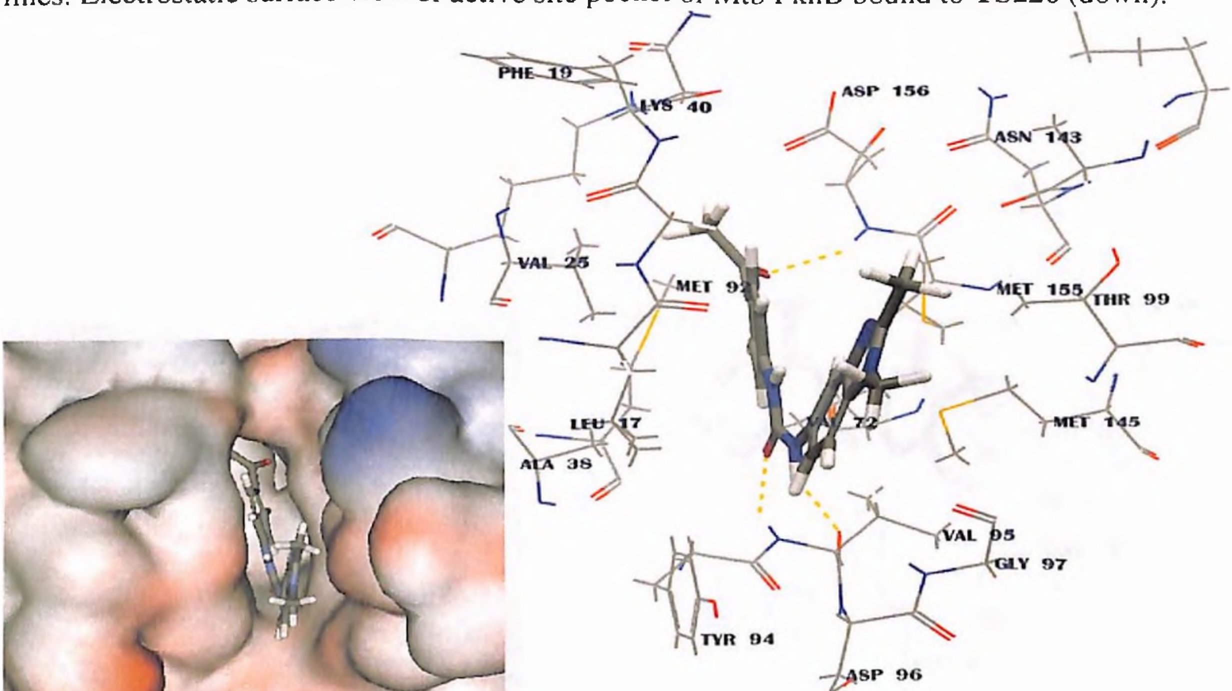

Figure 45: Schematic representation of the contact residues of **YS228** with Mtb PknB (left). Three H-bonds can be seen between Val95, Asp156 and **YS228** in the form of yellow dotted lines. Electrostatic surface view of active site pocket of Mtb PknB bound to **YS228** (down).

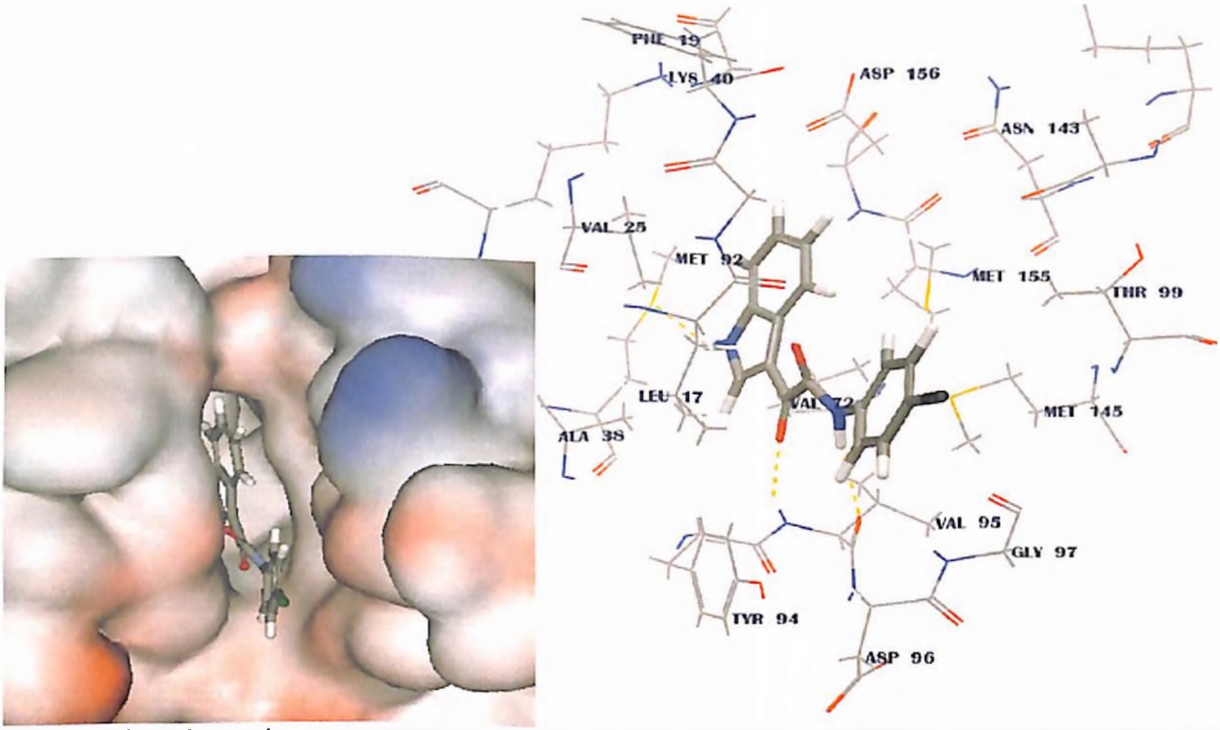

Figure 46: Schematic representation of the contact residues of **YS239** with Mtb PknB (left). Three H-bonds can be seen between Val95, Met92 and **YS239** in the form of yellow color dotted lines. Electrostatic surface view of active site pocket of Mtb PknB bound to **YS239** (down).

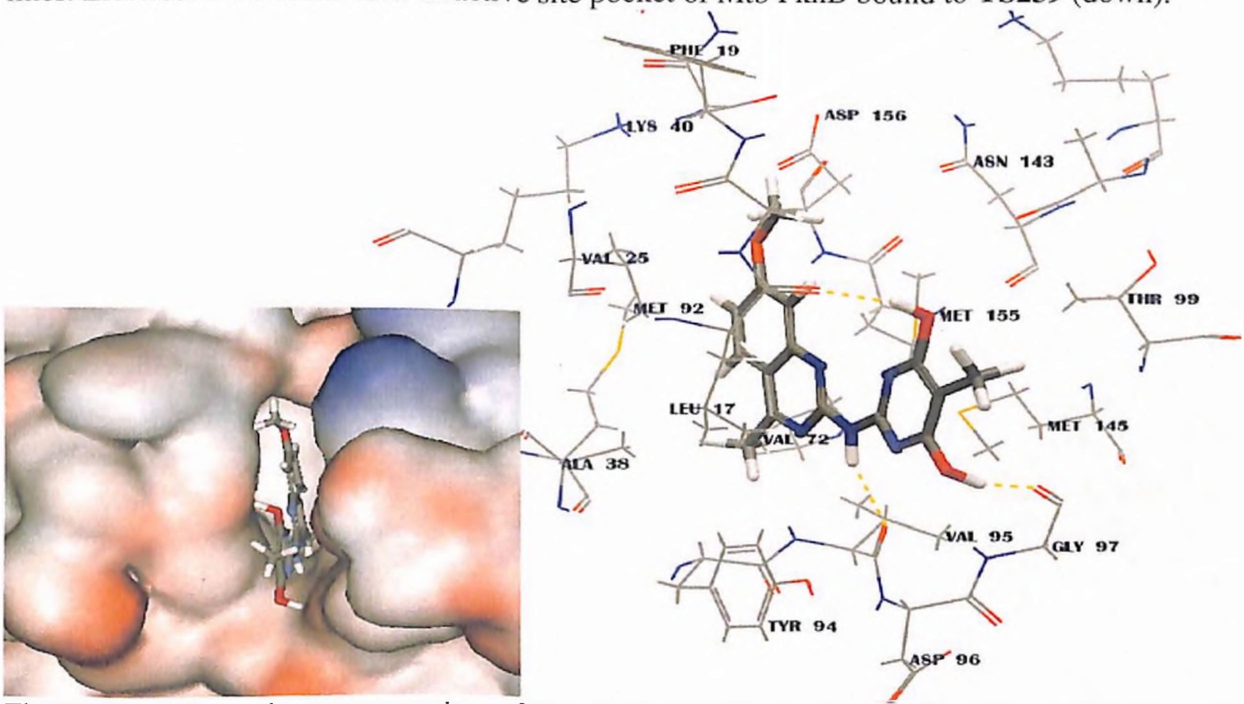

Figure 47: Schematic representation of the contact residues of **YS247** with Mtb PknB (left). Three H-bonds can be seen between Leu17, Val95, Gly97 and **YS247** in the form of yellow dotted lines. Electrostatic surface view of active site pocket of Mtb PknB bound to **YS247** (down).

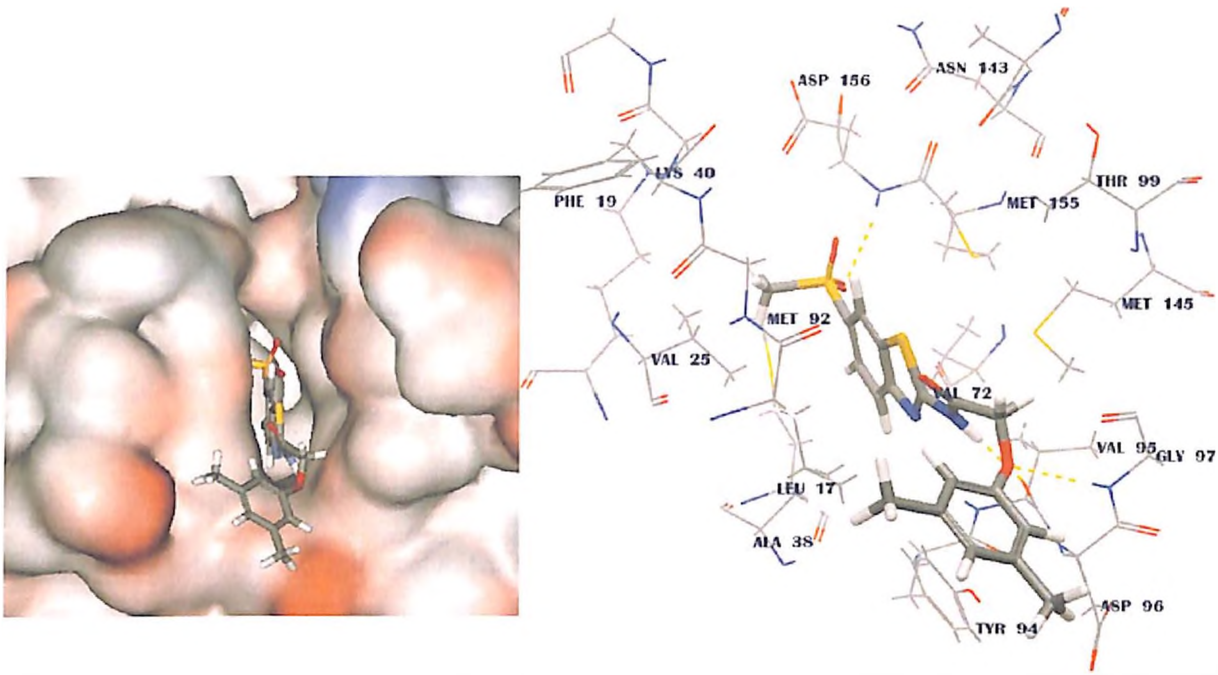

Figure 48: Schematic representation of the contact residues of **YS253** with Mtb PknB (left). Three H-bonds can be seen between Val95, Gly97, Asp156 and **YS253** in the form of yellow dotted lines. Electrostatic surface view of active site pocket of Mtb PknB bound to **YS253** (down).

Chapter VI

Isocitrate Lyase as anti-TB target & design of its Inhibitors

6.1 Introduction

The acquisition of essential nutrients by intracellular pathogens remains an area of considerable interest and ignorance. Biochemical studies suggest that in chronically infected lung tissues, fatty acids might be a major source of carbon and energy in Mtb metabolism [325]. Two pathways are required for fatty acid use by bacteria: the β-oxidation cycle and the glyoxylate shunt [304, 305]. The glyoxylate shunt is essential for carbon anaplerosis in the Krebs cycle during growth on C2 substrates such as fatty acids, which are the only abundant C2 carbon sources. The glyoxylate shunt is widespread among prokaryotes lower eukaryotes and plants, but is apparently absent in vertebrates. Recent studies revealed that expression of ICL, an enzyme of the glyoxylate shunt, is upregulated during infection of macrophages by *Mycobacterium spp.* [306, 307] Genes encoding isocitrate lyase activity in mycobacteria were identified by a genetic approach. A mutant of *M. smegmatis* was isolated which failed to grow on C2 substrates unless rescued by the *E. coli* aceA gene encoding ICL. Mtb expresses two enzymes with isocitrate lyase activity, ICL (Rv0467) and AceA (Rv1915/6) [306].

In *E. coli* and *Salmonella typhimurium*, induction of the fatty acid catabolic regulon is essential for survival in stationary phase [308, 309] and a similar role has been proposed in Mtb. ICL was induced when well aerated cultures of Mtb grew to saturation [310], which suggests a role for ICL in stationary phase survival. In another study, Mtb ICL was induced by oxygen limitation [311], and it was suggested that ICL might contribute to adaptation to hypoxia, but latter McKinney et all, found that wild-type and *Δicl* strains of Mtb were indistinguishable phenotypically when cultured in hypoxic or anoxic atmospheres [312]. McKinney et al., showed that the *Δicl* mutation had little effect on bacterial growth during the acute phase of infection, however the mutant was eliminated progressively from the lungs within two weeks onwards. These data show that ICL is important for survival of Mtb in the lungs of mice during the persistent phase of infection. These observations imply a 'C2 shift' in bacterial carbon metabolism concomitant with the host's response to infection. The observation that ICL expression is linked to the activation status of macrophages in the infected host cell suggests that ICL might be more important for bacterial survival in activated than in resting macrophages [312]. This finding supports that ICL is required for bacterial survival specifically during the persistent phase of infection in mice.

Persistence of bacteria and chronicity of infection are hallmarks of tuberculosis. Patients with chronic tuberculosis are thought to harbor bacteria in various metabolic states, ranging from active cell growth and division to stationary phase. Conventional drugs targeting cell-wall biogenesis and chromosome replication is responsible for poor activity against slow or non-growing bacteria is thought to be an important reason why conventional drugs take so long to eradicate infection. ICL promotes persistence of infection by enhancing bacterial survival within inflammatory macrophages makes it an attractive new target for chemotherapy.

More than half a century ago, Smith & Gunsalus (1954) reported the existence of the ICL, which cleaves isocitrate to glyoxylate and succinate, in extracts prepared from

Pseudomonas aeruginosa [313]. In 1957 Kornberg and co-workers demonstrated that the synthesis of C4 dicarboxylic acids from acetate occurs by a modified tricarboxylic acid (TCA) cycle that was termed the glyoxylate cycle or glyoxylate bypass [314, 315] (Figure 49). The

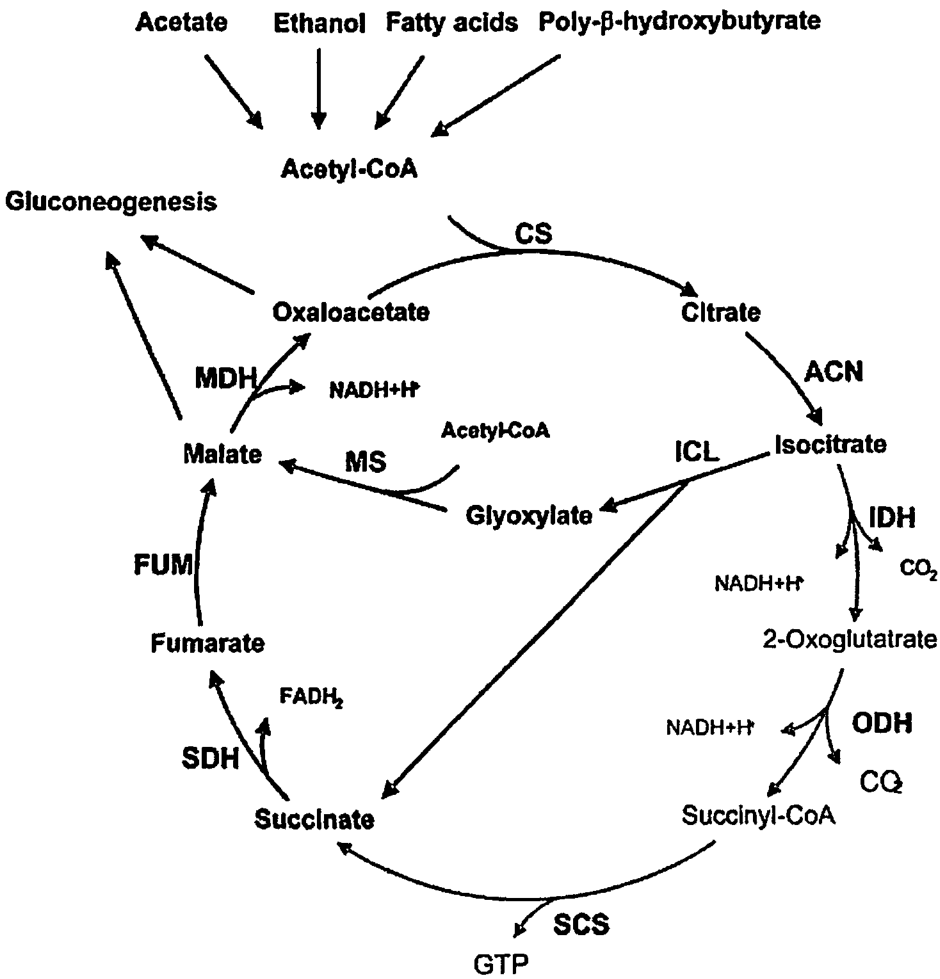

Figure 49: Enzymatic reactions of the glyoxalate and TCA cycles. A variety of metabolic processes can generate acetyl-CoA, the carbon from which can be preserved by metabolism via the glyoxalate cycle, which bypasses the CO_2-generating steps of TCA cycle. Abbreviations: CS-citrate synthase, ACN-aconitase, IDH- isocitrate dehydrogenase, ODH- 2-oxoglutarate dehydrogenase, SCS- succinyl-CoA synthase, SDH- succinate dehydrogenase, FUM- fumarase, MDH- malate dehydrogenase, MS-malate sythase, ICL- isocitrate lyase. [315]

pathway consists of the two initial steps of the TCA cycle catalyzed by citrate synthase and aconitase, followed by ICL, malate synthase and malate dehydrogenase. The glyoxylate cycle serves to bypass the CO_2-generating steps of the TCA cycle and allow the net assimilation of carbon from C2 compounds, allowing micro-organisms to replenish the pool of TCA cycle intermediates necessary for gluconeogenesis and other biosynthetic processes. The net result of the glyoxylate cycle is the production of malate and succinate from two molecules of acetyl-CoA derived from acetate or from the degradation of ethanol, fatty acids or poly-β-hydroxybutyrate,

ICL activity increases in pellicles in synthetic media as a consequence of fatty acid degradation [310] as well as under microaerophilic growth conditions [311]. Increased *aceA* (ICL) mRNA expression in response to human macrophages is also documented. Mtb expresses a 50 kDa protein during intracellular infection [307] and this was shown to be encoded by a second copy of an ICL gene that is present in several Mtb species. Expression analysis and biochemical characterization of ICL activity clearly show that Mtb and *M. avium* have two functional ICLs, ICL and *AceA* [306] *icl* mRNA levels markedly increase in lungs of mice [316] and in human lung granulomas, as well as in the lymphocyte region of necrotic granulomas. Munoz-Elias & McKinney (2005) reported that single mutations in ICL or *aceA* had no dramatic effect on bacterial growth on fatty acids, while an ICL *aceA* double mutant was unable to grow on this carbon source [317]. The double mutant inoculated into mice was eliminated from lungs and spleen and was unable to induce splenomegaly or alterations in lungs. ICL activity is thus essential for Mtb survival in the host. The recombinant *M. smegmatis*, transfected with Mtb ICL was phagocytized by macrophage. The transfected *M. smegmatis* exhibited significantly increased intracellular survival in the murine macrophage cell line. This increased intracellular survival was not accompanied by the upregulation of IFN-γ and NO in host macrophage. Mtb-ICL could promote the intracellular survival of transfected *M. smegmatis*, suppressing the apoptosis of host macrophage may be one of the important mechanisms involved in this increased intracellular survival [318].

ICL and to a lesser extent *AceA* were required for the growth of Mtb on propionate and on odd-chain fatty acids as a carbon source. The propionate or propionyl-CoA derived from β-oxidation of odd-chain fatty acids can be catabolized by the methylcitrate cycle, consisting of the enzymes 2-methylisocitrate lyase (MICL). However, structural and biochemical studies have demonstrated that unlike other ICLs and MICLs, the Mtb ICL possesses dual ICL/MICL activity and can support growth on acetate and propionate [319]. The *prpC* and *prpD* genes are upregulated during infection of macrophages [320], suggesting that the methylcitrate cycle could be important *in M. tuberculosis* pathogenesis. However, studies with a *prpC prpD* double mutant show that the methylcitrate cycle is required for Mtb replication in non-activated murine bone marrow derived macrophages, but that in IFN-γ-activated macrophages or in the lungs and spleen of inoculated mice the double mutant shows no alteration of in vivo growth, persistence or virulence. Thus, the functional role of ICL in Mtb virulence is in the glyoxylate cycle rather than the methylcitrate cycle.

Gengenbacher et al., recently showed that the ICL activity is very essential in maintaining the ATP homeostasis and intern Mtb viability under nutrient-starved, non-replicating condition [321]. To study the non-growing pathogen, culture models that generate quiescent organisms by either oxygen depletion in nutrient-rich medium (Wayne model) or nutrient deprivation in oxygen-rich medium (Loebel model) were developed [322, 323]. Upon shifting to the non-replicating state, the pathogen maintained a fivefold reduced but constant intracellular ATP level. Chemical probing of the F_0F_1 ATP synthase with the specific ATP synthase inhibitor TMC207 did not affect viability and only moderately reduced the intracellular ATP level of nutrient starved organisms. Depletion of oxygen killed Loebel bacilli, whereas death was prevented by nitrate, suggesting that respiration and an exogenous electron acceptor are required for maintaining viability. Nutrient starved bacilli lacking the ICL failed to reduce their intracellular ATP level and died, whereas wild-type Mtb reduced its ATP level rapidly upon the shift from growth in rich medium to carbon starvation, the ICL mutant failed to reduce its intracellular ATP concentration. These results suggest a link between ICL as part of the intermediary metabolism, intracellular ATP level regulation and nonreplicating survival.

The high-resolution structure of ICL from Mtb has been solved to 2.0 Å resolution. The apo-structure and the enzyme structure in complex with inhibitors, 3-nitropropionate with glyoxylate and 3-bromopyruvate have also been reported [324]. ICL is a tetrameric protein with subunits of 428 amino acids. The striking features of this structure are inter subunit helix-swapping, which in other enzymes have been proposed to enable the formation of stable dimers and a large conformational change in the active site loop upon binding of substrates.

Each subunit of the enzyme is composed of 14 α-helices and 14 β-strands. Eight α-helices (α4–α11) and eight β-strands (β2–β5, β8, β12–β14), representing the largest domain and the core of the structure, form an unusual α/β-barrel (Figure 50b). The α/β-barrel has a topology of (βα)2α(βα)5β, differing from the canonical (βα)8 pattern. An additional helix, present after the eighth β-strand (helix α12, composed of residues 349–367) projects away from the barrel and, together with the two ensuring helices α13 (residues 370–384) and α14 (residues 399–409), forms interactions exclusively with the neighboring subunit. Residues 184–200 and 235–254 (connecting the third and fourth β-strands to their consecutive helices, respectively) form a small β-domain consisting of a short five stranded β-sheet (β6, β7, β9, β10, β11) that lies atop the α/β-barrel. This domain is important as it contains several of the active site residues.

(connecting the third and fourth β-strands to their consecutive helices, respectively) form a small β-domain consisting of a short five stranded β-sheet (β6, β7, β9, β10, β11) that lies atop the α/β-barrel. This domain is important as it contains several of the active site residues.

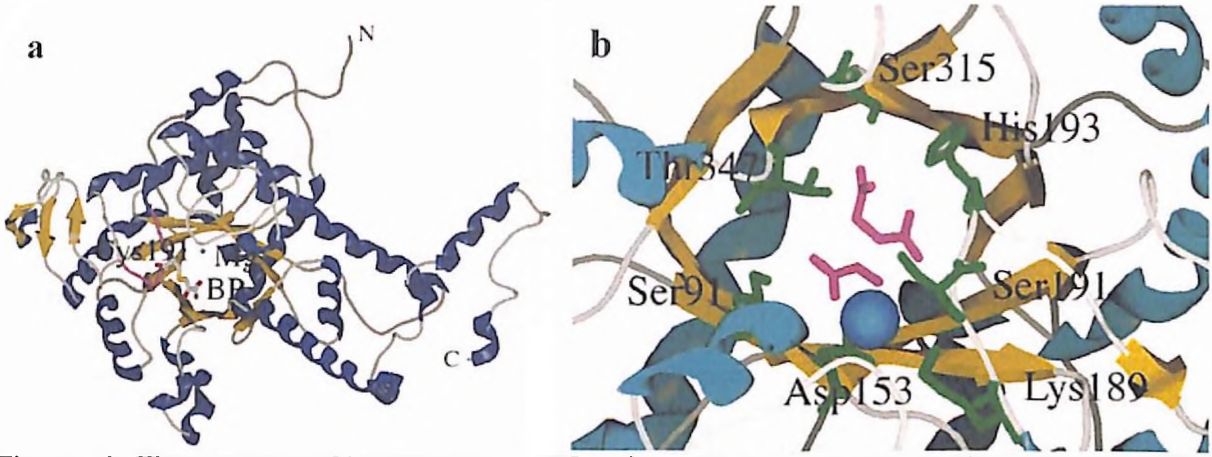

Figure 50: The structure of isocitrate lyase (ICL) from *M. tuberculosis*. (a) Single subunit of ICL, the a-helices are shown in blue and the b-strands in yellow. The positions of the N- and C-termini are indicated by N and C, respectively. The position of the active site cysteine (Cys191) is indicated covalently bound to the inhibitor 3-bromopyruvate. The active site Mg2+ ion is shown in cyan. (b) Binding of the succinate analog, 3-nitropropionate, and glyoxylate. The active site of the ternary complex between ICL C191S mutant and 3-nitropropionate and glyoxylate is shown. Important amino acids forming the active site are indicated. Glyoxylate and 3-nitropropionate are colored magenta, the active site Mg2+ ion is represented by the blue sphere.

Stable binding of both nitropropionate and glyoxylate was achieved by C191S mutant in ICL. As is seen typically in α/β barrels, the active site of ICL is located at the C-terminal ends of the β-strands (Figure 50a). Clear density was observed for glyoxylate, 3-nitropropionate and Mg^2+. The planar glyoxylate binds by coordination to the active site Mg^{2+} ion and forms hydrogen bonds with the residues Ser 91 OG, Gly 92 N, Trp 93 N and Arg 228 NH2 of the protein. As it was difficult to distinguish between the nitro and carboxylate groups of 3-nitro-propionate, a succinate molecule was fit to the density [324] such that one carboxylate makes specific hydrogen bonds with the side chains of residues Asn 313 ND1, Glu 295 OE2, Arg 228 of glyoxylate and 3.2 Å from the hydroxyl of Ser 191 of the C191S mutant. Inhibition of ICL by 3-bromopyruvate was accomplished through covalent bond formation via dehalogenation of the inhibitor with the active site nucleophile Cys 191. The pyruvyl moiety occupies the site where the second carboxylate of succinate was located and forms hydrogen bonds with the side chains of His 193 ND1, Asn 313 ND2, Ser 315 OG, Ser 317 OG, Thr 347 OG1 and a solvent molecule. The orientation of the carboxylate group differs in the two cases, due to covalent linkage with Cys 191 in the case of 3-bromopyruvate modified ICL. The residue Cys 191 adopts a conformation almost identical to Ser 191 in the C191S mutant, indicating that accommodation of the pyruvyl moiety did not require any additional rearrangement of the active site residues. In this complex, the glyoxylate binding site is occupied by solvent molecules that coordinate the Mg^{2}+ ion.

Comparison of the structures of the native and inhibitor bound forms of ICL showed large conformational differences in two regions that control access to the active site. The first region is an active site loop (residues 185–196) that contains the ICL sequence (K189KCGH193) and the second region consists of the last 18 residues (residues 411–428) at the C-terminal end of the adjacent subunit. In the ‘open’ conformation of the apo enzyme, Cys 191 in the active site loop is relatively far from other catalytic residues and the binding site is highly solvent accessible. Poor electron density was observed for residues His 193 and Leu 194 for one of the subunits in the asymmetric unit, suggesting that the active site loop is flexible in the ‘open’ conformation. Upon binding of inhibitor, the loop moves by 10–15 Å and adopts the ‘closed’ conformation. The inhibitor bound ‘closed’ conformation is completely blocked by the active site loop (residues 185–196). Closure of the active site loop invokes a movement of residues 411–428 of the adjacent subunit. Whereas the last 11 residues were somewhat disordered and extend into solvent in the apo enzyme crystal, clear electron density was observed for all except residue 428 of the C-terminus in the inhibited enzyme crystal. In the 'closed' conformation, residues 411–427 occupy the space created by closing of the active site loop. In the resulting orientation, the C-terminus lies on top of the active site loop, locking it into the catalytic conformation. This two-step conformational rearrangement is triggered by a 2.5 Å movement of a Mg^{2}+ ion that is bound in a highly electronegative depression formed by Asp 108, Asp 153, Glu 155 and Glu 182 in the apo enzyme. Binding of succinate appears to trigger the movement of the Mg^{2}+, allowing Lys 189 of the active site loop to form electrostatic interactions within this region, and facilitating closure of the active site loop over the bound substrates.

Occurrence of loop closure only when the succinate binding site is occupied by either nitropropionate or the pyruvyl moiety suggests that the presence of succinate be required to induce loop movement. Since crystals with 3-bromopyruvate were also obtained without glyoxylate, the interactions responsible for the loop closure can be narrowed down to the common carboxylate that binds in the pocket formed by residues His193, Asn313, Ser315, Ser317, and Thr347 in both the complexes. With the exception of residue Thr347, which is positioned identically in both bound and unbound states, all of these residues undergo significant movements upon binding. While His 193 is located on the flexible active site loop, residues Asn313, Ser315 and Ser317 are located at the C-terminal end of strand β14 and undergo a 1–2 Å shift upon binding.

ICL catalyzes the reversible lysis of a C–C bond of isocitrate to form glyoxylate and succinate. Since the glyoxylate is buried deeper in the active site than succinate and that loop closure requires succinate binding the glyoxylate must be first to bind the enzyme followed by succinate to form a ternary complex. The reaction mechanism involves Claisen condensation via the formation of an enolic intermediate. Deprotonation of the α-proton of a carboxylate of succinate by a base to form 4,4-dihydroxy-3-butenoate is the key step. The Cys 191 carries out the nucleophilic abstraction of the α-proton from the C2 position of the succinate. Mutagenesis studies carried on the enzyme from *E. coli* led to the proposal that deprotonation of the active site Cys 191 is carried out by a neighboring His residue (His 193 in Mtb ICL). In the crystal structures of inhibitor bound ICL, side chains of these residues are located 5 Å apart, suggesting that direct proton exchange may not occur between them. A general acid, probably Glu 295, protonates the carboxylate adjacent to the bond formed. The negative charge on the aldehyde oxygen of glyoxylate is stabilized by interactions with an oxyanion hole formed by the Mg2+ ion, Arg 228 and His 180.

The development of specific inhibitors against ICL is an attractive prospect. Several inhibitors of ICL have been identified, including itaconate, itaconic anhydride, bromopyruvate, nitropropionate, oxalate and malate [303, 325]. However, these are not pharmacologically suitable for use in vivo since they are toxic and non-specific. For example, nitropropionate inhibits ICL but also inhibits succinate dehydrogenase, a pivotal enzyme of the TCA cycle [326]. Efforts to isolate natural ICL inhibitors from plants revealed that extracts of *Illicium verum* and *Zingiber officinale* inhibit the ICL of Mtb [327].

Ki-Bong and coworkers have reported inhibitory activity against fungus *Candida albicans* ICL from natural origin and synthetic origin. Sesterterpene sulfates were isolated from the tropical sponge *Dysidea sp* (family Dysididea), and their inhibitory activities against ICL from *Candida albicans* were evaluated [328]. Among the isolated natural products two were found to be strong ICL inhibitors showed IC_{50} value of 20 µg/ml. The isolated compounds also showed potent antibacterial effect against *Bacillus subtilis* and *Proteus vulgaris*, but did not display antifungal activity.

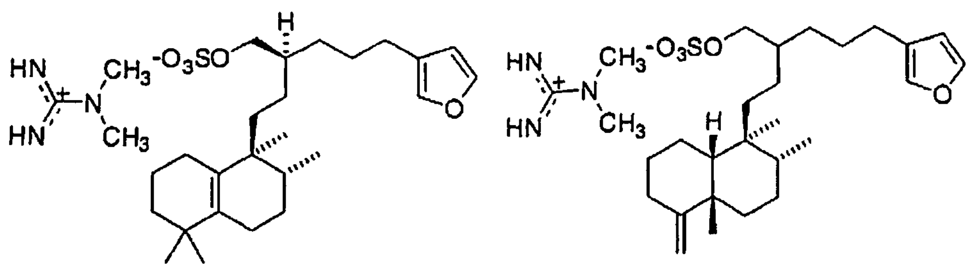

Alkaloids hyrtiosin B collected from tropical marine sponge *Hyrtios sp.* Hyrtiosin B displayed a potent inhibitory activity against ICL of *Candida albicans* with an IC_{50} value of 89.0 µM [329].

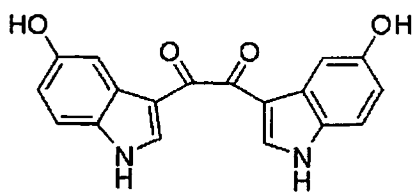

A series of bromophenols was synthesized by reactions of corresponding phenol analogs with bromine [330]. Upon testing of activity against ICL of *Candida albicans* bis(3-bromo-4,5-dihydroxyphenyl)methanone and (3-bromo-4,5-dihydroxyphenyl)(2,3-dibromo-4,5-dihydroxy-phenyl) methanone displayed potent inhibitory activities than found with natural bromophenol. These compounds also exibited very good antimicrobial activity against Gram-positive and, Gram-negative bacteria and fungi.

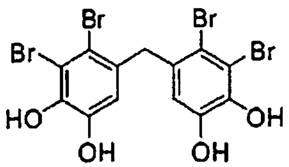

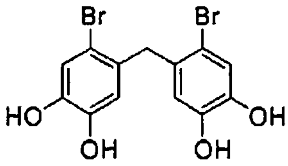

Work from our lab with an intention to identify the novel Mtb ICL inhibitors resulted in to identification of several potent synthetic compounds. Novel 2-[3-(4-bromo-2-fluorobenzyl)-4-oxo-3,4-dihydro-1-phthalazinyl]acetic acid hydrazones were synthesized from phthalic anhydride, and evaluated for in vitro, in vivo activities against eight Mtb species and Mtb ICL enzyme inhibition studies [331]. Among twenty six compounds N'1-[(4-nitrophenyl)methylene]-2-[3-(4-bromo-2-fluorobenzyl)-4-oxo-1,2,3,4-tetrahydro-1-phthalazinyl]ethanohydrazide was found to be the most active compound in-vitro with MIC's of 0.18 and <0.09 μM against log-phase cultures of Mtb and multi-drug resistant Mtb respectively. Compound inhibited all the eight mycobacterial species with MIC ranging from <0.09-12.25 μM. Compounds showed 55% inhibition against Mtb ICL enzyme at 10 μM. In the in vivo animal model decreased the bacterial load in lung and spleen tissues with 1.87 and 3.03-log10 protections respectively at 25 mg/kg body weight dose.

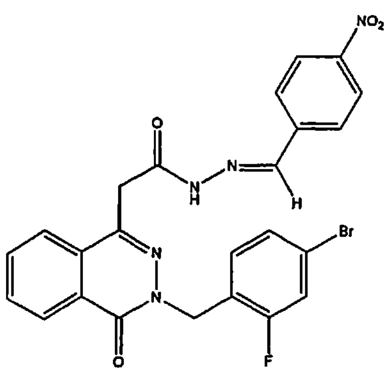

5-nitro-2,6-dioxohexahydro-4-pyrimidinecarboxamides were synthesized and evaluated for their in vitro activity against Mtb. H37Rv (Mtb), multidrug-resistant Mtb (MDR-TB), and *M.*

smegmatis as well as their cytotoxicity and Mtb ICL inhibition activity [332]. 1-Cyclopropyl-6-fuoro-8-methoxy-7-(3-methyl)-4-[(5-nitro-2,6-dioxohexahydro-4-pyrimidinyl) carbonyl]piperazino-4-oxo-1,4-dihydro-3-quinolinecarboxylic acid was found to be the most active compound in vitro with MICs of < 0.17 and 0.17 μM against log-phase Mtb and MDR-TB, respectively. Compounds showed 35% inhibition against Mtb ICL enzyme at 10 μM. Some other compounds showed 20–45% inhibition against Mtb ICL at 10 μM.

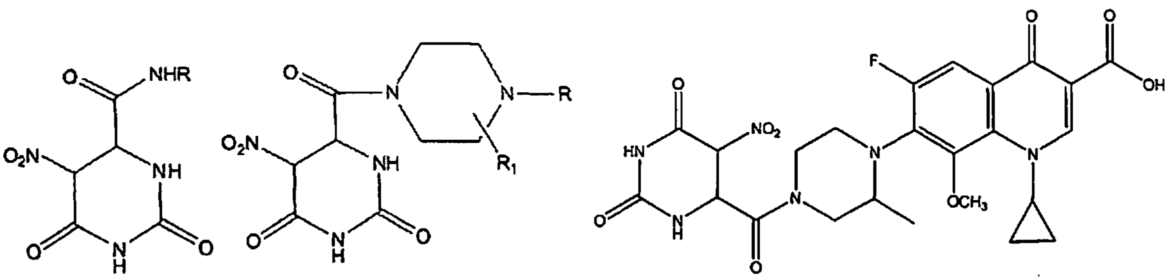

Various 5-nitro-2-furoic acid hydrazones were synthesized and evaluated for in vitro activities against log and starved phase culture of two Mtb species and Mtb ICL enzyme inhibition studies [333]. 5-nitro-N0-[(5-nitro-2-furyl)methylidene]-2-furohydrazide was found to be the most active compound in vitro with MICs of 2.65 and 10.64 μM against log- and starved-phase culture of Mtb. Compound also showed good enzyme inhibition of 86% Mtb ICL at 10 μM. Docking studies carried out confirmed the binding potential of compounds to ICL active site.

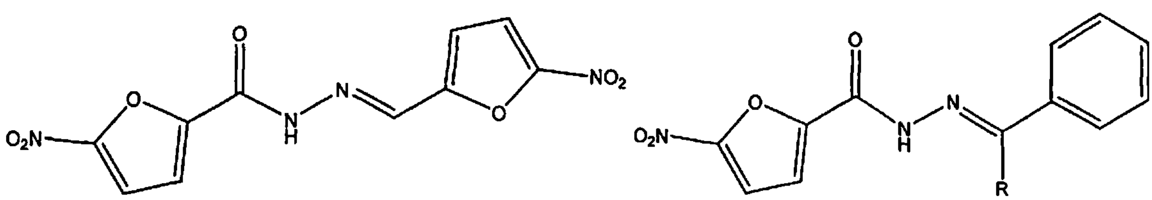

Novel 2-[3-(4-bromo-2-fluorobenzyl)-4-oxo-3,4-dihydro-1-phthalazinyl] acetic acid amides were synthesized from phthalicanhydride and were subjected to in vitro and in vivo evaluation against log- and starved phase of mycobacterial species and Mtb ICL enzyme inhibition studies [334]. Among the compounds screened, 2-(2-(4-bromo-2-fluorob-enzyl)-1,2-dihydro-1-oxophthalazin-4-yl)-N-(2,6-dim-methyl phenyl)acetamide inhibited all eight Mtb species with MIC's ranging from 0.08 to 5.05 μM. Compounds tested against starved culture of Mtb, and they inhibited with MIC's ranging from 3.78 to 23.2 μM. Some compounds showed 40–66% inhibition against Mtb ICL enzyme at 10 μM. The docking studies predicted the binding potential of the compounds at the ICL active site.

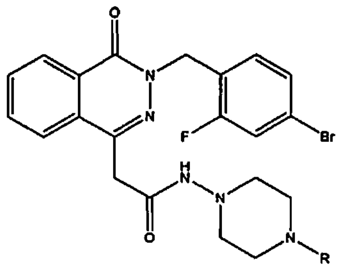

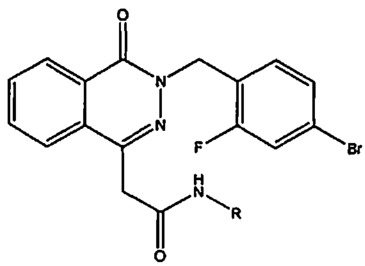

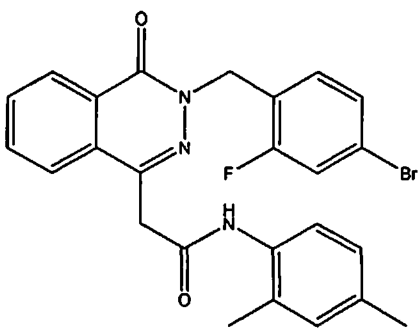

A series of novel 5-substituted-1-(arylmethyl/alkylmethyl)-1H-indole-2,3-dione-3-(N-hydroxy/methoxy thiosemicarbazone) analogueswere synthesized and evaluated for anti-tubercular activity in both log phase and starved cultures [335]. The compound 2-(1-{[4-(4-chlorophenyl)tetrahydropyrazin-1(2H)-yl]methyl}-5-methyl-2-oxo-1,2-dihydro-3H-indol-3-yliden)-N-(methyloxy)hydrazine-1-carbothioa-mide displayed promising activity against Mtb. It proved effective in inhibiting the growth of both log phase (MIC 3.30 μM) and starved (MIC 12.11 μM) Mtb cultures. The compounds from these series were careened against Mtb ICL shown to be inhibiting the enzyme from 20 to 63.44% at 10 mM.

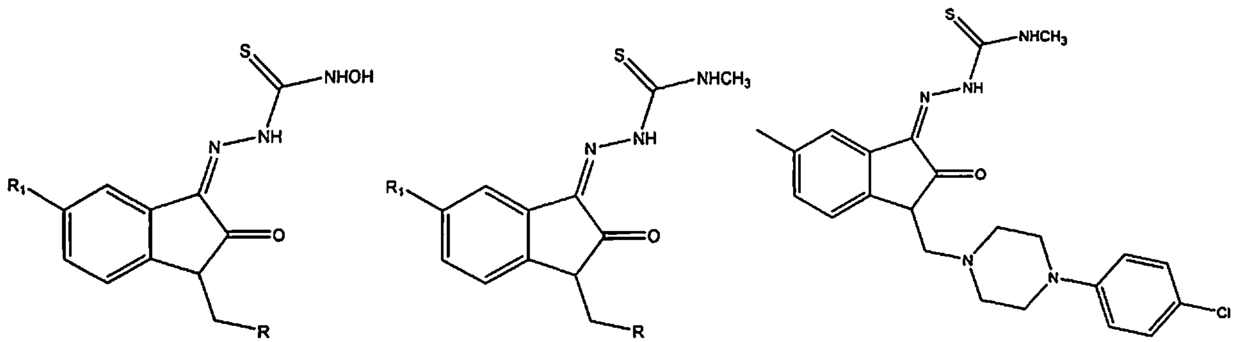

6.2 Materials and method

6.2.1 Collection of crystal structures The protein structural database, PDB was searched for the solved Mtb ICL X-ray crystals. There were three crystals structures reported, an apo-enzyme, without any substrate in the active site (1f61) and two crystal structures bound with the inhibitor nitro propionic acid (1f8m) and bromopyruvic acid (1f8i) respectively at the active site.

6.2.2 Structure preparation Coordinates for ICL crystal structure was taken from the PDB and prepared using the Protein Preparation Wizard, which is part of the Maestro software package (Maestro, v8.5, Schrodinger, LLC, New York, NY). Bond orders and formal charges were added for heterogroups, and hydrogens were added to all atoms in the system. To optimize the hydrogen bond network, Histidine tautomers and ionization states were predicted, 180° rotations of the terminal χ angle of Asn, Gln, and His residues were assigned, and hydroxyl and thiol hydrogens were sampled. Water molecules were removed. A brief relaxation was performed using an all-atom constrained minimization carried out with the Impact Refinement module (Impref) (Impact v5.0, Schrodinger, LLC, New York, NY) using the OPLS-2005 force field to alleviate steric clashes that may exist in the original PDB structures. The minimization was terminated when the energy converged or the rmsd reached a maximum cutoff of 0.30 Å.

6.2.3 Database preparation In-house database of 2000 molecule was used for the identification of the potential inhibitors of Mtb GluR. The molecular structures were built using Schrodinger Maestro. The 2D structures were saved in SDF format and then were subjected to Schrodinger LigPrep (LigPrep, version 2.3, Schrodinger, LLC, New York, NY) program, where the 2D molecules were converted to 3D form, the hydrogen was added to the molecules, different tautomeric form was generated, proper ionization state was generated at pH 7±2 and finally molecules were minimized to local minima. The prepared molecules were then used for further study.

6.2.4 Virtual screening of the database for inhibitor for inhibitor identification The prepared in-house database was used for the virtual screening, to identify the potential inhibitors of the Mtb GluR. The virtual screening was carried out by docking the molecules into active site. The protein was subjected initially to 10,000 steps of Steepest Descent (SD) minimization, followed by 15,000 steps of Conjugate Gradient (CG). The minimized protein was used for running the docking simulations. Glide was used for docking the database molecules. Glide grid was used for the carrying out docking calculations. The centroid of three amino acid residues Cys191, Thr347 and Asp153, taken as the center of the 13 Å rectangular grid box. Ligands were set free without application of any constrains during docking. The Glide flexible ligand docking was carried out with XP (extra precision) mode. Extra-precision (XP) docking and scoring is a more powerful and discriminating procedure, which takes longer to run than SP. XP is designed to be used on ligand poses that have a high score using SP docking. Epik state penalties were considered for the caution of dock score. The molecules with more than 300 atoms were not considered for the docking run, and also molecules with more than 50 rotatable bonds were restricted from docking. A Van-der-waal scaling factor of 0.8 Å was considered during docking to soften the potential for nonpolar parts of the ligand. A post docking minimization was then performed on the ligands with saved poses. 0.5 kcal/mol was kept as the threshold energy to reject the minimized poses. Poses with Columbic-Vdw energy more than 0.0 kcal/mol were rejected. 10,000 ligand poses were saved from the docking run, and for each molecule maximum 5 poses were saved. The poses were considered same when the rmsd between two poses were less than 0.5 Å.

6.2.5 Overexpression and purification of Mtb ICL A single colony from the *E. coli* BL21 plate was inoculated into 5 mL of LB broth having ampicillin at a concentration of 200 mg/mL and allowed to grow overnight at 37.8°C. It was then subcultured in 400 mL of LB broth containing similar ampicillin concentration at 37.8°C until A_{600} of 0.6 was achieved. The culture was then induced with 0.1 mM isopropyl-1-thio-β-D-galactopyranoside (IPTG) and incubated further at 20.8°C for 16 h. The cells were harvested at 8,000g for 10 min at 4° C and the resultant pellet was then stored at -20.0°C until further use. Histidine tagged protein was purified by resuspending the cell pellet in lysis buffer containing 50 mM potassium phosphate, 300 mM sodium chloride and 10% glycerol (pH 8.0) and PMSF. Cells were disrupted using a probe type ultrasonicator. Cell debris was removed by centrifugation at 12,000g for 1 h at 4° C. The supernatant obtained was applied on nickel-nitrilotriacetic acid-agarose affinity column equilibrated with the lysis buffer. The column was initially washed with lysis buffer and subsequently with same buffer containing

25 and 50 mM imidazole, respectively. The protein was eluted using 400 mM imidazole. The enzymatically active fractions with ICL activity were collected, pooled together and stored at -20.0 °C for 2 months with no loss of activity.

6.2.6 ICL inhibitory activity ICL activity was determined at 37°C by measuring the formation of glyoxylate-phenylhydrazone at 324 nm, with some modification in procedure described earlier. The reaction mixture contains 200 μM of 0.5mM potassium phosphate buffer, 2.4 μL of 1mM magnesium chloride, 48 μL of 100 mM 2-merceptoethanol, 16 μL of 100 mM phenyl hydrazine, 6 μL of 50 mM trisodiumisocitricacid and Mtb ICL enzyme (usually 6 to 10 μL). This mixture is made up to 400 μL with MilliQ water. At the end of the 20^{th} minute this reaction mixture is made up to 2 mL and UV absorbance was measured at 324 nM which serves as a control. For the test compound 3 μL of 100mM 3-nitropropionic acid was used and in case of the candidate molecules either 5 or 15 μL of 2 mg/ml concentration were added corresponding to the 3μg/mL or 9μg/mL respectively in the above mentioned reaction mixture. At the end of the 20^{th} minute this reaction mixture is made up to 2 mL and UV absorbance is measured at 324 nm which serves as a test. The % inhibition is calculated by the formulae control absorbance minus test absorbance divided by control absorbance multiplied by 100. All the measurements were run in triplicates.

6.3 Results and discussion

The limited number of the data available on the Mtb ICL inhibitor, the limited chemical diversity, activity range, made the drug discovery program difficult for the design of its inhibitors. Till now only from our group has identified and reported the Mtb ICL inhibitors. There are three crystals reported for the Mtb ICL. Two co-crystalized with the inhibitors and an apo-enzyme form. The enzyme is active in its closed form, whereas the apo-enzyme is inactive and is the open form. Crystal structure available with the two inhibitors are very small molecules, Nitropropionic acid, a competitive inhibitor and the other one is bromopyruvic acid is noncompetitive inhibitor forms a covalent bond at the active site. Both the inhibitors are very small molecules and also the active site of the enzyme is very small in the closed conformation. Moreover it is a metalo enzyme with larger proportion of polar surface area in the active site, made the drug design further problematic.

The Active site analysis carried out with the SiteMap, for the active, inhibitor bound, closed conformation of the ICL. The SiteMap generates scores for several parameters which can be used for the evaluation of the active site, its druggability etc. The scoring procedures are discussed in the SiteMap user manual. The number of site points that make up the site is a measure of the size of the site. As a rough rule of thumb, 2 to 3 site points typically correspond to each atom of the bound ligand, including hydrogens. The size of the site is often a good indicator of the preferred binding site. The two properties provide different measures of how open the site is to solvent exposure and enclosure scores. A shallow, open site would allow many more site points to be added, giving a high exposure score. The lower the exposure score, the better; the average for the tight-binding sites investigated is 0.49. For Mtb ICL the exposure score id far lower than the average value, 0.275. The enclosure score is the fraction of rays that strike the receptor surface within a distance of 10 Å, averaged over the original and the extension site points used in the exposure evaluation. Higher scores are better, with the average enclosure score for a tight-binding site being 0.78. The Mtb ICL presented an enclosure score of 0.973. The

SiteScore is based on a weighted sum of several of the properties like number of site points, enclosure score and hydrophilic score. Mtb ICL had a site score of 0.926, where as a score of greater than 1.0 suggests a site of particular promise. Dscore uses the same properties as SiteScore but different coefficients. Using this feature site can be distinguished undruggable from druggable ones. The Mtb ICL had a very low Dscore of 0.300. It is always to better to have balance between the hydrophobic to hydrophilic ratio or to have more towards the hydrophobic to have a very good druggable target. The average balance score for the investigated tight-binding sites, on the other hand is 1.6, not 1.0, because sites that have high phobic and low philic scores make large contributions to the average. The Mtb ICL had a hydrophobic character value of 0.057, which was too low whereas the hydrophilic character was 2.738, thus forming ratio of 0.021 which is very low suggesting a very bad dugable site in the closed form. The volume of the closed conformation of Mtb ICL was very low as 65.07 squares Å units.

Initially an effort was made to dock the earlier reported molecules to Mtb ICL using closed conformation. Since the crystal structure was available with the inhibitor bound form, an energy based pharmacophore was developed from Schrodinger scripts. But the active site had very low donor to acceptor ratio, 0.055 determined from SiteMap. Thus as expected a 4/5 feature hypothesis got generated with only single kind of feature in it, that is all acceptors. Presence of so many acceptor features was not good for the druggability, which was reflected upon the virtual screening. There were very few hits which were small fragments, with very high polar surface area similar to the known inhibitor nitripropionic acid. There have been many molecules earlier reported as Mtb ICL inhibitors, that inhibitor were tried to dock into active site of the closed conformation. Except few small molecules rest all big molecules failed to efficiently dock into active site. These all results indicated need of different approach for the identification of

Mtb ICL inhibitors. So instead of selecting inhibitor bound closed conformation the open inactive conformation of the enzyme was considered for the study.

The difference in the closed conformation and the open conformation is in the loop conformation. There two loops which in the closed form restrict the access to active site. The loop consisting of residue number 185 to 196 is an active loop (ICL signature sequence (K189KCGH193)) is the first one and the second loop consist of 18 amino acids with residue number 411–428 at the C-terminal end of the adjacent subunit. Binding of inhibitor leads the loop movement by 10-12 Å to adopt 'closed' conformation. This rearrangement appears to be triggered by a 2.5 Å movement of Mg^2+, that is bound in a highly electronegative depression formed by Asp108, Asp153, Glu155 and Glu182 in the apo enzyme. Since crystals with 3-bromopyruvate were also obtained without glyoxylate, the interactions responsible for the loop closure can be narrowed down to the common carboxylate that binds in the pocket formed by residues His193, Asn313, Ser315, Ser317, and Thr347 in both the complexes.

6.3.1 Virtual screening of database

To identify the hits with the potential to inhibit the Mtb ICL the virtual screening was carried out. Our own database molecules were used for the virtual screening. The molecules were docked to the open form of Mtb ICL, crystal structure collected from PDB (entry id 1f61). To the minimized protein the Glide docking was carried out with XP mode. The XP mode is more accurate and cover very diverse area of conformation during docking it was chosen over SP. Before running the virtual screening of database, the parameter for docking was set by running the docking simulation for earlier reported molecules. The highest active molecule which got docked in to the active site of the 'closed' conformation of Mtb ICL was taken and was docked into the 'open' form. The docked molecule was checked for orientation, binding pattern and the poses were compared with the docking poses generated with the closed conformation. The molecules presented not only the similar orientation, and pattern of binding presented a low rms deviation between the poses of "closed" and "open" forms. The superimposed docked molecules produced the rms deviations within 2.5 Å. This indicated no much change in the binding pattern of the inhibitor molecule to the 'open' as well as 'closed' form of the enzyme. Since there is no much difference in the binding of the inhibitor molecules to the 'open' and 'closed' forms, the 'open' form of the crystal structure can be used efficiently to identify the potential molecules which can inhibit the ICL enzyme.

Structure based virtual screening was carried out on our own database of about 2100 molecules. The Glide XP docking saved 1556 docked molecular poses. These molecules belonged to different class of the chemical moieties such as, Azetidines analogues, Pyridino-pyrimidines analogues, Thienoindoles derivatives, Pyridine derivatives, Pyrimidopyrimidine derivatives, Thiosemicarbazones etc. The docked molecules belonging to different class of the chemical moiety were assessed by docking score and binding pattern to the enzyme and molecules belonging to the best moiety were considered for the biochemical screening against the enzyme inhibitory activity. All the molecules available in our database belonging to the same class of moiety were screened. Once the biochemical activity was conducted the results were compared with the docking scores.

Azetidine analogues

Docking results presented a large number of azetidine analogue as hits. The 200 azetidine analogues were assessed for Mtb ICL enzyme inhibition at a concentration of 9 μg/mL. 56

molecules showed more than 50% enzyme inhibition, 14 molecules showed more than 80% enzyme inhibition compared to the nitropropionic acid which had 50% inhibitory activity at 100 μM. Table 15 presents the percentage inhibition of Mtb ICL activity by azetidine analogues. 21 series of compounds with 10 different analogues were considered for the biochemical activity assessment. All the analogues were present with different alkyl chains. Six molecules **3YS1, 3YS10, 3YS18, 5YS18, 8YS11** and **8YS17** exhibited more than 95% of Mtb ICL enzyme inhibition.

Out of the different alkyl groups substituted on the nitrogen atom of azetidine, the molecules with N-isopropyl substitution showed good activity followed by propyl substitution and benzyl substitution. Out of 21 analogues of N-isopropyl substitution 15 molecules had more than 50% inhibition. Even though most of the analogues with isopropyl substitution on nitrogen atom showed the inhibition, the extent of inhibition was moderate; **2YS2** exhibited the highest activity of 90.7% inhibition of Mtb ICL. The different amide analogues substitution on two and four position did not had much effect on enzyme inhibition activity.

·The analogues with N- propyl substitution on azetidine presented good activity following compared to the activity observed with N-isopropyl substitution. 10 molecules out of 21 analogues with substitution on two and four position of azetidine moiety showed activity more than 50%. Compound with 2- and 4-disubstituted phenylethylamine moiety **(1YS8)** showed highest percentage of inhibition activity of 89.31. Increasing the alkyl amine chain length from ethyl to propyl very moderately affected the activity. The branched alkyl chains increased the activity as can be seen with isopropyl moiety **(1YS4)** which showed 80% inhibition. Further increase in the chain length of alkyl chain length or increasing the bulkiness by disubstituted alkyl amines reduced activity compared to isopropyl amine. Aryl substitution had a positive effect on the activity. Compared to the cyclohexylamine (**1YS6**) which exhibited 47.18% inhibition, benzylamine (**1YS7**) and phenylethylamine (**1YS8**) presented higher activity (68% and 89% respectively). Substitution of piperidine at 2- and 4- position (**1YS13**) exhibited enzyme 60% inhibition. The substitution with 4-methylpiperidine at 2-and 4- position of azetidine (**1YS15**) affected activity moderately whereas the morpholine (**1YS14**) reduced inhibitory activity moderately. Substitution with the ethyl pyparazine (**1YS16**) showed a 65.89% enzyme inhibition. The activity reduced with the phenylpyperzine substitution (**1YS17**) to 38%, but with bezylpypeazine substitution (**1YS18**) the activity regained to 59%. The substitution on the 4-position of the phenyl pyperazin had a detrimental effect on the enzyme activity.

The benzyl substitution on nitrogen of azetidine presented very high activity compared to isopropyl moiety. Out of nine screened molecules five molecules presented activity more than 62%. Substitution with carboxycyclohexylamine, carboxypropylamine, carboxyhexylamine at 2- and 4-positions of azetidine showed enzyme inhibition of 89.46%, 86.76% and 83.34% respectively (**10YS6, 10YS2, 10YS5**).

Three molecules form the N-cyclopropyl substitution on azetidine presented very high activity. **3YS18**, (carboxybezylpyridine substitution at 2- and 4- position of azetidine) showed Mtb ICL inhibitory activity of 99.36%, **3YS10** (carboxydi-isopropylamine substitution at 2- and 4- position) showed enzyme inhibitory activity of 96% and **3YS1** (carboxyethlylamine substitution at 2- and 4- position) showed enzyme inhibitory activity of 95.76%. The similar trend to that observed with N-cyclopropyl substitution was seen for the N-propyl substitution. Here in this case the carboxyethylamine substitution (**3YS1**) showed a very high activity but the activity reduced with propyl (**3YS2**) or butyl (**3YS1**) substitutions. But with carboxy-isoporylamne substitution (**3YS4**) some activity regained (72%). The aryl substation did not increase the enzyme inhibitory activity to the extent observed with N-propyl or N-isopropyl substitutions. The carboxycyclohexylamine analogue (**3YS6**) presented 57.6% of enzyme inhibitory activity. Substitution of side chain with ethylpyperazine to phenyl pyperazine reduced the activity, but with the benzylpyperazine (**3YS18**) activity drastically increased to the extent of 99.36%. The carboxychlorophenyl-pyperazine derivative (**3YS19**) showed an ICL enzyme inhibitory activity of 55.86%.

As the alkyl chain length increased the overall Mtb ICL enzyme inhibitory activity moderately got reduced. Molecules with substitution of N-butyl, N-isobutyl, N-pentyl, N-cyclo-pentyl moieties in azetidine did show only moderate activity. A different tendency was observed with the alkyl substitution in 2- and 4- position. Ethylamine substitution (**4YS1**) showed highest activity (58.82%) in this series. The butylamine analogue (**4YS3**) shoed an activity of 52.71%, but the activity reduced with propylamine and cyclopropylamine (**4YS2**, **4YS4**) analogues. A similar tendency was observed with the N-isobutyl substitution even though the activity was low. With N-isobutyl substitution as usual tendency the benzylpyperazine analogue (**5YS18**) presented highest activity in that series with Mtb ICL inhibitory activity of 96.67%. Another molecule with 4-chlorophenyl pyperazine analogue (**5YS19**) showed 57.89% of enzyme inhibitory activity. All other analogues from N-isobutyl substituted series present Mtb ICL inhibitory activity less than 50%. Only two molecules with ehylpyperazine and 2-pyridine-ethanamine substitutions (**6YS16**, (56.16%); **6YS21**, (50.81%)) showed ICL inhibitory activity more than 50%.

Three molecules with N-hexyl substitution presented more than 50% of Mtb ICL enzyme inhibitory activity. The carboxydibutylamine analogue (**8YS11**) exhibited 99.28% of enzyme inhibitory activity. The carboxyethylpiperazine analogue (**8YS16**) showed 52.12% enzyme inhibition, whereas carboxyphenylpiperazine analogue (**8YS17**) exhibited 98.2% of enzyme inhibition. This tendency was different from the observed for analogues of other series where the benzylpyperazine analogue use to express higher activity, whereas with N-hexyl substitution reduced activity was observed (**8YS18**, 43.45% inhibition).

The N-cyclohexyl substituted analogues presented a different tendency. Out of 21 molecules from this series 7 molecules exhibited more than 50% Mtb ICL enzyme inhibition activity. The inhibitory activity observed to increase with carboxycyclohexyl substitution (**9YS6**) at 2- and 4- position of azetidine, which showed 47% enzyme inhibition. The inhibitory activity increased with the benzylamine substitution (**9YS7**) 83.94%, but the activity reduced with phenylethylamine substitution (**9YS8**) to 42.8%. Normally in all other analogues the bulky carboxydiamino substituted analogues revealed lower activity, but in case of N-cyclohexyl analogues the activity was found to increase. The activity increased in the order of diethylamine < di-isopropylamine < di-butylamine < di-bezylamine (**9YS9**, (26.4%) < (**9YS10**, (33.89%) < **9YS11**, (60.99%) < **9YS12**, (65.45%)). The pyperidne analogue (**9YS13**) exhibited good inhibitory activity of 75.8%, but he morpholin analogue and the 4-methylpyperidine analogue exhibited lesser enzyme inhibition. The ethylpyperizine analogue showed higher inhibitory activity compared to the phenylpiperazine or benzyle-piperazine analogues, but increased

Table 15: Structures of the different azetidine analogues with their Mtb ICL enzyme inhibitory activity. The enzyme inhibitory activity is expresses in terms of percentage inhibition.

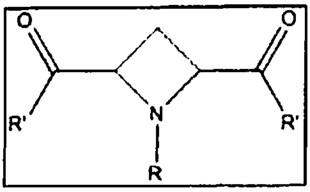

	R=propyl			R=isopropyl			R=cyclopropyl			R=butyl			R=isobutyl		
R'	name	% inhib	Mol Wt	name	% inhib	Mol Wt	name	% inhib	Mol Wt	name	% inhib	Mol Wt	name	% inhib	Mol Wt
ethylamine	1YS1	48.42	241.3	2YS1	45.64	241.3	3YS1	95.76	239.3	4YS1	58.82	255.4	5YS1	33.74	255.4
propylamine	1YS2	51.93	269.4	2YS2	90.69	269.4	3YS2	46.53	267.4	4YS2	34.81	283.4	5YS2	6.15	283.4
butylamine	1YS3	52.97	297.4	2YS3	42.03	297.4	3YS3	59.41	295.4	4YS3	52.71	311.5	5YS3	26.42	297.4
isopropylamine	1YS4	80.74	269.4	2YS4	63.12	269.4	3YS4	72.08	267.4	4YS4	35.62	283.4	5YS4	28.67	283.4
n-hexymamine	1YS5	34.01	353.5	2YS5	60.79	353.5	3YS5	44.60	351.5	4YS5	30.73	367.6	5YS5	9.51	367.6
cyclohexylamine	1YS6	47.18	349.5	2YS6	39.55	349.5	3YS6	57.62	347.5	4YS6	39.26	363.5	5YS6	30.33	363.5
benzylamine	1YS7	68.47	365.5	2YS7	58.42	365.5	3YS7	34.95	363.5	4YS7	45.81	379.5	5YS7	41.00	379.5
phenylethylamine	1YS8	89.31	393.5	2YS8	52.97	393.5	3YS8	40.10	391.5	4YS8	NA	407.6	5YS8	32.53	407.6
diethylamine	1YS9	53.51	297.4	2YS9	49.21	297.4	3YS9	30.79	295.4	4YS9	35.67	311.5	5YS9	NA	311.5
di-isopropylamine	1YS10	49.11	353.5	2YS10	66.44	353.5	3YS10	96.07	351.5	4YS10	33.92	367.6	5YS10	10.37	367.6
di-butylamine	1YS11	46.49	409.7	2YS11	55.00	409.7	3YS11	51.04	407.6	4YS11	27.23	423.7	5YS11	30.41	423.7
di-bezylamine	1YS12	18.07	545.7	2YS12	50.84	545.7	3YS12	30.45	543.7	4YS12	38.76	559.7	5YS12	30.65	559.7
piperidine	1YS13	60.15	321.5	2YS13	58.66	321.5	3YS13	46.29	319.4	4YS13	30.69	335.5	5YS13	15.25	335.5
morpholine	1YS14	46.78	325.4	2YS14	61.14	325.4	3YS14	39.70	323.4	4YS14	5.92	339.4	5YS14	27.10	339.4
4-methylpiperidine	1YS15	57.18	349.5	2YS15	51.78	349.5	3YS15	32.38	347.5	4YS15	44.91	363.5	5YS15	44.20	363.5
ethylpiperazine	1YS16	65.89	379.5	2YS16	53.66	379.5	3YS16	24.26	377.5	4YS16	13.37	393.6	5YS16	11.61	393.6
phenylpiperazine	1YS17	38.07	475.6	2YS17	58.32	475.6	3YS17	17.92	473.6	4YS17	9.87	489.7	5YS17	NA	489.7
benzyle-piperazine	1YS18	59.06	503.7	2YS18	64.01	503.7	3YS18	99.36	501.7	4YS18	42.08	517.7	5YS18	96.67	517.7
4-chlorophenyl-piperazine	1YS19	37.23	544.5	2YS19	34.21	544.5	3YS19	55.84	542.5	4YS19	30.33	558.5	5YS19	57.84	558.5
4-methoxyphenyl-piperazine	1YS20	44.21	535.7	2YS20	64.46	535.7	3YS20	41.54	533.7	4YS20	44.55	549.7	5YS20	20.51	549.7
2-pyridine-ethanamine	1YS21	31.44	395.5	2YS21	30.05	381.5	3YS21	45.54	379.5	4YS21	45.58	409.5	5YS21	49.60	395.5

	R=pentyl			R=cyclopentyl			R=hexyl			R=cyclohexyl			R=benzyl		
R'	name	% inhib	Mol Wt	name	% inhib	Mol Wt	name	% inhib	Mol Wt	name	% inhib	Mol Wt	name	% inhib	Mol Wt
ethylamine	6YS1	22.03	269.4	7YS1	20.05	267.4	8YS1	26.50	283.4	9YS1	NA	281.4	10YS1	26.97	289.4
propylamine	6YS2	38.51	297.4	7YS2	NA	295.4	8YS2	34.38	311.5	9YS2	15.81	309.5	10YS2	86.76	317.4
butylamine	6YS3	15.40	325.5	7YS3	26.48	323.5	8YS3	24.43	339.5	9YS3	42.96	337.5	10YS3	44.32	345.5
isopropylamine	6YS4	32.45	297.4	7YS4	52.33	295.4	8YS4	24.19	311.5	9YS4	30.10	309.5	10YS4	65.59	317.4
n-hexymamine	6YS5	41.26	381.6	7YS5	49.14	379.6	8YS5	26.65	395.6	9YS5	26.01	393.6	10YS5	83.34	401.6
cyclohexylamine	6YS6	13.50	377.6	7YS6	34.73	375.6	8YS6	36.90	391.6	9YS6	47.24	389.6	10YS6	89.46	397.6
benzylamine	6YS7	NA	393.5	7YS7	NA	391.5	8YS7	20.99	407.6	9YS7	83.94	405.5	10YS7	40.53	413.5
phenylethylamine	6YS8	32.16	421.6	7YS8	20.59	419.6	8YS8	17.09	435.6	9YS8	42.86	433.6	10YS8	NA	441.6
diethylamine	6YS9	48.03	325.5	7YS9	40.89	323.5	8YS9	30.49	339.5	9YS9	26.4	337.5	10YS9	62.21	345.5
di-isopropylamine	6YS10	36.10	381.6	7YS10	44.43	379.6	8YS10	24.68	395.6	9YS10	33.89	393.6	10YS10	ND	
di-butylamine	6YS11	42.24	437.7	7YS11	36.01	435.7	8YS11	99.28	451.7	9YS11	60.99	449.7	10YS11	ND	
di-bezylamine	6YS12	46.95	573.8	7YS12	27.14	571.8	8YS12	26.11	587.8	9YS12	65.45	585.8	10YS12	ND	
piperidine	6YS13	27.00	349.5	7YS13	23.65	347.5	8YS13	36.55	363.5	9YS13	75.81	361.5	10YS13	ND	
morpholine	6YS14	21.90	353.5	7YS14	19.11	351.4	8YS14	9.46	367.5	9YS14	41.49	365.5	10YS14	ND	
4-methylpiperidine	6YS15	45.14	377.6	7YS15	26.31	375.6	8YS15	14.98	391.6	9YS15	40.99	389.6	10YS15	ND	
ethylpiperazine	6YS16	56.14	407.6	7YS16	42.32	405.6	8YS16	52.12	421.6	9YS16	30.63	419.6	10YS16	ND	
phenylpiperazine	6YS17	33.90	503.7	7YS17	50.89	501.7	8YS17	98.28	517.7	9YS17	19.67	515.7	10YS17	ND	
benzyle-piperazine	6YS18	14.38	531.7	7YS18	34.04	529.7	8YS18	43.45	545.8	9YS18	11.55	543.7	10YS18	ND	
4-chlorophenyl-piperazine	6YS19	9.05	572.6	7YS19	35.02	570.6	8YS19	25.52	586.6	9YS19	69.42	584.6	10YS19	ND	
4-methoxyphenyl-piperazine	6YS20	25.29	563.7	7YS20	27.78	561.7	8YS20	15.12	577.8	9YS20	76.59	575.7	10YS20	ND	
2-pyridine-ethanamine	6YS21	50.81	423.6	7YS21	26.11	421.5	8YS21	NA	437.6	9YS21	85.44	435.6	10YS21	ND	

*NA= not active, ND= not determined

activity was observed with 4-chlorophenyl-piperazine analogue, **9YS19** (69.4%) and 4-methoxyphenyl-piperazine analogue, **9YS20** (76.6%). The 2-pyridine-ethanamine analogue **9YS21** exhibited Mtb ICL inhibitory activity of 85.4%.

Across the different series The N-ispropyl substituted compounds were most efficient in producing the Mtb ICL enzyme inhibition. Many compounds belonging to this series showed inhibitory activity more than 50%. As the N-substituted alkyl chain length increased the activity reduced. Following N-isopropyl substitution, the number of N-propyl substituted compounds stood second, which showed activity more than 50% enzyme inhibition. The N-cyclohexyl substitution had good effect on the ICL inhibitory activity. But the N-benzyl substituted compounds presented higher inhibitory activity. Along the different series corboxybenzyle-piperazine substitution at 2- and 4- position of azetidine showed good enzyme inhibitory activity.

Pyrido-pyrimidine analogues

Pyridopyrimidine analogues were another major hits identified by the docking studies. A total of 30 molecules belonging to pyridopyrimidine class were subjected to Mtb ICL inhibitory activity assessment. There were 2 series with 15 analogues in each series. The enzyme activity was monitored by at 9 μg/mL concentration of each analogue. Table 16 contains the structural details of the molecules and its activity expresses in terms of percentage inhibition of Mtb ICL enzyme.

The first series had 2,4,5-triflurophenylaniline attached at 4-position of the pyrido-pyrimidine (**11YS** series). The 15 analogues present, had different aryl amine substitutions at 2-position of pyridopyrimidine moiety. The molecules from **11YS** series exhibited a moderate to high Mtb ICL enzyme inhibitory activity. The aniline analogue, **11YS1** showed 86.24% of Mtb

ICL enzyme inhibition at 9 µg/mL concentration. The 4-methoxyaniline analogue **11YS2** presented a higher inhibitory activity of 94.75%, but the activity got reduced with 4-nitoraniline (**11YS3**) to 59.11%. *o,p*-dimethyl substitution had a detrimental effect on the enzyme inhibitory activity, **11YS4** showed 43.57% of inhibitory activity. Halogens on the *para* position had moderate effect on the activity. The 4-chloroaniline analogue (**11YS12**) exhibited 62.24% of ICL inhibition, whereas the 4-bromoaniline analogue (**11YS11**) exhibited 41.62% enzyme inhibition. Compound **11YS13** with 2,4-dimethylaniline substitution exhibited highest, 98.43% of Mtb ICL enzyme inhibitory activity. The 2-methyl-5-fluroaniline analogue (**11YS5**) and 2-methyl-3-chloroaniline analogue (**11YS15**) showed moderate enzyme inhibitory activity of 61.7% and 75.76% respectively. Except **11YS7**, 2-(3-methyl)pyridylamine analogue (65.71% inhibition) all other different pyridyl and benzyl amine substituted compounds exhibited low to moderate Mtb ICL inhibition activity. The 2-(5-nitro)thiazolylamine analogue **11YS8** was totally inactive molecules but 2-(6-nitrobenzo)thiazolylamine analogue **11YS9** exhibited excellent Mtb ICL enzyme inhibitory activity.

The second series had benzothiazole-6-amine attached at 4-position of the pyrido-pyrimidine (**12YS** series). The 15 analogues present, had different aryl amine substitutions at 2-position of pyridopyrimidine moiety. The molecules from **12YS** series showed low to moderate Mtb ICL enzyme inhibitory activity. The 4-pyridylamine analogue (**12YS14**) exhibited 79.24% of enzyme inhibition, but substituted pyridylamine, 2-(3-methyl)pyridylamine reduced the activity (53.19%). The 2-pyridylamine analogue, **12YS6** was totally inactive. Both thiazolyl substituted analogues **12YS8** and **12YS9** exhibited 42% ICL enzyme inhibition. The Benzyl aniline analogue **12YS10** showed 47.2% enzyme inhibition. All unsubstituted and monosubstituted analogues exhibited very low inhibitory activity, except 2-methyl-3-chloroaniline analogue **12YS15**, which showed 96.9% of Mtb ICL enzyme inhibition.

Table 16: Structures of the different Pyridopyrimidine analogues with their Mtb ICL enzyme inhibitory activity. The enzyme inhibitory activity is expresses in terms of percentage inhibition. *na = not active

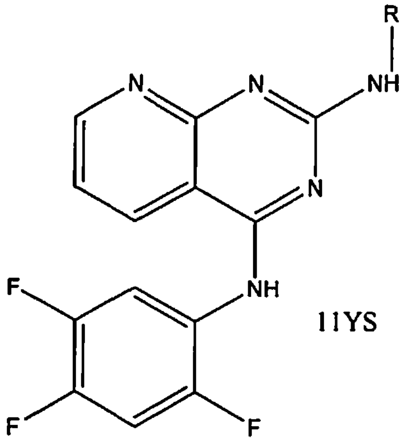

11YS

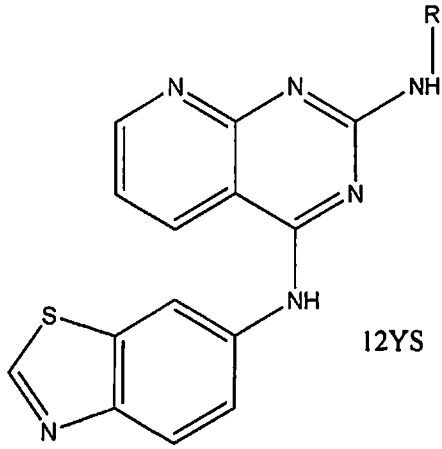

12YS

R	Comp	Mol. Wt.	% inhib	Comp	Mol. Wt.	% inhib
	2,4,5-trifluropenyl			benzothiazole		
phenyl	11YS1	367.33	86.24	12YS1	370.43	10.62
4-methoxyphenyl	11YS2	397.35	94.75	12YS2	400.46	24.10
4-nitrophenyl	11YS3	412.32	59.11	12YS3	415.43	35.86
2,4-dimethoxyphenyl	11YS4	427.38	43.57	12YS4	430.48	19.19
2-methyl-5-flurophenyl	11YS5	399.34	61.71	12YS5	402.45	6.29
2-pyridyl	11YS6	368.32	13.71	12YS6	371.42	na
2-(3-methyl)-pyridyl	11YS7	382.34	67.71	12YS7	385.44	53.19
5-nitro-2thiazolyl	11YS8	419.34	na	12YS8	422.44	42.33
6-nitrobenzo-2-thiazolyl	11YS9	469.4	95.52	12YS9	472.5	42.57
benzyl	11YS10	381.35	18.33	12YS10	384.46	47.29
4-bromophenyl	11YS11	446.22	41.62	12YS11	449.33	na
4-chlorophenyl	11YS12	401.77	62.24	12YS12	404.88	7.81
2,5-diethylphenyl	11YS13	423.43	98.43	12YS13	426.54	28.43
4-pyridyl	11YS14	368.32	45.90	12YS14	371.42	79.24
2-methyl-3-chlorophenyl	11YS15	415.8	75.76	12YS15	418.9	96.90

Benzo-thiazolo-pyrimido-pyrimidine-one analogues

A major number of benzo-thiazolo-pyrimido-pyrimidine-one analogues were obtained as hits during the docking studies. 90 molecules belonging to this class of the molecules were monosubstituted analogues exhibited very low inhibitory activity, except 2-methyl-3-chloroaniline analogue **12YS15**, which showed 96.9% of Mtb ICL enzyme inhibition.

Table 16: Structures of the different Pyridopyrimidine analogues with their Mtb ICL enzyme inhibitory activity. The enzyme inhibitory activity is expresses in terms of percentage inhibition. *na = not active

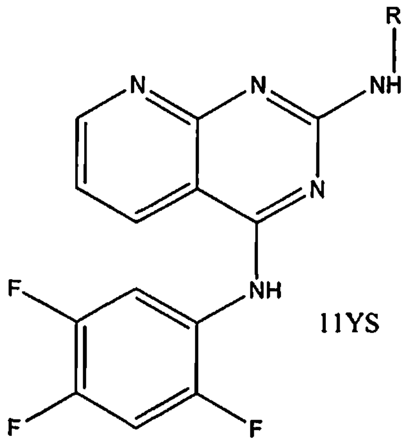

11YS

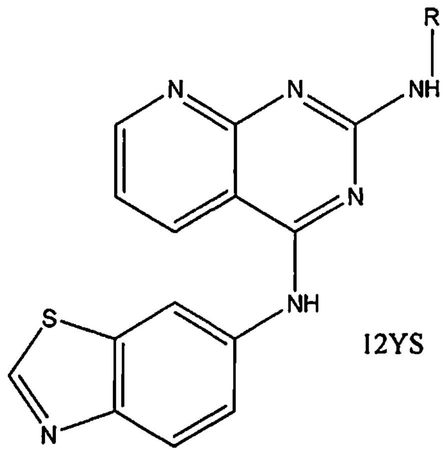

12YS

R	Comp	Mol. Wt.	% inhib	Comp	Mol. Wt.	% inhib
	2,4,5-triflurophenyl			benzothiazole		
phenyl	11YS1	367.33	86.24	12YS1	370.43	10.62
4-methoxyphenyl	11YS2	397.35	94.75	12YS2	400.46	24.10
4-nitrophenyl	11YS3	412.32	59.11	12YS3	415.43	35.86
2,4-dimethoxyphenyl	11YS4	427.38	43.57	12YS4	430.48	19.19
2-methyl-5-flurophenyl	11YS5	399.34	61.71	12YS5	402.45	6.29
2-pyridyl	11YS6	368.32	13.71	12YS6	371.42	na
2-(3-methyl)-pyridyl	11YS7	382.34	67.71	12YS7	385.44	53.19
5-nitro-2thiazolyl	11YS8	419.34	na	12YS8	422.44	42.33
6-nitrobenzo-2-thiazolyl	11YS9	469.4	95.52	12YS9	472.5	42.57
benzyl	11YS10	381.35	18.33	12YS10	384.46	47.29
4-bromophenyl	11YS11	446.22	41.62	12YS11	449.33	na
4-chlorophenyl	11YS12	401.77	62.24	12YS12	404.88	7.81
2,5-diethylphenyl	11YS13	423.43	98.43	12YS13	426.54	28.43
4-pyridyl	11YS14	368.32	45.90	12YS14	371.42	79.24
2-methyl-3-chlorophenyl	11YS15	415.8	75.76	12YS15	418.9	96.90

Benzo-thiazolo-pyrimido-pyrimidine-one analogues

A major number of benzo-thiazolo-pyrimido-pyrimidine-one analogues were obtained as hits during the docking studies. 90 molecules belonging to this class of the molecules were subjected to the biochemical screening where they were assayed for the Mtb ICL inhibitory activity. There were 15 analogues belonging to the 6 different series. The percentage inhibition of the candidate analogues were assessed at 3 μg/mL concentration. Table 17 contains the structural details of the molecules and its activity expresses in terms of percentage inhibition of Mtb ICL activity.

The first series was of benzo-thiazolo-pyrimido-pyrimidine-one analogues named **13YS** series. It had benzo-thiazolo-pyrimido-pyrimidine-one analogues with 4,5- attached dihydropyrimidine-2-one. 15 analogues were present in the **13YS** series with different aryl substituents at 6-position of attached dihydro-pyrimidineone. Molecules belonging to this series produced moderately low activity. The highest active molecule was **13YS10** analogues with the *p*-dimethylamino-benzaldehyde substitution at 6 position of dihydropyrimidineone. It exhibited 24.25% inhibition of Mtb ICL enzyme. The next highest active molecule in this series was **13YS12**, exhibited 22.16% of enzyme inhibition. All other molecules were either inactive or had Mtb ICL enzyme inhibitory activity less than 20%.

The second series was of benzo-thiazolo-pyrimido-pyrimidine-one analogues named **14YS** series. It had benzo-thiazolo-pyrimido-pyrimidine-one analogues with 4,5- attached dihydropyrimidine-2-thone. 15 analogues were present in the **14YS** series with different aryl substituents at 6-position of attached dihydropyrimidine-thione. Three molecules in this series exhibited Mtb inhibitory activity more than 50%. **14YS14** with 2-(trifluoromethyl)-benzaldehyde substitution at 6-position of dihydropyrimidine-thione showed highest of 71.23% ICL inhibitory activity. **14YS10** analogue with p-dimethylaminobenzaldehyde substitution, **14YS1** analogue with benzaldehyde substitution presented Mtb ICL inhibitory activity of 53.74% and 50.8% respectively. Other than **14YS8**, (the molecule with 4-methoxybenzaldehyde substitution which showed 34.49% of enzyme inhibition) all other molecules exhibited Mtb ICL inhibition less than 30%.

The third series was of 3-nitrobenzo-thiazolo-pirimido-pirimidine-one analogues, named **15YS** series. It had 3-nitrobenzo-thiazolo-pirimido-pirimidine-one analogues with 4,5- attached dihydro-pyrimidine-2-one. 15 analogues were present in the **15YS** series with different aryl substituents at 6-position of attached dihydropyrimidine-one. Three molecules in this series exhibited Mtb inhibitory activity more than 50%. They were **15YS14** with 2-(trifluoromethyl)-benzaldehyde substitution at 6-position of dihydropyrimidine-one exhibited 71.23% of Mtb ICL inhibitory activity, **15YS15** analogue with vanillin substitution exhibited 66% of enzyme inhibition, and **15YS3** analogue with 2nitrobenzaldehyde substitution presented Mtb ICL inhibitory activity of 54.89%. All other molecules wee inactive with activity less than 25%.

The fourth series was of 3-nitrobenzo-thiazolo-pirimido-pirimidine-7-one analogues, named **16YS** series. It had 3-nitrobenzo-thiazolo-pirimido-pirimidine-one analogues with 4,5-attached dihydro-pyrimidine-2-thione. 15 analogues were present in the **16YS** series with different aryl substituents at 6-position of attached dihydropyrimidine-one. At concentration of 3 μg/mL, all the molecules were inactive with the with Mtb ICL enzyme inhibitory activity less than 30%, except **16YS10**, p-dimethylamino analogue which exhibited 41.45% of ICL inhibition.

The fifth series was of 2-nitrobenzo-thiazolo-pyrimido-pyrimidine-one analogues, named **17YS** series. It had 3-nitrobenzo-thiazolo-pyrimido-pyrimidine-one analogues with 4,5- attached dihydropyrimidine-2-one. 15 analogues were present in the **17YS** series with different aryl substituents at 6-position of attached dihydropyrimidine-one. Two molecules, **17YS6** (4-bromobenzaldehyde analogue, 79.97% enzyme inhibition) and **17YS12** (p-tolylaldehyde analogue 67.14% enzyme inhibition) exhibited Mtb ICL enzyme inhibitory activity more than 50%. Four molecules, **17YS2** (salicyaldehyde), **17YS7** (4-fluorobenzaldehyde), **17YS10** (p-dimethylaminobenzaldehyde), **17YS1** (benzaldehyde) exhibited a moderate activity of 43.86%, 34.87%, 32.65%, 30.18% of

Table 17: Structures of the different benzo-thiazolo-pyrimido-pyrimidine-one analogues with their Mtb ICL enzyme inhibitory activity. The enzyme inhibitory activity is expresses in terms of percentage inhibition. *NA = not active

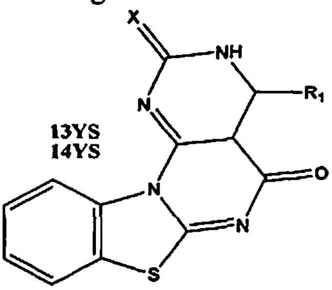

13YS
14YS

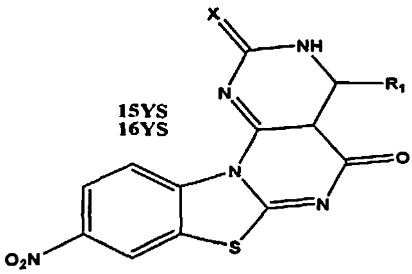

15YS
16YS

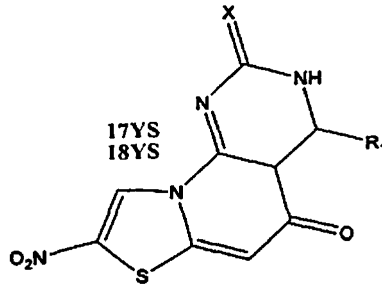

17YS
18YS

R_1	X	Comp	Mol. wt	% inhib	Comp	Mol. wt	% inhib	Comp	Mol. wt	% inhib
Benzaldehyde	O	13YS1	376.39	9.53	15YS1	423.40	21.13	17YS1	371.33	30.18
salicyaldehyde	O	13YS2	392.39	10.59	15YS2	439.40	7.61	17YS2	387.33	43.86
2-nitrobenzaldehyde	O	13YS3	421.39	10.20	15YS3	468.40	54.89	17YS3	416.33	NA
4-nitrobenzaldehyde	O	13YS4	421.39	3.78	15YS4	468.40	13.37	17YS4	416.33	3.81
3-bromobenzaldehyde	O	13YS5	455.29	17.44	15YS5	502.30	NA	17YS5	450.22	NA
4-bromobenzaldehyde	O	13YS6	455.29	NA	15YS6	502.30	20.08	17YS6	450.22	79.97
4-fluorobenzaldehyde	O	13YS7	394.38	NA	15YS7	441.39	18.19	17YS7	389.32	34.88
4-methoxybenzaldehyde	O	13YS8	406.42	6.26	15YS8	453.43	NA	17YS8	401.35	16.08
4-chlorobenzaldehyde	O	13YS9	410.83	8.56	15YS9	457.85	2.44	17YS9	405.77	NA
p-dimethylaminobenzaldehyde	O	13YS10	419.46	24.25	15YS10	466.47	29.80	17YS10	414.40	32.65
o-tolylaldehyde	O	13YS11	390.42	17.32	15YS11	437.43	0.86	17YS11	385.35	NA
p-tolylaldehyde	O	13YS12	390.42	22.16	15YS12	437.43	8.26	17YS12	385.35	67.14
2,6-dichlorobenzaldehyde	O	13YS13	445.28	5.87	15YS13	492.29	17.71	17YS13	440.22	NA
2-(trifluoromethyl)- benzaldehyde	O	13YS14	444.39	NA	15YS14	491.40	74.74	17YS14	439.33	NA
vanillin	O	13YS15	422.41	17.86	15YS15	469.43	66.08	17YS15	417.35	3.48
Benzaldehyde	S	14YS1	392.45	50.66	16YS1	439.47	NA	18YS1	387.39	NA
salicyaldehyde	S	14YS2	408.45	NA	16YS2	455.47	34.34	18YS2	403.39	NA
2-nitrobenzaldehyde	S	14YS3	437.45	24.47	16YS3	484.47	NA	18YS3	432.39	15.87
4-nitrobenzaldehyde	S	14YS4	437.45	28.98	16YS4	484.47	NA	18YS4	432.39	11.84
3-bromobenzaldehyde	S	14YS5	471.35	22.36	16YS5	518.36	10.54	18YS5	466.29	39.28
4-bromobenzaldehyde	S	14YS6	471.35	NA	16YS6	518.36	22.60	18YS6	466.29	37.41
4-fluorobenzaldehyde	S	14YS7	410.45	10.65	16YS7	457.46	27.62	18YS7	405.38	25.53
4-methoxybenzaldehyde	S	14YS8	422.48	34.49	16YS8	469.49	4.05	18YS8	417.42	NA
4-chlorobenzaldehyde	S	14YS9	426.90	NA	16YS9	473.91	35.13	18YS9	421.84	33.71
p-dimethylaminobenzaldehyde	S	14YS10	435.52	53.74	16YS10	482.54	41.45	18YS10	430.46	12.69
o-tolylaldehyde	S	14YS11	406.48	25.74	16YS11	453.49	4.95	18YS11	401.42	43.86
p-tolylaldehyde	S	14YS12	406.48	26.30	16YS12	453.49	NA	18YS12	401.42	6.47
2,6-dichlorobenzaldehyde	S	14YS13	461.34	6.77	16YS13	508.36	NA	18YS13	456.28	NA
2-(trifluoromethyl)- benzaldehyde	S	14YS14	460.45	71.23	16YS14	507.47	0.21	18YS14	455.39	NA
vanillin	S	14YS15	438.48	21.30	16YS15	485.49	28.61	18YS15	433.42	0.21

enzyme inhibition respectively. All other molecules were inactive with activity less than 30% of enzyme inhibition.

The sixth series was of 2-nitrobenzo-thiazolo-pyrimido-pyrimidine-one analogues, named **18YS** series. It had 3-nitrobenzo-thiazolo-pyrimido-pyrimidine-one analogues with 4,5- attached dihydro-pyrimidine-2-thione. 15 analogues were present in the **18YS** series with different aryl substituents at 6-position of attached dihydropyrimidine-thione. Except four molecules, which were moderately active, all other molecules belonged to this series were inactive with the Mtb ICL inhibitor activity less than 30% at concentration of 3 μg/mL. Those moderately active molecules were, **18YS11** (o-tolylaldehyde), **18YS5** (3-bromobenzaldehyde), **18YS6** (4-bromobenzaldehyde), **18YS9** (4-chlorobenzaldehyde) which exhibited Mtb ICl enzyme inhibitory activity 43.86%, 39.28%, 37.41%, 33.70% respectively.

6.4 Comparison of the biochemical activity with computational results

The both active as well as the inactive form of the Mtb ICL enzyme crystal structures are available. The active form is the closed form. In the closed form two loops closes and limits the accessibility to the active site. The active site is characterized by presence of many polar residues like, Ser91, Asp108, Lys189, His193, Arg228, Glu285, Asn313, Ser315, Ser317 and Thr347. The small size and the highly polar nature of the active site in the closed form has made it unsuitable for use to identify newer inhibitors, rather the closed form failed to identify newer hits in the closed form. There have been many reports of larger molecules from natural sources efficiently inhibiting the ICL enzyme from different species. The active site of the ICL enzyme is very flexible. In the open form the enzyme accommodates large area. To change the conformation from open form to closed form, there occurs 10-12 Å of movement in the loop. So there is very high probability that the larger molecule can fit into the active site.

The use of the closed form of crystal, because of its smaller area and the high polar nature, during the high through put virtual screening by docking, failed to identify newer hits. To identify larger scaffolds with the potential to inhibit Mtb ICL necessitated an alternate method. The little amount of information on already reported inhibitors limited the use of the pharmacophore modeling. The crystal ligands present were very small (nitropropionic acid and bromopyruvic acid). Effort was made to construct a crystal based pharmacophore with these reported molecules. But the pharmacophores were inefficient to identify good hits. The pharmacophore had single feature type of feature with many sites; more over the site present was polar kind (hydrogen acceptor) and the feature lied very close to each other. The database molecules either failed to map to the generated pharmacophore efficiently or failed to dock into active site of the active form of Mtb ICL crystal.

The other alternate available was to use the apo enzyme, open form of the crystal structure. The open form has to be used with much care as it is inactive form. It needs to be checked and validated before its use in the high throughput screening so that it can efficiently identify the inhibitors. So as it was discussed earlier (in section Virtual screening of database) the highest active molecule reported earlier was taken and docked to crystal structure of apo enzyme of Mtb ICL at ligand binding site. The ligand binding site in the apo enzyme was identified by super imposing it with the active form of enzyme. The inhibitor binding pattern, orientation and the contact residues were checked. The inhibitor poses reproduced the similar binding pattern and the orientation. The rms deviation observed was less than 2.5 Å. Usually two poses are considered same only if the rms deviation is less than 2.0 Å units. But in this case, even though rms deviation was slightly more than the allowed limits it was considered same. It could be noted from the figure 51, that the loop closer was responsible for the ligand displacement in the binding site. In the closed conformation the two loops comprising of residue number Asp183 to Lys197 and Cys314 to Asn319 moved closer making the active site area small. The major ICL signature loop moved about 10-12 Å distance restricting access to the active site, while the loop comprising of residues Glu285 to Asp290 moved a bit away making a cavity to hold the ligand. But in the open form this loop has a closed conformation. These movements in the loops are largely responsible for the observed deviation of 2.5 Å in ligand binding pose. But it could be clearly seen that in both 'closed' as well as in 'open' conformation of ICL the ligand has taken similar head to tail orientation of binding. Thus these results gave the confidence to use the apo enzyme form for the high through put virtual screening to identify potential hits which can inhibit Mtb ICL. The apo enzyme has large active site compared to the 'closed' form, made it possible to identify the lager molecules during the virtual screening.

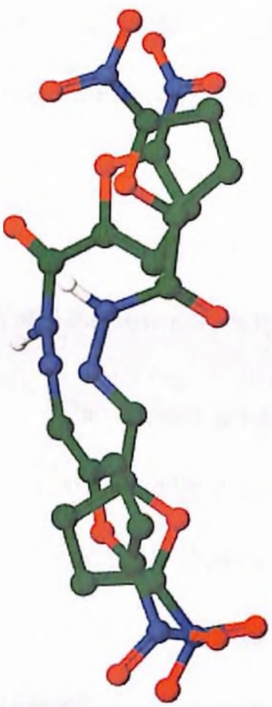

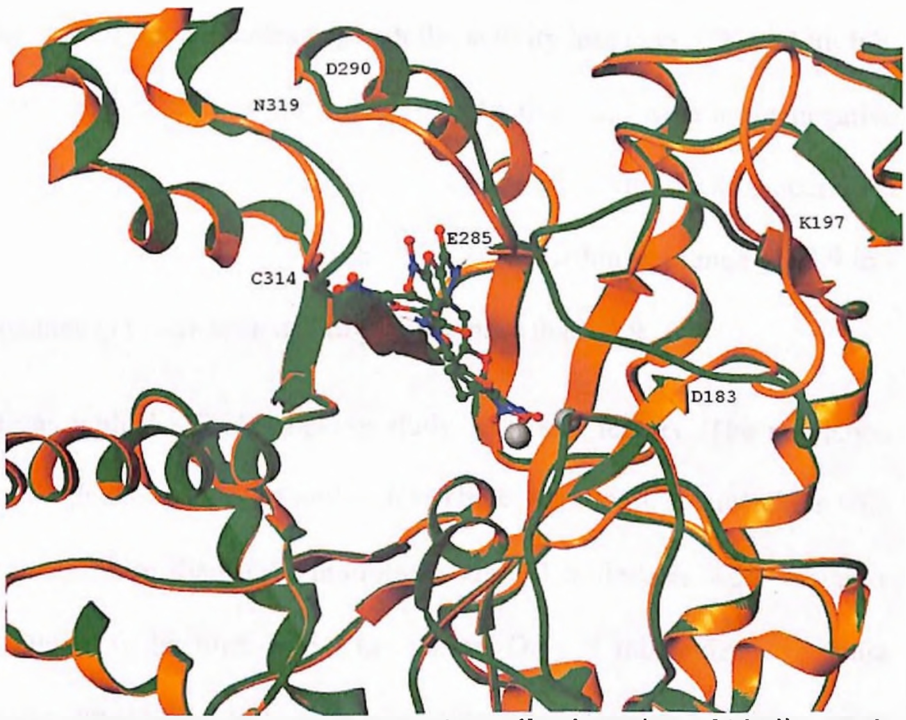

Figure 51: The superimposed inhibitor showing similar head to tail orientation of binding at the active site of Mtb ICL open and closed forms (left). Superimposed inhibitor bound 'open' and 'closed' conformation of the Mtb ICL enzyme (right). The 'closed' protein is presented in green color, and the 'open' form is represented in orange color. The gray spears are the Mg^{2+} ions.

Initially our own proprietary database molecules were subjected to high throughput virtual screening. The hits were clustered into different series. Then the biochemical assay was carried out not only just on the hits obtained from virtual screening but also on all the molecules available belonging to those series. That was to avoid the missing out of potential inhibitor molecule, since the ICL crystal with 'open' conformation was used for the virtual screening. Thus total of about 300 molecules were screened based of the hits obtained from the high throughput virtual screening. A correlation was tried to bring between the computational docking result and the actual ICL inhibition activity collected from biochemical assessment. The dock score, and percentage of ICL inhibition was divided in to activity scale. The activity scale for the Mtb ICL inhibition had three groups in it, the high active molecules (+++) with activity more than 65% of enzyme inhibition, moderate active molecules (++) with the activity within the range of 65 to 35%, and the low active molecules (+) with the activity less than 35% of Mtb ICL enzyme inhibition. The Glide docking scores were energy based values and were in the negative side of scale. The activity scale comprised of the active molecules (+++) with docking score less than -3.9, moderate active molecules (++) were with the dock score within the range of -3.9 to -2.9, and the low active molecules (+) were with docking score more than -2.9.

The overall predictions with the Glide docking study were satisfactory. The prediction carried was excellent for the high active class of molecules. There were total 36 molecules with the Mtb ICL inhibitory activity more than 65% inhibition. The 33 molecules were correctly predicted by the docking studies to be high active molecules. Only 3 molecules were miss interpreted as moderate active molecules, and none were wrongly interpreted as low active molecules. The docking did not result into any false negative results. The docking

Table 18: The comparison of the actual percentage inhibition and the docking scores of the each molecule screened against Mtb ICL enzyme with the activity scale.

Comp	%inhiYS	Activity Scale	Dock Score	Activity Scale	Comp	%inhiYS	Activity Scale	Dock Score	Activity Scale	Comp	%inhiYS	Activity Scale	Dock Score	Activity Scale
3YS18	99.36	+++	-4.58	+++	14YS14	71.23	+++	-3.91	+++	2YS7	58.42	++	-3.06	++
8YS11	99.28	+++	-3.96	+++	9YS19	69.42	+++	-3.74	+++	2YS17	58.32	++	-2.96	++
11YS13	98.43	+++	-4.51	+++	1YS7	68.47	+++	-4.12	+++	5YS19	57.84	++	-3.19	++
8YS17	98.28	+++	-4.83	+++	11YS7	67.71	+++	-4.30	+++	3YS6	57.62	++	-3.07	++
12YS15	96.90	+++	-4.25	+++	17YS12	67.14	+++	-4.10	+++	1YS15	57.18	++	-2.89	++
3YS10	96.07	+++	-3.84	++	2YS10	66.44	+++	-4.51	+++	6YS16	56.14	++	-3.56	++
3YS1	95.75	+++	-4.10	+++	15YS15	66.08	+++	-4.51	+++	3YS19	55.84	++	-3.68	++
11YS9	95.52	+++	-4.03	+++	1YS16	65.89	+++	-2.94	++	2YS11	55.00	++	-3.90	++
11YS2	94.75	+++	-4.21	+++	10YS4	65.59	+++	-4.18	+++	15YS3	54.89	++	-3.10	++
2YS2	90.69	+++	-3.94	+++	9YS12	65.45	+++	-4.60	+++	14YS10	53.74	++	-3.04	++
10YS6	89.46	+++	-3.75	+++	2YS20	64.46	++	-3.47	++	2YS16	53.66	++	-3.00	++
1YS8	89.31	+++	-4.50	+++	2YS18	64.01	++	-3.83	++	1YS9	53.51	++	-4.25	+++
10YS2	86.76	+++	-3.93	+++	2YS4	63.12	++	-3.27	++	12YS7	53.19	++	-2.47	+
11YS1	86.24	+++	-3.96	+++	11YS12	62.24	++	-2.02	+	1YS3	52.97	++	-3.39	++
9YS21	85.44	+++	-3.90	+++	10YS9	62.21	++	-5.50	+++	2YS8	52.97	++	-3.62	++
9YS7	83.94	+++	-4.19	+++	11YS5	61.71	++	-3.86	++	4YS3	52.71	++	-3.00	++
10YS5	83.34	+++	-4.20	+++	2YS14	61.14	++	-3.70	++	7YS4	52.33	++	-3.88	++
1YS4	80.74	+++	-3.89	++	9YS11	60.99	++	-2.91	++	8YS16	52.12	++	-3.50	++
17YS6	79.97	+++	-4.27	+++	2YS5	60.79	++	-3.50	++	1YS2	51.93	++	-3.51	++
12YS14	79.24	+++	-4.39	+++	1YS13	60.15	++	-3.89	++	2YS15	51.78	++	-2.78	++
9YS20	76.59	+++	-5.86	+++	3YS3	59.41	++	-3.64	++	3YS11	51.04	++	-3.43	++
9YS13	75.81	+++	-3.92	+++	11YS3	59.11	++	-3.82	++	7YS17	50.89	++	-3.15	++
11YS15	74.76	+++	-4.18	+++	1YS18	59.06	++	-3.69	++	2YS12	50.84	++	-3.69	++
15YS14	74.74	+++	-3.92	+++	4YS1	58.82	++	-3.31	++	6YS21	50.81	++	-3.68	++
3YS4	72.08	+++	-4.04	+++	2YS13	58.66	++	-2.94	++	14YS1	50.66	++	-3.90	++
Comp	%inhib	Activity Scale	Dock Score	Activity Scale	Comp	%inhib	Activity Scale	Dock Score	Activity Scale	Comp	%inhib	Activity Scale	Dock Score	Activity Scale
5YS21	49.60	++	-3.20	++	5YS15	44.20	++	-3.85	++	18YS5	39.28	++	-3.15	++
2YS9	49.21	++			18YS11	43.86	++	-3.46	++	4YS6	39.26	++	-3.53	++
7YS5	49.14	++			17YS2	43.86	++	-5.39	+++	4YS12	38.76	++	-3.69	++
1YS10	49.11	++	-2.99	++	11B4	43.57	++	-3.80	++	6YS2	38.51	++	-3.69	++
1YS1	48.42	++	-3.87	++	8YS18	43.45	++	-3.62	+++	1YS17	38.07	++	-3.51	++
6YS9	48.03	++	-4.72	+++	9YS3	42.96	++	-3.23	++	18YS6	37.41	++	-3.83	++
12B10	47.29	++	-3.57	++	9YS8	42.86	++	-3.18	++	9YS6	37.24	++	-2.09	+
1YS6	47.18	++	-3.89	++	12B9	42.57	++	-3.81	++	1YS19	37.23	++	-3.60	++
6YS12	46.95	++	-3.62	++	12B8	42.33	++	-3.81	++	8YS6	36.90	++	-3.04	++
1YS14	46.78	++	-5.23	+++	7YS16	42.32	++	-3.25	++	8YS13	36.55	++	-3.06	++
3YS2	46.53	++	-3.90	++	6YS11	42.24	++	-4.33	+++	9YS9	36.40	++	-3.07	++
1YS11	46.49	++	-3.90	++	4YS18	42.08	++	-3.64	++	6YS10	36.10	++	-3.16	++
3YS13	46.29	++	-3.32	++	2YS3	42.03	++	-3.35	++	7YS11	36.01	++		
11B14	45.90	++	-4.29	+++	11B11	41.62	++	-3.13	++	23B3	35.86	++	-3.66	++
4YS7	45.81	++	-3.89	++	3YS20	41.54	++	-2.35	+	4YS9	35.67	++	-3.07	++
2YS1	45.64	++	-3.69	++	9YS14	41.49	++	-3.35	++	4YS4	35.62	++	-3.36	++
4YS21	45.58	++	-3.90	++	16YS10	41.45	++	-3.39	++	16YS9	35.13	++	-3.49	++
3YS21	45.54	++	-3.62	++	6YS5	41.26	++	-3.51	++	7YS19	35.02	++		
6YS15	45.14	++	-3.52	++	5YS7	41.00	++	-3.29	++	3YS7	34.95	+	-4.55	+++
4YS15	44.91	++	-3.73	++	9YS15	40.99	++	-3.32	++	17YS7	34.88	+	-3.90	++
3YS5	44.60	++	-3.57	++	7YS9	40.89	++	-3.66	++	4YS2	34.81	+	-2.22	+
4YS20	44.55	++	-4.51	+++	10YS7	40.53	++	-3.55	++	7YS6	34.73	+	-2.32	+
7YS10	44.43	++	-3.08	++	3YS8	40.10	++	-3.17	++	14YS8	34.49	+	-2.76	+
10YS3	44.32	++	-3.13	++	3YS14	39.70	++	-3.87	++	8YS2	34.38	+	-2.45	+
1YS20	44.21	++	-3.81	++	2YS6	39.55	++	-2.03	+	16YS2	34.34	+	-4.85	+++

Table 17: The comparison of the actual percentage inhibition and the docking scores of the each molecule screened against Mtb ICL enzyme with the activity scale. (Continued)

Comp	%inhib	Activity Scale	Dock Score	Activity Scale	Comp	%inhib	Activity Scale	Dock Score	Activity Scale	Comp	%inhib	Activity Scale	Dock Score	Activity Scale
2YS19	34.21	+	-3.62	++	2YS21	30.05	+	-4.74	+++	6YS20	25.29	+	-2.90	+
7YS18	34.04	+			15YS10	29.80	+	-3.46	++	8YS10	24.68	+	-2.90	+
1YS5	34.01	+	-2.62	+	14YS4	28.98	+	-2.33	+	14YS3	24.47	+	-2.86	+
4YS10	33.92	+	-2.66	+	5YS4	28.67	+	-2.07	+	8YS3	24.43	+	-2.45	+
6YS17	33.90	+	-2.90	+	16YS15	28.61	+	-4.78	+++	3YS16	24.26	+	-3.50	++
5YS1	33.74	+	-3.22	++	12B13	28.43	+	-2.68	+	13YS10	24.25	+	-2.99	+
18YS9	33.71	+	-4.02	+++	7YS20	27.78	+			8YS4	24.19	+	-2.10	+
17YS10	32.65	+	-2.64	+	16YS7	27.62	+	-3.44	++	12B2	24.10	+	-3.73	++
5YS8	32.53	+	-5.30	+++	4YS11	27.23	+	-2.84	+	7YS13	23.65	+		
6YS4	32.45	+	-2.68	+	7YS12	27.14	+	-2.36	+	16YS6	22.60	+	-3.63	++
3YS15	32.38	+	-2.89	+	5YS14	27.10	+	-2.90	+	14YS5	22.36	+	-3.45	++
6YS8	32.16	+	-1.68	+	6YS13	27.00	+	-2.81	+	13YS12	22.16	+	-3.58	++
1YS21	31.44	+	-2.21	+	10YS1	26.97	+	-2.44	+	6YS1	22.03	+	-3.07	++
3YS9	30.79	+	-3.47	++	8YS5	26.65	+	-2.31	+	6YS14	21.90	+	-2.59	+
4YS5	30.73	+	-4.56	+++	8YS1	26.50	+	-2.84	+	14YS15	21.30	+	-4.83	+++
4YS13	30.69	+	-2.35	+	7YS3	26.48	+	-2.88	+	15YS1	21.13	+	-3.50	++
5YS12	30.65	+	-2.60	+	5YS3	26.42	+			8YS7	20.99	+	-2.63	+
9YS16	30.63	+	-2.90	+	7YS15	26.31	+	-2.15	+	7YS8	20.59	+		
8YS9	30.49	+	-4.98	+++	14YS12	26.30	+	-3.53	++	5YS20	20.51	+	-2.41	+
3YS12	30.45	+	-2.89	+	7YS21	26.11	+	-2.90	+	15YS6	20.08	+	-3.90	++
5YS11	30.41	+	-2.08	+	8YS12	26.11	+	-4.99	+++	7YS1	20.05	+	-2.22	+
4YS19	30.33	+	-3.13	++	9YS5	26.01	+	-2.60	+	9D17	19.67	+	-2.76	+
5YS6	30.33	+	-2.25	+	14YS11	25.74	+	-3.90	++	7D14	19.11	+	-2.09	+
17YS1	30.18	+	-2.07	+	18YS7	25.53	+	-3.79	++	1D12	18.07	+	-2.67	+
9YS4	30.10	+	-2.50	+	8YS19	25.52	+	-2.61	+	3D17	17.92	+	-2.49	+

simulation did not miss out identifying potential molecule from the database during the high throughput virtual screening. This shows the efficiency of the docking study, indicating the open form of crystal structure of the Mtb ICL can be used as alternative to closed form to identify potential inhibitor molecules. Table 18 contains the comparison of the actual percentage inhibition and the docking scores of the each molecule screened against Mtb ICL enzyme with the activity scale. The molecules are arranged in the descending order of the Mtb ICL enzyme inhibitory activity. The molecules with activity less than 20% inhibition did not show correlation to the prediction so was omitted from the table.

There were 22 molecules in the azetidine series which presented the Mtb ICL inhibitory activity more than 65%. During docking studies **3YS10, 1YS4** and **1YS16** were interpreted as ++

instead of +++. Except these three molecules from the high active molecules (+++), all others were correctly predicted during docking simulation. There were 88 molecules which exhibited moderate range (++) of the Mtb ICL enzyme activity from azetidine series. Out of 88 molecules in 78 molecules were predicted correctly by the docking study. Out of 10 wrongly predicted molecules 7 were predicted as high active molecules (+++). Those molecules are **10YS9**, **1YS9**, **6YS9**, **1YS14**, **4YS20**, **8YS18** and **6YS11**. It could be noted that the mostly the caboxycyclo-hexylamine substituted analogues were wrongly predicted. The 3 molecules were predicted low active molecules (+). The **3YS20**, **2YS6** and **9YS6** were predicted as false negative. The 2 molecules **7YS19** and **7YS11** did not get dock into the active site of open form of Mtb ICL but exhibited a moderate enzyme inhibitory activity of 35% and 36% respectively. There were 55 molecules which exhibited low range (+) of the Mtb ICL enzyme inhibitory activity from azetidine series. Out of these 6 molecules, **3YS7**, **5YS8**, **4YS5**, **8YS9**, **2YS21** and **8YS12** were predicted as high active molecules (+++) during docking simulation. The 6 molecules were predicted moderate active molecules (++). They are **2YS19**, **5YS1**, **3YS9**, **4YS19**, **3YS16** and **6YS1** predicted as false positive. The **7YS20**, **5YS3**, **7YS13** and **7YS1** did not get dock into the active site of open form of Mtb ICL but exhibited a low (+) enzyme inhibitory activity.

From pyridopyridine series 8 molecules belonged to the highly active molecules (+++) which exhibited more than 65% of the Mtb ICL inhibitory activity. No molecule was wrongly predicted from these highly active molecules in the docking simulation. There were 11 molecules which exhibited moderate range (++) of the Mtb ICL enzyme activity from pyridopyridine series. Out of 11 molecules, 8 molecules were predicted correctly by the docking simulations. Out of 3 wrongly predicted molecules one molecule, **11YS14** was predicted as high active molecule (+++) during simulation. The 2 molecules were predicted low active molecules (+).

The **11YS12** and **12YS7** were predicted as false negative by dock studies carried using the open form of Mtb ICL, but exhibited a moderate enzyme inhibitory activity of 62.2% and 53.1% respectively. There were 2 molecules which exhibited low range (+) of the Mtb ICL enzyme inhibitory activity from pyridopyridine series. Out of these one molecule, **12YS2** was predicted as moderate active molecules (++) during docking simulation.

In case of benzo-thiazolo-pyrimido-pyrimidine-one analogues, 5 molecules belonged to the highly active molecules (+++), which exhibited more than 65% of the Mtb ICL inhibitory activity. No molecule was wrongly predicted from these highly active molecules in the docking simulation. There were 9 molecules which exhibited moderate range (++) of the Mtb ICL enzyme activity from benzo-thiazolo-pyrimido-pyrimidine-one series. Out of 9 molecules, 6 molecules were predicted correctly by the docking simulations. All the 3 were wrongly predicted to be high active molecule (+++) during simulation. They were **15YS3**, **17YS2** and **18YS6**. There were 21 molecules which exhibited low range (+) of the Mtb ICL enzyme inhibitory activity from benzo-thiazolo-pyrimido-pyrimidine-one series. Out of these 4 molecules, **17YS7**, **16YS2**, **18YS9** and **16YS15** were predicted as high active molecules (+++) during docking simulation. 11 molecules, **17YS7**, **15YS10**, **16YS7**, **14YS12**, **14YS11**, **18YS7**, **16YS6**, **14YS5**, **13YS12**, **15YS1** and **15YS6** were predicted to be false positive with moderate activity (++).

Many molecules from thiazolo-pyrimidine-one series were predicted false positive. The selected low concentration may be a reason for the lack of the visible correlation to the biochemical activity and the computational predictions. The azetidine analogues and the pyridopyrimidines analogues presented very good correlation to the computational docking prediction with actual biochemical activity carried out in the form of percentage inhibition of

Mtb ICL. The azetidine analogues and the pyridopyrimidines analogues were assessed for the Mtb ICL inhibition activity at 9 μg/mL concentration. Since many molecules exhibited good percentage of enzyme inhibition from the azetidine analogues and the pyridopyrimidines analogues, the benzo-thiazolo-pyrimido-pyrimidine-one series was checked for its activity at a lower dose of 3 μg/mL. The decreased dose might be reason for the observed lower activity of the compounds from the benzo-thiazolo-pyrimido-pyrimidine-one series compared to the other two series.

Figure 52 shows one of high active molecule **3YS18**, form azetidine series. It produced, 99.4% of Mtb ICL enzyme inhibition. The molecule presented very good combination of polar and non-polar (hydrophobic) interactions with the enzyme residues. There were two H-bonds, one was found with carboxy group of carboxy-4-benzylpiperazine group with side chain of Ser317 (C=O, 44...HO, S317; 2.035 Å) , and the other H-bond was found between N atom of the indole ring of the Trp93 and the nitrogen atom of the carboxy-4-benzylpiperazine (N, 8...N, T93; 3.0 Å). Strong hydrophobic interactions were observed between the benzene and piperazine moieties of one of carboxy-4-benzylpiperazine with side chain of Pro107, Trp93. The other carboxy-4-benzylpiperazine substituted part of the azetidine in 3YS18 formed hydrophobic interactions with amino acid residues Leu348, Pro316 and Trp93.

The **8YS11** is another high active molecule from azetidine series. It had carboxydibutyl-amine side chains, and n-hexane chain attachment on N of azetidine moiety. It produced, 99.28% of Mtb ICL enzyme inhibition. The molecule presented very good combination of polar and non-polar (hydrophobic) interactions with the enzyme residues (Figure 53). There were four H-bonds, a bifurcated H-bond was observed between carboxy group of one of the carboxydibutylamine group with side chain of Arg228 (C=O, 54...HN, R228; 2.3 Å and C=O, 54...HN, R228; 1.7 Å), and the other bifurcated H-bond was found between other carboxydibutylamine with side chain OH of Thr347 (C=O, 32...HO, T347; 2.13 Å) and side chain amine group of Asn313 (C=O, 32...HN, N313; 2.6 Å). Other than this a C=O...CH induced bipolar interaction was observed between backbone carboxy group of Thr286 and C8 atom of the butyl group of one of the carboxydibutylamine. Hydrophobic interactions were observed between the butyl chains of one of carboxydibutylamine with side chain of Pro107, Trp93 and Ala186. The other carboxy-4-benzylpiperazine substituted part of the azetidine in **3YS18** formed hydrophobic interactions with amino acid residues Leu348, Pro316 and Trp283. The azetidine moiety also showed hydrophobic interaction with Trp93.

The **11YS9** is a high active molecule from the pyridopyrimidine group. It had 2,4,5-trifluroaniline substitution at 4-position of pyidopyrimidine moiety and 2,6-diethylaninile substitution at 2-position of pyridopyrimidine. It produced 98.4% of Mtb ICL enzyme inhibition. Strong combinations of the polar and hydrophobic interactions were seen between the **11YS9** and the Mtb ICL. Figure 54 illustrates the interaction pattern of **11YS9** with Mtb ICL enzyme residues. The ligand produced six H-bonds with enzyme. A bifurcated H-bond was observed between the 2-fluro atom and indole nitrogen of Trp93 and backbone nitrogen of Asp108 (2F, 32...HN, T93; 2.3 Å, and 2F, 32...N, D108; 2.4 Å,). The 5-fluro atom formed H-bond with side chain amine group of Lys189 (5F, 44...NH3, K189; 2.3 Å). The nitrogen atom of 2,6-diethylaninile moiety formed strong electrostatic interaction with side chain carboxy group of Glu285 (N, 11...C=O, E285; 1.9 Å). The N1 atom of the pyridopyrimidine moiety formed H-bond with side amine group of Arg228 (N1, 10...NH, R228; 2.3 Å). The N8 atom of the pyridopyrimidine moiety formed H-bond with side amine group of Gln184 (N8, 2...NH, Q184;

2.0 Å). Hydrophobic interactions were seen between the phenyl moiety of diethylaniline group and amino acid residues Trp93, Leu348 and Pro316. The 2-ehtyl moiety from diethylaniline formed hydrophobic interactions with amino acid residue Trp93. The phenyl moiety of 2,4,5-trifluroaniline group formed hydrophobic interactions with amino acid residue Pro107.

The **12YS14** is a high active molecule from the pyridopyrimidine group. It had benzothiazle substitution at 4-position of pyridopyrimidine moiety and 4-pyridylamine substitution at 2-position of pyridopyrimidine. It produced 79.24% of Mtb ICL enzyme inhibition. A good combination of the polar and hydrophobic interactions was seen between the **12YS14** and the Mtb ICL. Figure 55 illustrates the interaction pattern of **12YS14** with Mtb ICL enzyme residues. The ligand produced four H-bonds with enzyme. A H-bond was observed between the N atom of the pyridyl moiety and side chain OH group of Thr347 (N, 15...HO, T347; 1.8 Å). The amine group nitrogen atom of 4-pyridylamine moiety formed strong electrostatic interaction with side chain carboxy group of Glu285 (N, 11...C=O, E285; 1.8 Å). The N1 atom of the pyridopyrimidine moiety formed H-bond with side amine group of Arg228 (N1, 10...NH, R228; 1.9 Å). The N8 atom of the pyridopyrimidine moiety formed H-bond with side amine group of Gln184 (N8, 2...NH, Q184; 3.3 Å). Hydrophobic interactions were seen between the pyridyl moiety of 4-pyridylamine group and amino acid residues Trp93, Leu348 and Pro316. The pyridyl moiety from pyridopyrimidine formed hydrophobic interactions with amino acid residue Ala186. The thiazole group formed hydrophobic interactions with amino acid residue Ala233.

The **15YS14** is a high active molecule from the nitrobenzo-thiazolo-pyrimido-pyrimidine-one group. It had 2-(trifluoromethyl)-benzaldehyde substitution. It produced 74.74%

of Mtb ICL enzyme inhibition. A very good combination of the polar and hydrophobic interactions was seen between the **15YS14** and the Mtb ICL. Figure 56 illustrates the interaction pattern of **15YS14** with Mtb ICL enzyme residues. The ligand produced five H-bonds with enzyme. A bifurcating H-bond was observed between the carboxy moiety of atom of the 2-(trifluoromethyl)-benzaldehyde group and side chain NH group of Arg228 (C=O, 36...NH, R228; 1.9 Å and C=O, 36...NH, R228; 2.2 Å). The N1 atom of thiazalopyrimidine-7-one formed H-bond with N atom of and indole nitrogen of Trp93 (N1, 13...HN, T93; 2. Å). The nitro group atom formed H-bond with side chain amine group of Lys189 (NO2, 42...NH3, K189; 2.3 Å). The carbonyl group of the pyrididopyrimidine moiety formed H-bond with side amine group of Gln184 (N8, 2...NH, Q184; 2.0 Å). Hydrophobic interactions were seen between the phenyl moiety of 2-(trifluoromethyl)-benzaldehyde group and amino acid residues Leu348 and Pro316. The pyridinopyrimidine moiety formed hydrophobic interactions with amino acid residue Trp93. The phenyl group of nitrobenzo group formed hydrophobic interactions with amino acid residue Pro107.

The **17YS12** is a high active molecule belonged to the nitrobenzo-thiazolo-pyrimido-pyrimidine-one group. It had *p*-tolylaldehyde substitution. It produced 67.14% of Mtb ICL enzyme inhibition. A combination of the polar and hydrophobic interactions was observed between the **17YS12** and the Mtb ICL. Figure 60 illustrates the interaction pattern of **17YS12** with Mtb ICL enzyme residues. The ligand produced five H-bonds with enzyme. Two H-bonds were seen between nitro group of nitrothiazolo-pyrimidine-7-one moiety, one with backbone nitrogen of Asp108 (NO2, 37...HN, D93; 2. 8 Å) and other one with side chain amine group of Lys189 (NO2, 36...HN, K189; 2.8 Å). A H-bond was observed between the carbonyl moiety of the pyridinopyrimidine group and side chain NH group of Arg228 (C=O, 31...NH, R228; 2.2 Å).

Another H-bond was observed between N atom of the pyridinopyrimidine moiety and N of indole side chain of Trp93 (N, 5…NH, T93; 2.1 Å). One more H-bond was observed between N atom of the pyridinopyrimidine moiety and side chain carbonyl group of Gln285 (N,11…C=O, E285; 1.70 Å). Hydrophobic interactions were seen between the phenyl moiety of *p*-tolylaldedhyde group and residues Tyr89, Trp93, Trp283, Leu348 and Pro316. The pyridinopyrimidine moiety formed hydrophobic interactions with amino acid residue Trp93.

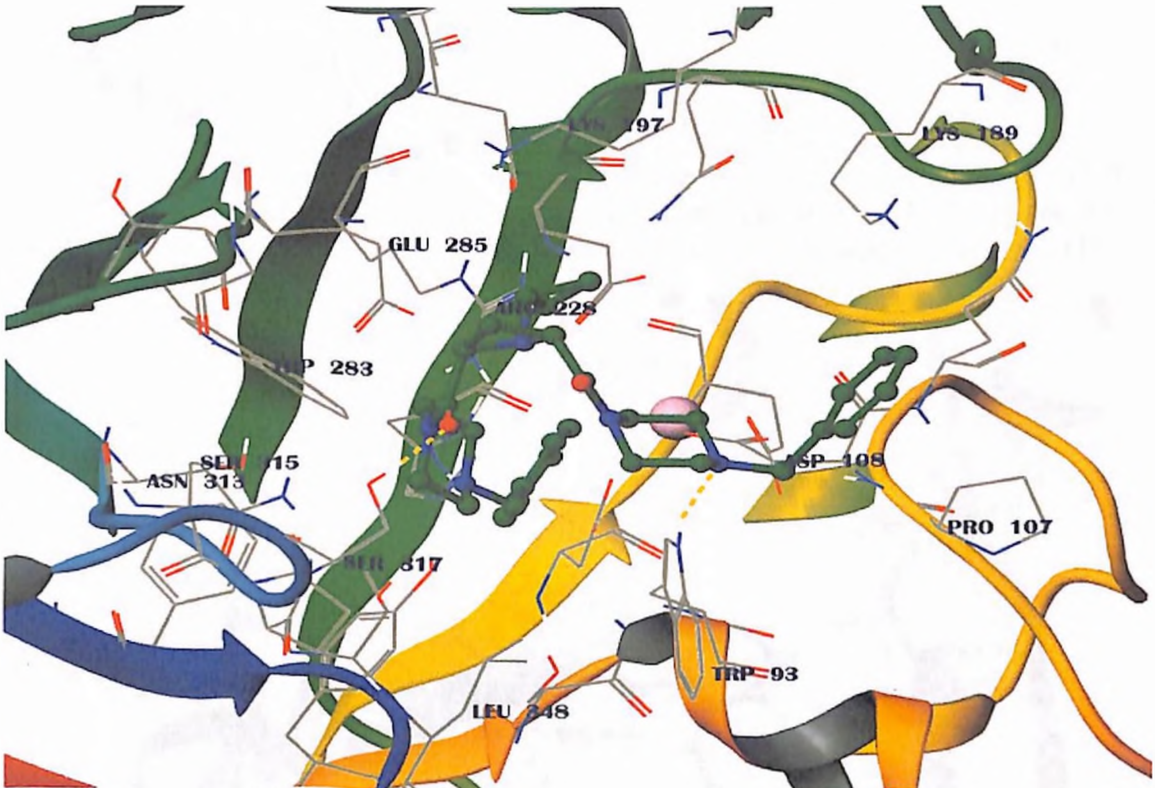

Figure 52: Contact residues of one of the highest active molecule from azetidine series **3YS18** docked in to Mtb ICL. The molecule in green color is the ligand. Two H-bonds are shown as yellow dotted lines.

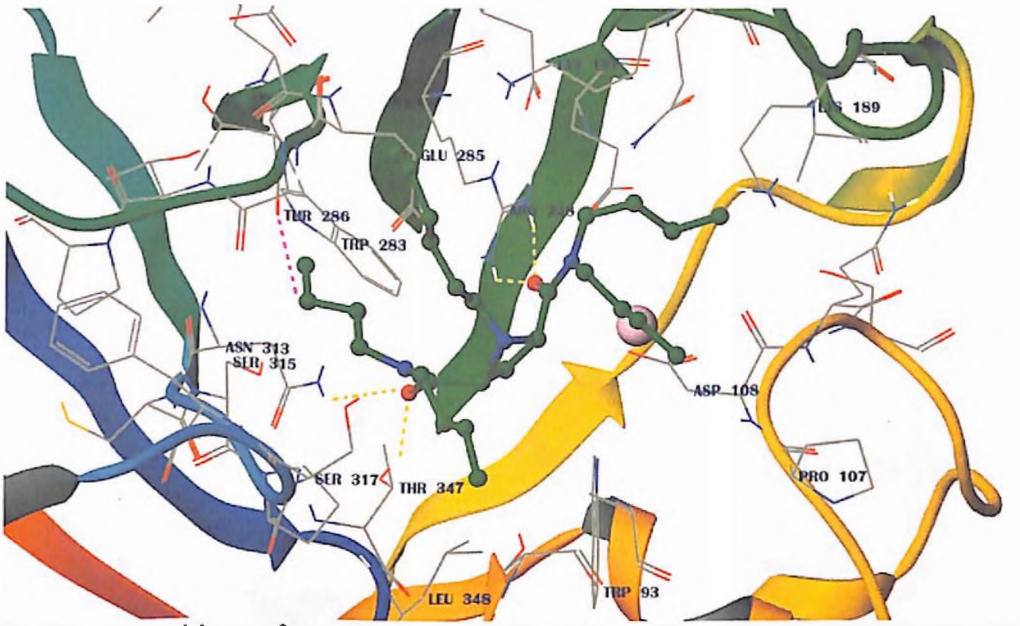

Figure 53: Contact residues of one of the highest active molecule from azetidine series **8YS11** docked in to Mtb ICL. The molecule in green color is the ligand. Four H-bonds are shown as yellow dotted lines. The induced bipolar interaction (C=O…HC) showed in pink dotted lines.

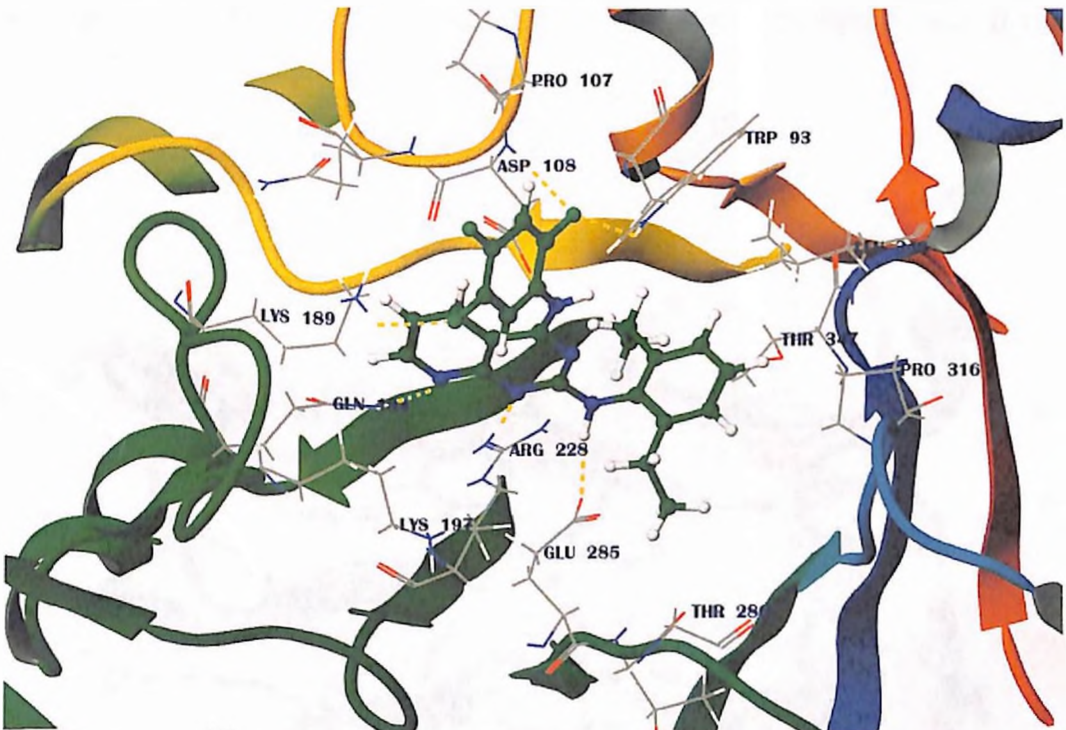

Figure 54: Contact residues of one of the highest active molecule from pyridopyrimidine series **11YS9** docked in to Mtb ICL. The molecule in green color is the ligand. Six H-bonds are shown as yellow dotted lines.

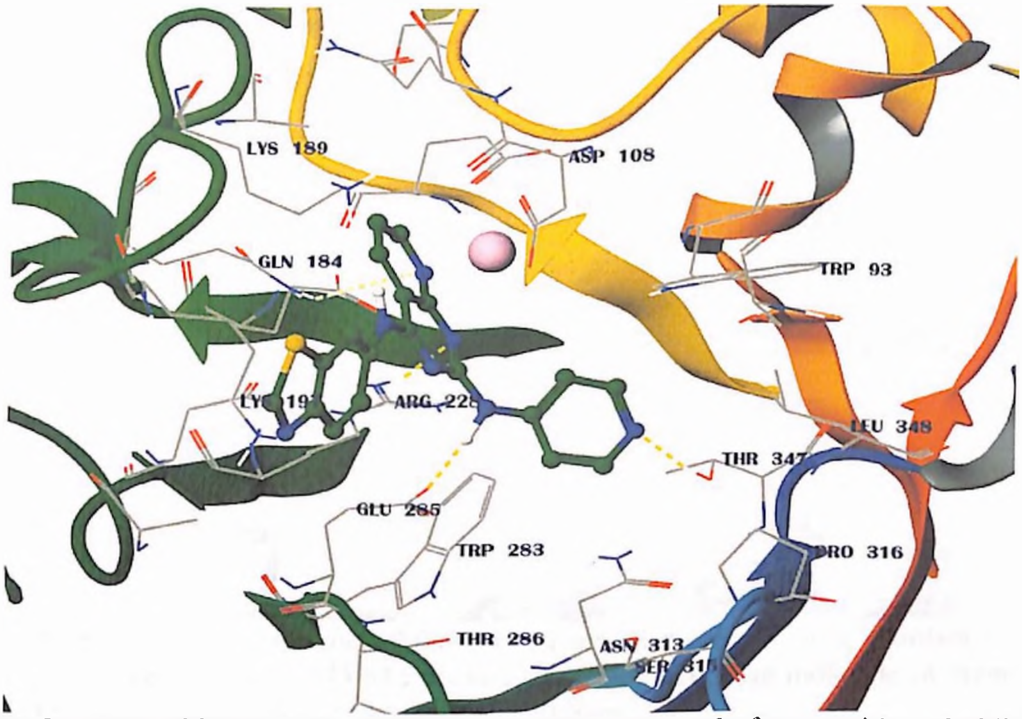

Figure 55: Contact residues of one of the highest active molecule from pyridopyrimidine series **12YS14** docked in to Mtb ICL. The molecule in green color is the ligand. Four H-bonds are shown as yellow dotted lines.

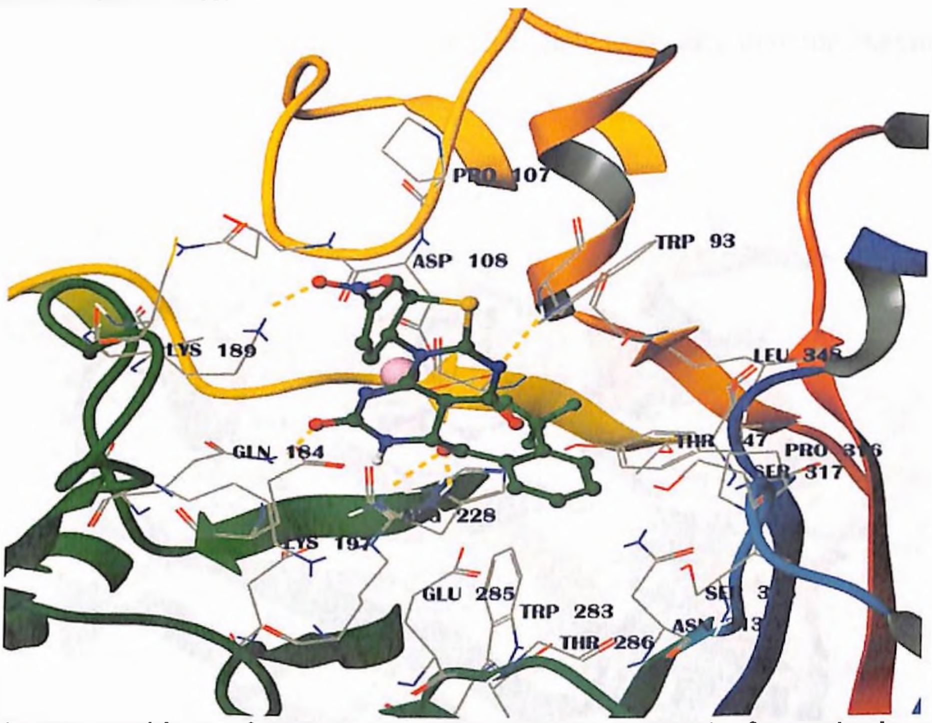

Figure 56: Contact residues of one of the highest active molecule from nitrobenzo-thiazolo-pyrimido-pyrimidine-one series **15YS14** docked in to Mtb ICL. The molecule in green color is the ligand. Six H-bonds are shown as yellow dotted lines.

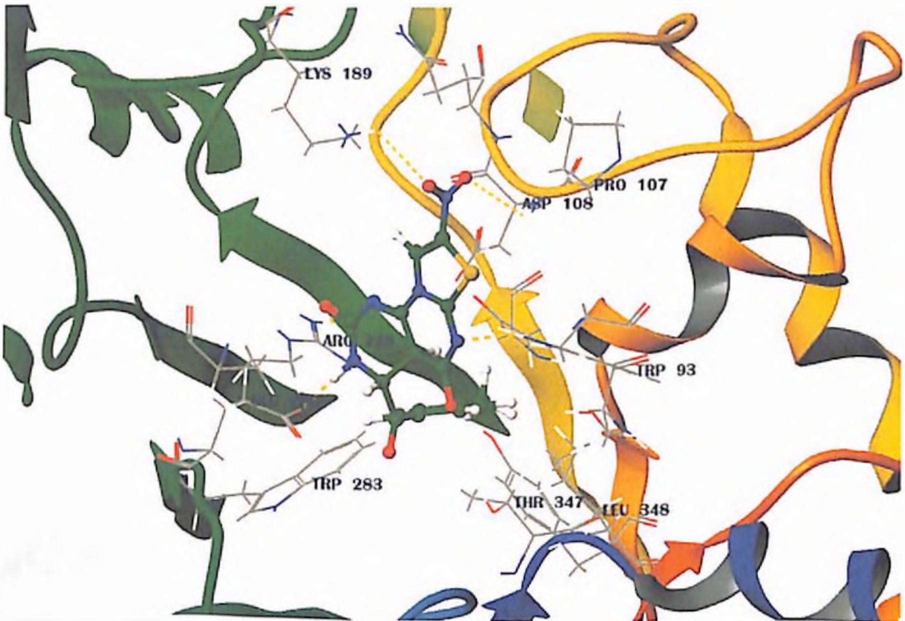

Figure 57: Contact residues of one of the highest active molecule from nitrobenzo-thiazolo-pyrimido-pyrimidine-one series **17YS12** docked in to Mtb ICL. The molecule in green color is the ligand. Five H-bonds are shown as yellow dotted lines.

Below are the pictures (Figure 58 to 62) of some inactive molecules of Mtb ICL. These inactive molecules did lack some of interactions which were essential for enzyme inhibitory activity.

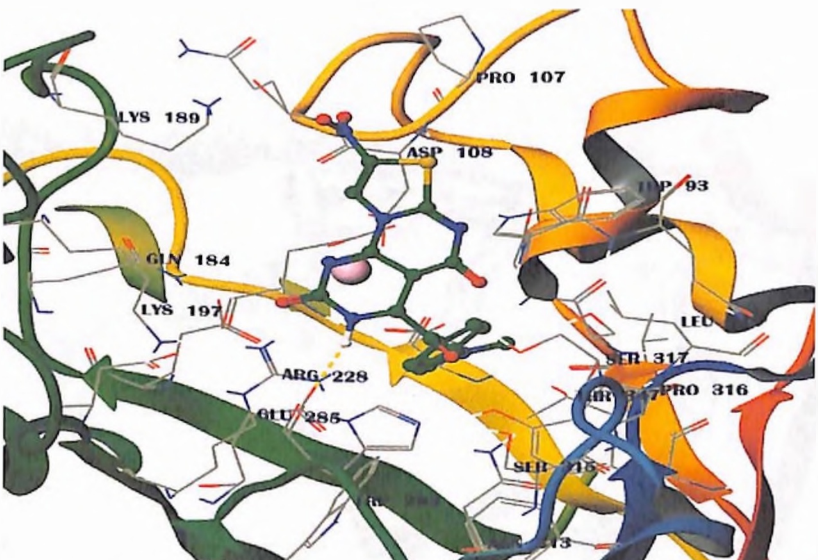

Figure 58: Contact residues of one of the low active molecule from nitrobenzo-thiazolo-pyrimido-pyrimidine-one series **17YS10** docked in to Mtb ICL. The molecule in green color is the ligand. H-bonds are shown as yellow dotted lines.

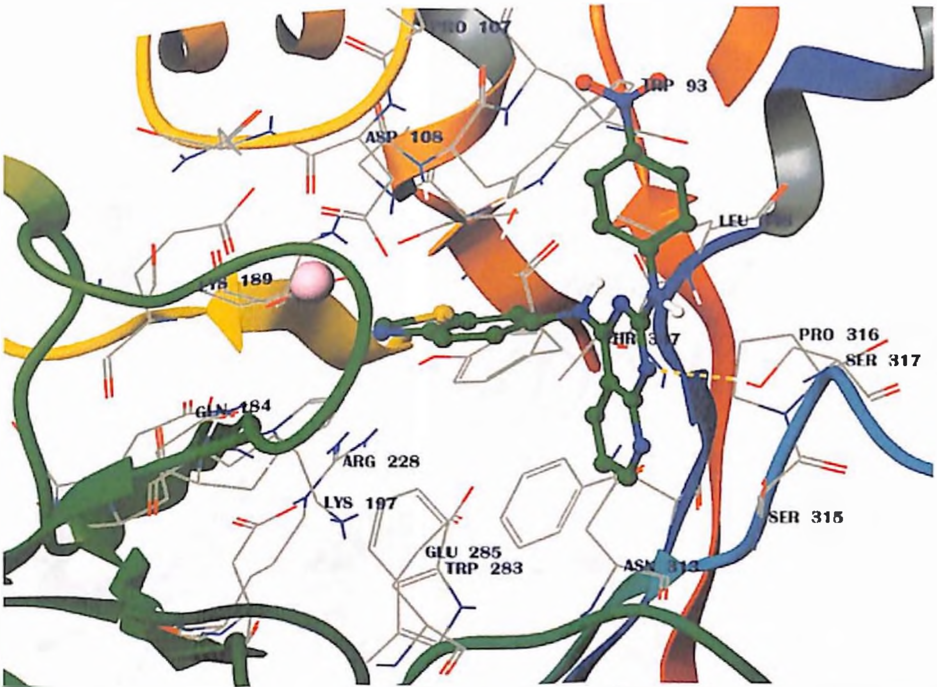

Figure 59: Contact residues of one of the low active molecule from pyridopyrimidine series **12YS3** docked in to Mtb ICL. The molecule in green color is the ligand. H-bonds are shown as yellow dotted lines.

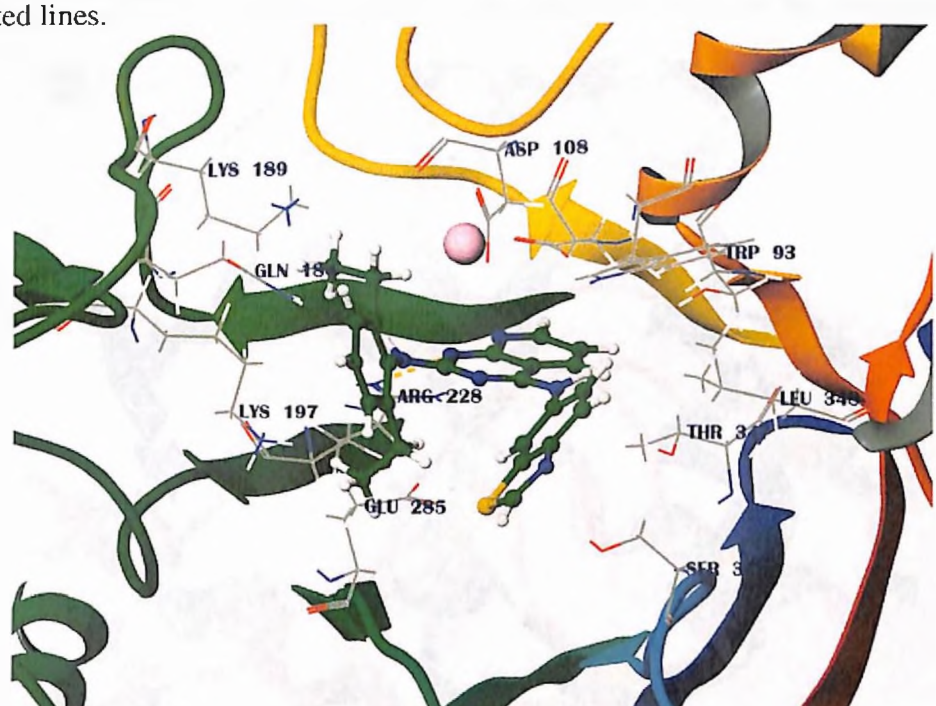

Figure 60: Contact residues of one of the low active molecule from pyriopyrimidine series **12YS13** docked in to Mtb ICL. The molecule in green color is the ligand. H-bonds are shown as yellow dotted lines.

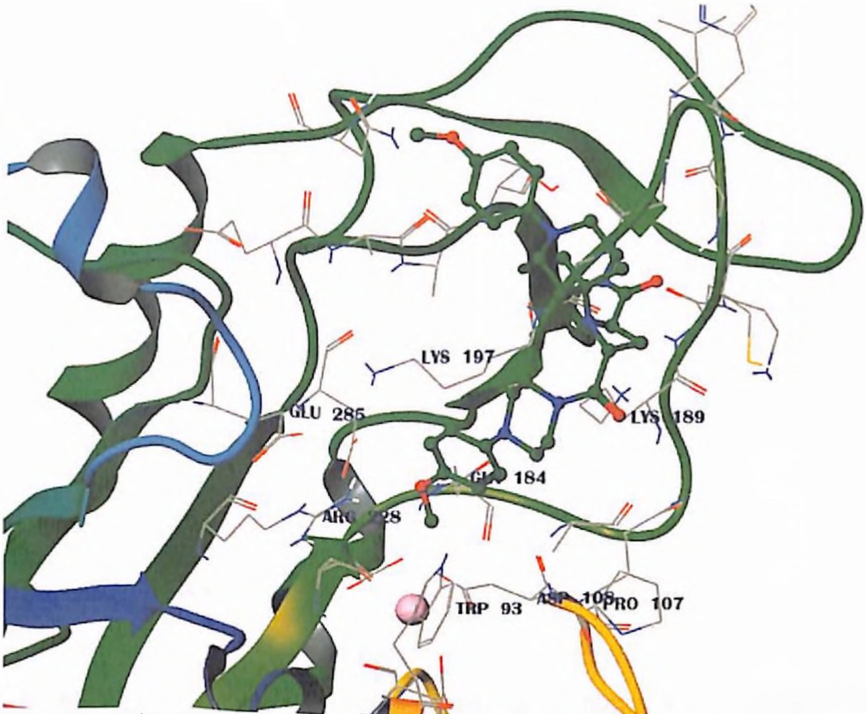

Figure 61: Contact residues of one of the low active molecule from azetidine series **5YS20** docked in to Mtb ICL. The molecule in green color is the ligand. H-bonds are shown as yellow dotted lines. It could be seen that the ligand has binding totally outside the active site, along the flexible loop.

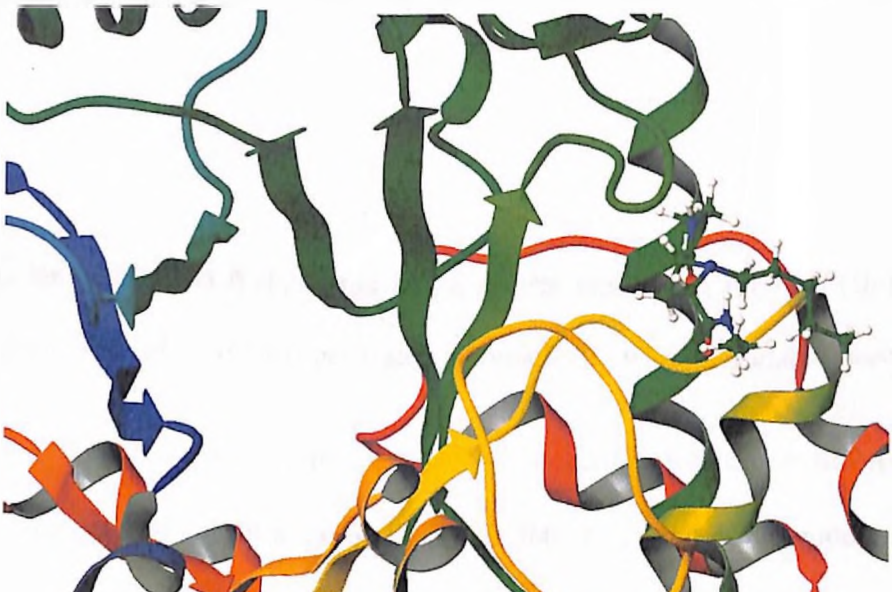

Figure 62: Contact residues of one of the low active molecule from azetidine series **6YS1** docked in to Mtb ICL. The molecule in green color is the ligand. H-bonds are shown as yellow dotted lines. It could be seen that the ligand has binding totally outside the active site.

Chapter VII

Summary and Conclusions

With the intention of the developing new anti-tubercular molecules, three new enzyme targets of Mtb were explored to identify new hits with the potential to inhibit Mtb. The targets explored were GluR, PknB, ICL. Because of their inherited features different approaches were implemented to identify hits which can inhibit these Mtb enzymes.

Glutamate Racemase (GluR)

- The GluR crystal structure is till now not resolved, to construct a structural model for Mtb GluR, using BLAST search by amino acid alignment, most suitable homologues template GluR of *E. faecalis* (PDB id 2vvt) was selected.

- Based on the ClustalW alignment with manual inspection for the alignment, the model for Mtb GluR was constructed using MOELLER program.

- There was another model that existed in Swiss-prot repository, for Mtb GluR, which was built based on GluR of *B. subtilis* generated automatically without human interventions.

- To compare both the model with respect to the better structure a molecular dynamic simulation was carried for duration of 1.2 ns, at 300° K, for both the models and structures evolved during the simulation were collected as trajectory and compared.

- The trajectory structures of both the models were evaluated by different parameters, to compare the stability of the models and to find out comparatively better structure. The backbone rms deviation, rms deviation of the ligand, ligand binding pattern and distance parameters between important amino acid residues in the GluR structure models were monitored during the molecular dynamics simulation.

- The model collected from Swiss-prot repository exhibited large deviation in the distance parameters measured between amino acid residues and ligand, especially the loop region amino acids comprised of Ser10, Trp44 and Gly45. The H-bond which is very essential to hold the ligand firmly during the catalytic activity got broken during the simulation for Swiss-prot model, resulted into the flipping of the glutamate with in the active site during simulation, which is totally unacceptable according to the two base mechanisms reported earlier for GluR.

- The basic difference between the models was amino acid rotamer (conformation of amino acid). During MD simulation the rotameric conformations were stable, and presented very low rms deviation for model developed by us, whereas Swiss-prot model during the simulation changed the original conformation. This was to attain a lower energy conformation by utilizing the energy provided during MD simulation. The Swiss model during MD evolution tried to attain similar rotameric conformation which was present in GluR model developed by us. These rotameric changes brought during the MD simulation, in Swiss-prot model resulted into the distortion of the overall architecture of the model.

- The Mtb GluR model built by us presented a very steady structure with very low backbone deviation measured during the MD simulation, which is within 0.4 Å units, indicating good stability of model over Swiss-prot model.

- The validated new structural model of Mtb GluR was used for identification of the hits with the potential to inhibit the enzyme. For this structure based drug design was implemented. Our own proprietary database molecules were docked to the active site of Mtb GluR, and molecules with the better binding tendency were identified.

- To identify potential inhibitor molecules different docking programs, Gold, Glide SP, and Glide XP were utilized with different parameters. The molecules with best binding pattern with good score were listed out.

- Finally 15 molecules were shortlisted, which are **10YS21, 10YS6, 10YS8, 1YS8, 4YS7, 6YS8, 8YS12, 3YS21, 2YS12, 3YS12, 4YS8, 5YS7, 10YS7, 11YS21, 4YS12.** These molecules either came as top hits in all the three docking programs, or were highest scoring molecule from any one of the docking program.

Protein kinase B (PknB)

- PknB is a signal translator enzyme, essential for growth of the Mtb. To identify hits with potential to inhibit PknB enzyme, first the reported crystal structure from PDB were collected. There were crystals reported with endogenous ligand, as well as bound with inhibitors.

- A combination approach involving both pharmacophoric approach and Structure based design approach were utilized for the identification of the potential inhibitor of PknB.

- Using already reported inhibitors analogue based pharmacophore was constructed. Based on the interaction energetics of the highest active inhibitor with Mtb PknB enzyme, energy based pharmacophore was constructed.

- The pharmacophore developed were validated before its use. Both pharmacophores had 4 features in each of them, and both pharmacophores had a site representing hinge region interaction, an important interaction needed for better binding of ligand to the enzyme. The ligand based pharmacophore reproduced the crystal binding pose for Mtz with very low rms deviation of 0.97 Å.

- The pharmacophores developed were utilized for identification of potential inhibitors of Mtb PknB by carrying out the virtual screening of database molecules. The web based commercial database Asinex was utilized for the virtual screening.

- Based on the fitness score the molecules were shortlisted. The shortlisted molecules were subjected to the Glide SP docking. The molecules with less than -6.5 glide score were only considered, filtered molecules were then manually inspected for binding pattern and also the docking alignment was compared with the pharmacophore alignment. Only molecules with similar alignment pattern were selected.

- The shortlisted molecules were clustered. To collect most diverse set of molecules from the hits, best molecules from each cluster were selected. Molecular hits from ligand based pharmacophores formed 19 clusters and molecular hits form energy based pharmacophore formed 32 clusters.

- These shortlisted molecules were subjected to the XP Glide docking, by taking the XP docking pose. The rms deviation for each molecule was measured between SP Glide pose and XP glide pose. Since SP dock produced a minimum energy docking pose most of the molecules had rms deviation of XP pose with in 2 Å of SP docking pose.

- Then the XP glide docking poses were visually inspected and best 58 molecules were shortlisted.

Isocitrate lyase (ICL)

- ICL provides the carbon source for the mycobacteria under starvation condition. Thus bacteria use the rich fatty acid as source of nutrition from its peptidoglycan cell layer.

- Three crystal structures reported for Mtb ICL, bound with competitive inhibitor niopropionic acid, another one covalently bound to bromopyruvic acid and the third one is apo-enzyme.

- The 'closed' form is the active form, and inhibitor bound closed form had very small active site, which made it not suitable for use in the virtual screening of database molecules. So as an alternate 'open' form of the ICL was utilized for virtual screening of the database.

- The known reported molecules were used first to validate the 'open' from. The highest active molecules docked to the 'closed' form and to 'open' form and binding pattern of both was compared. Both produced similar binding pattern.

- In-house proprietary database was subjected to virtual screening by using XP Glide docking. The hits were clustered into groups. The biochemical ICL inhibition was carried out not only just on the hits obtained from virtual screening but also on all the molecules available belonging to those series.

- A biochemical assay developed based on the measurement of the quantity of phenyl-hydrazine glyoxalate formed at 324 nm. About 300 molecules were assesses for its ability to inhibit Mtb ICL at either 9 µg/mL or at 3 µg/mL. The activity expressed as percentage inhibition.

- Different series belonging to series if benzo-thiazolo-pyrimido-pyrimidine-one, pyridopirimidine and azetidine were obtained as hits in virtual screening, were assesses for percentage ICL inhibitory activity. Total of about 300 molecules were subjected to biochemical activity assessment.

- There were 36 molecules which exhibited more than 65 % of Mtb ICL inhibition. A comparison with the predictions made with the docking study presented good reliability of the docking procedure, where out of 36 highest active molecules 33 molecules were predicted correctly, indicating the open of the ICL can be utilized for identifying the potential inhibitors with very less fear of false hits.

- Out of 200 screened azetidine analogues 14 molecules had inhibitory activity more than 80% at 9 µg/mL. Six molecules **3YS1, 3YS10, 3YS18, 5YS18, 8YS11** and **8YS17** exhibited more than 95% of Mtb ICL enzyme inhibition. Out of the different alkyl groups substituted on the nitrogen atom of azetidine, the molecules with N-isopropyl substitution showed good activity followed by propyl substitution and benzyl substitution.

- As the N-substituted alkyl chain length increased in azetidine series the activity reduced. Following N-isopropyl substitution, the number of N-propyl substituted compounds stood second, which showed activity more than 50% enzyme inhibition. The N-cyclohexyl substitution had good effect on the ICL inhibitory activity. But the N-benzyl substituted compounds presented higher inhibitory activity. Along the different series corboxybenzyle-piperazine substitution at 2- and 4- position of azetidine showed good enzyme inhibitory activity.

- Out of 30 molecules screened from pyridopyrimidine, 8 molecules had Mtb ICL inhibitory activity more than 65%. Five molecules, **11YS13**, **12YS15**, **11YS9**, **11YS2** and **11YS1** exhibited more than 85% of enzyme inhibition at concentration 9 μg/mL.

- The 2,4,5-triflurophenylanimine analogues were more active compare to the benzothiazole analogues. Electro negative moieties at the *para*-position of the phenylamine substitution had detrimental effect on the ICL activity. The 4-mothoxy substitution analogue **11YS2** had 94% of enzyme inhibition.

- Out of 90 compounds screened from benzo-thiazolo-pyrimido-pyrimidine-one 5 molecules exhibited inhibitory activity more than 65% at concentration 3 μg/mL. Three molecules, **17YS6**, **15YS14** and **14YS14** exhibited activity more than 70%.

- Benzo-thiazolo-pyrimido-pyrimidine-one series was screened at lower concentration 3 μg/mL less number of molecules exhibited good percentage of activity.

Chapter VIII

Future Perspectives

The present study involved the identification of the hits for Mtb enzymes GluR, PknB, and ICL, by utilizing different computational and simulation techniques.

For GluR a model has been developed and validated. Its stability was checked by running 1.2 ns MD simulation. Comparison of the model structure with the Mtb GluR crystal structure would be more interesting, more over it will give more confidence on homology model based drug discovery program. Biochemical assessment of the identified hits will give better understanding for further development of leads. The allosteric site exploration is also an attractive target site for the future development of Mtb GluR inhibitors.

For PknB hits were identified based on the combination approach of pharmacophore and the structure based approach. Biochemical assessment of the identified hits will give better understanding for the further development to form leads. Synthesis of the analogues of the active molecules will be usefull for the development of hit to lead. The crystal structure amino acid interaction assessment with newly developed inhibitor by X-ray crystallographic method would further help in lead development steps.

For ICL the inhibitor activity representation in the form of IC_{50} would enhance the understanding in terms of better lead design perspective. Since identified hits were with considerable good sizes (molecular weight ranging from 350-400 Daltons) the crystallization study will be beneficial in better understanding the flexible part of loop region of receptor. It will also useful in the future design of new hits or for the development of hits to lead against the Mtb ICL enzyme.

References

1. Daniel, T. M., The history of tuberculosis. *Respir. Med.* 2006, 100, 1862-1870.

2. Corbett, E. L., Watt, C. J., Walker, N., Maher, D., Williams, B. G, Raviglione, M. C., The growing burden of tuberculosis: global trends and interactions with the HIV epidemic. *Arch. Intern. Med.* 2003, 163, 1009-1021.

3. Badri, M., Wilson, D., Wood, R. Effect of highly active antiretroviral therapy on incidence of tuberculosis in South Africa: a cohort study. *Lancet* 2002, 359, 2059–2064.

4. Wood, R., Maartens, G., Lombard, C. J. Risk factors for developing tuberculosis in HIV-1-infected adults from communities with a low or very high incidence of tuberculosis. *J. Acquir. Immune.Defic.Syndr.* 2000, 23, 75–80.

5. Lawn, S. D., Bekker, L. G., Miller, R. F. Immune reconstitution disease associated with mycobacterial infections in HIV-infected individuals receiving antiretrovirals. *Lancet Infect. Dis.* 2005, 5, 361–373.

6. Gutierrez, M. C., Brisse, S., Brosch, R., Fabre, M., Omaïs, B., Marmiesse, M., Supply, P., Vincent, V. Ancient Origin and Gene Mosaicism of the Progenitor of *Mycobacterium tuberculosis*. *PLoS Pathogens* 2005, 1, e5.

7. http://en.wikipedia.org/wiki/History of tuberculosis.

8. Dye, C., Scheele, S., Dolin, P., Pathania, V., Raviglione, M. C. Global Burden of Tuberculosis, Estimated Incidence, Prevalence, and Mortality by Country *Journal of the American Medical Association* 1999, 282, 677–686.

9.Van, Soolingen, D., Hoogenboezem, T., Haas, P. E., Hermans, P. W., Koedam, M. A. A novel pathogenic taxon of the Mycobacterium tuberculosis complex, Canetti: Characterization of an exceptional isolate from Africa. *Int. J. Syst. Bacteriol* 1997, 47, 1236–1245.

10. World Health Organization (2009). "The Stop TB Strategy, case reports, treatment outcomes and estimates of TB burden". Global tuberculosis control: epidemiology, strategy, financing. pp. 187–300. ISBN 9789241563802.

11. http://wapedia.mobi/en/Tuberculosis_treatment

12. Schatz, A., Bugie, E., Waksman, S. A. Streptomycin, a substance exhibiting antibiotic activity against Gram-positive and Gram-negative bacteria. *Proc. Soc. Exp. Biol. Med.* 1944, 55, 66-69.

13. WHO Global Tuberculosis Program. Global tuberculosis control (WHO/GTB/97/225). Geneva. World Health Organization, 1997.

14. Spigelman, M., Gillespie, S. Tuberculosis drug development pipeline. Progress and hope. *Lancet* 2006, 367, 945-47.

15. O'Brien, R. J., Spigelman, M. KNew drugs for tuberculosis: current status and future prospects.*Clin. Chest Med.* 2005, 26, 327-340.

16. Canetti, G. The tubercle bacillus in the pulmonary lesion of man.Histobacteriology and its bearing on the herapy of pulmonary tuberculosis, Springer Publishing Company.New York, 1955.

17. Warner, D. F., Mizrahi, V. Tuberculosis Chemotherapy. the Influence of Bacillary Stress and Damage Response Pathways on Drug Efficacy *Clin. Microbiol. Rev.* 2006, 19, 558-570.

18.East African-British Medical Research Councils.Controlled clinical trial of four short-course (6-month) regimens of chemotherapy for treatment of pulmonary tuberculosis *Lancet*, 1974, 304, 237-240.

19. Ying, Z.Y., Wade, M. M. Scorpio, A., Zhang, H., Sun, Z. J. Mode of Action of Pyrazinamide. Disruption of *Mycobacterium tuberculosis* Membrane Transport and Energetics by Pyrazinoic Acid*J. Antimicrob. Chemother.* 2003, 52, 790-795.

20. A controlled trial of 6 months' chemotherapy in pulmonary tuberculosis. Final report.results during the 36 months after the end of chemotherapy and beyond. British Thoracic Society. *Brit. J. Diseases Chest*, 1984, 78, 330-336.

21. Instructions for applying to the Green Light Committee for access to second line anti-tuberculosis drugs, World Health Organization. 2006 http.//whqlibdoc.who.int/hq/2006/WHO_HTM_TB_2006.369_eng.pdf).

22. CDC. Notice to Readers. Revised Definition of Extensively Drug-Resistant Tuberculosis.MMWR, 2006, 55, 1176. http://www.cdc.gov/mmwr/preview/mmwrhtml/mm5543a4.htm

23.Corbett, E. L. Watt, C. J., Walker, N. The growing burden of tuberculosis.global trends and interactions with the HIV epidemic *Arch. Intern. Med.*, 2003, 163, 1009-1021.

24. Daley, C. L., Small, P. M., Schecter, G. F., Schoolnik, G. K., McAdam, R. A., Jacobs, W. R. Hopewell, P.C. An outbreak of tuberculosis with accelerated progression among persons infected with the human immunodeficiency virus. An analysis using restriction-fragment-length polymorphisms *N. Engl. J. Med.*, 1992, 326, 231-235.

25.De Cock, K. M., Soro, B., Coulibaly, I. M., Lucas, S. B. Tuberculosis and HIV infection in sub-Saharan Africa. *JAMA*, 1992, 268,1581-1587.

26. Markowitz, N., Hansen, N. I., Hopewell, P. C., Glassroth, J., Kvale, P. A., Mangura, B.T., Wilcosky, T. C., Wallace, J. M., Rosen, M. J., Reichman, L.B. Incidence of tuberculosis in the

United States among HIV-infected persons. The Pulmonary Complications of HIV Infection Study Group, *Ann. Intern. Med.*, 1997, 126, 123-132.

27. Protopopova, M., Hanrahan, C., Nikonenko, B., Samala, R., Chen, P., Gearhart, J. Einck, L, Nacy, C.A. Identification of a new antitubercular drug candidate, SQ109, from a combinatorial library of 1,2-ethylenediamines. *J. Antimicrob. Chemother.*, 2005, 56, 968-974.

28. Chen, P, Gearhart, J., Protopopova, M., Einck, L, Nacy, C.A. Synergistic interactions of SQ109, a new ethylene diamine, with front-line antitubercular drugs in vitro *J. Antimicrob. Chemother.*, 2006, 58, 332-337.

29. Nikonenko, B.V., Protopopova, M., Samala, R., Einck, L., Nacy, C. A. Drug therapy of experimental tuberculosis (TB). improved outcome by combining SQ109, a new diamine antibiotic, with existing TB drugs. *Antimicrob.Agents Chemother.* 2007, 51, 1563-1565.

30. Christine F., Sizemore, Ph.D., Barbara E. Laughon, Ph.D., and Anthony S. Fauci, M.D. Successful Public-Private Partnership Between NIAID and Sequella Yields Promising New TB Drug for Clinical Testing, http.//www.nih.gov/news/pr/sep2006/niaid-12.htm

31. Bøsling, J., Poulsen, S. M., Vester, B., Long, K. S. Resistance to the Peptidyl Transferase Inhibitor Tiamulin Caused by Mutation of Ribosomal Protein L3. *Antimicrob.Agents Chemother.* 2003, 47, 2892-2896.

32. Wayne, L. G., Sramek, H. A. Metronidazole is bactericidal to dormant cells of *Mycobacterium tuberculosis. Antimicrob.Agents Chemother.* 1994, 38, 2054-2058.

33. Tyagi, S., Nuermberger, E., Yoshimatsu, T., Williams, K., Rosenthal, I., Lounis, N., Bishai, W., Grosset, J. Bactericidal activity of the nitroimidazopyran PA-824 in a murine model of tuberculosis. *Antimicrob. Agents Chemother.*, 2005, 49, 2289-2293.

34. Lenaerts, A. J., Gruppo, V., Marietta, K. S., Johnson, C. M., Driscoll, D. K., Tompkins, N. M., Rose, J. D., Reynolds, R. C., Orme, I. M. Preclinical testing of the nitroimidazopyran PA-824 for activity against *Mycobacterium tuberculosis* in a series of in vitro and in vivo models. *Antimicrob. Agents Chemother.*, 2005, 49, 2294.

35. Stover C. K., Warrener, P., VanDevanter, D. R., Sherman, D. R., Arain, T. M., Langhorne, M. H., Anderson, S. W., Towell, J. A., Yuan, Y., McMurray, D. N., Kreiswirth, B. N., Barry, C. E., Baker, W. R. A small-molecule nitroimidazopyran drug candidate for the treatment of tuberculosis.*Nature*, 2000, 405, 962-966.

36. Manjunatha, U. H., Boshoff, H., Dowd, C. S., Zhang, L., Albert, T. J., Norton, J. E., Daniels, L., Dick, T., Pang, S., Barry, C. E. Identification of a nitroimidazo-oxazine-specific protein involved in PA-824 resistance in *Mycobacterium tuberculosis. Proc. Natl. Acad. Sci. USA*, 2006, 103, 431-436.

37. Nuermberger, E., Rosenthal, I., Tyagi, S, Williams, K. N., Almeida, D., Peloquin, C. A., Bishai, W. R., Grosset, J. *Antimicrob. Agents Chemother.*Combination Chemotherapy with the

Nitroimidazopyran PA-824 and First-Line Drugs in a Murine Model of Tuberculosis, 2006, 50, 2621-2625.

38. Barbachyn, M. R., D. K. Hutchinson, S. J. Brickner, M. H. Cynamon, J. O. Kilburn, S. P. Klemens, S. E. Glickman, K. C. Grega, S. K. Hendges, D. S. Toops, C. W. Ford, and G. E. Zurenko. 1996. Identification of a novel oxazolidinone (U-100480) with potent antimycobacterial activity. *J. Med. Chem.* 1996, 39,680–685.

39. Williams, K. N., Stover, C. K., Zhu, T., Tasneen, R., Tyagi, S., Grosset, J. H., Nuermberger, E. Promising Antituberculosis Activity of the Oxazolidinone PNU-100480 Relative to That of Linezolid in a Murine Model. *Antimicrob. Agents Chemother*, 2009, 53, 1314–1319.

40. Williams, K. N., Steven J. B., Charles, K. S., Tong Zhu, Adam O., Rokeya T., Sandeep T., Jacques H. G., Eric L. N. Addition of PNU-100480 to First-Line Drugs Shortens the Time Needed to Cure Murine Tuberculosis. *Am. J. Respir. Crit. Care Med.* 2009, 180, 371–376.

41. Matsumoto,M. OPC-67683, a nitro-dihydro-imidazooxazole derivative with promising action against tuberculosis in vitro and in mice. *PLoS Med.* 2006, 3, 2131–2144.

42. http.//www.clinicaltrials.gov/ct/gui/show/NCT00401271,jsessionid=BA98700 1885DF9EF2 4458721E400B6B4?order=38

43. http.//www.kaisernetwork.org/health_cast/uploaded_files/110306_wlh_drugd evelopment_ transcript.pdf

44. Andries, K., Verhasselt, P., Guillemont, J., Gohlmann, H. W., Neefs, J. M., Winkler, H., Van Gestel, J., Timmerman, P., Zhu, M., Lee, EWilliams, P., de Chaffoy, D., Huitric, E., Hoffner, S., Cambau, E., Truffot-Pernot, C., Lounis, N., Jarlier, V. A diarylquinoline drug active on the ATP synthase of *Mycobacterium tuberculosisScience* 2005, 307, 223- 227.

45. Lounis, N., Veziris, N., Chauffour, A., Truffot-Pernot, C., Andries, K., Jarlier, V. Antimicrob. Combinations of R207910 with Drugs Used To Treat Multidrug-Resistant Tuberculosis Have the Potential To Shorten Treatment Duration. *Agents Chemother.*, 2006, 50, 3543-3547.

46. Lenaerts, A. J., Hoff, D., Aly, S., Ehlers, S., Andries, K., Cantarero, L., Orme, I. M., Basaraba, R. J. Location of persisting mycobacteria in a guinea pig model of tuberculosis revealed by R207910. *Antimicrob. Agents Chemother*, 2007, 51, 3338–3345.

47. Ma, Z., Ginsburg, A. M., Spigelman, M. Antibacterial. antimycobacterial agents. In. Taylor J B, Triggle D, eds. Comprehensive Medicinal Chemistry II. Elsevier. Oxford, 2007

48. Rosenthal, I. M., Zhang, M., Williams, K. N, Daily dosing of rifapentine cures tuberculosis in three months or less in the murine model. *PLoS Med.* 2007, 4, e344.

49. Keung, A. C., Owens, R. C. Jr., Eller, M. G., Weir, S. J., Nicolau, D. P., Nightingale, C, H. Pharmacokinetics of rifapentine in subjects seropositive for the human immunodeficiency virus. a phase I study. *Antimicrob.Agents Chemother.* 1999, 43, 1230–1233.

50. Li, A. P., Reith, M. K., Rasmussen, A, Gorski, J. C., Hall, S. D., Xu, L., Kaminski, D. L., Cheng, L.K. Primary human hepatocytes as a tool for the evaluation of structure-activity relationship in cytochrome P450 induction potential of xenobiotics. evaluation of rifampin, rifapentine and rifabutin. *Chem Biol Interact* 1997, 107, 17–30.

51. Tsukamura, M., Nakamura, E., Yoshii, S., Amano, H. Therapeutic effect of a new antibacterial substance ofloxacin (DL8280) on pulmonary tuberculosis. *Am. Rev. Respir. Dis.*, 1985, 131, 352-356.

52. Grosset, J. H. Treatment of tuberculosis in HIV infection. *Tuber.Lung Dis.*, 1992, 73, 378-383.

53. Crofton, J., Chaulet, P., Maher, D., Grosset, J., Harris, W, Horne, N., Iseman, M., Watt, B. Guidelines for the management of drug-resistant tuberculosis, WHO. Switzerland, 1997.

54. Bozeman, L, Burman, W., Metchock, B., Welch, L., Weiner, M. Fluoroquinolone susceptibility among *Mycobacterium tuberculosis* isolates from the United States and Canada. *Clin. Infect. Dis.*, 2005, 40, 386-391.

55. Blum, R. A. Influence of renal function on the pharmacokinetics of lomefloxacin compared with other fluoroquinolones. *Am. J. Med.*, 1992, 92,18S-21S.

56. Oliphant, C. M., Green, G. M. Quinolones. a comprehensive review. *Am. Fam. Physician*, 2002, 65, 455-464.

57. Tuberculosis Research Centre. Shortening Short Course Chemotherapy: A Randomised Clinical Trial for treatment of smear Positive Pulmonary Tuberculosis with regimens using Oflaxacin In the intensive phase *Ind. J. Tub.*, 2002, 49, 27-39.

58. Hu, Y., Coates, A. R. M., Mitchison, D. A. Sterilizing Activities of Fluoroquinolones against Rifampin-Tolerant Populations of *Mycobacterium tuberculosis Antimicrob. Agents Chemother.*, 2003, 47, 653-657.

59. http.//www.fda.gov/bbs/topics/news/2006/NEW01318.html

60. Paramasivan, C. N., Sulochana, S., Kubendiran, G., Venkatesan, P., Mitchison, D. A. Bactericidal action of gatifloxacin, rifampin, and isoniazid on logarithmic- and stationary-phase cultures of *Mycobacterium tuberculosis.Antimicrob.Agents Chemother.*2005, 49, 627-631.

61. Cynamon, M. H., Sklaney, M. Gatifloxacin and ethionamide as the foundation for therapy of tuberculosis. *Antimicrob Agents Chemother*, 2003, 47, 2442-2444.

62. http.//www.kaisernetwork.org/health_cast/hcast_index.cfm?display=detail&hc=1948

63. Davies, P.D.O., Yew, W.W. Recent developments in the treatment of tuberculosis, *Expert Opin. Invest. Drugs*, 2003, 12, 1297-1312.

64. http.//www.fda.gov/bbs/topics/news/2006/NEW01318.html

65. http.//www.fda.gov/cder/drug/InfoSheets/patient/moxifloxacin_hclPIS.htm

66. Ji, B, Lounis, N, Maslo, C., Truffot-Pernot, C., Bonnafous, P., Grosset, J. Antimicrob. Agents Chemother., 1998,42, 2066.

67. Gillespie, S. H., Gosling, R. D., Uiso, L., Sam, N. E., Kanduma, E. G., McHugh, T. D. Early bactericidal activity of a moxifloxacin and isoniazid combination in smear-positive pulmonary tuberculosis.*J. Antimicrob. Chemother.*, 2005, 56, 1169- 1171.

68. Nuermberger, E. L., Yoshimatsu, T., Tyagi, S., O'Brien, R. J., Vernon, A. N., Chaisson, R. E., Bishai, W. R., Grosset, J. H. Moxifloxacin-containing regimen greatly reduces time to culture conversion in murine tuberculosis. *Amer.J. Respir. Crit. Care Med.*, 2004, 16, 421-426.

69. Zhenkun M., Christian L., Helen M., Andrew J. N., Xiexiu W. Global tuberculosis drug development pipeline. the need and the reality. *Lancet* 2010, 375. 2100–2109.

70. Humer F (2005) Innovation in the Pharmaceutical Industry—Future Prospects. Available. http.//www.roche.com/fbh_zvg05_e.pdf. (Accessed 31 Dec 2010).

71. Bloom, B. R., Fine PEM. The BCG experience.Implications for future vaccines against tuberculosis. In. Bloom BR, eds. Tuberculosis. Pathogenesis, protection, and control. Washington DC, American Society for Microbiology, 1994, pp. 531–557.

72. Fine P. E. M., Variation in protection by BCG. implications of and for heterologous immunity. *Lancet* 1995, 346.1339–1345.

73. Styblo, K. Impact of BCG vaccination programmes in children and young adults on the tuberculosis program. *Tubercle* 1976, 57.17–43.

74. Anon. Randomised controlled trial of single BCG, repeated BCG, or combined BCG and killed Mycobacterium leprae vaccine for prevention of leprosy and tuberculosis in Malawi. Karonga Prevention Trial Group. *Lancet* 1996, 348.17–24.

75. Samiul H., Sabine D., P. S. Srinivasa R., Mark S. Prioritizing Genomic Drug Targets in Pathogens. Application to *Mycobacterium tuberculosis.PLoS Comput. Biol.* 2006, 2, e61.

76. Adams, P. D., Pannu, N. S., Read, R. J., Brunger, A. T., Cross-validated maximum likelihood enhances crystallographic simulated annealing refinement. *Proc. Natl. Acad. Sci. U. S. A.* 1997, 94, 5018-5023.

77. Terwilliger, T. C., Berendzen, J. Automated MAD and MIR structure solution. *Acta Crystallogr.* 1999, 55, 849-861.

78. Morris, R. J., Perrakis, A., Lamzin, V. S. ARP/wARP and automatic interpretation of protein electron density maps. *Methods Enzymol.*2003, 374, 229-244.

79. McCoy, A. J., Grosse-Kunstleve, R. W., Adams, P. D., Winn, M. D., Storoni, L. C., Read, R. J. Phaser crystallographic software. *J. Appl. Cryst.* 2007, 40, 658-674.

80. Manjasetty, B. A., Turnbull, A.P., Panjikar, S., Bussow, K., Chance, M. R. Automated technologies and novel techniques to accelerate protein crystallography for structural genomics. *Proteomics*, 2008, 8, 612-625.

81. Thomas, R. I, James, C. S. Structural genomics approach to drug discovery for *Mycobacterium tuberculosis.Curr.Opin.Microbiol.* 2009, 12, 318–325.

82. Arcus, V. L., Lott, J. S, Johnston, J. M., Baker, E. N. The potential impact of structural genomics on *Mycobacterium tuberculosis* drugdiscovery.*Drug Discov. Today*, 2006, 11, 28-34.

83. Murillo, A. C., Li, H. Y., Alber, T., Baker, E. N., Berger, J. M., Cherney, L. T., Cherney, M. M., Cho, Y. S., Eisenberg, D., Garen, C. R. High throughput crystallography of TB drug targets. *Infect. Disord. Drug Targets* 2007, 7, 127-139.

84. Johnston, J. M., Arcus, V. L., Morton, C. J., Parker, M. W., Baker, E. N. Crystal structure of a putative methyltransferase from *Mycobacterium tuberculosis.* misannotation of a genome clarified by protein structural analysis. *J. Bacteriol.* 2003, 185, 4057-4065.

85. Lee, K., Zhan, X., Gao, J., Qiu, J., Feng, Y., Meganathan, R., Cohen, S. N., Georgiou, G. RraA. a protein inhibitor of RNase E activity that globally modulates RNA abundance in *E. coli. Cell* 2003,114, 623-634.

86. Schneider, G.Virtual screening. an endless staircase? *Nat. Rev. Drug. Discov.* 2010, 9, 273–276.

87. Ekins, S., Bradford, J., Dole, K., Spektor, A., Gregory, K., Blondeau, D., Hohman, M., Bunin, B. A. A Collaborative Database And Computational Models For Tuberculosis Drug Discovery. *Mol. Biosyst.* 2010, 6, 840–851.

88. Squires, B., Catherine, M., Garcia-Sastre, A., Shubhada G., Jyothi N., Victoria H., Roger C., Christopher N. L., Ed, K., Kevin B., Richard H. S. BioHealthBase. informatics support in the elucidation of influenza virus host pathogen interactions and virulence. Nucleic Acids Res. 2008, 36, D497–503.

89. Hohman, M., Gregory, K., Chibale, K., Smith, P. J., Ekins, S., Bunin, B. Novel web-based tools combining chemistry informatics, biology and social networks for drug discovery.DrugDisc.Today.2009, 14,261–270.

90. Makarov, V., Manina, G., Mikusova, K., Möllmann, U., Ryabova, O., Saint-Joanis, B., Dhar, N., Pasca, M. R., Buroni, S., Lucarelli, A. P., Milano, A., De-Rossi, E., Belanova, M., Bobovska, A., Dianiskova, P., Kordulakova, J., Sala, C., Fullam, E., Schneider, P., McKinney, J. D., Brodin,

P., Christophe, T., Waddell, S., Butcher, P., Albrethsen, J., Rosenkrands, I., Brosch, R., Nandi, V., Bharath, S., Gaonkar, S., Shandil, R. K., Balasubramanian, V., Balganesh, T., Tyagi, S., Grosset, J., Riccardi, G., Cole, S. T. Benzothiazinones kill *Mycobacterium tuberculosis* by blocking arabinan synthesis. *Science*, 2009, 324, 801–804.

91. Catanho, M., Mascarenhas, D., Degrave, W., Miranda, A. B. GenoMycDB.a database for comparative analysis of mycobacterial genes and genomes. *Genet. Mol. Res.* 2006, 5, 115–126.

92. Bhardwaj, A., Bhartiya, D., Kumar, N., Open Source Drug Discovery Consortium, Scaria V. (2009) TBrowse. an integrative genomics map of *Mycobacterium tuberculosis*. *Tuberculosis,* 2009, 89, 386–387.

93. Aguero, F., Al-Lazikani, B., Aslett, M., Berriman, M., Buckner, F. S., Campbell, R. K., Carmona, S., Carruthers, I. M., Chan, A. W., Chen, F., Crowther, G. J., Doyle, M. A., Hertz-Fowler, C., Hopkins, A. L, McAllister, G., Nwaka, S., Overington, J. P., Pain, A., Paolini, G. V., Pieper, U., Ralph, S. A., Riechers, A., Roos, D. S., Sali, A., Shanmugam, D., Suzuki, T., Van Voorhis, W. C., Verlinde, C. L. (2008) Genomic-scale prioritization of drug targets.the TDR Targets database. *Nat. Rev. Drug Discov.* 2008, 7, 900–907.

94. Sandgren, A., Strong, M., Muthukrishnan, P., Weiner, B. K., Church, G. M., Murray, M. B. Tuberculosis drug resistance mutation database. *PLoS medicine* 2009, 6, e2.

95. Cole, S.T. Learning from the genome sequence of *Mycobacterium tuberculosis* H37Rv. *FEBS Lett.* 1999, 452, 7–10.

96. Reddy, T. B., Riley, R., Wymore, F., Montgomery, P., DeCaprio, D., Engels, R., Gellesch, M., Hubble, J., Jen, D., Jin, H., Koehrsen, M., Larson, L., Mao, M., Nitzberg, M., Sisk, P., Stolte, C., Weiner, B., White, J., Zachariah, Z. K., Sherlock, G., Galagan, J. E., Ball, C. A., Schoolnik, G. K. TB database. an integrated platform for tuberculosis research. *Nucleic Acids Res.* 2009, 209, 37, D499–508.

97. (i)Terwilliger, T. C., Park, M. S., Waldo, G. S., Berendzen, J., Hung, L. W., Kim, C. Y., Smith, C. V., Sacchettini, J. C., Bellinzoni, M., Bossi, R., De-Rossi, E., Mattevi, A., Milano, A., Riccardi, G., Rizzi, M., Roberts, M. M., Coker, A. R., Fossati, G., Mascagni, P., Coates, A. R., Wood, S. P., Goulding, C. W., Apostol, M. I., Anderson, D. H., Gill, H. S., Eisenberg, D. S., Taneja, B., Mande, S., Pohl, E., Lamzin, V., Tucker, P., Wilmanns, M., Colovos, C., Meyer-Klaucke, W., Munro, A. W., McLean, K. J., Marshall, K. R., Leys, D., Yang, J. K., Yoon, H. J., Lee, B. I., Lee, M. G., Kwak, J. E., Han, B. W., Lee, J. Y., Baek, S. H., Suh, S. W., Komen, M. M., Arcus, V. L., Baker, E. N., Lott, J. S., Jacobs, W. Jr., Alber, T., Rupp, B., The TB structural genomics consortium. a resource for *Mycobacterium tuberculosis* biology. *Tuberculosis.* 2003, 83, 223–249. (ii)Goulding, C. W., Apostol, M., Anderson, D. H., Gill, H. S., Smith, C. V., Kuo, M. R., Yang, J. K., Waldo, G. S., Suh, S. W., Chauhan, R., Kale, A., Bachhawat, N., Mande, S. C., Johnston, J. M., Lott, J. S., Baker, E. N., Arcus, V. L., Leys, D., McLean, K. J., Munro, A. W., Berendzen, J., Sharma, V., Park, M. S., Eisenberg, D., Sacchettini, J., Alber, T., Rupp, B., Jacobs, W. Jr., Terwilliger, T. C. The TB structural genomics consortium.providing a structural foundation for drug discovery. *Curr. Drug Targets Infect. Disord.* 2002, 2, 121–141. (iii)Rupp,

B., Segelke, B. W., Krupka, H. I., Lekin, T., Schäfer, J., Zemla, A., Toppani, D., Snell, G., Earnest, T. (2002) The TB structural genomics consortium crystallization facility.towards automation from protein to electron density. *Acta Crystallographica.* 2002, 58, 1514–1518.

98. Talcott, C., Eker, S., Knapp, M., Lincoln, P., Laderoute, K. Pathway logic modeling of protein functional domains in signal transduction.*Pac. Symp.on Biocomput.* 2004, 6, 568–580.

99. Caspi, R. Foerster, H., Fulcher, C. A., Hopkinson, R., Ingraham, J., Kaipa, P., Krummenacker, M., Paley, S., Pick, J., Rhee, S. Y., Tissier, C., Zhang, P., Karp, P. D. Meta Cyc. a multiorganism database of metabolic pathways and enzymes. *Nucleic Acids Res.* 2006, 34, D511–516.

100. Paley, S. and Karp, P. D.The pathway tools cellular overview diagram and omics viewer. *Nucleic Acids Res.* 2006, 34, 3771–3778.

101. Anishetty, S., Pulimi, M., Pennathur, G. Potential drug targets in *Mycobacterium tuberculosis* through metabolic pathway analysis. *Comput. Biol. Chem.* 2005, 29, 368–378.

102. Sud,M., Fahy, E., Cotter, D., Brown, A., Dennis, E. A., Glass, C. K., Merrill, A. H. Jr., Murphy, R. C., Raetz, C. R., Russell, D. W., Subramaniam, S. LMSD. LIPIDMAPS structure database. *Nucleic Acids Res.* 2007, 35, D527–532.

103. Cabusora, L., Sutton, E., Fulmer, A., Forst, C. V. Differential network expression during drug and stress response. *Bioinformatics.* 2005, 21, 2898–2905.

104. Lipinski, C., Lombardo, F., Dominy, B., Feeney, P. Experimental and computational approaches to estimate solubility in drug discovery and development settings. *Adv. Drug Deliv. Rev.*1997, 23, 3-25.

105. Chhabria, M., Mitesh, J., Shailesh, P. New frontiers in the therapy of tuberculosis: Fighting with the global menace. *Mini Rev. Med.* 2009, 9, 401–430.

106. O'Shea, R., Moser, H.E. Physicochemical properties of antibacterial compounds. implications for drug discovery. *J. Med. Chem.* 51, 2871–2878.

107. Payne, D. A., Gwynn, M. N., Holmes, D. J., Pompliano, D. L. Drugs for bad bugs.confronting the challenges of antibacterial discovery. *Nat. Rev. Drug Disc.* 2007, 6, 29–40.

108.Barry, C.E., Slayden, R. A., Sampson, A. E., Lee, R. E. Use of genomics and combinatorial chemistry in the development of new antimycobacterial drugs. *Biochem.Pharmacol.* 2000, 59, 221–231.

109. Ritchie, T. J., Luscombe, C. N., Macdonald, S. J. Analysis of the calculated physicochemicalproperties of respiratory drugs.canwe design for inhaled drugs yet? *J. Chem. Inf. Model.* 2009, 49, 1025–1032.

110. Fernandes, J. P., Pasqualoto, K. F., Felli, V. M., Ferreira, E. I.,Brandt, C. A. QSAR modeling of a set of pyrazinoate esters as antituberculosis prodrugs.*Arch. Pharm.* 2010, 343, 91–97.

111. Dolezal, R., Waisser, K., Petrlíková, E., Kunes, J., Kubicová, L., Machácek, M., Kaustová, J., Dahse, H. M. N-benzylsalicylthioamides.highly active potential antituberculotics. *Arch. Pharm.* 2009, 342, 113–119.

112. Nayyar, A., Malde, A., Coutinho, E., Jain, R. Synthesis, anti-tuberculosis activity, and 3D-QSAR study of ring-substituted-2/4-quinolinecarbaldehyde derivatives. *Bioorg. Med. Chem.* 2006, 14, 7302–7310.

113. Macaev, F., Rusu, G., Pogrebnoi, S., Gudima, A., Stingaci, E., Vlad, L., Shvets, N., Kandemirli, F., Dimoglo, A., Reynolds, R. Synthesis of novel 5-aryl-2-thio-1,3,4-oxadiazoles and the study of their structure-anti-mycobacterial activities. *Bioorg. Med. Chem.* 2005, 13, 4842–4850

114. Ventura, C., Martins, F. Application of quantitative structure-activity relationships to the modeling of antitubercular compounds. 1. The hydrazide family. *J. Med. Chem.* 2008, 51, 612–624.

115. Andrade, C. H., Salum, Lde. B., Castilho, M. S., Pasqualoto, K. F., Ferreira, E. I.,Andricopulo, A. D. Fragment-based and classical quantitative structure-activity relationships for a series of hydrazides as antituberculosis agents.*Mol. Divers.*2008, 12, 47–59.

116. Sivakumar, P. M., Sethu, K. G. B., Doble, M. QSAR studies on chalcones and flavonoids as anti-tuberculosis agents using genetic function approximation (GFA) method. *Chem. Pharm. Bull.* 2007, 55, 44–49.

117. Kortagere, S., Ekins, S. Troubleshooting computational methods in drug discovery. *J. Pharmacol. Toxicol.*Methods 2010, 61, 67–75.

118. Manvar, A. T., Pissurlenkar, R. R., Virsodia, V. R., Upadhyay, K. D., Manvar, D. R., Mishra, A. K., Acharya, H. D., Parecha, A. R., Dholakia, C. D., Shah, A. K., Coutinho, E. C. Synthesis, in vitro antitubercular activity and 3D-QSAR study of 1,4-dihydropyridines. *Mol. Divers.* 2010, 14, 285–305.

119. Shagufta, Kumar, A., Panda, G., Siddiqi, M. I. CoMFA and CoMSIA 3D-QSAR analysis of diaryloxy-methano-phenanthrene derivatives as anti-tubercular agents. *J. Mol. Model.* 2007, 13, 99–109.

120. Aparna, V., Jeevan. J., Ravi, M., Desiraju, G. R., Gopalakrishnan, B. 3D-QSAR studies on antitubercular thymidine monophosphate kinase inhibitors based on different alignment methods. *Bioorg. Med. Chem. Lett.* 2006,16, 1014–1020.

121. Hevener, K. E., Ball, D. M., Buolamwini, J. K., Lee, R. E. Quantitative structure-activity relationship studies on nitrofuranyl anti-tubercular agents. *Bioorg. Med. Chem.* 2008, 16, 8042–8053.

122. Nayyar, A., Monga, V., Malde, A., Coutinho, E., Jain, R. Synthesis, anti-tuberculosis activity, and 3D-QSAR study of 4-(adamantan-1-yl)-2-substituted quinolines. *Bioorg. Med. Chem.* 2007, 15, 626–640.

123. Nayyar, A., Malde, A., Coutinho, E., Jain, R. 3D-QSAR study of ring-substituted quinoline class of anti-tuberculosis agents. *Bioorg. Med. Chem.* 2006, 14, 847–856.

124. Kim, P., Kang, S., Boshoff, H. I., Jiricek, J., Collins, M., Singh, R., Manjunatha, U. H., Niyomrattanakit, P., Zhang, L., Goodwin, M., Dick, T., Keller, T. H., Dowd, C. S., Barry, C. E. 3rd. Structure-Activity Relationships of Antitubercular Nitroimidazoles. 2. Determinants of Aerobic Activity and Quantitative Structure-Activity Relationships. *J. Med. Chem.* 2009, 52, 1329–1344.

125. Biava, M., Porretta, G. C., Poce, G., Supino, S., Deidda, D., Pompei, R., Molicotti, P., Manetti, F., Botta, M. Antimycobacterial agents: Novel diarylpyrrole derivatives of BM212 endowed with high activity toward *Mycobacterium tuberculosis* and low cytotoxicity. *J. Med. Chem.* 2006, 49, 4946–4952.

126. Kolb, P., Ferreira, R. S., Irwin, J. J., Shoichet, B. K. Docking and chemoinformatic screens for new ligands and targets.*Curr. Opin.Biotechnol.* 2009, 20, 429–436.

127. Biava, M., Porretta, G. C., Poce, G., Supino, S., Deidda, D., Pompei, R., Molicotti, P., Manetti, F., Botta, M. Antimycobacterial agents. Novel diarylpyrrole derivatives of BM212 endowed with high activity toward *Mycobacterium tuberculosis* and low cytotoxicity. *J. Med. Chem.* 2006, 49, 4946–4952.

128. Gupta, R. K., Thakur, T. S., Desiraju, G. R., Tyagi, J. S. Structure-based design of DevR inhibitor active against nonreplicating *Mycobacterium tuberculosis J. Med. Chem.* 2009, 52, 6324–6334.

129. Kumar, A., Siddiqi, M. I. CoMFA based de novo design of pyrrolidine carboxamides as inhibitors of enoyl acyl carrier protein reductase from *Mycobacterium tuberculosis. J. Mol. Model.* 2008, 14, 923–935.

130. Kumar, A., Siddiqi, M. I. Receptor based 3D-QSAR to identify putative binders of *Mycobacterium tuberculosis* Enoyl acyl carrier protein reductase. *J. Mol. Model.* 2010, 16, 877–893.

131. Kumar, A., Mohammad, I. S., Stanislav, M. New molecular scaffolds for the design of *Mycobacterium tuberculosis* type II dehydroquinase inhibitors identified using ligand and receptor based virtual screening. *J. Mol. Model.* 2010, 16, 693–712.

132. Banfi, E., Scialino, G., Zampieri, D., Mamolo, M. G., Vio, L., Ferrone, M., Fermeglia, M., Paneni, M. S., Pricl, S. Antifungal and antimycobacterial activity of new imidazole and triazole derivatives.A combined experimental and computational approach.*J. Antimicrob. Chemother.* 2006, 58, 76–84.

133. Andrade, C.H., Kerly, F. M., Pasqualoto, E. I. Ferreira, Anton, J., Hopfinger. Rational design and 3D-pharmacophore mapping of 50 -thiourea-substituted alpha-thymidine analogues as mycobacterial TMPK inhibitors.*J. Chem. Inf. Model.* 2009, 49, 1070–1078.

134. Labello, N.P., Eric M. B., David, M., Ferguson, Courtney, C. A. Quantitative three dimensional structure linear interaction energymodel of 5 -O-[N-(salicyl)sulfamoyl]adenosine and the aryl acid adenylating enzyme MbtA. *J. Med. Chem.* 2008, 51, 7154–7160.

135. Wahab, H. A. Choong, Y. S., Ibrahim, P., Sadikun, A., Scior, T. Elucidating isoniazid resistance using molecular modeling.*J. Chem. Inf. Model.* 2009, 49, 97–107.

136. Kumar, M., Vijayakrishnan, R., Subba, R. G. In silico structure-based design of a novel class of potent and selective small peptide inhibitor of *Mycobacterium tuberculosis* dihydrofolate reductase, a potential target for anti-TB drug discovery. *Mol. Divers.* 2009, 14, 595–604.

137. Hegymegi-Barakonyi, B., Székely, R., Varga, Z., Kiss, R., Borbély, G., Németh, G., Bánhegyi, P., Pató, J., Greff, Z., Horváth, Z., Mészáros, G., Marosfalvi, J., Erõs, D., Szántai-Kis, C., Breza, N., Garavaglia, S., Perozzi, S., Rizzi, M., Hafenbradl, D., Ko, M., Av-Gay, Y., Klebl, B. M., Orfi, L., Kéri, G. Signalling inhibitors against *Mycobacterium tuberculosis*–early days of a new therapeutic concept in tuberculosis.*Curr. Med. Chem.* 2008, 15, 2760–2770.

138. Gopalakrishnan, B., Aparna, V., Jeevan, J., Ravi, M., Desiraju, G. R. A virtual screening approach for thymidinemonophosphate kinase inhibitors as antitubercular agents based on docking and pharmacophoremodels.*J. Chem. Inf.Model.* 2005, 45, 1101–1108.

139. Lin, T. W., Melgar, M. M., Kurth, D., Swamidass, S. J., Purdon, J., Tseng, T., Gago, G., Baldi, P., Gramajo, H., Tsai, S. C. Structure-based inhibitor design of AccD5, an essential acyl-CoA carboxylase carboxyltransferase domain of *Mycobacterium tuberculosis.Proc. Natl. Acad. Sci. U. S. A.* 2006, 103, 3072–3077.

140.Metaferia, B. B., Brandon, J., Fetterolf, S., Shazad-ul-Hussan, Matthew, M., Jeremy, A. S., Satyajit, R., Maria-Teresa, Gutierrez-Lugo, Carole, A. B. Synthesis of natural product-inspired inhibitors of *Mycobacterium tuberculosis* mycothiol-associated enzymes. The first inhibitors of GlcNAc-Ins deacetylase.*J. Med. Chem.* 2007, 50, 6326–6336.

141. Srivastava, S.K. et al. Rama Pati Tripathi, and Ravishankar Ramachandran (2005)NAD+-dependent DNA Ligase (Rv3014c) from *Mycobacterium tuberculosis*. Crystal structure of the adenylation domain and identification of novel inhibitors. J. Biol. Chem. 2005, 280, 30273–30281

142. Andrade, C. H., Pasqualoto, K. F., Ferreira, E. I.,Hopfinger, A. J. 3D-Pharmacophore mapping of thymidinebased inhibitors of TMPK as potential antituberculosis agents.*J. Comput. Aided Mol. Des.*2010, 24, 157–172.

143. Lu, X. Y., Chen, Y. D., Jiang, Y. J., You, Q. D. Discovery of potential new InhA direct inhibitors based on pharmacophore and 3D-QSAR analysis followed by in silico screening.*Eur. J. Med. Chem.* 2009, 44, 3718–3730.

144. Kumar, A., Chaturvedi, V., Bhatnagar, S., Sinha, S., Siddiqi, M. I. Knowledge based identification of potent antitubercular compounds using structure based virtual screening and structure interaction fingerprints. *J. Chem. Inf. Model.* 2009, 49, 35–42.

145. Kumar, V., Saravanan, P., Arvind, A., Mohan, C. G. Identification of hotspot regions of MurB oxidoreductase enzyme using homology modeling, molecular dynamics and molecular docking techniques.*J. Mol. Model.*2010, in press.

146. Jatana, N., Jangid, S., Khare, G., Tyagi, A. K., Latha, N. Molecular modeling studies of Fatty acyl-CoA synthetase (FadD13) from *Mycobacterium tuberculosis*-a potential target for the development of antitubercular drugs. *J. Mol. Model.*2010, in press.

147. Manina, G., Bellinzoni, M., Pasca, M. R., Neres, J., Milano, A., Ribeiro, A. L., Buroni, S., Skovierová, H., Dianišková, P., Mikušová, K., Marák, J., Makarov, V., Giganti, D., Haouz, A., Lucarelli, A. P., Degiacomi, G., Piazza, A., Chiarelli, L. R., De-Rossi, E., Salina, E., Cole, S. T, Alzari, P. M., Riccardi, G. Biological and structural characterization of the Mycobacterium smegmatis nitroreductase NfnB, and its role in benzothiazinone resistance.*Mol. Microbiol.* 2010, 5, 1172-85.

148. Sean, E., Joel, S., Freundlich, I. C., Malabika, S., Carolyn, T. Computational databases, pathwayand cheminformatics tools fortuberculosis drug discovery. *Cell Press (Article n Press)*

149. Hunt, E., Pleuromutilin antibiotics *Drugs Fut.*, 2000, 25, 1163-1168.

150. Schlünzen, F., Pyetan, E., Fucini, P., Yonath, A., Harms, Inhibition of peptide bond formation by pleuromutilins. the structure of the 50S ribosomal subunit from Deinococcus radiodurans in complex with tiamulin.*J.M. Mol. Microbiol.*, 2004, 54, 1287-1294.

151. Karlsson, M., Oxberry, S. L., Hampson, D. J. Veter. Antimicrobial susceptibility testing of Australian isolates of Brachyspira hyodysenteriae using a new broth dilution method.*Microbiol.*, 2002, 84, 123-133.

152. Schuster, I., Fleschurz, C., Helm, I. On the interaction of a lipophilic drug with different sites of rat-liver microsomes. Equilibrium studies with a substituted pleuromutilin.*Eur. J. Biochem.*, 1975, 51, 511-519.

153. Long, K. S., Poehlsgaard, J., Kehrenberg, C., Schwarz, S., Vester, B. The Cfr rRNA methyltransferase confers resistance to Phenicols, Lincosamides, Oxazolidinones,

Pleuromutilins, and Streptogramin A antibiotics. *Antibiotics Antimicrob. Agents Chemother.*, 2006, 50, 2500-2505.

154. Cox, R. J., Sutherland, A., Vederas, J. C. Bacterial diaminopimelate metabolism as a target for antibiotic design. *Bioorganic & Medicinal Chemistry* (2000), 8, 843-871.

155. Bugg, T. D. H., Walsh, C. T. Intracellular steps of bacterial cell wall peptidoglycan biosynthesis: enzymology, antibiotics, and antibiotic resistance. *Nat. Prod. Rep.* 1992, 9,199–215.

156. Chu, D. T., W., Plattner, J. J., Katz, L., New Directions in Antibacterial Research. *J. Med. Chem* 1996, 39, 3853-3874.

157. De, D. A., Prieto, L., Martín, J. A., Rubio, A., Ezquerra, J., Tebbe, M., López, U. B., Martín, J., Sánchez, A., LeTourneau, D. L., McGee, J. E., Boylan, C., Parr, T. R. Jr., Smith, M. C. 4-Substituted D-glutamic acid analogues: the first potent inhibitors of glutamate racemase (MurI) enzyme with antibacterial activity. *J. Med. Chem.* 2002, 45, 4559-70.

158. Neu, H. C. The crisis in antibiotic resistance.*Science*. 1992, 257, 1064-73.

159. Stewart, L. Fisher. Glutamate racemase as a target for drug discovery.*Microbial Biotechnology*2008, 5, 345–360.

160. Ayengar, P., Roberts, E. Utilization of D-glutamic acid by Lactobacillus arabinosus. glutamic racemase. *J. Biol. Chem.* 1952, 197.453–460.

161. Narrod, S. A., Wood, W. A. Evidence for a glutamic acid racemase in Lactobacillus arabinosus. *Arch. Biochem. Biophys.* 1952, 35.462–463.

162. Glaser, L. Glutamic acid racemase from Lactobacillus arabinosus. *J. Biol. Chem.* 1960, 235.2095–2098.

163. Tanaka, M., Kato, Y., Kinoshita, S. Glutamic acid racemase from Lactobacillus fermenti. purification and properties. *Biochem.Biophys.Res. Comm.* 1961, 4.114–117.

164. Diven, W.F. Studies on amino acid racemases. purification and properties of the glutamate racemase from *Lactobacillus fermenti. Biochim.Biophys.Acta* 1969, 191.702–706.

165. Doublet, P., van Heijenoort, J., Mengin-LeCreulx, D. Identification of the Escherichia coli murI gene, which is required for the biosynthesis of D-glutamic acid, a specific component of the bacterial peptidoglycan. *J. Bacteriol,* 1992, 174. 5772–5779.

166. Doublet, P., van Heijenoort, J., Bohin, J. P., MenginLeCreulx, D. The murI gene of Escherichia coli is an essential gene that encodes a glutamate racemase activity. *J. Bacteriol.* 1993, 175. 2970–2979.

167. Dougherty, T.J., Thanassi, J.A., and Pucci, M.J. The Escherichia coli mutant requiring D-glutamic acid is the result of mutations in two distinct genetic loci. *J. Bacteriol.* 1993, 175.111–116.

168. Baliko, G., Venetianer, P. An Escherichia coli gene in search of a function.phenotypic effects of the gene recently identified as murl. *J. Bacteriol.* 1993, 175. 6571–6577.

169. Pucci, M. J., Novotny, J., Discotto, L. F., Dougherty, T.J. The Escherichia coli Dga (MurI) protein shares biological activity and structural domains with the Pediococcus pentosaceus glutamate racemase. *J. Bacteriol.* 1994, 176.528–530.

170. Ashiuchi, M., Kuwana, E., Yamamoto, T., Komatsu, K., Soda, K., and Misono, H. Glutamate racemase is an endogenous DNA gyrase inhibitor. *J. Biol. Chem.* 2002, 277.39070–39073.

171. Sengupta, S., Shah, M., Nagaraja, V. Glutamate racemase from *Mycobacterium tuberculosis* inhibits DNA gyrase by affecting its DNA binding. *Nucleic.Acids.Res.* 2006, 34. 5567–5576.

172. Sengupta, S., and Nagaraja, V. Inhibition of DNA gyrase activity by Mycobacterium smegmatis MurI. *FEMS Microbiol.Lett.* 2008, 279.40–47.

173. Ashiuchi, M., Kuwana, E., Komatsu, K., Soda, K., and Misono, H. Differences in effects on DNA gyrase activity between two glutamate racemases of Bacillus subtilis, the poly-g-glutamate synthesis-linking Glr enzyme and the YrpC (MurI) isozyme. *FEMS Microbiol.Lett.* 2003, 223.221–225.

174. Drysdale, M., Heninger, S., Hutt, J., Chen, Y., Lyons, C. R., and Koehler, T. M. Capsule synthesis by Bacillus anthracis is required for dissemination in murine inhalation anthrax. *EMBO J.* 2005, 24.221–227.

175. Kada, S., Nanamiya, H., Kawamura, F., and Horinouchi, S. Glr, a glutamate racemase, supplies D-lutamate to both peptidoglycan synthesis and poly-g-glutamate production in g-PGA-producing Bacillus subtilis. *FEMS Microbiol.Lett.* 2004, 236.13–20.

176. Kimura, K., Phan Tran, L.-S., and Itoh, Y. Roles and regulation of the glutamate racemase isogenes, racE and yrpC,in Bacillus subtilis. *Microbiology,* 2004, 150. 2911–2920.

177. Shatalin, K. Y., Neyfakh, A. A. Efficient gene inactivation in Bacillus anthracis. *FEMS Microbiol.Lett.* 2005, 245.315–319.

178. Ashiuchi, M., Soda, K., and Misono, H. Characterization of yrpC gene product of Bacillus subtilis IFO 3336 as glutamate racemase isozyme. *Biosci.Biotech.Biochem.* 1999, 63.792–798.

179. Dodd, D., Reese, J. G., Louer, C. R., Ballard, J. D., Spies, M. A., Blanke, S.R. Functional comparison of the two Bacillus anthracis glutamate racemases. *J. Bacteriol.* 2007, 189. 5265–5275.

180. May, M., Mehboob, S., Mulhearn, D. C., Wang, Z., Yu, H., Thatcher, G. R. J.Structural and functional analysis of two glutamate racemase isozymes from Bacillus anthracis and implications for inhibitor design. *J. Mol. Biol.* 2007, 371.1219–1237.

181. Glavas S, Tanner ME. Active site residues of glutamate racemase.Biochemistry.2001 40 (21) 6199–6204.

182. Baltz, R. H., Hoskins, J. A., Solenberg, P. J. & Treadway, P. J. (1999). US Patent 5 981 281.

183. Pucci, M. J., Thanassi, J. A., Ho, H. T., Falk, P. J. & Dougherty, T. J. Staphylococcus haemolyticus contains two D-glutamic acid biosynthetic activities, a glutamate racemase and a D-amino acid transaminase. *J. Bacteriol.* 1995, 177, 336-342.

184. Kobayashi, K., Ehrlich, S. D., Albertini, A., Amati, G., Andersen, K.K. , Arnaud, M., Asai, K., Ashikaga, S., Aymerich, S., Bessieres, P., Boland, F., Brignell, S. C., Bron, S., Bunai, K., Chapuis, J., Christiansen, L. C., Danchin, A., Débarbouille, M., Dervyn, E., Deuerling, E., Devine, K., Devine, S. K., Dreesen, O., Errington, J., Fillinger, S., Foster, S. J., Fujita, Y., Galizzi, A., Gardan, R., Eschevins, C., Fukushima, T., Haga, K., Harwood, C. R., Hecker, M., Hosoya, D., Hull, M. F., Kakeshita, H., Karamata, D., Kasahara, Y., Kawamura, F., Koga, K., Koski, P., Kuwana, R., Imamura, D., Ishimaru, M., Ishikawa, S., Ishio, I., Le, Coq, D., Masson, A., Mauël, C., Meima, R., Mellado, R. P., Moir, A., Moriya, S., Nagakawa, E., Nanamiya, H., Nakai, S., Nygaard, P., Ogura, M., Ohanan, T., O'Reilly, M., O'Rourke, M., Pragai, Z., Pooley, H. M., Rapoport, G., Rawlins, J. P., Rivas, L. A., Rivolta, C., Sadaie, A., Sadaie, Y., Sarvas, M., Sato, T., Saxild, H. H., Scanlan, E., Schumann, W., Seegers, J. F., Sekiguchi, J., Sekowska, A., Séror, S. J., Simon, M., Stragier, P., Studer, R., Takamatsu, H., Tanaka, T., Takeuchi, M., Thomaides, H. B., Vagner, V., van-Dijl, J. M., Watabe, K., Wipat, A., Yamamoto, H., Yamamoto, M., Yamamoto, Y., Yamane, K., Yata, K., Yoshida, K., Yoshikawa, H., Zuber, U., Ogasawara, N. Essential *Bacillus subtilis* genes.*Proc. Natl. Acad. Sci. USA,* 2003, 100, 4678-4683.

185. (a) Park, J. T., In Escherichia coli and Salmonella. Neidhardt, F. C., Curtis, R. I., Ingraham, J. L., Lin, E. C. C., Low, K. B., Magasanik, B., Resnikoff, W. S., Riley, M., Schaechter, M. and Umbarger, H. E., Eds., *American Society for Microbiology*: Washington, DC, 1996, 48-57. (b) van Heijenoort, J. In Escherichia coli and Salmonella, Neidhardt, F. C., Curtis, R., III, Ingraham, J. L., Lin, E. C. C., Low, K. B., Magasanik, B., Resnikoff, W. S., Riley, M., Schaechter, M. and Umbarger, H. E., Eds., *American Society for Microbiology*: Washington, DC, 1996, 1025-1034.

186. Gale, E. F., Cundliffe, E., Reynolds, P. E., Richmond, M. H., Waring, M. J. The Molecular Basis of Antibiotic Action, 2nd ed., Wiley and Sons: London, 1981.

187. Hwang, K. Y., Cho, C. S., Kim, S. S., Sung, H. C., Yu, Y. G., Cho, Y. Structure and mechanism of glutamate racemase from Aquifex pyrophilus *Nature Struct. Biol.* 1999, 6, 422-426.

188. Ruzheinikov, S. N., Taal, M. A., Sedelnikova, S. E., Baker, P. J. & Rice, D. W. Substrate-induced conformational changes in Bacillus subtilis glutamate racemase and their implications for drug discovery. *Structure* 2005, 13, 1707–1713.

189. Kook-Han Kim, Young-Jong Bong, Joon Kyu Park, Key-Jung Shin, Kwang Yeon Hwang and Eunice Eun Kyeong Kim. Structural Basis for Glutamate Racemase Inhibition, *J. Mol. Biol.* 2007, 372, 434–443

190. Glavas, S., Tanner, M. E. Catalytic Acid/Base Residues of Glutamate Racemase. *Biochemistry*, 1999, 38, 4106–4113.

191. Tanner, M. E. Understanding Nature's Strategies for Enzyme-Catalyzed Racemization and Epimerization. *Acc. Chem. Res.*, 2002, 35, 237–246.

192. Yoshimura, T., Esaki, N. Amino Acid Racemases: Functions and Mechanisms, *J. Biosci. Bioeng*, 2003, 96, 103-109.

193. Fisher, L. M., Albery, W. J., Knowles, J. R. Energetics of proline racemase: racemization of unlabeled proline in the unsaturated, saturated, and oversaturated regimes. *Biochemistry*. 1986, 25, 2529–2537.

194. Fsher, L. M., Albery, W. J., Knowles, J. R. Energetics of proline racemase: tracer perturbation experiments using [14C]proline that measure the interconversion rate of the two forms of free enzyme. *Biochemistry*. 1986, 6, 25, 2538–2542.

195. Fisher, L. M., Belasco, J. G., Bruice, T. W., Albery, W. J, Knowles, J. R. Energetics of proline racemase: transition-state fractionation factors for the two protons involved in the catalytic steps. *Biochemistry* 25, 1986, 2543-2551.

196. Gallo, K. A., Knowles, J. R. Purification, cloning, and cofactor independence of glutamate racemase from Lactobacillus. *Biochemistry*. 1993, 20, 32, 3981–3990.

197. Gallo, K. A., Tanner, M. E., Knowles, J. R. Mechanism of the reaction catalyzed by glutamate racemase. *Biochemistry*. 1993, 32, 3991–3997.

198. Schlippe, Y. V. G., Hedstrom, L. A twisted base?The role of arginine in enzyme-catalyzed proton abstractions*Arch. Biochem. Biophys*. 2005, 433, 266–278.

199. Ondrechen, M. J., Briggs, J. M., McCammon, A Model for Enzyme−Substrate Interaction in Alanine Racemase. *J. Am. Chem. Soc.*, 2001, 123, 2830–2834.

200. Sun, S., Toney, M. D. Evidence for a Two-Base Mechanism Involving Tyrosine-265 from Arginine-219 Mutants of Alanine Racemase, *Biochemistry*, 1999, 38, 4058–4065.

201. Major, D. T., Nam, K., Gao, J. Transition State Stabilization and α-Amino Acidity in Alanine Racemase. *J. Am. Chem. Soc.* 2006, 128, 8114-8115.

202. Major, D. T., Gao, J. A Combined Quantum Mechanical and Molecular Mechanical Study of the Reaction Mechanism and α-Amino Acidity in Alanine Racemase. *J. Am. Chem. Soc.*, 2006, 128, 16345–16357.

203. Eduard, P., Edgar, M., Mireia, G., Gonza, A., Jose, M. L. How the Substrate D-Glutamate Drives the Catalytic Action of Bacillus subtilis Glutamate Racemase. *J. Am. Chem. Soc.* 2009, 131, 3509–3521.

204. Henrik, M., Thomas, C. B. Multiple Substrate Binding States and Chiral Recognition in Cofactor-independent Glutamate Racemase: A Molecular Dynamics Study. *Biochemistry* 2004, 43, 9685-9694.

205. Eduard, P., Mireia, G., Gonzalez, A., Jose, M. L., Martin, J. F. New Insights into the Reaction Mechanism Catalyzed by the Glutamate Racemase Enzyme: pH Titration Curves and Classical Molecular Dynamics Simulations. *J. Phys. Chem. B* 2007, 111, 2385-2397.

206. Ashley, M. S., Joseph, G. R. Dylan, D., Katherine, L. P., Steven, R. B., Baudry. Determinants of Catalytic Power and Ligand Binding in Glutamate Racemase.*J. Am. Chem. Soc.* 2009, 131, 5274–5284.

207. Tomas, L., Stewart, L. F., Gunther, K., Rutger, H. A. F., Yafeng, X. D. Trevor Newton, Thomas A. Keating, Richard A. Alm, Boudewijn L. M. de Jonge. Exploitation of structural and regulatory diversity in glutamate racemases.*Nature*. 447, 2007, 817-822.

208. Doublet, P., van Heijenoort, J. Mengin-Lecreulx, D. The glutamate Racemase activity from Escherichia coli is regulated by peptidoglycan precursor UDP-N-acetylmuramoyl-L-alanine. *Biochemistry* 1994, 33, 5285–5290.

209. Ho, H.-T., Falk, P. J., Ervin, K. M., Krishnan, B. S., Discotto, L. F., Dougherty, T. J., Pucci, M. J. UDP-N-acetylmuramyl-L-alanine functions as an activator in the regulation of the Escherichia coli glutamate racemase activity. *Biochemistry* 1995, 34, 2464–2470.

210. Doublet, P., van Heijenoort, J. Mengin-Lecreulx, D. Regulation of the glutamate racemase of Escherichia coli investigated by site-directed mutagenesis. *Microb. Drug Resist. Mechanisms Epidemiol. Dis.* 1996, 2, 43–49.

211. Fotheringham, I. G., Bledig, S. A., Taylor, P. P. Characterization of the genes encoding D-amino acid transaminase and glutamate racemase, two D-glutamate biosynthetic enzymes of Bacillus sphaericus ATCC 10208. *J. Bacteriol.* 1998, 180, 4319–4323.

212. Song, J. H., Ko, K. S., Lee, J. Y., Baek, J. Y., Oh, W. S., Yoon, H. S., Jeong, J. Y., Chun, J. Identification of essential genes in Streptococcus pneumoniae by allelic replacement mutagenesis. *Mol. Cells* 2005, 19, 365–374.

213. Wang, L., Zamudio, C. A method for predicting operons in prokaryotes. US patent number US2005/0026189A1 (2005).

214.http://modbase.compbio.ucsf.edu/modbasecgi/model_details.cgi?queryfile=1293038595_344&searchmode=default&filtermode=off&displaymode=moddetail&seq_id=&model_id= b0cf2a914 b0d78c41970a641f240b130 (visited on Dec 30th 2010)

21. http://www.ncbi.nlm.nih.gov/Education/BLASTinfo/psi1.html (visited on Dec 30th 2010)

216. Tanner, M. E. Shichang, M. The Synthesis and Stability of Aziridino-glutamate, an Irreversible Inhibitor of Glutamate Racemase.*Terrahedron Letters*, 1994, 35, 4073-4076.

217. Glavas, S., Tanner, M. E., The Inhibition Of Glutamate Racemase By D-*N*-Hydroxyglutamate, *Bioorg. & Med. Chem. Lett.* 1997, 7, 2265-2270.

218.Bolin, G., Gloria, B., Comita-Prevoir, J., Randy, P., Charles, E., Tomas, L., Peter, D., Elise, G., Brian, N. Exploring 9-benzyl purines as inhibitors of glutamate racemase (MurI) in Gram-positive bacteria. *Bioorg.& Med. Chem. Lett.* 2008, 18, 4368–4372.

219. Gregory, S. B., Pamela, J. H., Abdullah, R., Peter, J. H. W. Design of Helicobacter pylori glutamate racemase inhibitors as selective antibacterial agents. A novel pro-drug approach to increase exposure.*Bioorg.& Med. Chem. Lett.* 2008, 18, 4716–4722.

220. Gloria, A. B., Comita-Prevoir, J., Charles, J. E., Bolin, G., Randy, P., Peter, D., Elise, G., Brian, N. Exploring 8-benzyl pteridine-6,7-diones as inhibitors of glutamate racemase (MurI) in Gram-positive bacteria. *Bioorg.& Med. Chem. Lett.* 2008, 18, 6100–6103.

221. Bolin, G., Gregory, B., Comita-Prevoir, J., Madhusudhan, G., Pamela, H., Andrew, K., James, L., Lawrence, M., Marshall, M., George, M., Ekundayo, O., Alexander, S., Charles, E., Tomas, L. Potent and selective inhibitors of Helicobacter pylori glutamate Racemase (MurI). Pyridodiazepine amines.*Bioorg.& Med. Chem. Lett.* 2009, 19, 930–936.

222. Priscila-de-Almeida, L., Anthony, R. C, Leanne, T., Gordon, K., Bernadette, M. M., Gunther, K., Stewart, F., John, N. A. H., Ronald, J. Q. Exiguaquinol. A Novel Pentacyclic Hydroquinone from Neopetrosia exigua that Inhibits Helicobacter pylori MurI.*Org. Lett.*, 2008, 10, 2585-2588.

223. Katie, L., W., Katherine, L. P., Steven, R. B., Ashley M. S. Exploiting Enzyme Plasticity in Virtual Screening. High Efficiency Inhibitors of Glutamate Racemase.*ACS Med. Chem. Lett.* 2010, 1, 9–13.

224. Henikoff, S., Henikoff, J. G. Amino acid substitution matrices from protein blocks. *Proc. Natl. Acad. Sci. USA* 1992, 89, 10915–10919.

225. Sali, A., Blundell, T. L. Comparative protein modelling by satisfaction of spatial restraints. *J. Mol. Biol.* 1993, 234,779–815.

226. Whittle, P. J., Blundell, T. L Protein structure-based drug design, *Ann. Rev.Biophys. Biomole.Structure.* 1994, 23, 349-375.

227. Schrödinger Suite 2009 Protein Preparation Wizard, Epik version 2.0, Schrödinger, LLC, New York, NY, 2009, Impact version 5.5, Schrödinger, LLC, New York, NY, 2009, Prime version 2.1, Schrödinger, LLC, New York, NY, 2009.

228. Impact, version 5.5, Schrödinger, LLC, New York, NY, 2005.

229. Laskowski, R. A., MacArthur, M. W., Moss, D. S., Thornton, J. M. PROCHECK: a program to check the stereochemical quality of protein structures. *J. Appl. Cryst.* 1993, 26, 283-293.

230. Luthy, R., Bowie, J. U., Eisenberg, D. Assessment of protein models with three-dimensional profiles. *Nature* 1992, 3, 56, 83-93.

231. SiteMap, version 2.3, Schrödinger, LLC, New York, NY, 2009.

232. Friesner, R. A., Murphy, R. B., Repasky, M. P., Frye, L. L., Greenwood, J. R., Halgren, T. A., Sanschagrin, P. C., Mainz, D. T. Extra precision glide: docking and scoring incorporating a model of hydrophobic enclosure for protein-ligand complexes. *J. Med. Chem.* 2006, 49, 6177–6196

233. Desmond Molecular Dynamics System, version 2.2, D. E. Shaw Research, New York, NY,2009. Maestro-Desmond Interoperability Tools, version 2.2, Schrödinger, New York, NY,2009

234. Kevin, J. B., Edmond, C., Huafeng, Xu, Ron, O. D., Michael, P. E., Brent, A.G., John, L. K., Istvan, K., Mark, A. M., Federico, D., John, K. S., Yibing, S., David, E. S., "Scalable Algorithms for Molecular DynamicsSimulations on Commodity Clusters," Proceedings of the ACM/IEEE Conference on Supercomputing (SC06), Tampa, Florida, November 11-17, 2006.

235. Jorgensen, W. L., Chandrasekhar, J., Madura, J. Klein, M. L. Comparison of simple potential functions for simulating liquid water. *J. Chem. Phys.* 1983, 79, 926–935.

236Berendsen, H. J. C., Postma, J. P. M., van Gunsteren, W. F., DiNola, A., Haak, J. R. Molecular dynamics with coupling to an external bath. *J. Comput. Phys.* 1984, 81, 3684–3690.

237. (a) Darden, T.; York, D. L. Pedersen, Particle mesh Ewald: An N log(N) method for Ewald sums in large system. *J. Chem. Phys.* 1993,98, 10089–10092. (b) Essmann, U., Perera, L., Berkowitz, M. L., Darden, T., Lee, H., Pedersen, L. G. A smooth particle mesh Ewald method. *J. Chem. Phys.*1995, 103, 8577–8593.

238. Ryckaert, J. P., Ciccotti, G., Berendsen, H. J. C. Numerical integration of the Cartesian equations of motion of a system with constraints: Molecular synamics of n-alkanes. *J. Comput. Phys.* 1977, 23, 327–341.

239. West, A. H., Stock, A. M. Histidine kinases and response regulator proteins in two-component signaling systems. *Trends Biochem. Sci.* 2001, 26, 369–376.

240. Cole, S. T., Brosch, R., Parkhill, J, Garnier, T., Churcher, C., Harris, D., Gordon, S. V., Eiglmeier, K., Gas, S., C. E., Barry, 3rd, Tekaia, F., K., Badcock, Basham, D., Brown D., Chillingworth, T., Connor, R., Davies R., Devlin, K., Feltwell, T., S., Gentles, N. H, Holroyd, S., Hornsby, T., Jagels, K., Krogh, A., McLean, J., Moule, S., Murphy, L., Oliver, K., Osborne J., Quail, M. A., Rajandream, M. A., Rogers, J., Rutter, S., Seeger, K., Skelton, J., Squares, R., quares, S., Sulston, J. E., Taylor, K., Whitehead, S., Barrell, B. G. Deciphering the biology of *Mycobacterium tuberculosis* from the complete genome sequence. *Nature* 1998, 393, 537–544.

241. Fontan, P., Walters, S., Smith I. Cellular signaling pathways and transcriptional regulation in *Mycobacterium tuberculosis*. stress control and virulence. *Curr.Sci.* 2004, 86,122–134.

242. Parish, T., Smith, D. A., Kendall, S., Casali N., Bancroft, G. J., Stoker, N. G. Deletion of two-component regulatory systems increases the virulence of *Mycobacterium tuberculosis*. *Infect. Immun.* 2003, 71, 1134–1140.

243. Parish, T., Smith, D. A., Roberts, G., Betts, J., Stoker, N. G. The senX3-regX3 two-component regulatory system of *Mycobacterium tuberculosis* is required for virulence. *Microbiology* 2003, 149, 1423–1435.

244. Perez, E., Samper, S., Bordas, Y., Guilhot, C., Gicquel, B., Martin, C. An essential role for phoP in *Mycobacterium tuberculosis* virulence.*Mol. Microbiol.* 2001, 41, 179–187.

245. Rickman, L., Saldanha, J. W., Hunt, D. M., Hoar, D. N., Colston, M. J., Millar, J. B., Buxton, R. S. A two-component signal transduction system with a PAS domain-containing sensor is required for virulence of *Mycobacterium tuberculosis* in mice. *Biochem.Biophys. Res. Commun.* 2004, 314, 259–267.

246. Zahrt, T. C., Deretic, V. *Mycobacterium tuberculosis* signal transduction system required for persistent infections. *Proc. Natl. Acad. Sci. USA* 2001, 98, 12706–12711.

247. Zahrt, T. C., Deretic, V. An essential two-component signal transduction system in *Mycobacterium tuberculosis*. *J. Bacteriol.* 2000, 182, 3832–3838.

248. Cole, S. T., Eiglmeier, K., Parkhill, J., James, K. D., Thomson, N. R., Wheeler, P. R., Honore, N., Garnier, T., Churcher, C., Harris, D., Mungall, K., Basham, D., Brown, D., Chillingworth, T., Connor, R., Davies, R. M., Devlin, K., Duthoy, S., Feltwell, T., Fraser, A., Hamlin, N., Holroyd, S., Hornsby, T., Jagels, K., Lacroix, C., Maclean, J., Moule, S., Murphy, L., Oliver, K., Quail, M. A., Rajandream, M. A., Rutherford, K. M., Rutter, S., Seeger, K., Simon, S., Simmonds, M., Skelton, J., Squares, R., Squares, S., Stevens, K., Taylor, K., Whitehead, S., Woodward, J. R., Barrell, B. G. Massive gene decay in the leprosy bacillus. *Nature*, 2001, 409, 1007–1011.

249. Sassetti, C. M., Boyd, D. H., Rubin, E. J. Genes required for mycobacterial growth defined by high density mutagenesis. *Mol. Microbiol.* 2003,48, 77–84.

250. Cowley, S., Ko, M., Pick, N., Chow, R., Downing, K. J., Gordhan, B. G., Betts, J. C., Mizrahi, Smith V. Stokes, Stokes, R. W., Y. Av-Gay. The *Mycobacterium tuberculosis* protein serine/threonine kinase PknG is linked to cellular glutamate/glutamine levels and is important for growth in vivo. *Mol. Microbiol.* 2004, 52, 1691–1702.

251. Nguyen, L., Walburger, A., Houben, E., Koul, A., Muller, S., Morbitzer, M., Klebl, B., Ferrari, G., Pieters, J. Role of protein kinase G in growth and glutamine metabolism of Mycobacterium bovis BCG*J. Bacteriol.* 2005, 187, 5852–5856.

252. Papavinasasundaram, K. G., Chan, B., Chung, J. H., Colston, M. J., Davis, E. O., Y. Av-Gay. Deletion of the *Mycobacterium tuberculosis* pknH gene confers a higher bacillary load during the chronic phase of infection in BALB/c mice. *J. Bacteriol.* 2005, 187, 5751–5760.

253. Perez, J., Garcia, R., Bach, H., Waard, J. H. de, Jacobs, W. R., Jr., Y. Av-Gay, Bubis, J., Takiff, H. E. *Mycobacterium tuberculosis* transporter MmpL7 is a potential substrate for kinase PknD. *Biochem. Biophys. Res. Commun.* 2006, 348, 6–12.

254. Deol, P., Vohra, R., Saini, A. K., Singh, A., Chandra, H., Chopra, P., Das, T. K., Tyagi, A. K., Singh, Y. Role of *Mycobacterium tuberculosis* Ser/Thr kinase PknF. implications in glucose transport and cell division. *J. Bacteriol.* 2005, 187, 3415–3420.

255. Av-Gay, Y., Everett, M. The eukaryotic-like Ser/Thr protein kinases of *Mycobacterium tuberculosis.Trends Microbiol.*2000, 8, 238–244.

256. Kang, C. M., Abbott, D. W., Park, S. T., Dascher, C. C., Cantley, L. C., Husson, R. N. The *Mycobacterium tuberculosis* serine/threonine kinases PknA and PknB. substrate identification and regulation of cell shape. *Genes Dev.* 2005, 19, 1692–1704.

257. Pablo, F., Brigitte, Saint-Joanis, Nathalie, B., Mary, J., Brigitte, G., Stewart, T. C., Pedro, M. Alzari. The Ser/Thr Protein Kinase PknB Is Essential for Sustaining Mycobacterial Growth. *J. Bacteriol.* 2006, 43, 7778–7784.

258. Zhang, W., Munoz-Dorado, J., Inouye, M., Inouye, S. Identification of a putative eukaryotic like protein kinase family in the developmental bacterium *Myxococcus xanthus. J. Bacteriol.* 1992, 174, 5450–5453.

259. Matsumoto, A., Hong, S. K., Ishizuka, H., Horinouchi, S., Beppu, T. Phosphorylation of the AfsR protein involved in secondary metabolism in Streptomyces species by a eukaryotic-type protein kinase. *Gene* 1994,146, 47–56.

260. Peirs, P., De Wit, L., Braibant, M., Huygen, K., Content, J. A serine/threonine protein kinase from *Mycobacterium tuberculosis.Eur. J. Biochem.* 1997, 244, 604–612.

261. Av-Gay, Y., Jamil, S., Drews, S. J. Expression and characterization of the *Mycobacterium tuberculosis* serine/threonine protein kinase PknB. *Infect. Immun.* 1999, 67, 5676–5682.

262. Gaidenko, T. A., Kim, T. J., Price, C. W. The PrpC serine-threonine phosphatase and PrkC kinase have opposing physiological roles in stationary-phase Bacillus subtilis cells. *J. Bacteriol.* 2002, 184, 6109–6114.

263. Koul, A., Choidas, A., Tyagi, A. K., Drlica, K., Singh, Y., Ullrich, A. Serine/threonine protein kinases PknF and PknG of *Mycobacterium tuberculosis*. characterization and localization. *Microbiology* 2001, 147, 2307–2314.

264. Chaba, R., Raje, M., Chakraborti, P. K. Evidence that a eukaryotic-type serine/threonine protein kinase from *Mycobacterium tuberculosis* regulates morphological changes associated with cell division. *Eur. J. Biochem.* 2002, 269, 1078–1085.

265. Molle, V., Girard-Blanc, C., Kremer, L., Doublet, P., Cozzone, A.J., Prost, J. F.. Protein PknE, a novel transmembrane eukaryotic-like serine/threonine kinase from *Mycobacterium tuberculosis .Biochem.Biophys. Res. Commun.* 2003, 308, 820–825. b Molle, V., Kremer, L., Girard-Blanc, C., Besra, G. S., Cozzone, A. J. ,Prost, J. F. An FHA phosphoprotein recognition domain mediates protein EmbR phosphorylation by PknH, a Ser/Thr protein kinase from *Mycobacterium tuberculosis. Biochemistry* 2003, 42, 15300–15309.

266. Gopalaswamy, R., Narayanan, P.R., Narayanan, S. Cloning, overexpression, and characterization of a serine/threonine protein kinase pknI from *Mycobacterium tuberculosis* H37Rv. *Protein. Expr.Purif.* 2004, 36, 82–89.

267. Young, T. A., Delagoutte, B., Endrizzi, J. A., Falick, A. M., Alber, T. Structure of *Mycobacterium tuberculosis* PknB supports a universal activation mechanism for Ser/Thr protein kinases. *Nat. Struct. Biol.* 2003, 10, 168–174.

268. Boitel, B., Ortiz-Lombardia, M., Duran, R., Pompeo, F., Cole, S. T., Cervenansky, C., Alzari, P. M. PknB kinase activity is regulated by phosphorylation in two Thr residues and dephosphorylation by PstP, the cognate phospho-Ser/Thr phosphatase, in *Mycobacterium tuberculosis . Mol. Microbiol.* 2003, 49, 1493–1508.

269. Huse, M., Kuriyan, J. The conformational plasticity of protein kinases.*Cell* 2002, 109, 275–282.

270. Grundner, C., Gay, L.M., Alber, T. *Mycobacterium tuberculosis* serine/threonine kinases PknB, PknD, PknE, and PknF phosphorylate multiple FHA domains. *Protein. Sci.* 2005, 14, 1918–1921.

271. Villarino, A., Duran, R., Wehenkel, A., Fernandez, P., England, P., Brodin, P., Cole, S. T., ZimnyArndt, U., Jungblut, P. R., Cervenansky, C., Alzari P. M. Proteomic identification of *M. tuberculosis* protein kinase substrates. PknB recruits GarA, a FHA domain-containing protein, through activation loop-mediated interactions. *J. Mol. Biol.* 2005, 350, 953–963.

272.Duran, R., Villarino, A., Bellinzoni, M., Wehenkel, A., Fernandez, P., Boitel, B., Cole, S.T., Alzari, P.M., Cervenansky C. Conserved autophosphorylation pattern in activation loops and juxtamembrane regions of *Mycobacterium tuberculosis* Ser/Thr protein kinases. *Biochem Biophys Res Commun* 2005, 333, 858–867.

273. Belanger, A. E., Hatfull, G. F. Exponential-phase glycogen recycling is essential for growth of *Mycobacterium smegmatis. J. Bacteriol.* 1999, 181, 6670–6678.

274. Niebisch, A., Kabus, A., Schultz, Weil, C., B., Bott, M. Corynebacterial protein kinase G controls 2-oxoglutarate dehydrogenase activity via the phosphorylation status of the OdhI protein.*J. Biol. Chem.* 2006, 281, 12300–12307.

275. Yeats, C., Finn, R.D., Bateman, A., The PASTA domain. α β-lactam binding domain, *Trends Biochem. Sci.* 2002, 27, 438–440

276. Good, M. C., Greenstein, A. E., Young, T. A., Ng, H.-L., Alber T., Sensor domain of the *Mycobacterium tuberculosis* receptor Ser/Thr protein kinase, PknD, forms a highly symmetric b propeller, *J. Mol. Biol.* 2004, 339, 459–469.

277. Jones, G., Dyson, P. Evolution of transmembrane protein kinase implicated in coordinating remodelling of Gram-positive peptidoglycan. inside versus outside, *J. Bacteriol.* 2006, 188, 7470–7476.

278. Keep, N.H., Ward, J.M., Cohen-Gonsaud, M., Henderson, B., Wake up! Peptidoglycan lysis and bacterial non-growth states, *Trends Microbiol.* 2006, 14, 271–276.

279. Puneet C., Bhuminder, S., Ramandeep S., Reena, V., Anil, K., Laxman S. M., Harshavardhan, K., Megha, G., Parampal, D., Taposh, K. D., Anil, K. T., Yogendra, S. Phosphoprotein phosphatase of *Mycobacterium tuberculosis* dephosphorylates serine–threonine kinases PknA and PknB. *Biochem. Biophysi. Res.h Comm.* 2003, 311, 112–120.

280. Fernandes, N. D., Wu, Q. L., Kong, D., Puyang, X., Garg, S., Husson, R. N., A mycobacterial extracytoplasmic sigma factor involved in survival following heat shock and oxidative stress. *J Bacteriol* 1999, 181, 4266–4274.

281. Raman, S., Song, T., Puyang, X., Bardarov, S., Jacobs, W. R., Jr, Husson, R. N. The alternative sigma factor SigH regulates major components of oxidative and heat stress responses in *Mycobacterium tuberculosis. J Bacteriol* 2001, 183, 6119–6125.

282. Song, T., Dove, S. L., Lee, K. H., Husson, R. N RshA, an anti-sigma factor that regulates the activity of the mycobacterial stress response sigma factor SigH. *Mol. Microbiol.* 2003, 50, 949–959.

283. Darwin, K. H., Ehrt, S., Gutierrez-Ramos, J. C., Weich, N., Nathan, C. F The proteasome of *Mycobacterium tuberculosis* is required for resistance to nitric oxide. *Science* 2003, 302, 1963–1966.

284. Li, W., Bottrill, A. R., Bibb, M. J., Buttner, M. J., Paget, M. S., Kleanthous, C.The Role of zinc in the disulphide stress-regulated anti-sigma factor RsrA from Streptomyces coelicolor. *J. Mol. Biol.*2003, 333, 461–472.

285. Newman, J. D., Anthony, J. R., Donohue, T. J. The importance of zinc-binding to the function of Rhodobacter sphaeroides ChrR as an anti-sigma factor.*J. Mol. Biol.* 2001, 313, 485–499.

286. Paget, M. S., Bae, J. B., Hahn, M. Y., Li, W., Kleanthous, C., Roe, J. H., Buttner, M. J. Mutational analysis of RsrA, a zinc-binding anti-sigma factor with a thiol-disulphide redox switch.*Mol. Microbiol.* 2001, 39, 1036–1047.

287. Sang T. P., Choong-Min, K., Robert, N. H. Regulation of the SigH stress response regulon by an essential protein kinase in *Mycobacterium tuberculosis*. *PNAS*, 2008, 105, 13105–13110.

288. Amit, P., Sunil, K. V., Shazia, K., Balaji, P., Vinay, K. N. PknB-Mediated Phosphorylation of a Novel Substrate, N-Acetylglucosamine-1-Phosphate Uridyltransferase, Modulates Its Acetyltransferase Activity. *J. Mol. Biol.* 2009, 386, 451–464.

289. O'Hare, H. M., Duran, R., Cervenansky, C., Bellinzoni, M., Wehenkel, A. M., Pritsch, O., Obal, G., Baumgartner, J., Vialaret, J., Johnsson, K., Alzari, P. M. *Mol. Microbiol.* 2008, 70, 1408–1423.

290. An intramolecular switch regulates phosphoindependent FHA domain interactions in Mycobacterium tuberculosis. Nott, T. J., Kelly, G., Stach, L., Li, J., Westcott, S., Patel, D., Hunt, D. M., Howell, S., Buxton, R. S., O'Hare, H. M., Smerdon, S.J.*Sci. Signal.* 2009, 2, Ra12

291. Malgorzata, M., Stefanie, D., Sonja, R., Thilo, S., Thijs, R. H. M. K., Sander, H. D., Annette, D., Ewoud, R., Katrin, G., Dorte, B., Maikel, P. D., Knut, O. Staphylococcal PknB as the First Prokaryotic Representative of the Proline-Directed Kinases. *PLoS ONE* 2010, 5, e9057.

292. Dasgupta, A., P. Datta, M. K., Basu, J. The serine/threonine kinase PknB of *Mycobacterium tuberculosis* phosphorylates PBPA, a penicillin-binding protein required for cell division. Microbiology 2006, 152, 493–504.

293. Ortiz-Lombardia, M., Pompeo, F., Boitel, B., Alzari, P. M. Crystal structure of the catalytic domain of the PknB Serine/Threonine kinase from *Mycobacterium tuberculosis* . *J Biol Chem* 2003, 278, 13094–13100.

294. Goldberg, J., Nairn, A. C., Kuriyan, J. Structural basis for the autoinhibition of calcium/calmodulin-dependent protein kinase I. *Cell* 1996, 84, 875–887.

295. Xu, W., Doshi, A., Lei, M., Eck, M. J., Harrison, S. C. Crystal structures of c-Src reveal features of its autoinhibitory mechanism. *Mol Cell* 1999, 3, 629–638.

296. Young, M. A., Gonfloni, S., Superti-Furga, G., Roux, B., Kuriyan, J. Dynamic coupling between the SH2 and SH3 domains of c-Src and Hck underlies their inactivation by C-terminal tyrosine phosphorylation. *Cell* 2001, 105, 115–126.

297. Annemarie, W., Pablo, F., Marco, B., Vincent, C., Nathalie, B., Gilles, L., Mary, J., Pedro M. Alzari. The structure of PknB in complex with mitoxantrone, an ATP-competitive inhibitor, suggests a mode of protein kinase regulation in mycobacteria. *FEBS Letters* 2006, 580, 3018–3022.

298. Steven, J. D., Firmin, H., Av-Gay, Y. A protein kinase inhibitor as an antimycobacterial agent, *FEMS.Microbio.Lett.* 2001, 205, 369-374.

299. Rita, S., Frigyes, W., Istvan, S., Gabor, N., Hegymegi-Barakonyi, B., Daniel, E., Balint, S., Janos, P., Doris, H., Jacqueline, S., Saint-Joanis, B., Stewart, T. C., Laszlo, O., Bert, M. K., Gyorgy, K. A novel drug discovery concept for tuberculosis. Inhibition of bacterial and host cell signaling. *Immunol.Lett.* 2008, 116, 225–231.

300. Eldridge, M. D., Murray, C. W., Auton, T. R., Paolini, G. V., Mee, R. P. Empirical scoring functions: I. The development of a fast empirical scoring function to estimate the binding affinity of ligands in receptor complexes. *J. Comput.-Aided Mol. Des.* 1997, 11, 425–445.

301. Friesner, R. A., Banks, J. L., Murphy, R. B., Halgren, T. A., Klicic, J. J., Mainz, D. T., Repasky, M. P., Knoll, E. H., Shelley, M., Perry, J. K., Shaw, D. E., Francis, P., Shenkin, P. S. Glide: a new approach for rapid, accurate docking and scoring. 1. Method and assessment of docking accuracy. *J. Med. Chem.* 2004, 47, 1739–1749.

302. Steven L. Dixon, Alexander M. Smondyrev, Eric H. Knoll, Shashidhar N. Rao, David E. Shaw, Richard A. Friesner. PHASE: a new engine for pharmacophore perception, 3D QSAR model development, and 3D database screening: 1. Methodology and preliminary results. *J. Comput. Aided. Mol. Des.* 2006. 20, 647–671.

303. Segal, W. in The Mycobacteria. A Sourcebook (eds Kubica, G. P. & Wayne, L. G.) 547-573 (Dekker,New York, 1984).

304. Clark, D. P., Cronan, J. E. Jr in Escherichia coli and Salmonella. Cellular and Molecular Biology (ed. Neidhardt, F. C.) 343-357 (ASM Press, Washington DC, 1996).

305.Cronan, J. E. Jr. LaPorte, D. in Escherichia coli and Salmonella. Cellular and Molecular Biology (ed. Neidhardt, F. C.) 206-216 (ASM Press, Washington DC, 1996).

306.Ho-Ènerzu, B. K., Miczak, A., Swenson, D. L., Russell, D. G. Characterization of activity and expression of isocitrate lyase in *Mycobacterium avium* and *Mycobacterium tuberculosis*. *J. Bacteriol.* 1999, 181, 7161-7167.

307.Sturgill-Koszycki, S., Haddix, P. L., Russell, D. G. The interaction between Mycobacterium and the macrophage analyzed by two-dimensional polyacrylamide gel electrophoresis.*Electrophoresis* 1997, 18, 2558-2565.

308.Farewell, A., Diez, A. A., DiRusso, C. C., Nystrom, T. Role of the Escherichia coli FadR regulator in stasis survival and growth phase-dependent expression of the uspA, fad, and fab genes. *J. Bacteriol.* 1996, 178, 6443-6450.

309.Spector, M. P. DiRusso, C. C., Pallen, M. J., Garciadel, P. F., Dougan, G., Finlay, B. B. The medium/long-chain fatty acyl-CoA dehydrogenase (fadF) gene of *Salmonella typhimurium* is a phase 1 starvation-stress response (SSR) locus. *Microbiol.* 1999, 145, 15-31.

310.SuryanarayanaMurthy, P., Sirsi, M., Ramakrishnan, T. Effect of age on the enzymes of tricarboxylic acid and related cycles in *Mycobacterium tuberculosis* H37Rv. *Amer. Rev. Resp. Dis.* 1973, 108, 689-690.

311.Wayne, L. G., Lin, K. Y. Glyoxylate metabolism and adaptation of *Mycobacterium tuberculosis* to survival under anaerobic conditions. *Infect. Immunol.* 1982, 37, 1042-1049.

312.McKinney, J. D., Bentrup, K. H. E., Munaoz-Eloaas, E. J., Andras, M., Bing, C., Wai-Tsing, C., Dana, S., Sacchettinik, J. C., Jacobs, W. R., Russell. D. G. Persistence of *Mycobacterium tuberculosis* in macrophages and mice requires the glyoxylate shunt enzyme isocitrate lyase. *Nature* 2000, 406, 735-738.

313.Smith, R. A., Gunsalus, I. C. Isocitritase. a new tricarboxylic acid cleavage system. *J. Am. Chem. Soc.* 1954, 76, 5002–5003.

314.Kornberg, H. L., Krebs, H. A. Synthesis of cell constituents from C2-units by a modified tricarboxylic acid cycle. *Nature* 1957, 179, 988–991.

315.Kornberg, H. L., Madsen, N. B. Synthesis of C4-dicarboxylic acids from acetate by a glyoxylate bypass of the tricarboxylic acid cycle. *Biochim Biophys Acta* 1957, 24, 651–653.

316.Timm, J., Post, F. A., Bekker, L. G., Walther, G. B., Wainwright, H. C., Manganelli, R., Chan, W. T., Tsenova, L., Gold, B. Differential expression of iron-, carbon-, and oxygenresponsive mycobacterial genes in the lungs of chronically infected mice and tuberculosis patients. *Proc. Natl. Acad Sci. U S A* 2003, 100, 14321–14326.

317.Munoz-Elias, E. J. McKinney, J. D. *Mycobacterium tuberculosis* isocitrate lyases 1 and 2 are jointly required for in vivo growth and virulence. *Nat. Med.* 2005, 11, 638–644.

318.Jun-ming, L., Na, L., Dao-yin, Z., La-gen, W., Yong-lin H., Chun, Y. Isocitrate lyase from *Mycobacterium tuberculosis* promotes survival of *Mycobacterium smegmatis* within macrophage by suppressing cell apoptosis. *Chin. Med. J.* 2008, 121, 1114-1119.

319.Gould, T. A., Langemheen, H., Munoz-Elias, E. J., McKinney, J. D., Sacchettini, J. C. Dual role of isocitrate lyase 1 in the glyoxylate and methylcitrate cycles in *Mycobacterium tuberculosis*. *Mol. Microbiol.* 2006, 61, 940–947.

320.Schnappinger, D., Ehrt, S., Voskuil, M. I., Liu, Y., Mangan, J. A., Monahan, I. M., Dolganov, G., Efron, B., Butcher, P. D., Transcriptional adaptation of *Mycobacterium* *tuberculosis* within macrophages.insights into the phagosomal environment. *J. Exp. Med.* 2003, 198, 693–704.

321.Martin, G., Srinivasa, P. S. R., Kevin, P., Thomas, D. Nutrient-starved, non-replicating *Mycobacterium tuberculosis* requires respiration, ATP synthase and isocitrate lyase for maintenance of ATP homeostasis and viability. *Microbiology* 2010, 156, 81–87.

322.Betts, J. C., Lukey, P. T., Robb, L. C., McAdam, R. A., Duncan, K. Evaluation of a nutrient starvation model of *Mycobacterium tuberculosis* persistence by gene and protein expression profiling. *Mol. Microbiol.* 2002, 43, 717–731.

323.Wayne, L. G., Hayes, L. G. An in vitro model for sequential study of shiftdown of *Mycobacterium tuberculosis* through two stages of nonreplicating persistence.*Infect. Immun.* 1996, 64, 2062–2069.

324.Sharma, V., Sharma, S., Honerzu, B. K., McKinney, J. D., Russell, D. G., Jacobs, Jr. W. R., Structure of isocitrate lyase, a persistence factor of *Mycobacterium tuberculosis*. *Nat. Struct. Biol.* 2000, 7.663–668.

325.McFadden, B. A., Purohit, S. Itaconate, an isocitrate lyase directed inhibitor in Pseudomonas indigofera. *J. Bacteriol* 1977, 131, 136–144.

326.Alston, T. A., Mela, L., Bright, H. J. 3-Nitropropionate, the toxic substance of Indigofera, is a suicide inactivator of succinate dehydrogenase. *Proc. Natl. Acad. Sci. U S A* 1977, 74, 3767–3771.

327.Bai, B., Xie, J.-P., Yan, J.-F., Wang, H.-H. & Hu, C.-H. A high throughput screening approach to identify isocitrate lyase inhibitors from traditional Chinese medicine sources.*Drug Dev Res* 2007, 67, 818–823.

328.Dongha, L., Jongheon, S., Kyung-Mi Y., Tae-Im, K., So-Hyoung, L., Hyi-Seung, L., Ki-Bong, O. Inhibition of Candida albicans isocitrate lyase activity by sesterterpene sulfates from the tropical sponge Dysidea sp. *Bioorg. Med. Chem. Lett.* 2008, 18, 5377–5380.

329.Hyi-Seung, L., Kyung-Mi, Y., Yu-Ri, H., Kyung, J. L., Soon-Chun, C., Tae-Im, K., So-Hyoung, L., Jongheon, S., Ki-Bong, O. 5-Hydroxyindole-type alkaloids, as Candida albicans isocitrate lyase inhibitors, from the tropical sponge Hyrtios sp. *Bioorg. Med. Chem. Lett.* 2009, 19, 1051–1053.

330.Ki-Bong, O., Heung, B. J., Yu-Ri, H., Yeon-Ju, L., Jiyoung, P., So-Hyoung, L., Dongsik, Y., Mihyun, K., Jongheon, S., Hyi-Seung, L. Bromophenols as Candida albicans isocitrate lyase inhibitors. *Bioorg. Med. Chem. Lett.* 2010, 20, 6644–6648.

331.Sriram, D., Yogeeswari, P., Senthilkumar, P., Sangaraju, D., Nelli, R., Banerjee, D., Bhat, P., Veugopal , B., Pavan, V.V.S., Manjashetty, T.H. Novlel pthalazinyl derivatives. Synthesis, antimycobacterial activities, and inhibition of *Mycobacterium tuberculosis* isocitrate lyase enzyme.*Med. Chem.* 2009, 5, 422-433.

332.Sriram, D., Yogeeswari, P., Senthilkumar, P., Geetanjali, N., Pritesh, B. 5-Nitro-2,6-dioxohexahydro-4-pyrimidinecarbox- amides Synthesis and antimycobacterial activities. *J. Enzyme Inhib. Med. Chem.* 2009, 25, 765-772.

333.Sriram, D., Yogeeswari, P., Devambatla, R. K. V., Senthilkumar, P., Pritesh, B., Madala S., 5-Nitro-2-furoic acid hydrazones. Design, synthesis and in-vitro antimycobacterial evaluation against log and starved phase cultures. . *Bioorg. Med. Chem. Lett.* 2010, 20, 4313-4316.

334.Sriram, D., Yogeeswari, P., Senthilkumar, P., Sangaraju, D., Nelli, R., Banerjee, D., Bhat, P., Manjashetty. T. H Synthesis and antimycobacterial evaluation of novel phthalazin-4-ylacetamides against log- and starved phase cultures. *Chem. Biol. Drug Design*, 2010, 75, 381-391.

335.Debjani, B., Yogeeswari, P., Pritesh, B., Anisha, T., Madala, S., Sriram, D., Novel isatinyl thiosemicarbazones derivatives as potential molecule to combat HIV-TB co-infection. *Euro. J. Med. Chem.* 2011, 46, 106-121.

APPENDIX

List of Publications

1. Debjani Banerjee, Perumal Yogeeswari, **Pritesh Bhat**, Anisha Thomas, Madala Srividya, Dharmarajan Sriram. Novel isatinyl thiosemicarbazones derivatives as potential molecule to combat HIV-TB co-infection. ***Eur. J. Med. Chem.***, 46, 106-121, 2011.
2. Dharmarajan Sriram, Perumal Yogeeswari, Devambatla Ravi Kumar Vyas, Palaniappan Senthilkumar, **Pritesh Bhat**, Madala Srividya. 5-Nitro-2-furoic acid hydrazones: Design, synthesis and in-vitro antimycobacterial evaluation against log and starved phase cultures. ***Bioorg. Med. Chem. Lett.***, 20, 4313-4316, 2010.
3. Dharmarajan Sriram, Perumal Yogeeswari, Palaniappan Senthilkumar, D. Sangaraju, Rohith Nelli, Debjani Banerjee, **Pritesh Bhat**, T.H. Manjashetty. Synthesis and antimycobacterial evaluation of novel phthalazin-4-ylacetamides against log and starved phase cultures. ***Chem. Biol. & Drug Design***, 75, 381-391, 2010.
4. Dharmarajan Sriram, Perumal Yogeeswari, M. Dinakaran, Debjani Banerjee, **Pritesh Bhat**, Sunil Gadhwal. Discovery of Newer Antitubercular 2,10-Dihydro-4aH-chromeno[3,2-c]pyridin-3-yl Derivatives. ***Eur. J. Med. Chem.***, 45, 120-123, 2010.
5. Debjani Banerjee, Perumal Yogeeswari, **Pritesh Bhat**, Anisha Thomas, Dharmarajan Sriram. Synthesis, in-vitro evaluation and computational studies of novel isatinyl derivatives for their activity against HIV-TB co-infection. ***Int. J. Drug Des. & Discov.***, 1, 65-80, 2010.
6. Dharmarajan Sriram, Perumal Yogeeswari, Palaniappan Senthilkumar, Geetanjali Naidu, **Pritesh Bhat**. 5-Nitro-2,6-dioxohexahydro-4-pyrimidinecarbox- amides : Synthesis and antimycobacterial activities. ***J. Enzyme Inhib. Med. Chem.***, 25, 765-772, 2010.

7. Dharmarajan Sriram, Perumal Yogeeswari, Palaniappan Senthilkumar, D. Sangaraju, Rohith Nelli, Debjai Banerjee, **Pritesh Bhat**, B. Veugopal, V.V.S. Pavan, T.H Manjashetty. Novlel pthalazinyl derivatives: Synthesis, antimycobacterial activities, and inhibition of Mycobacterium tuberculosis isocitrate lyase enzyme. ***Med. Chem.***, 5, 422-433, 2009.

8. Raju Ranjith Kumar, Subbu Perumal, S.C. Manju, **Pritesh Bhat**, Perumal Yogeeswari, D Sriram. An atom economic synthesis and antitubercular evaluation of novel spiro-cyclohexanones. ***Bioorg. Med. Chem. Lett.,*** 19, 3461-3465, 2009.

9. **Pritesh Bhat**, Dharmarajan Sriram, Ramakrishna Vadrevu, Perumal Yogeeswari. Homology modeling and molecular dynamics of Glutamate Racemase of Mycobacterium tuberculosis. ***J. Chem. Inf. Mod.*** In communication.

BIOGRAPHY OF PRITESH BHAT

Mr. Pritesh Bhat has completed his Bachelor's degree in Pharmacy from Manipal College of Pharmaceutical Sciences Manipal, in the year 2004. He acquired his Master's degree in Pharmacy in Pharmaceutical chemistry from Manipal College of pharmaceutical sciences, Manipal, Karnataka in 2007. He had been working as a research scholar at BITS, Pilani from 2007-2011. During his post-graduation studies he availed GATE scholarship and during his doctoral studies he was awarded Senior Research Fellowship (SRF) by the, Department of Biotechnology, (Centre of Excellence Project) New Delhi, India. He has few publications in international journals.

BIOGRAPHY OF Dr. P.YOGEESWARI

Dr. P. Yogeeswari is presently working in the capacity of Associate Professor and Head, Department of Pharmacy, Birla Institute of Technology and Science, Pilani, Hyderabad Campus. She received her Ph.D. degree in the year 2001 from BanarasHinduUniversity; Varanasi. She has been involved in research for the last 12yrs and in teaching for 11 yrs. APTI honored her with YOUNG PHARMACY TEACHER AWARD for the year 2007. She has collaborations with various national and international organizations that include National Institute of Health, Bethesda, USA, National Cancer Institute, and USA, National Institute of Mental Health and Neurosciences, Bangalore, Indian Institute of Science, Bangalore, and Department of Ophthalmology & Visual Science, University of Illinois, Chicago, USA. She has to her credit more than 125 research publications and one patent under process. She is an expert reviewer of many international journals like Journal of Medicinal Chemistry (ACS), Bioorganic Medicinal Chemistry (Elsevier), Recent Patents on CNS Drug Discovery (Bentham), Current Enzyme Inhibition (Bentham), ActaPharmacologicaSinica (Blackwell Publishing), European Journal of Medicinal Chemistry (Elsevier) and Natural Product Resources (Taylor and Francis).She has also co-authored a textbook on organic medicinal chemistry with Dr.D Sriram titled "Medicinal Chemistry", published by Pearson Education. She is the co-editor for "Internal Journal of Drug Design and Discovery". She is a lifetime member of Association of Pharmacy Teachers of India and Indian Pharmacological Society. She has successively completed three projects, one of DST SERC Fast Track under Young Scientist Scheme and other two of CSIR. In addition she is working on two another projects of UGCand DBT. She has guided fourPh.D students and currently she is guiding 7 students.